
Site Investigation and Dynamic Soil Properties

Outline

Geophysical Exploration Methods
Laboratory Techniques and Field-Lab. Comparisons
Nonlinear Soil Behavior (soil stiffness and damping)

Short course notes: A. Elgamal, Chicago, Illinois, April 29 - 30, 2013

1

Acknowledgments

Reference papers and figures generously contributed by the following
Individuals are greatly appreciated:

Professor Kenneth H. Stokoe II
University of Texas, Civil Engineering Dept.
Austin, TX

Professor Richard D. Woods
University of Michigan
2360 GG Brown Laboratory
Ann Arbor, MI

Dr. Michael Fraser, PE
Naval Facilities Engineering Command Southwest
San Diego, CA

Short course notes: A. Elgamal, Chicago, Illinois, April 29 - 30, 2013

2

Primary References

Kenneth H. Stokoe II and J. Carlos Santamarina (2000). **Seismic Wave-Based Testing in Geotechnical Engineering**, International Conference on Geotechnical and Geological Engineering, GeoEng 2000, Melbourne, Australia, November, 19-24.

Kenneth H. Stokoe II, Seon Keun Hwang, James Ngar-Kok Lee, and Ronald D. Arduis (1994). **Effects of Various Parameters on the Stiffness and Damping of Soils at Small to Medium Strains**, International Symposium on Prefailure Deformation Characteristics of Geomaterials, Keynote Lecture, Sapporo, Japan, September 12 – 14.

Kenneth H. Stokoe II, M. B. Darendeli, R. D. Arduis, and L. T. Brown (1999). **Dynamic Soil Properties: Laboratory, Field and Correlation Studies**, Theme Lecture, Session I: Dynamic Characterization of Soils, Second International Conference on Earthquake Geotechnical Engineering, Vol. 3, Lisbon, Portugal, June .

Kenneth H.; Stokoe, II, M. B. Darendeli, , F. - Y. Menq and W. - K. Choi, (2004). **Comparison of the Linear and Nonlinear Dynamic Properties of Gravels, Sands, Silts and Clays**, University of California, Berkeley, The 11th International Conference on Soil Dynamics & Earthquake Engineering (11th ICSDEE). The 3rd Intl Conference on Earthquake Geotechnical Eng (3rd ICEGE). University of California, Berkeley, January 7-9.

Richard D. Woods, Ed. (1994). **Geophysical Characterization of Sites**, Volume prepared by ISSMFE Technical Committee # 10, XIII ICSMFE, New Delhi, India, Oxford & IBH Publishing CO. PVT. LTD.

Ronald J. Ebelhar, Vincent P. Drnevich, and Bruce L. Kutter, Eds. (1994). **Dynamic Geotechnical Testing II**, Symposium Proc., San Francisco, CA, 27-28 June, STP 1213, ASTM publication code number (PCN):04-012130-38.

Richard D. Woods (1994). **Laboratory Measurement of Dynamic Soil Properties**, Dynamic Geotechnical Testing II, Symposium Proc., San Francisco, CA, 27-28 June, Ronald J. Ebelhar, Vincent P. Drnevich, and Bruce L. Kutter, Eds., STP 1213, ASTM publication code number (PCN):04-012130-38.

Short course notes: A. Elgamal, Chicago, Illinois, April 29 - 30, 2013

3

R. G. Campanella (1994). **Field Methods for Dynamic Geotechnical Testing: An Overview of Capabilities and Needs**, Dynamic Geotechnical Testing II, Symposium Proc., San Francisco, CA, 27-28 June , Ronald J. Ebelhar, Vincent P. Drnevich, and Bruce L. Kutter, Eds., STP 1213, ASTM publication code number (PCN):04-012130-38.

E. Kavazanjian, Jr., N. Matasovic, T. Hadj-Hamou, and P. J. Sabatini (1997). **Geotechnical Engineering Circular No. 3 – Design Guidance: Geotechnical Earthquake Engineering for Highways**, Design Principles, Volume 1, SA-97-076 (NTIS # PB98-11560)

E. Kavazanjian, Jr., N. Matasovic, T. Hadj-Hamou, and P. J. Sabatini (1997). **Geotechnical Engineering Circular No. 3 – Design Guidance: Geotechnical Earthquake Engineering for Highways**, Design Examples, Volume 2, SA-97-077 (NTIS # PB98-11578)

NRC (2000). **Seeing into the Earth**, Committee for Noninvasive Characterization of the Shallow Subsurface for Environmental and Engineering Applications, P. R. Roming, Chair, 129 pp.

Rosenblad, B. L., Li, J., Menq, F-Y, Stokoe, K. H. (2007). **Deep Shear Wave Velocity Profiles from Surface Wave Measurements in the Mississippi Embayment**, Earthquake Spectra , November 200, Vol.23, Issue 4, pp. 791-808.

Zhang, J, Andrus, R. D., and Juang, C. H. (2005). **“Normalized Shear Modulus and Damping Relationships**, Journal of Geotechnical and Geoenvironmental Engineering, ASCE, Vol. 131, No. 4, April.

Zhang, J., Andrus, R. D., and Juang, C. H. (2008). **Model uncertainty in Normalized Shear Modulus and Damping Relationships**, Journal of Geotechnical and Geoenvironmental Engineering, Vol. 34, No. 1, January.

Short course notes: A. Elgamal, Chicago, Illinois, April 29 - 30, 2013

4

Additional References

Bray, J.D., Zekkos, D., Kavazanjian, E., Jr., Athanasopoulos, G.A. and Riemer, M.F. (2009). Shear Strength of Municipal Solid Waste, *J. Geotech. and Geoenvironmental Engineering*, Volume 135, Issue 6, pp. 709-722.

Darendeli, M.B. (2001). Development of a new family of normalized modulus reduction and material damping curves, PhD dissertation, U. of Texas at Austin, 362 p.

Duhee, P. and Hashash, Y. (2008). Rate-dependent soil behavior in seismic site response analysis, *Canadian Geotechnical Journal*, Volume 45, Number 4, 1 April, pp. 454-469(16), NRC Research Press.

Khan, Z.H., Cascante, G., El Naggar, M.H. and Lai, C.G. (2008). Measurement of frequency-dependent dynamic properties of soils using the resonant-column device, *J. Geotechnical and Geoenvironmental Engineering*, Volume 134, Issue 9, pp. 1319-1326.

Menq, F.-Y. (2003). Dynamic Properties of Sandy and Gravelly Soils. PhD Dissertation (supervisor: Prof. Kenneth H. Stokoe), Department of Civil Engineering, The University of Texas at Austin, May.

Menq, F. Y., Stokoe, K. H., II and Kavazanjian, E. 2003. "Linear dynamic properties of sandy and gravelly soils from large-scale resonant tests." Proc., Int. Symp. IS Lyon 03, Deformation Characteristics of Geomaterials, H. Di Benedetto, T. Doahn, H. Geoffroy, and C. Sauzeat, eds., Balkema, Lyon, France.

Kishida, T., Wehling, T.M., Boulanger, R.W., Driller, M.W. and Kenneth H. Stokoe K.H., II (2009). Dynamic Properties of Highly Organic Soils from Montezuma Slough and Clifton Court, *Journal of Geotechnical and Geoenvironmental Engineering*, Vol. 135, No. 4, April, 525-532.

Kurtulus, A. and Stokoe, II, K.H (2008). In Situ Measurement of Nonlinear Shear Modulus of Silty Soil, *J. Geotechnical and Geoenvironmental Engineering*, Volume 134, Issue 10, pp. 1531-1540, October.

Short course notes: A. Elgamal, Chicago, Illinois, April 29 - 30, 2013

5

Additional References (cont.)

Stokoe, K. H., II, Darendeli, M.B., Menq, F.-Y. and Choi, W.-K. (2004). Comparison of the Linear and Nonlinear Dynamic Properties of Gravels, Sands, Silts and Clays, University of California, Berkeley, The 11th International Conference on Soil Dynamics & Earthquake Engineering (11th ICSDEE). The 3rd International Conference on Earthquake Geotechnical Engineering (3rd ICEGE). University of California, Berkeley, January 7-9.

Zekkos, D., Bray, J., Athanasopoulos, G.A., Reimer, M., Kavazanjian, E., Jr., Founta, P.A., and Grizi, A.F. (2007). Compositional and loading rate effects on the shear strength of municipal solid waste, 4th International Conference on Earthquake Geotechnical Engineering, June 25-28,, Paper No. 1525.

Zekkos, D., Bray, J., Stokoe, K.H., II, Kavazanjian, Jr. E., Rathje, E., Athanasopoulos, G.A., Reimer, M., Matasovic, N., Lee, J.J., and Seos, B. (2008). Recent findings on the static and dynamic properties of municipal solid waste, *Geocongress 2008, Geotechnics of waste management and remediation, ASCE, GSP 177*, March 9-12, New Orleans, LA.

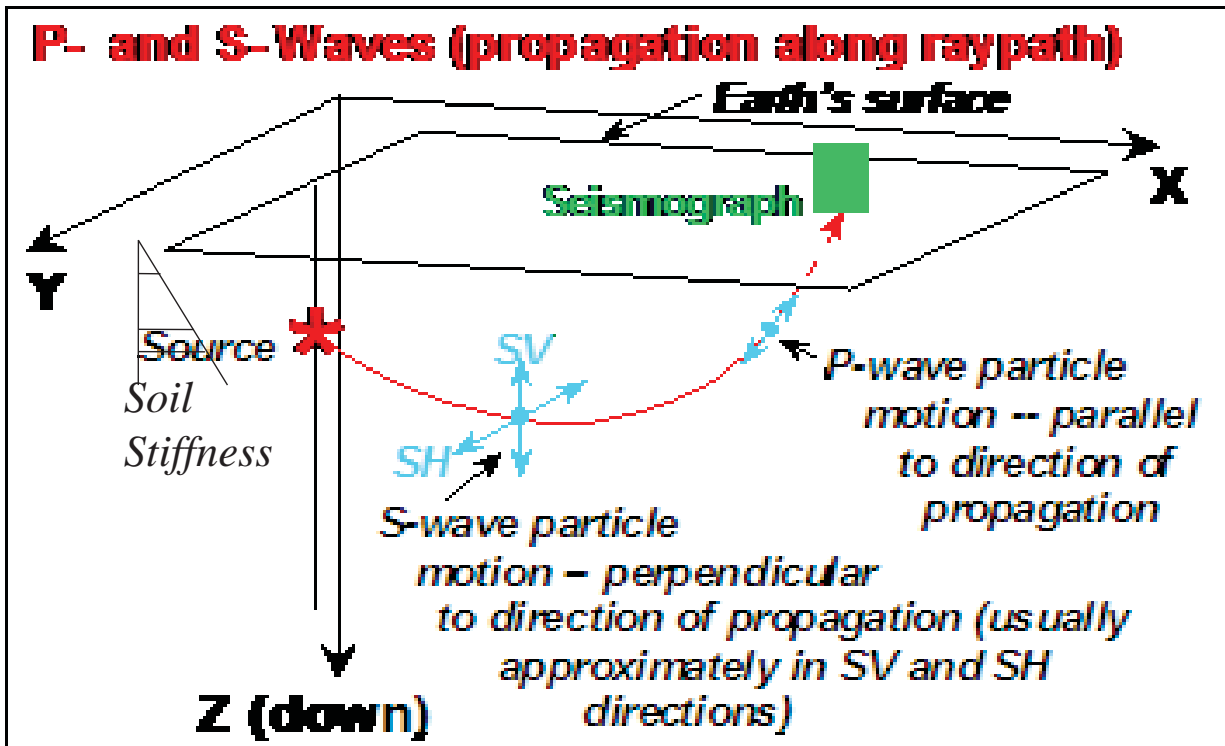
Short course notes: A. Elgamal, Chicago, Illinois, April 29 - 30, 2013

6

Wave Propagation and Seismic Waves

Short course notes: A. Elgamal, Chicago, Illinois, April 29 - 30, 2013

7

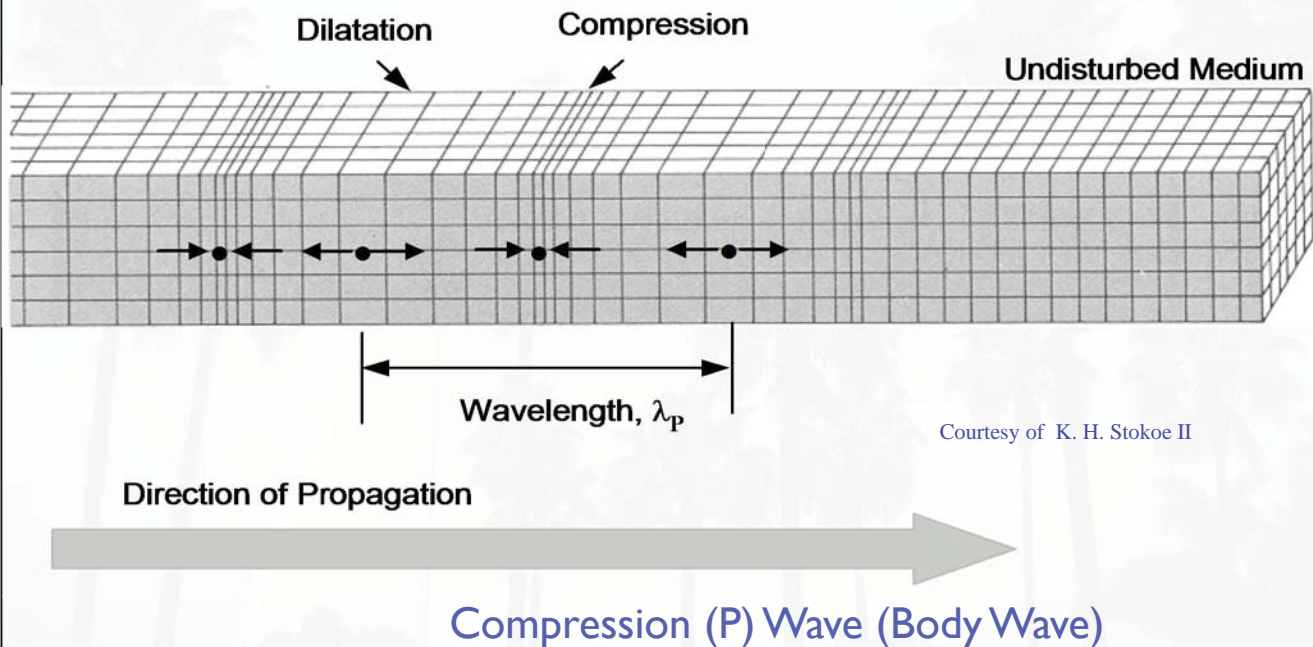


after: <http://web.ics.purdue.edu/~braile/edumod/slinky/slinky.htm>

Short course notes: A. Elgamal, Chicago, Illinois, April 29 - 30, 2013

8

Wave Propagation Modes. Body Waves within a Uniform, Infinite Medium (after Bolt, 1976)



Short course notes: A. Elgamal, Chicago, Illinois, April 29 - 30, 2013

9

P-waves propagate through solids and fluids. May emerge to ground surface as an audible sound wave (to animals and humans, if >15 cycles per second).

$$\text{P-wave velocity } \alpha = \sqrt{(B + \frac{4}{3}G)/\rho} = V_p$$

where:

B = Modulus of incompressibility / bulk modulus

G = Modulus of rigidity / shear modulus (G or μ)

ρ = Density

Note: B and G can be expressed in terms of E and ν , where E = Young's modulus and ν = Poisson's ratio

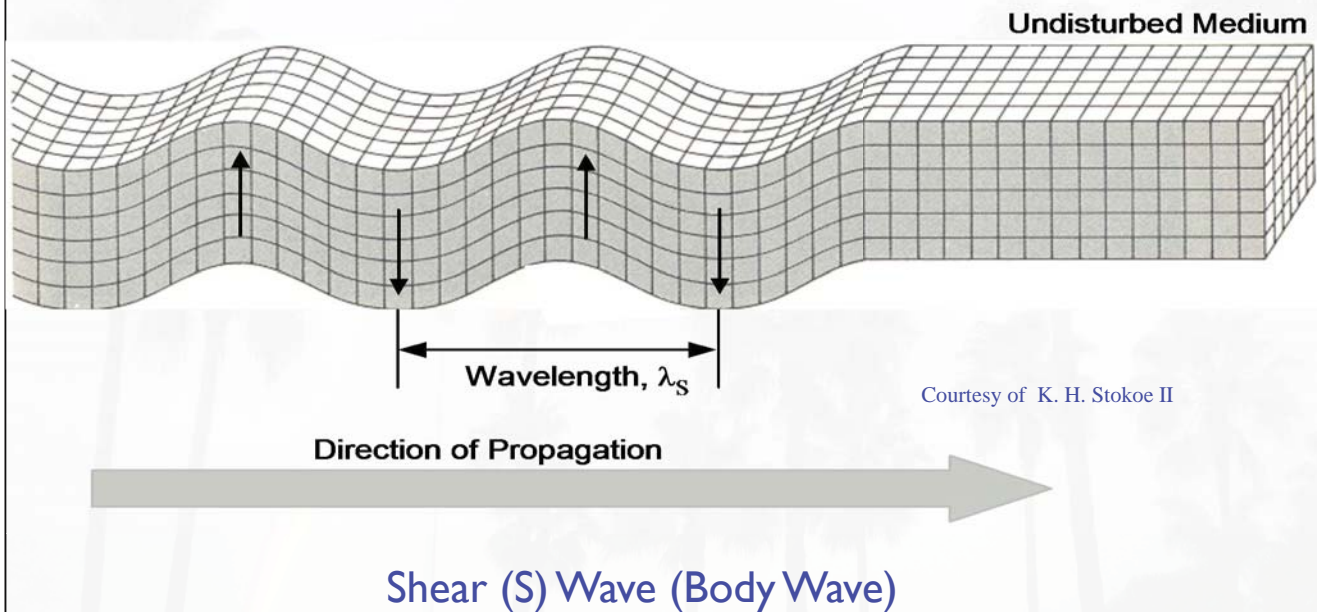
For granite $\alpha = 4.8$ km/sec

For water $\alpha = 1.5$ km/sec

Short course notes: A. Elgamal, Chicago, Illinois, April 29 - 30, 2013

10

Wave Propagation Modes. Body Waves within a Uniform, Infinite Medium (after Bolt, 1976)



Short course notes: A. Elgamal, Chicago, Illinois, April 29 - 30, 2013

11

S-waves travel through solids only

S-wave velocity $\beta = \sqrt{G/\rho} = V_s$

For granite, $\beta = 3.0$ km/sec

For water, $\beta = 0$ km/sec (G or μ of fluids = 0)

Accordingly, the P-wave is faster than the S-wave.

Arrives first to a site during an earthquake. S-wave follows after a few seconds and causes most damage due to side-to-side motion. Most earthquake energy is in shear with high shaking amplitude.

Alternate forms for G , B , E and ν

$$G = \rho V_s^2 \quad B = \rho \left(V_p^2 - \frac{4}{3} V_s^2 \right) \quad E = 2\rho V_s^2 (1 + \nu)$$

$$\nu = \text{Poisson's ratio} = \frac{0.5(V_p/V_s)^2 - 1}{(V_p/V_s)^2}$$

Short course notes: A. Elgamal, Chicago, Illinois, April 29 - 30, 2013

12

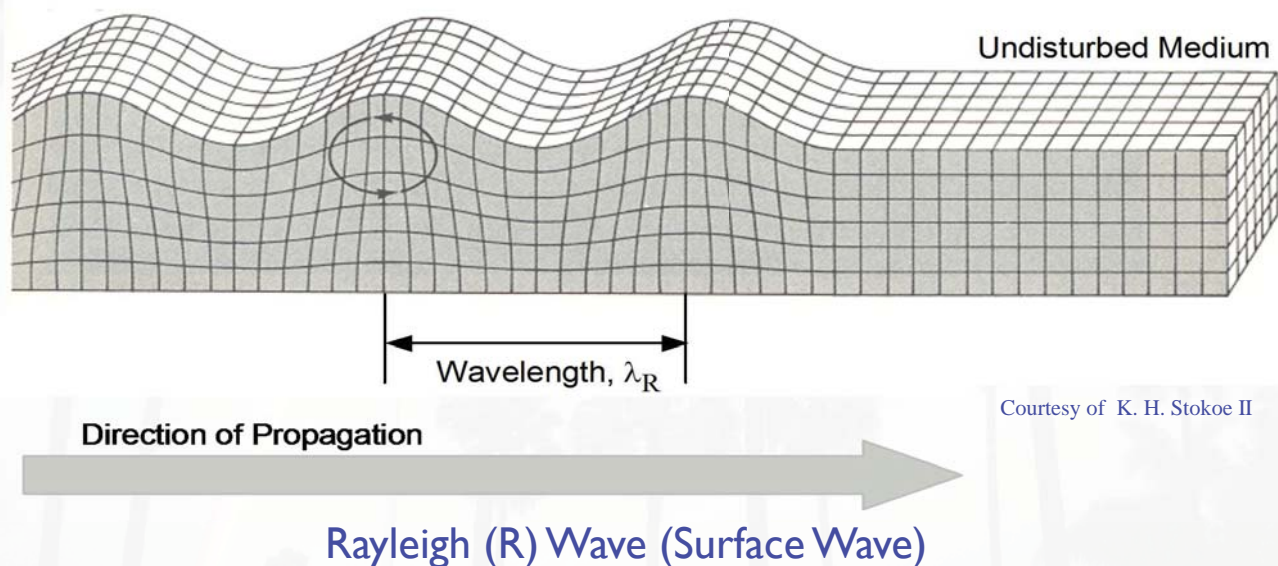
P-wave velocities (approximate)

Material	V_p (m/sec)
Air	340
Soft soil	250-550
Stiff soil	450-600
Water	1450-1500
Dense gravel	450-1200
Cemented gravel	1200-2000
Soft shale	900-2000
Hard shale	1800-3000
Sandstone	1500-3000
Limestone	2400-5500
Basalt	2400-4000
Granite	3000-6100

Short course notes: A. Elgamal, Chicago, Illinois, April 29 - 30, 2013

13

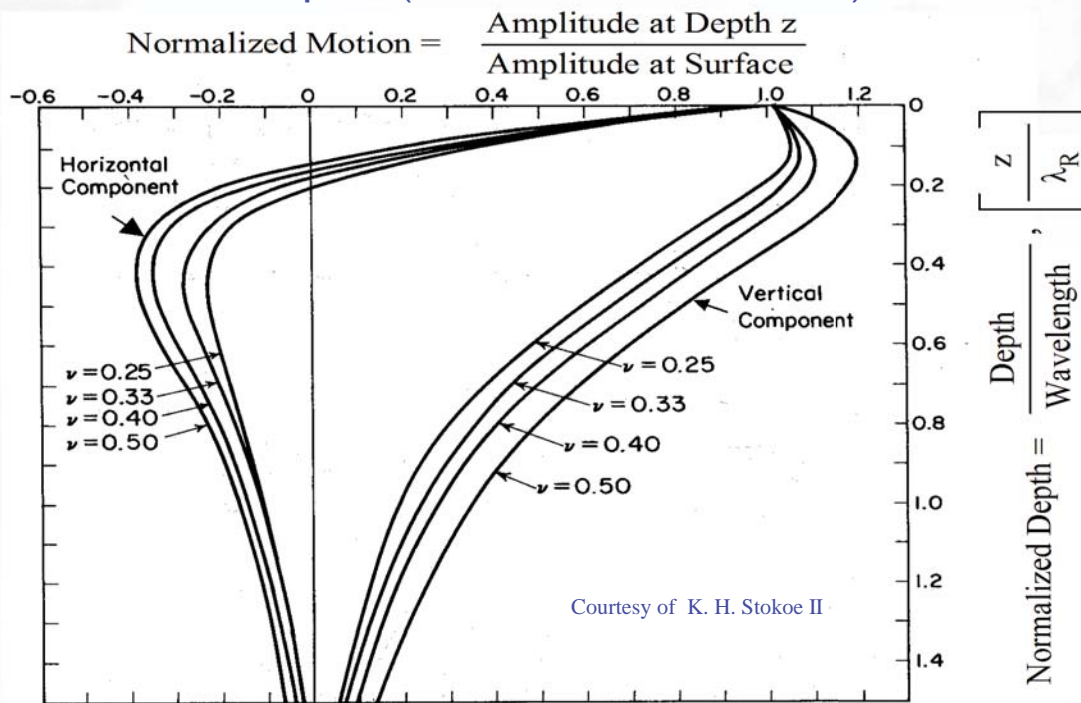
Wave Propagation Modes: Rayleigh (R) Waves along the surface of a uniform half space (after Bolt, 1976)



Short course notes: A. Elgamal, Chicago, Illinois, April 29 - 30, 2013

14

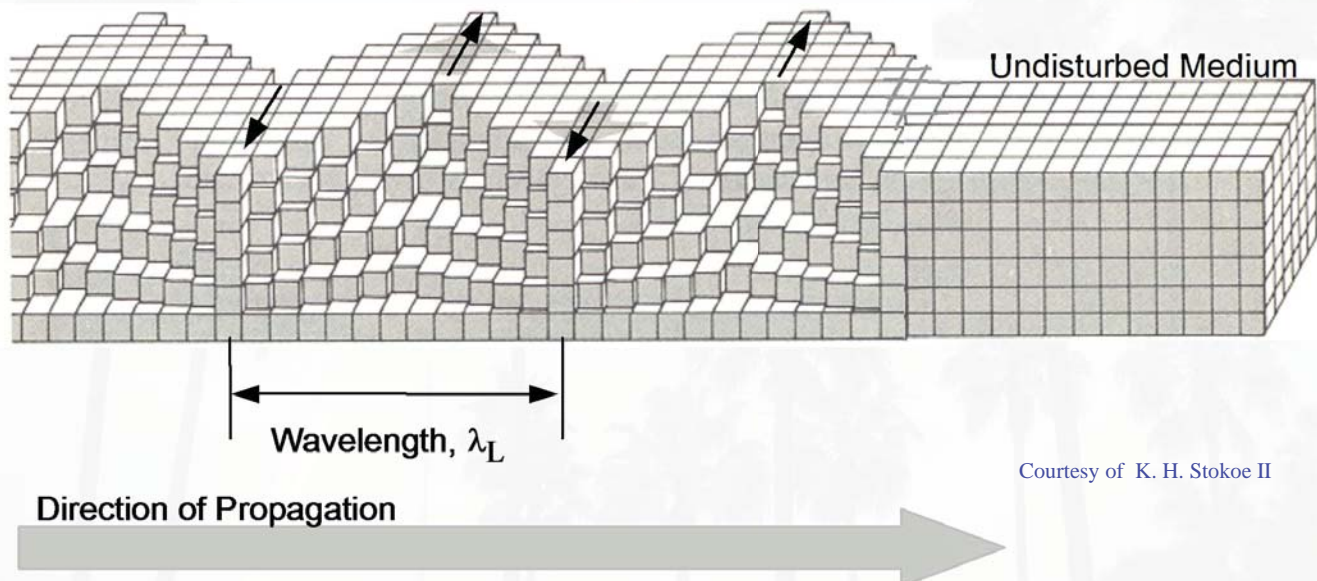
Variation in Normalized Particle Motions with Normalized Depth for Rayleigh Waves Propagating Along a Uniform Half Space (from Richart et al., 1970)



Short course notes: A. Elgamal, Chicago, Illinois, April 29 - 30, 2013

15

Surface Wave: Love (L) Wave Propagating in the Top Layer of a Layered Half Space (after Bolt, 1976)



Short course notes: A. Elgamal, Chicago, Illinois, April 29 - 30, 2013

16

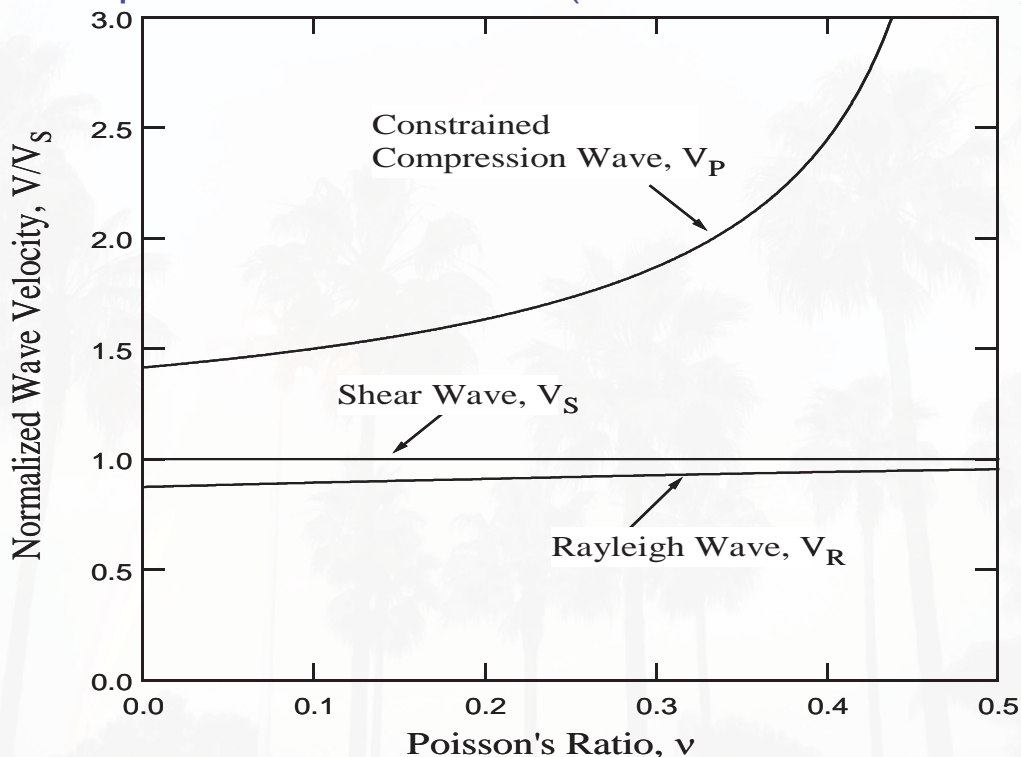
Surface waves: Waves with motion restricted to near ground surface (wave displacement decreases with depth, like ripples of water across a lake). Surface waves travel slower than body waves (Love waves generally travel faster than Rayleigh waves)

- Rayleigh waves can appear in vert. and horiz. recorded accelerations
- Love waves only appear in horizontal accelerations

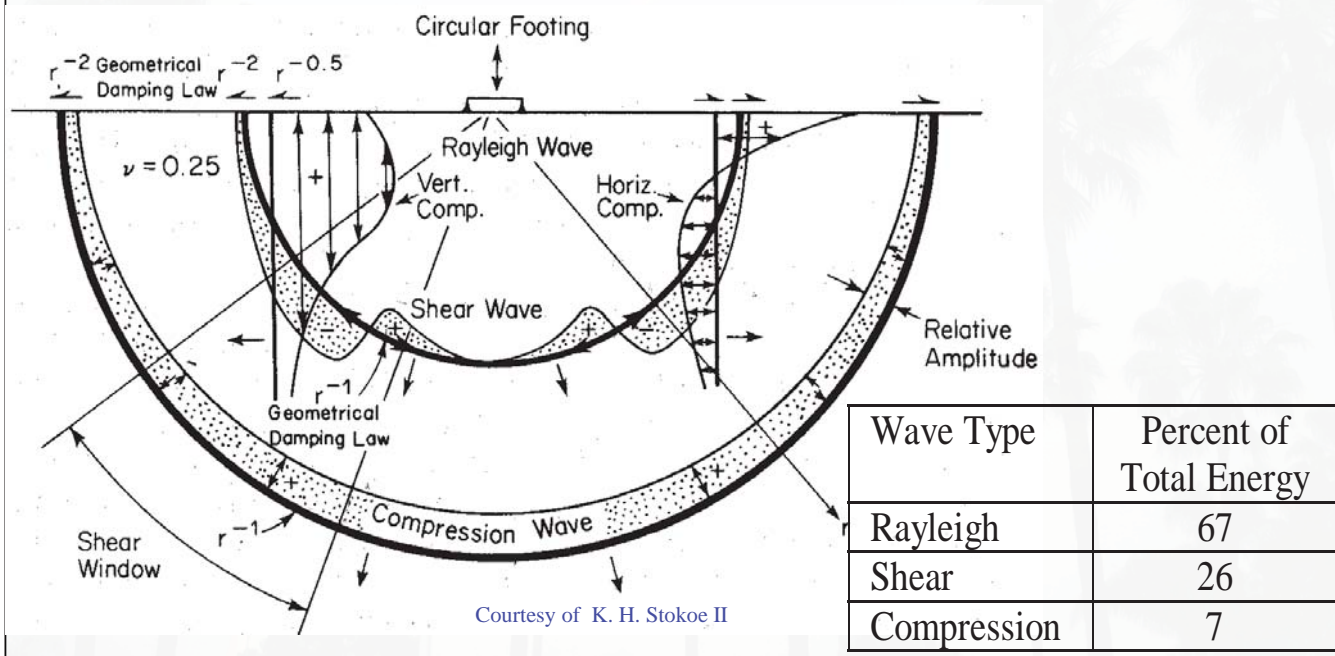
Velocity: P-wave > S-wave > Love wave > Rayleigh wave (in general)

- Surface waves (Rayleigh and Love) spread out into a train of motion as they propagate (**dispersion**). Waves with longer wavelength travel quicker than waves with shorter wavelength, because longer waves penetrate deeper into the earth where the ground is stiffer and transmittal of waves is faster. Time of arrival of each wavelength in the surface train of waves can be used to back-figure the dispersion relation and the elastic properties of rocks through which the waves traveled.

Relationship Between Stress Wave Velocities in a Uniform Half Space and Poisson's ratio (from Richart et al., 1970)

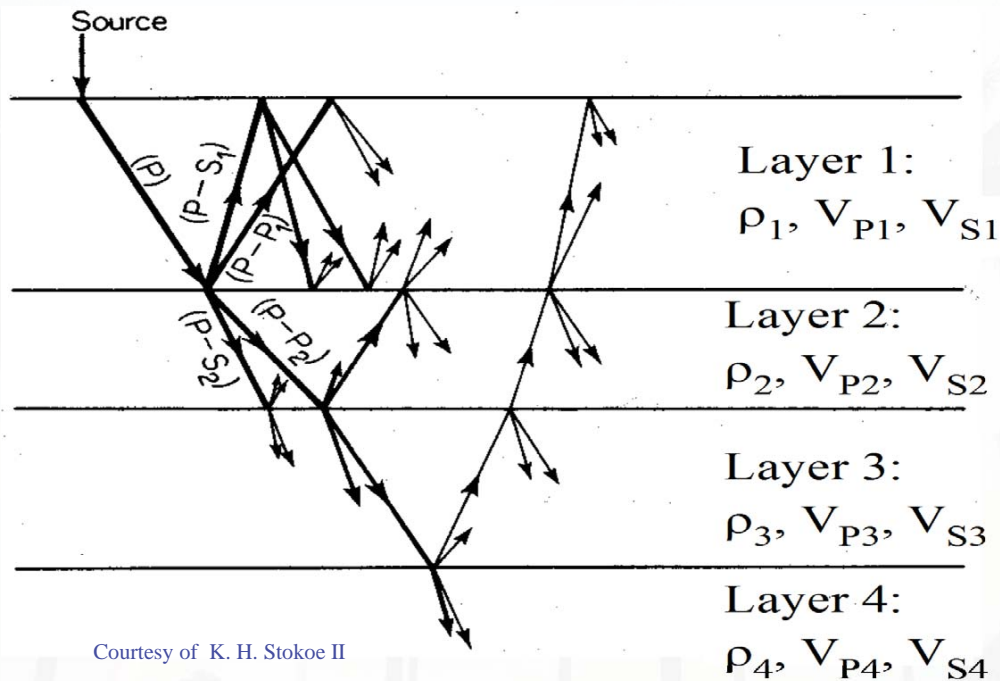


Distribution of Stress Wave Motions from a Vibrating Circular Footing on a Homogeneous, Isotropic, Elastic Half Space (from Woods, 1968)



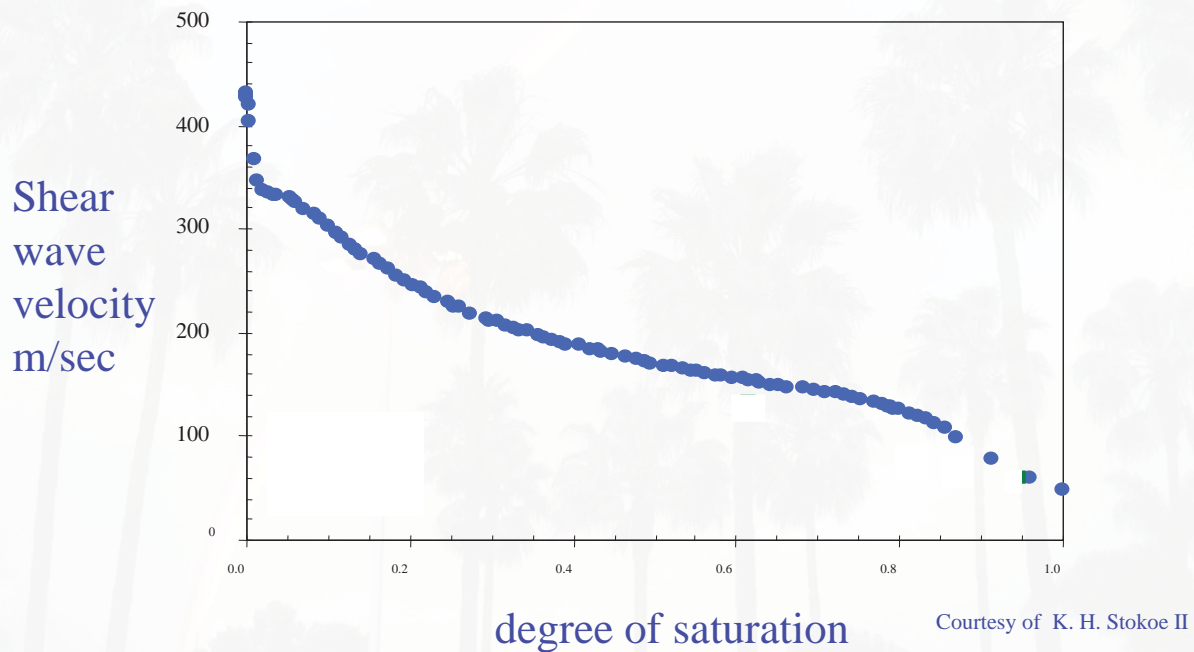
Short course notes: A. Elgamal, Chicago, Illinois, April 29 - 30, 2013

Multiple Wave Reflections and Refractions in a Layered Half-Space and the Resulting Mode Conversions (from Richart et al., 1970)

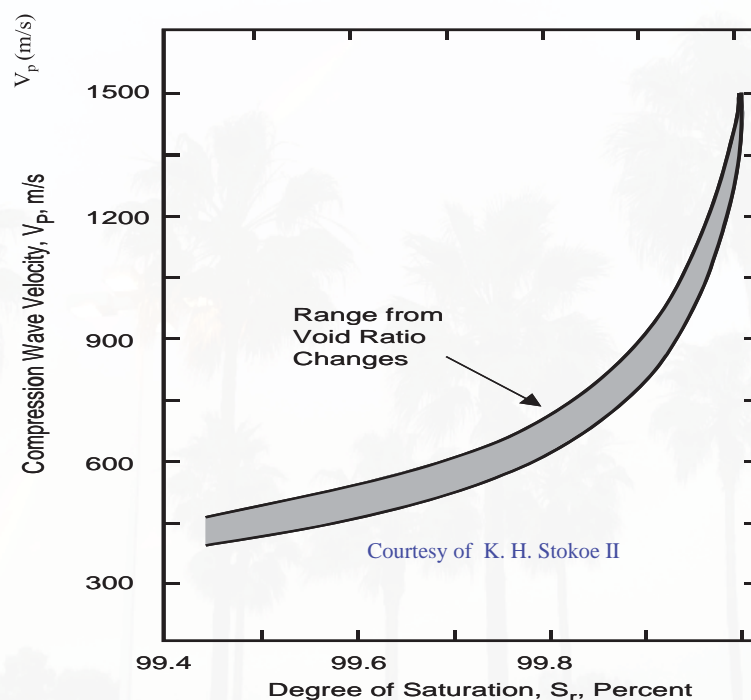


Short course notes: A. Elgamal, Chicago, Illinois, April 29 - 30, 2013

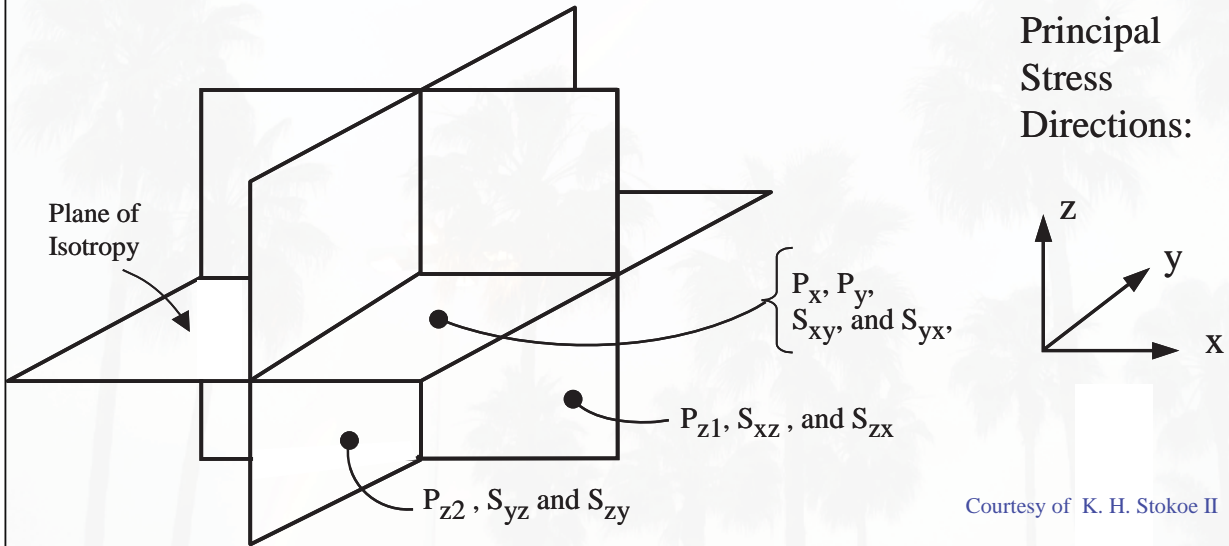
Shear wave velocity versus degree of saturation (granite powder, $d_{50}=89 \mu\text{m}$, applied $\sigma_v=1.5 \text{ kPa}$; Cho and Santamarina, 2000)



Typical Variation in Compression Wave Velocity with Degree of Saturation Changing from 99.4 to 100 % for Sand (after Allen et al., 1980)

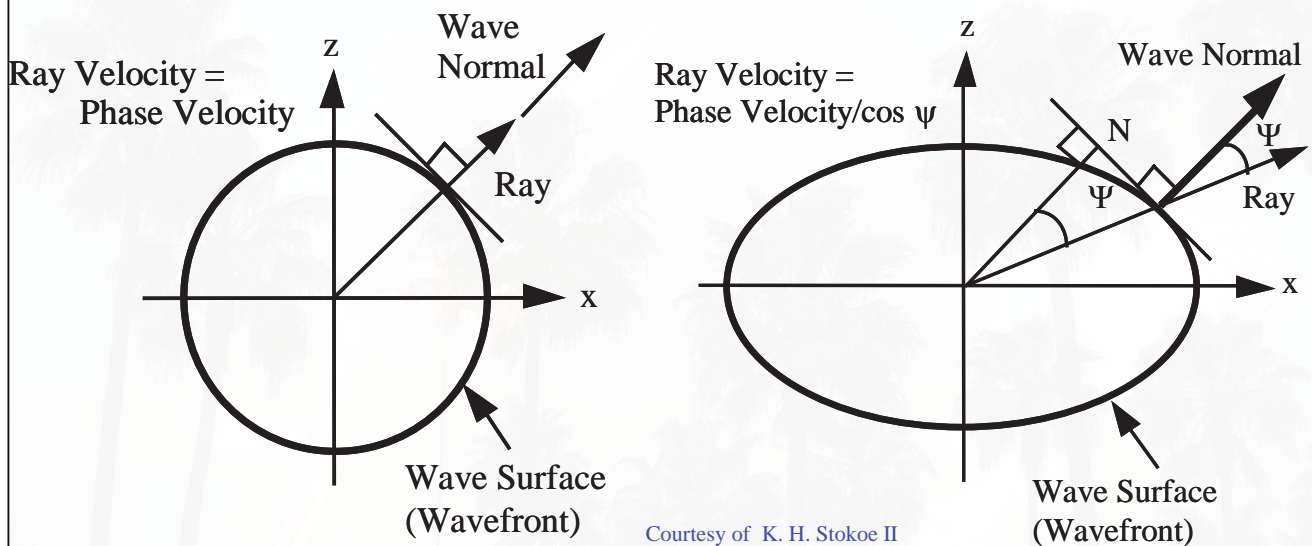


Principal Planes and Associated Polarized Body Waves in a Cross-Anisotropic Model with the Plane of Isotropy Oriented Horizontally



Short course notes: A. Elgamal, Chicago, Illinois, April 29 - 30, 2013

Direction of Ray and Wave Normals on Wavefronts Generated by a Point Source in Isotropic and Anisotropic Infinite Spaces



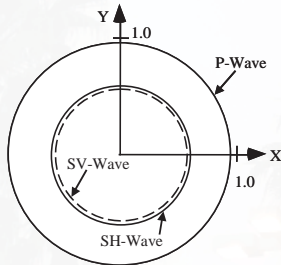
Isotropic Infinite Space

Anisotropic Infinite Space

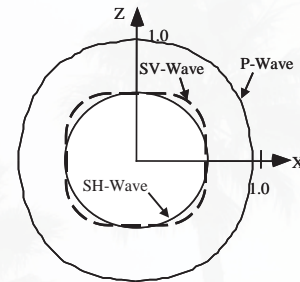
Short course notes: A. Elgamal, Chicago, Illinois, April 29 - 30, 2013

Theoretical Wave Velocity Surfaces in the Horizontal and Vertical Planes for a Cross-Anisotropic Material Under Normally Consolidated (a) and Mildly Overconsolidated (b) States (from Stokoe et al., 1994a)

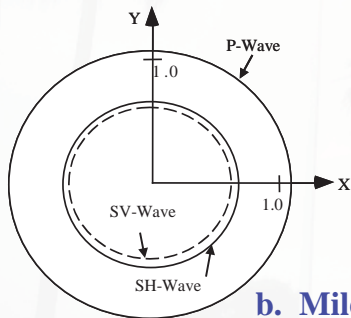
Horizontal Plane



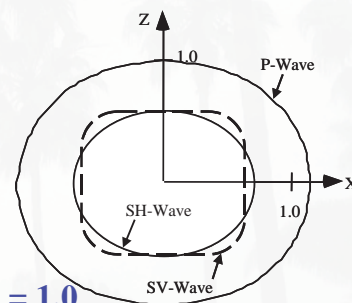
Vertical Plane



a. Normally Consolidated, $K_0 = 0.5$



Courtesy of K. H. Stokoe II



b. Mildly Overconsolidated, $K_0 = 1.0$

Short course notes: A. Elgamal, Chicago, Illinois, April 29 - 30, 2013

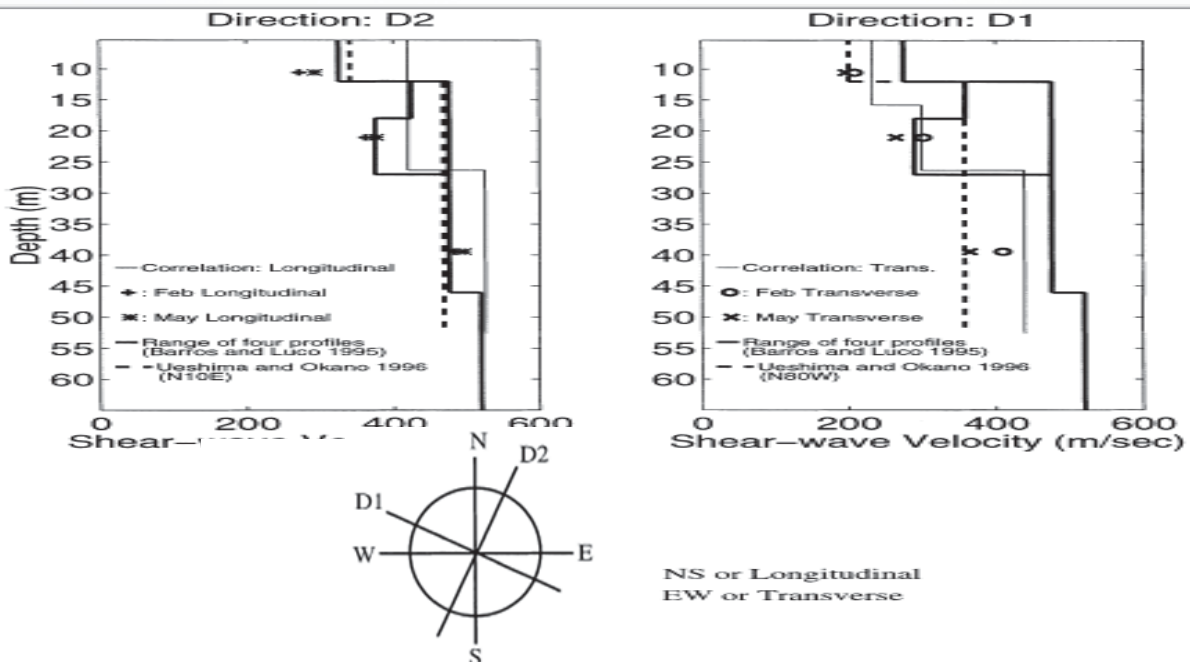
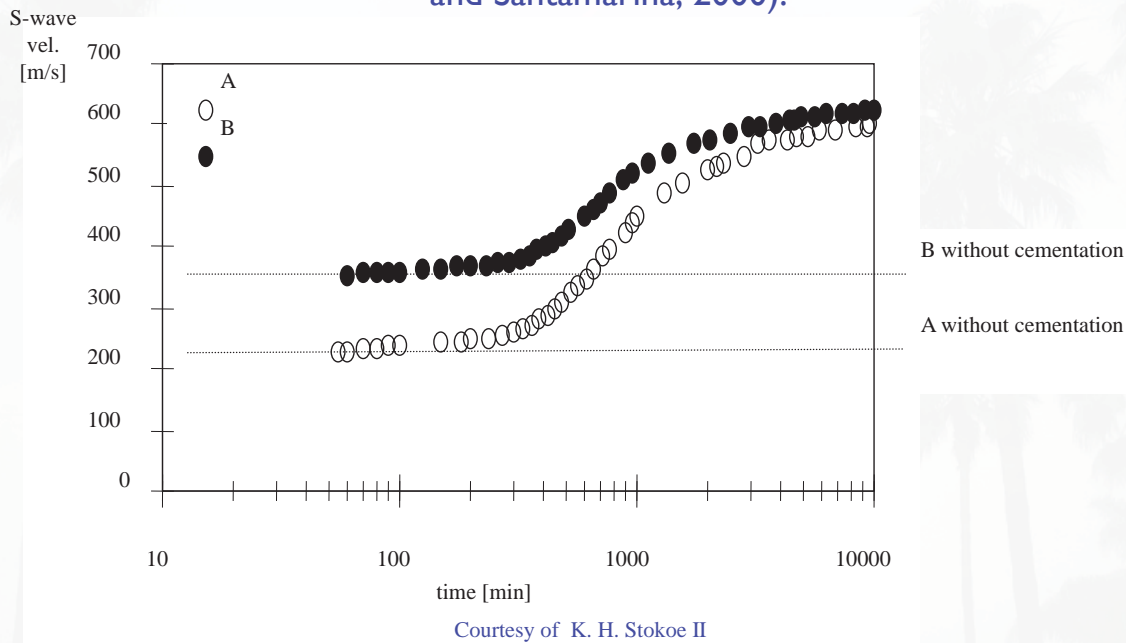


Fig. 26. Comparison of shear wave profiles identified from: (i) forced vibration foundation impedance functions [after Barros and Luco (1995)]; and (ii) earthquake downhole ground response.

Engineering Geology 50 (1998) 9–29: Hualien seismic downhole data analysis, V.R. Gunturi, A.-W.M. Elgamal, and H.T. Tang

The effect of cementation on shear wave velocity. Sand specimens with 2% Portland cement by weight. In specimen A, the fresh mixture is isotropically confined to 70 kPa and allowed to harden. The level of confinement for specimen B is 415 kPa (Fernandez and Santamarina, 2000).



Short course notes: A. Elgamal, Chicago, Illinois, April 29 - 30, 2013

27

Geophysical Exploration Methods

Short course notes: A. Elgamal, Chicago, Illinois, April 29 - 30, 2013

28

General Applicability of Selected Noninvasive Geophysical Methods to Typical Sites Assessments and Monitoring Objectives (from NRC, 2000)

Example Objectives	Seismic Refraction	Seismic Reflection	Ground-Penetrating Radar	Electrical Resistivity	Electromagnetics	Induced Polarization	Microgravity	Airborne Sensing	Magnetics
Geologic mapping	①	①	①	①	①	②	②	②	②
Hydrogeology characteristics	①	②	①	①	①	③	③	③	na
Water table depth	①	②	③	①	①	③	na	②	na
Top of bedrock	①	①	②	①	①	②	②	②	na
Cavity detection	②	②	①	①	①	③	①	③	③
Disposal trench mapping	③	②	①	①	①	na	②	②	②
Nature of trench fill	③	na	①	①	①	?	①	na	①
Inorganic contaminant plume	na	na	①	①	①	①	na	②	na
Organic contaminant plume	na	na	②	?	?	?	na	②	na
Disposal container (metal drum)	na	na	①	②	①	③	③	na	①
Underground storage tanks	③	③	①	②	①	③	②	na	①
UXO detection	na	na	①	①	①	na	na	③	①

KEY: ① = primary applicability; ② = secondary supporting applicability; ③ = limited applicability; na = no general applicability or not widely used; and ? = area of active research and rapidly evolving technology or questionable application.

Courtesy of K. H. Stokoe II

Short course notes: A. Elgamal, Chicago, Illinois, April 29 - 30, 2013

29

Wave phenomena: complexity and richness

Example Objectives	Seismic Refraction	Seismic Reflection	Ground-Penetrating Radar	Electrical Resistivity	Electromagnetics	Induced Polarization	Microgravity	Airborne Sensing	Magnetics
Geologic mapping	①	①	①	①	①	②	②	②	②
Hydrogeology characteristics	①	②	①	①	①	③	③	③	na
Water table depth	①	②	②	①	①	③	na	②	na
Top of bedrock	①	①	②	①	①	②	②	②	na
Cavity detection	②	②	①	①	①	③	①	③	③
Disposal trench mapping	③	②	①	①	①	na	②	②	②
Nature of trench fill	③	na	①	①	①	?	①	na	①
Inorganic contaminant plume	na	na	①	①	①	①	na	②	na
Organic contaminant plume	na	na	②	?	?	?	na	②	na
Disposal container (metal drum)	na	na	①	②	①	③	③	na	①
Underground storage tanks	③	③	①	②	①	③	②	na	①
UXO detection	na	na	①	①	①	na	na	③	①

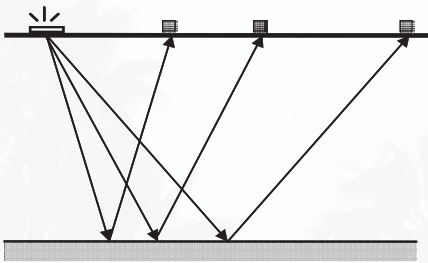
KEY: ① = primary applicability; ② = secondary supporting applicability; ③ = limited applicability; na = no general applicability or not widely used; and ? = area of active research and rapidly evolving technology or questionable application.

Courtesy of K. H. Stokoe II

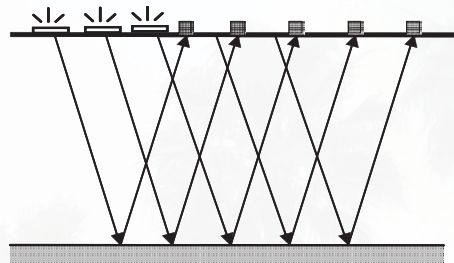
Short course notes: A. Elgamal, Chicago, Illinois, April 29 - 30, 2013

30

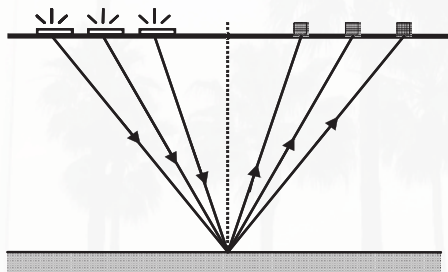
Field Arrangements Used in Surface Reflection Testing. (a) Normal moveout. (b) Common offset. (c) Common depth point



a. Normal moveout (NMO)



b. Common offset

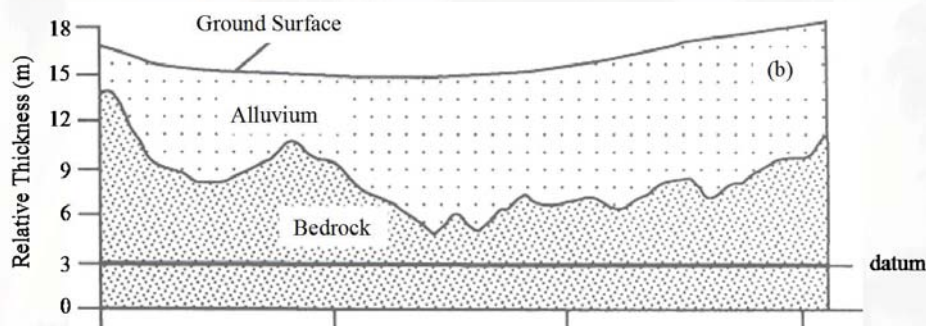
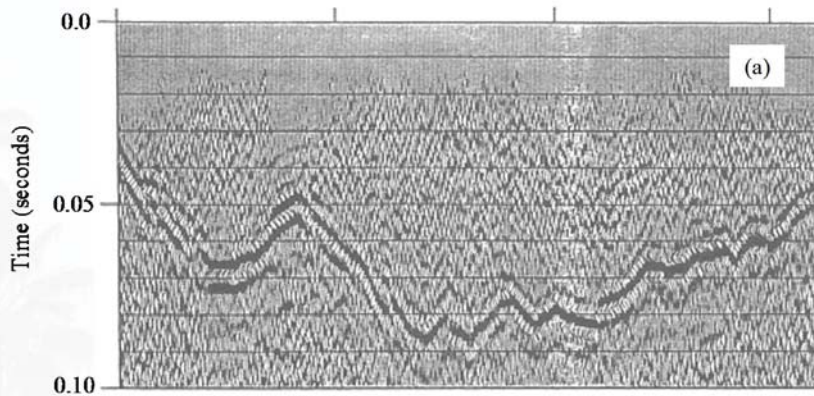


c. Common depth point

Courtesy of K. H. Stokoe II

Short course notes: A. Elgamal, Chicago, Illinois, April 29 - 30, 2013

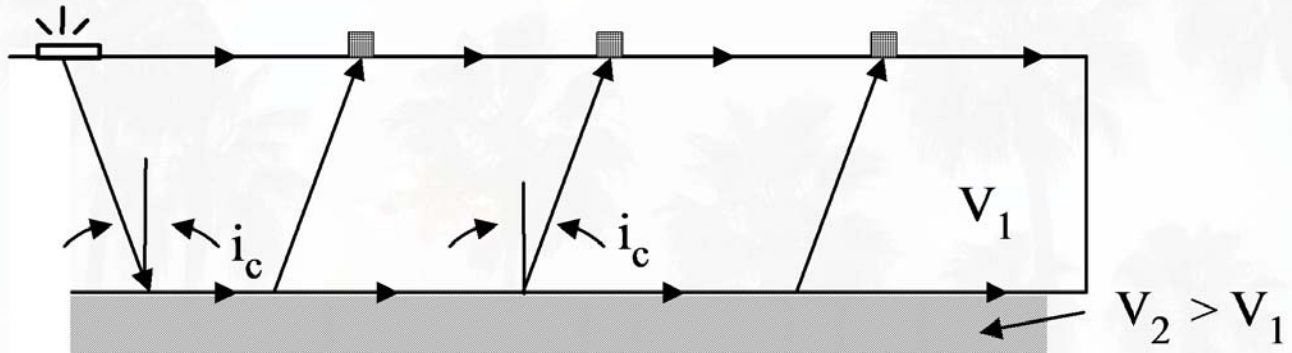
Seismic Reflection Cross Section (a) and Interpreted Geotechnical Cross Section (b) Used to Locate the Alluvium-Bedrock Contact (from NRC, 2000)



Courtesy of K. H. Stokoe II

Short course notes: A. Elgamal, Chicago, Illinois, April 29 - 30, 2013

Field Arrangement Used in Surface Refraction Testing



Courtesy of K. H. Stokoe II

Short course notes: A. Elgamal, Chicago, Illinois, April 29 - 30, 2013

33

Advantages and Disadvantage of Seismic Refraction and Seismic Reflection Methods (from NRC, 2000)

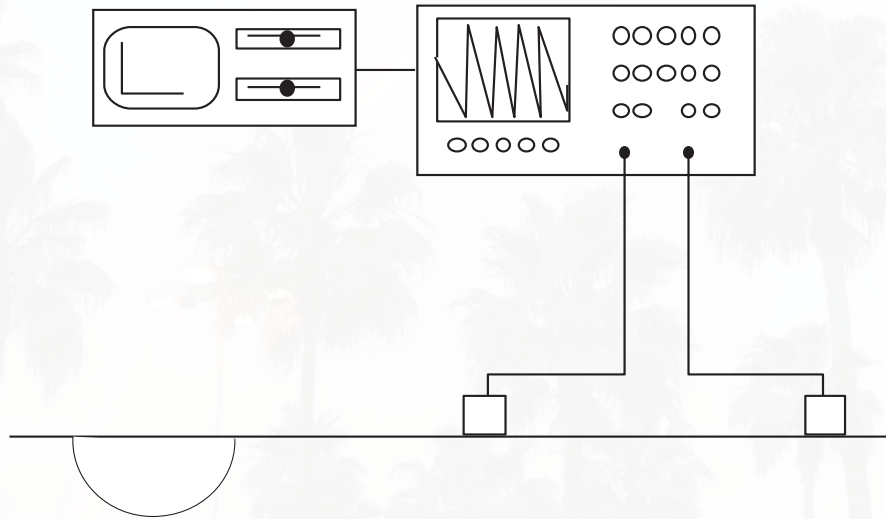
Refraction Method		Reflection Method	
Advantage	Disadvantage	Advantage	Disadvantage
Observation generally use fewer source and receiver locations: relatively cheap to acquire	Observation require relatively large source-receiver offset	Observations are collected at small source-receiver offsets	Many source and receiver locations must be used to produce meaningful images; expensive to acquire
Little processing is needed except for trace scaling or filtering to help pick arrival times of the initial ground motion	Only works if the speed at which motions propagate increases with depth	Method can work no matter how the propagation speed varies with depth	Processing can be expensive as it is very computer intensive, needed sophisticated hardware and high-level of expertise
Modeling and interpretation fairly straightforward	Observation generally interpreted in layers that can be dip and topography; produces simplified models	Reflection observations can be more readily interpreted in terms of complex geology; subsurface directly imaged from observations	Interpretations require more sophistication and knowledge of the reflection process

Courtesy of K. H. Stokoe II

Short course notes: A. Elgamal, Chicago, Illinois, April 29 - 30, 2013

34

Field Arrangement Used in SASW Testing with a Common- Receivers Midpoint Geometry

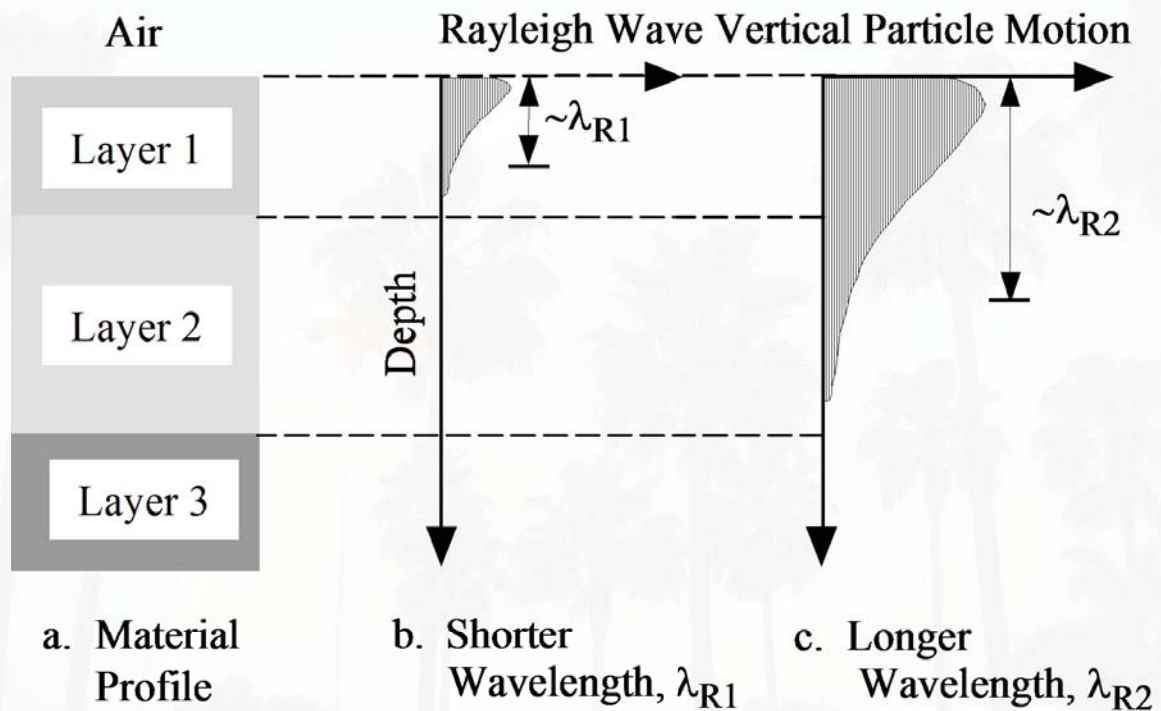


Courtesy of K. H. Stokoe II

Short course notes: A. Elgamal, Chicago, Illinois, April 29 - 30, 2013

35

Schematic Representation of Rayleigh Waves of Different Wavelengths Sampling Material to Different Depths

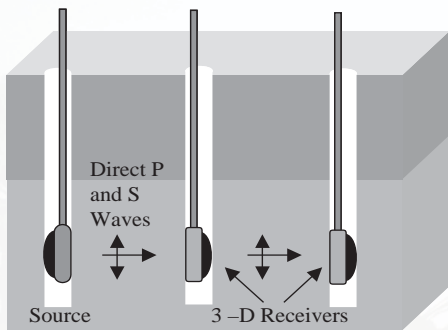


Courtesy of K. H. Stokoe II

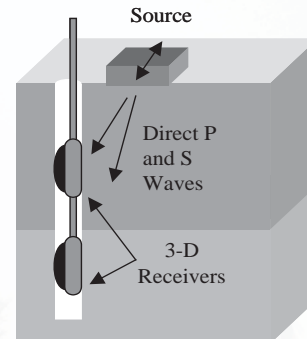
Short course notes: A. Elgamal, Chicago, Illinois, April 29 - 30, 2013

36

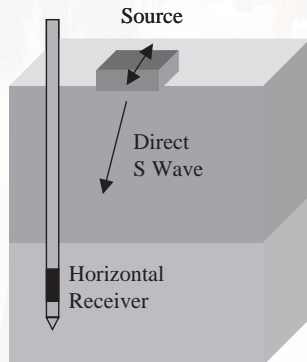
Field Arrangements Used to Perform Intrusive Seismic Tests



a. Crosshole Testing

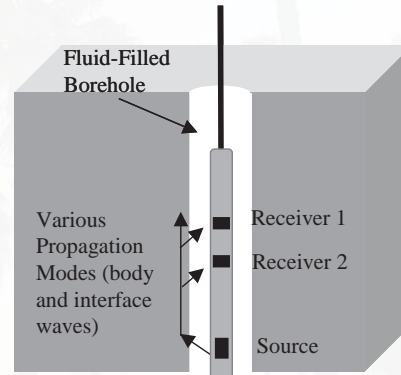


b. Downhole Testing



c. Seismic Cone Penetrometer

Courtesy of K. H. Stokoe II

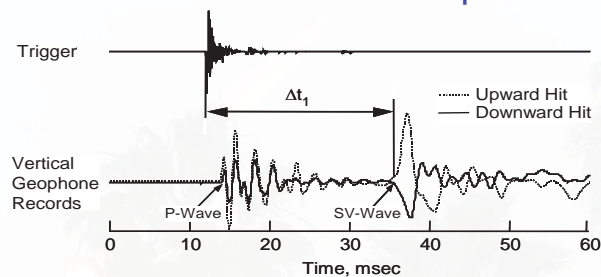


d. Suspension Logging

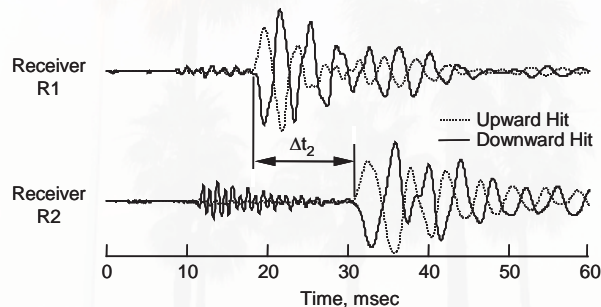
Short course notes: A. Elgamal, Chicago, Illinois, April 29 - 30, 2013

37

Example Shear Wave Records Measured in Traditional Crosshole Testing Using Upward and Downward Impacts to Help Identify the Initial SV-Wave Arrival (from Fuhriman, 1993). Note: the P-wave signal may also reverse, depending on the directivity of the source and the relative position of the receiver.



a. Record Illustrating a Direct Travel Time Measurement of an SV Wave



b. Record Illustrating an Interval Travel Time Measurement of an SV Wave

Courtesy of K. H. Stokoe II

Short course notes: A. Elgamal, Chicago, Illinois, April 29 - 30, 2013

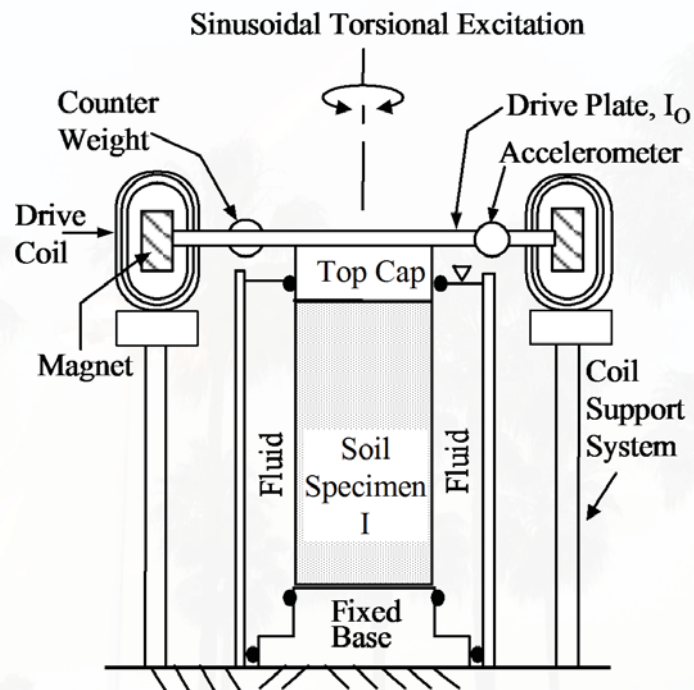
38

Laboratory Techniques

Short course notes: A. Elgamal, Chicago, Illinois, April 29 - 30, 2013

39

Simplified Diagram of a Fixed-Free, Torsional Resonant Column (Confining chamber not shown)

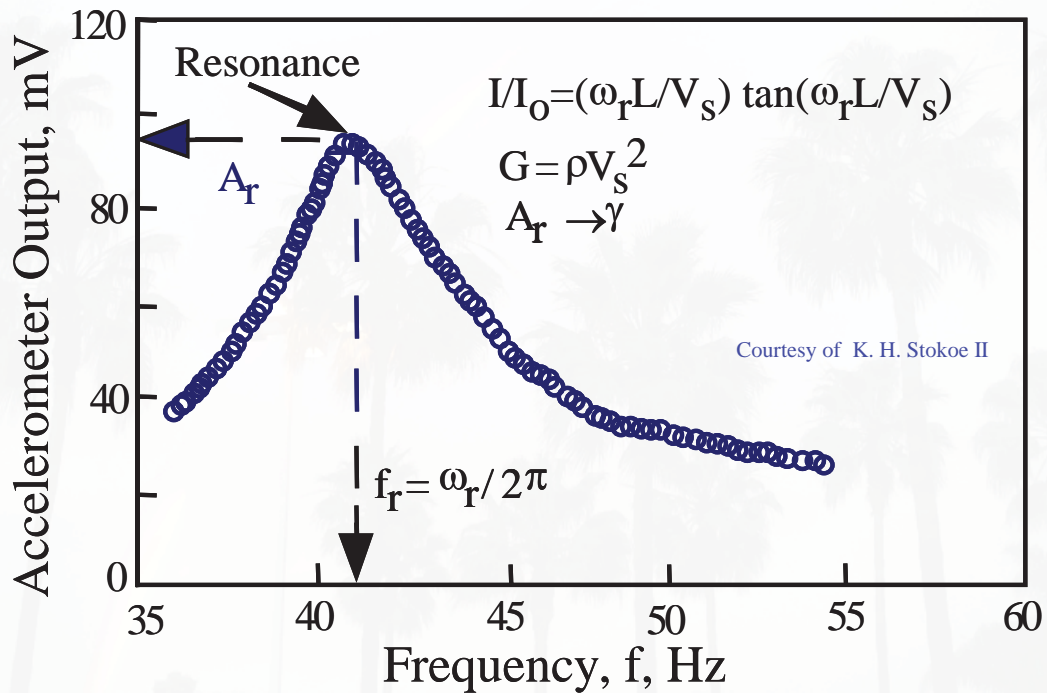


Courtesy of K. H. Stokoe II

Short course notes: A. Elgamal, Chicago, Illinois, April 29 - 30, 2013

40

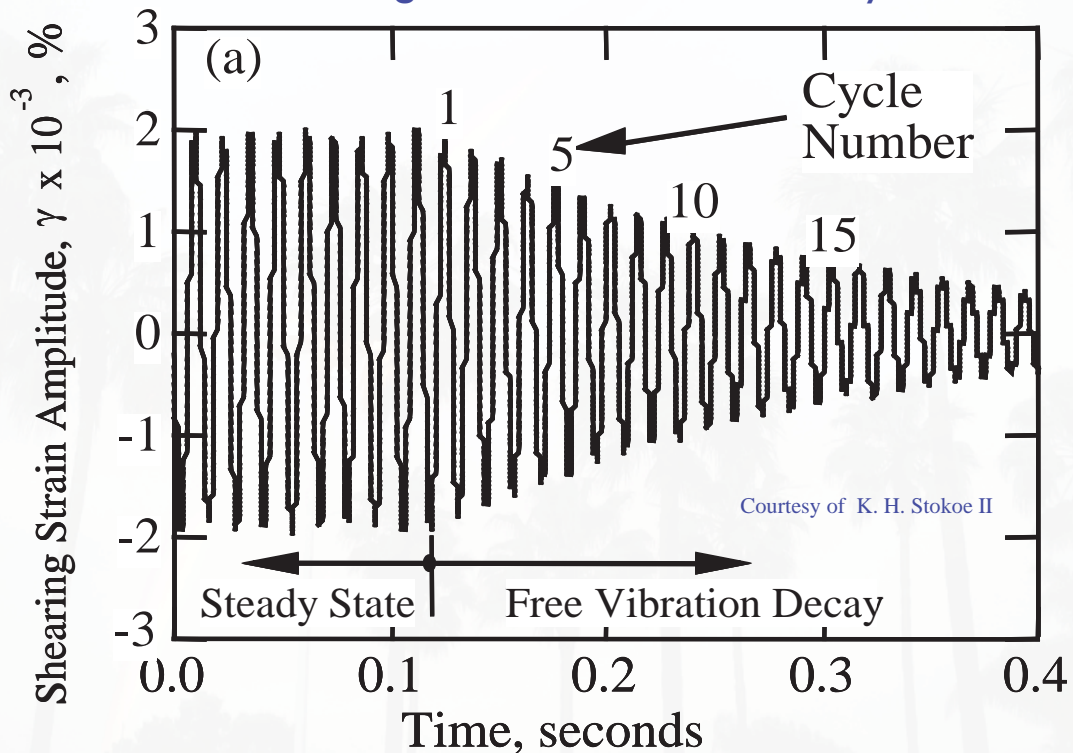
Dynamic Response Curve Measured with a Fixed-Free Torsional Resonant Column



Short course notes: A. Elgamal, Chicago, Illinois, April 29 - 30, 2013

41

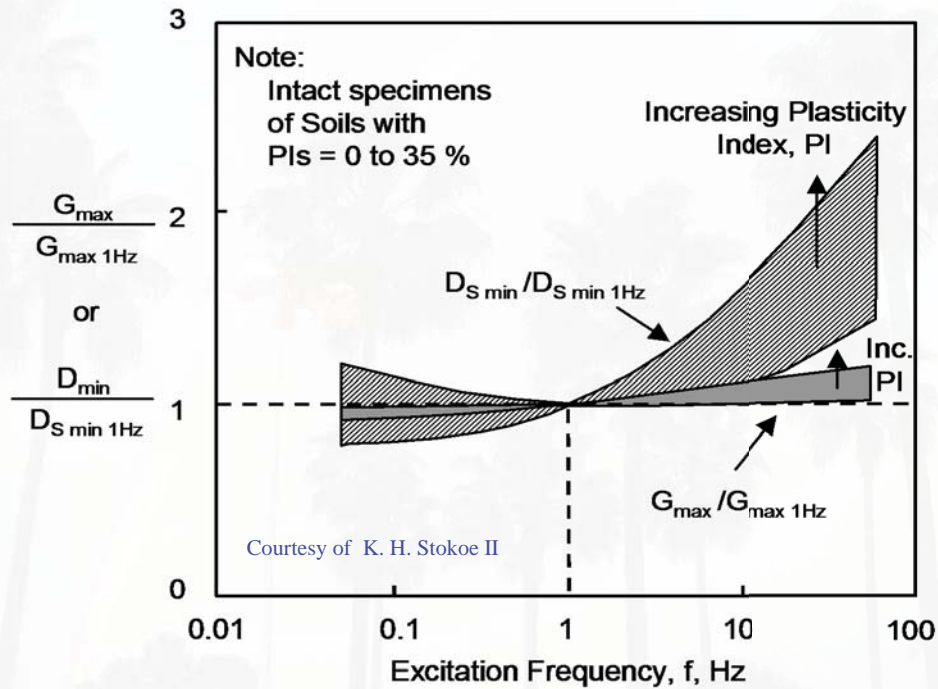
Material Damping Measurement with a Fixed-Free Torsional Resonant Column Test Using the Free-Vibration Decay Curve



Short course notes: A. Elgamal, Chicago, Illinois, April 29 - 30, 2013

42

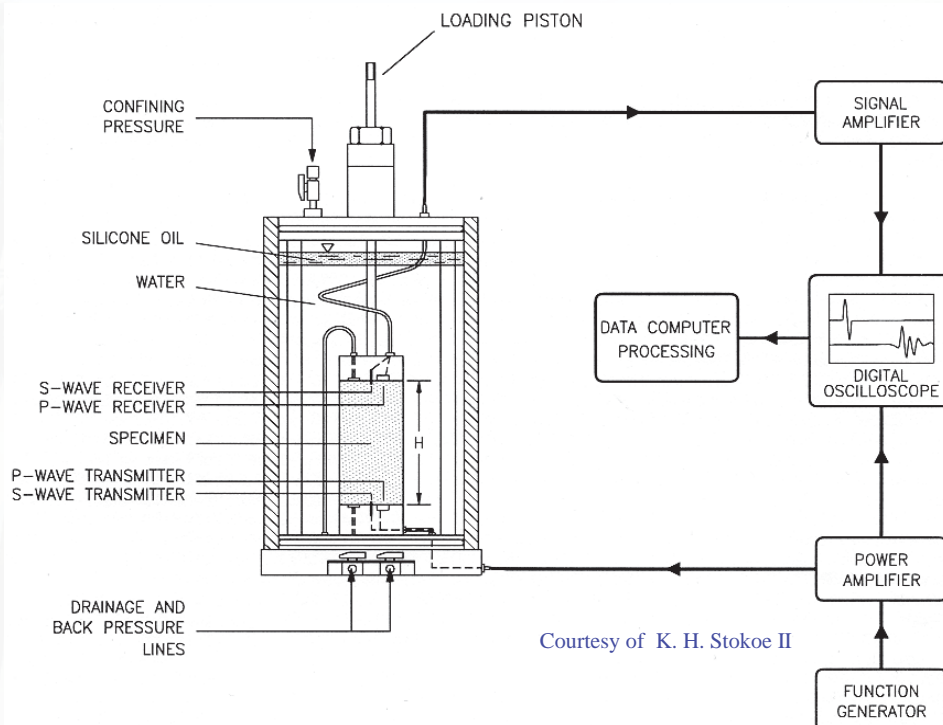
General Effect of Excitation Frequency on Small-Strain Shear Modulus, G_{max} , and Small-Strain Material Damping Ratio in Shear, $D_{S min}$ (after Stokoe, et al., 1999)



Short course notes: A. Elgamal, Chicago, Illinois, April 29 - 30, 2013

43

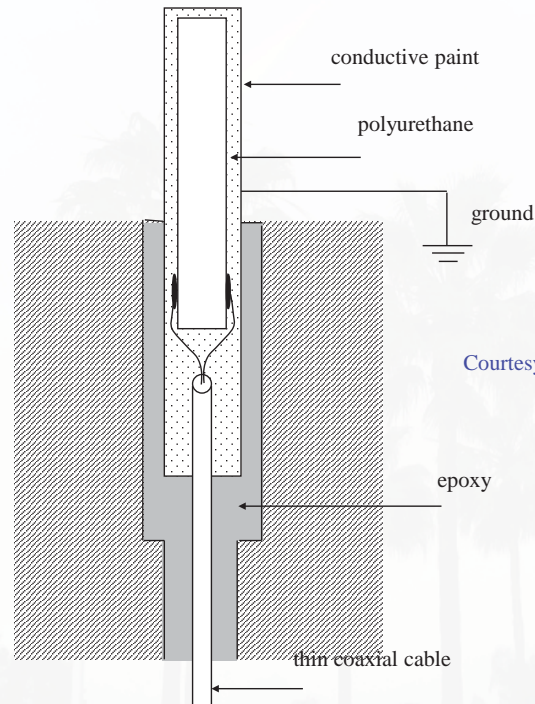
Schematic of Piezoelectric Transducers and Associated Electronics Used During Triaxial Testing (from Brignoli, et al., 1996)



Short course notes: A. Elgamal, Chicago, Illinois, April 29 - 30, 2013

44

Mounting bender elements. The element is coated with polyurethane to prevent moisture and with conductive paint and grounded to avoid cross-talk and antenna-effects (see details in Dyvik and Madshus, 1985; Santamarina et al., 2000)

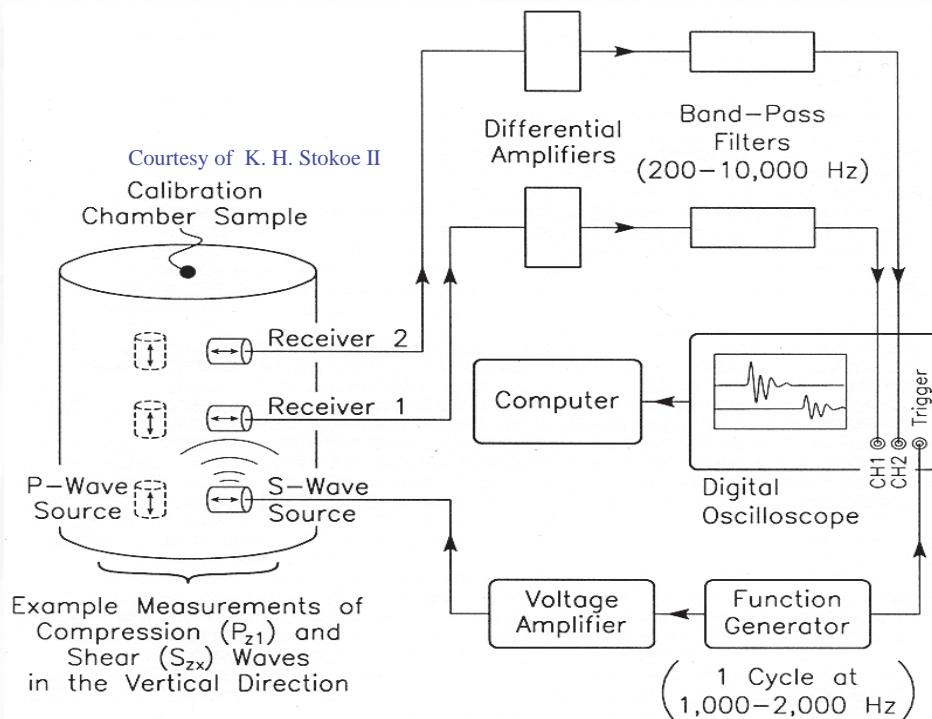


Courtesy of K. H. Stokoe II

Short course notes: A. Elgamal, Chicago, Illinois, April 29 - 30, 2013

45

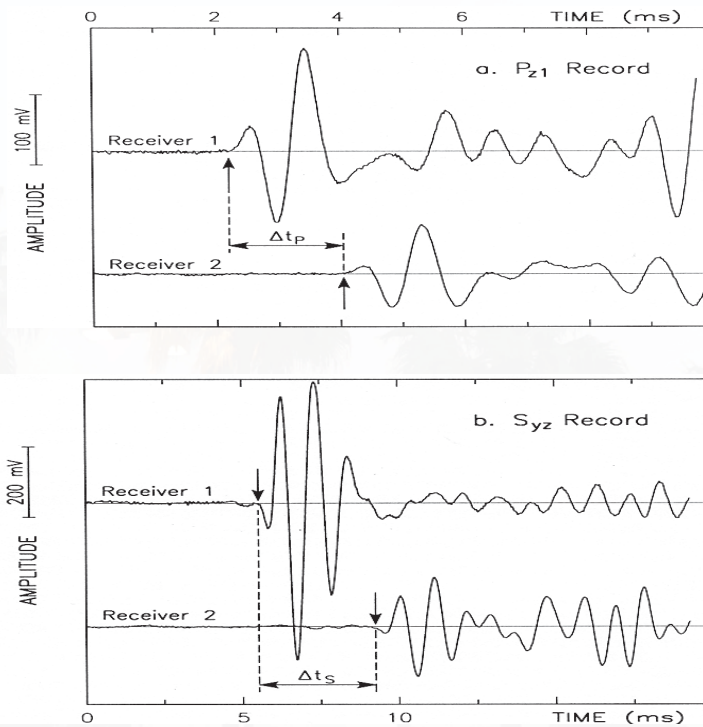
Schematic Diagram of Embedded Geophones and Electronics Used in Seismic Measurements in Calibration Chamber (from Brignoli et al., 1997)



Short course notes: A. Elgamal, Chicago, Illinois, April 29 - 30, 2013

46

Example Compression Wave (a) and Shear Wave (b) Records Measured in a Calibration Chamber Test (from Brignoli et al., 1997)



Courtesy of K. H. Stokoe II

Short course notes: A. Elgamal, Chicago, Illinois, April 29 - 30, 2013

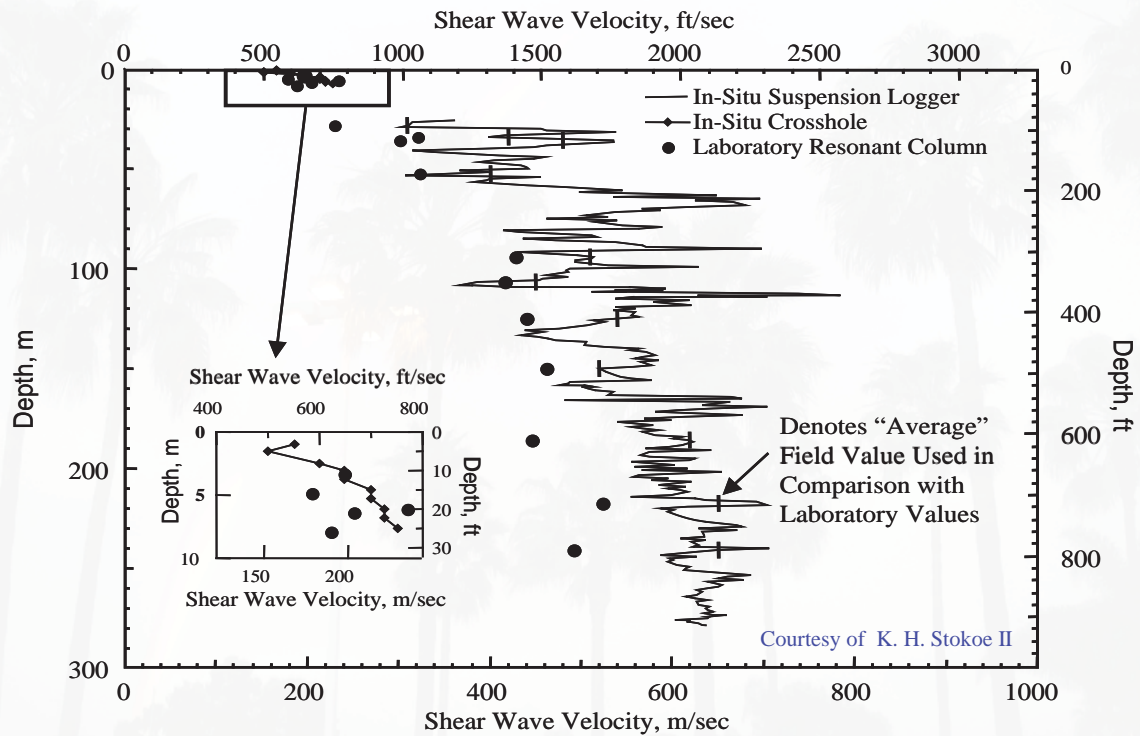
47

Field-Laboratory Comparison

Short course notes: A. Elgamal, Chicago, Illinois, April 29 - 30, 2013

48

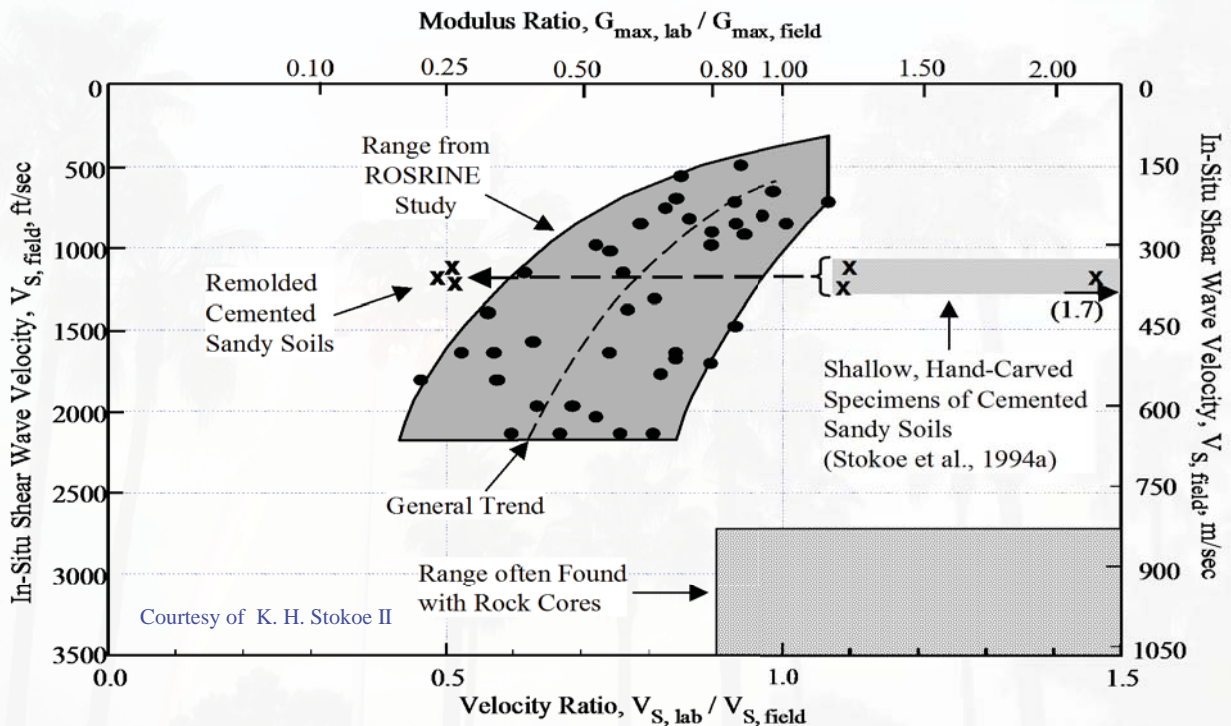
Example Profile of Field and Laboratory Shear Wave Velocities Evaluated at a Strong-Motion Earthquake Site on the ROSRINE Study



Short course notes: A. Elgamal, Chicago, Illinois, April 29 - 30, 2013

49

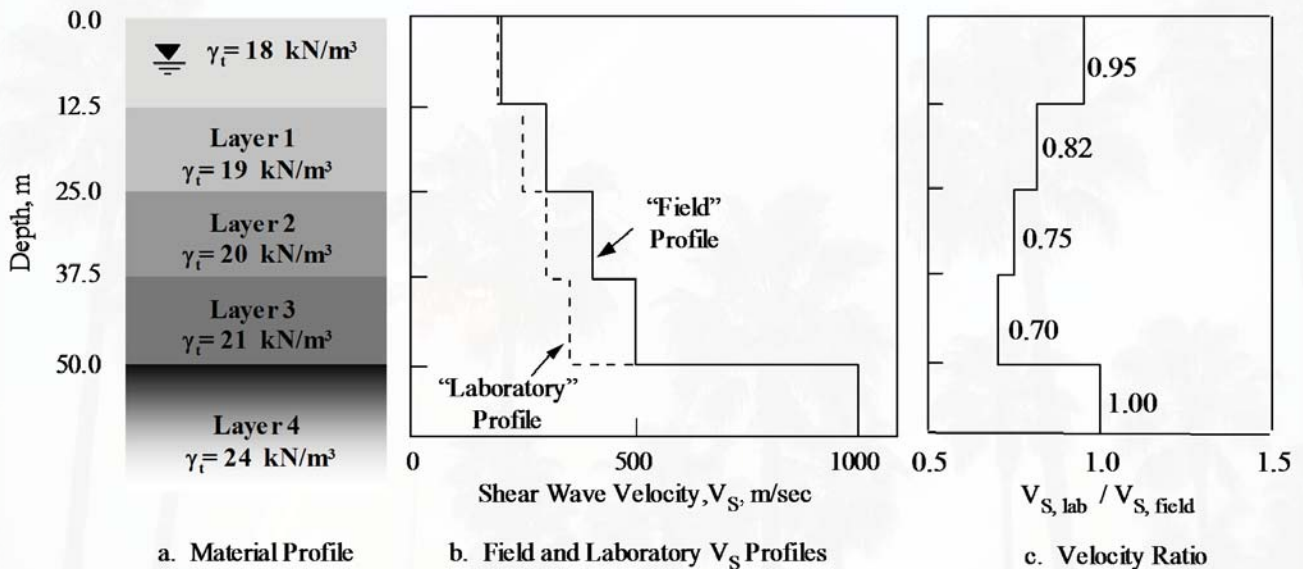
Variation in the Ratio of Laboratory-to-Field Stiffness ($V_{S,lab} / V_{S,field}$) with respect to the In Situ Value of V_S



Short course notes: A. Elgamal, Chicago, Illinois, April 29 - 30, 2013

50

Idealized Geotechnical Site Used to Illustrate the Importance of In Situ Seismic Testing

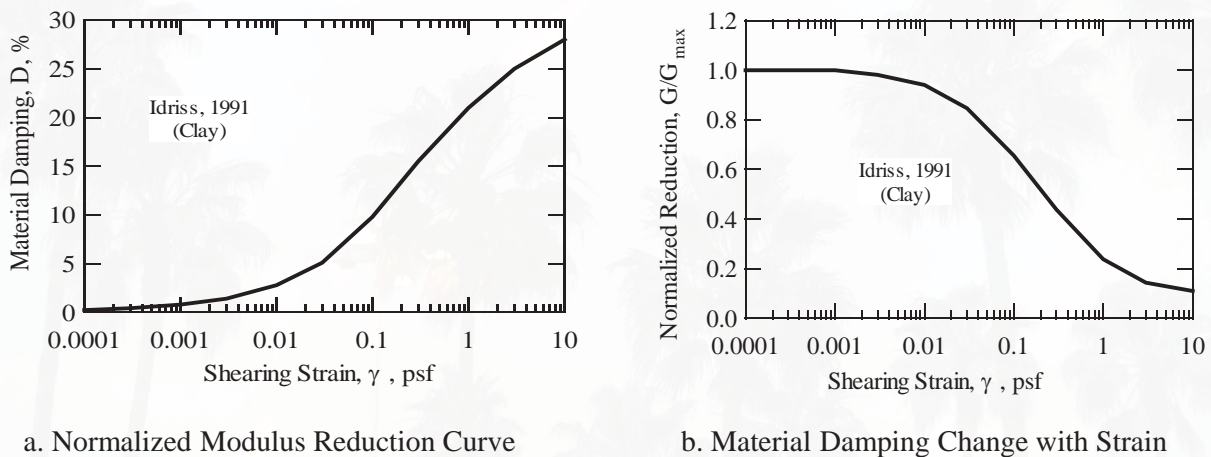


Courtesy of K. H. Stokoe II

Short course notes: A. Elgamal, Chicago, Illinois, April 29 - 30, 2013

51

Nonlinear Soil Characteristics Used to Represent Each Layer

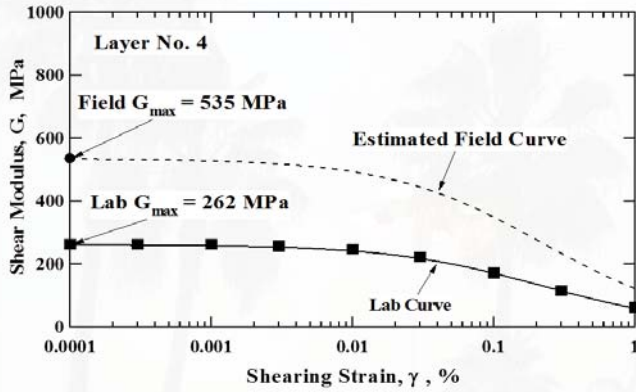


Courtesy of K. H. Stokoe II

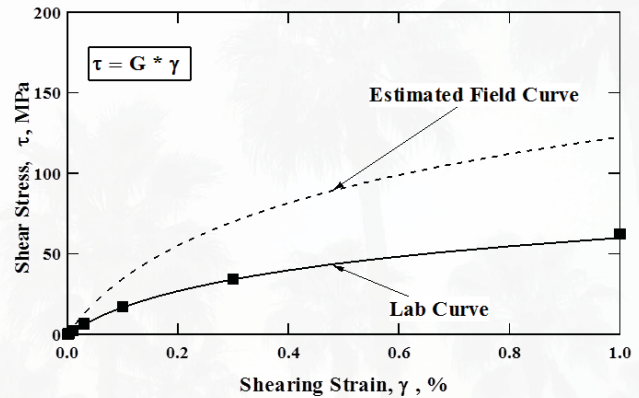
Short course notes: A. Elgamal, Chicago, Illinois, April 29 - 30, 2013

52

Comparison of the Estimated Field and Laboratory Nonlinear Stiffness Characteristics



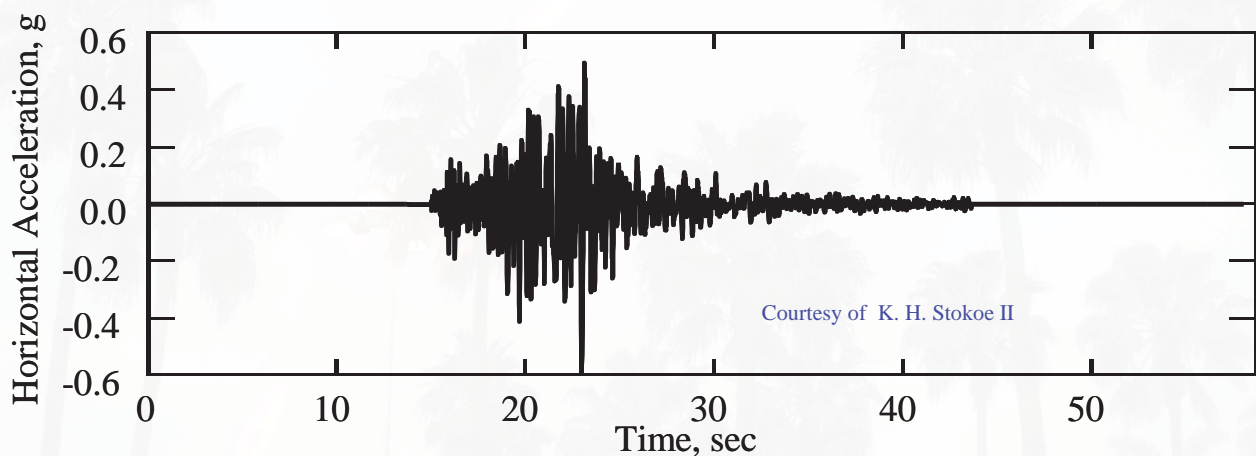
a. Estimated Field and Laboratory Modulus Reduction Curves



b. Estimated Field and Laboratory Stress-Strain Curves

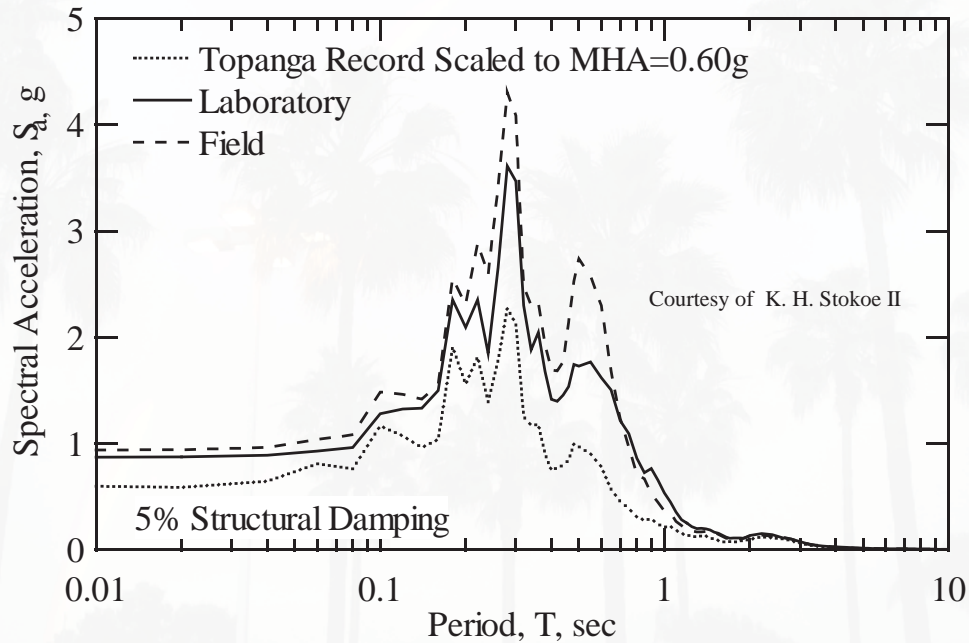
Courtesy of K. H. Stokoe II

Rock Outcrop Motion from the Topanga 1994 Strong-Motion Record Scaled to 0.6 g



Courtesy of K. H. Stokoe II

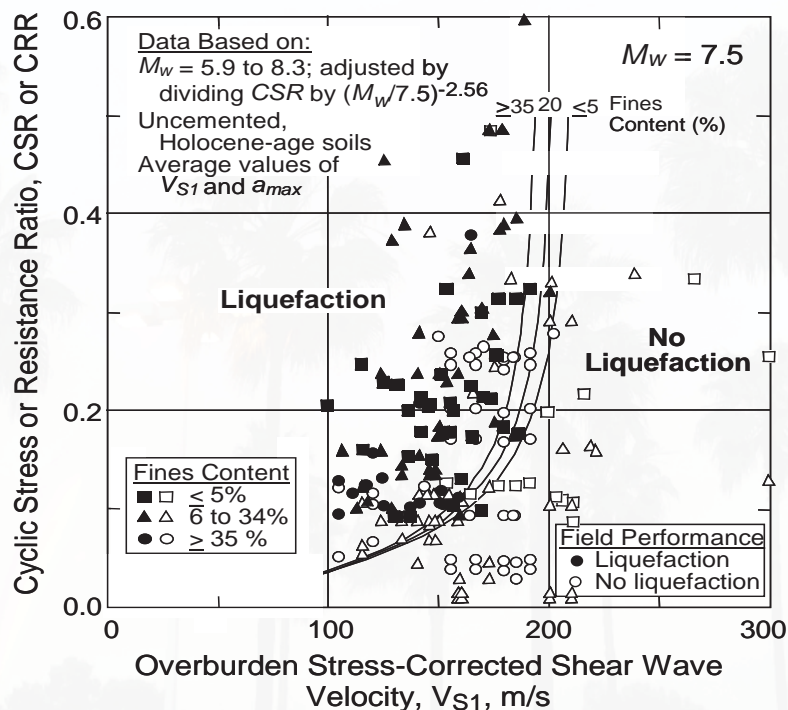
Comparison of Surface Spectral Accelerations Predicted for the Clay Deposit in Figure 30 Using Laboratory and Field V_s Profiles



Short course notes: A. Elgamal, Chicago, Illinois, April 29 - 30, 2013

55

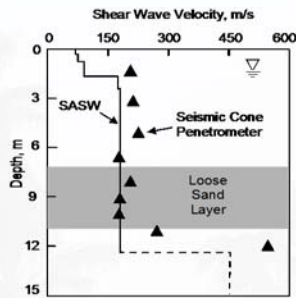
Curves Proposed by Andrus et al. (1999) for Delineating Liquefiable and Nonliquefiable Granular Soils Based on Field V_s Measurements



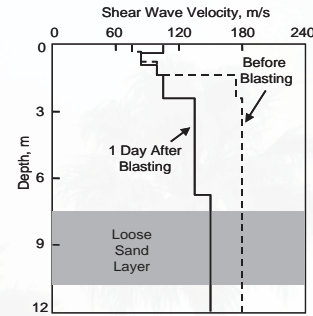
Short course notes: A. Elgamal, Chicago, Illinois, April 29 - 30, 2013

56

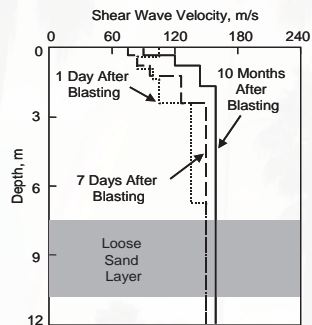
Evaluation of the Effectiveness of Blast Densification of a Loose Sand Layer with Field V_s Measurements



a. V_s Profile before Blasting

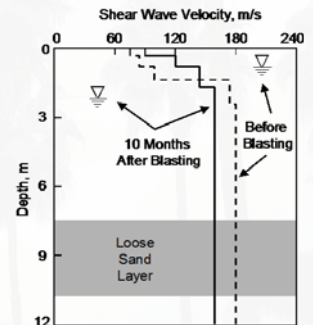


b. Comparison of V_s Profiles before and after Blasting



c. Change in V_s Profiles with Time after Blasting

Courtesy of K. H. Stokoe II

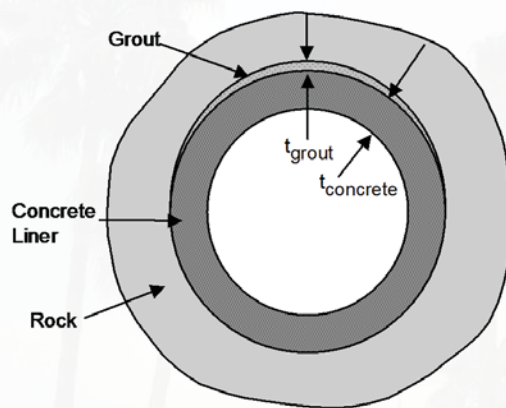


d. Comparison of V_s Profiles before and 10 Months after Blasting

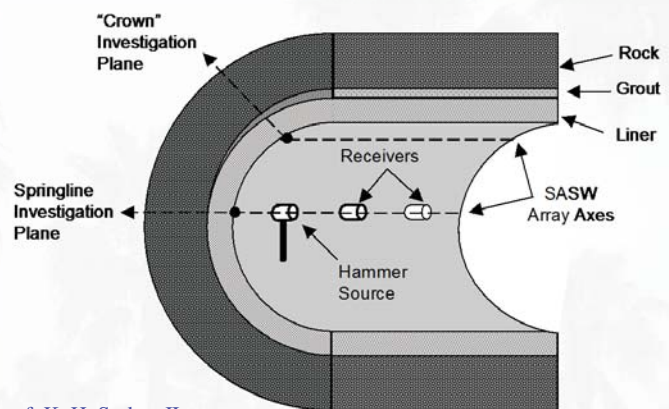
Short course notes: A. Elgamal, Chicago, Illinois, April 29 - 30, 2013

57

SASW Testing Performed Inside a Concrete-Lined Tunnel



a. Generalized Tunnel Cross Section



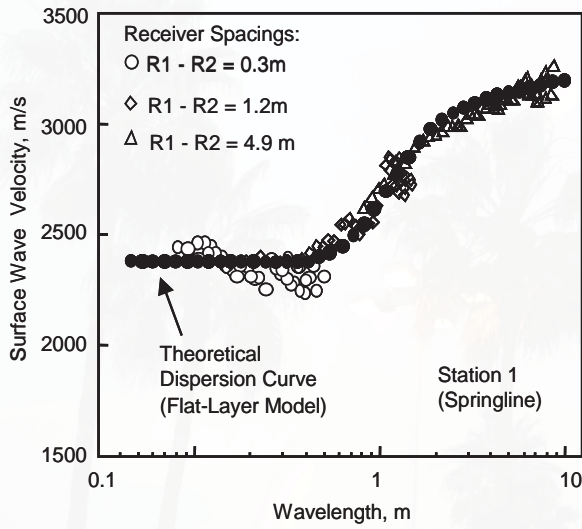
b. SASW Testing Arrangement and Planes of Investigation

Courtesy of K. H. Stokoe II

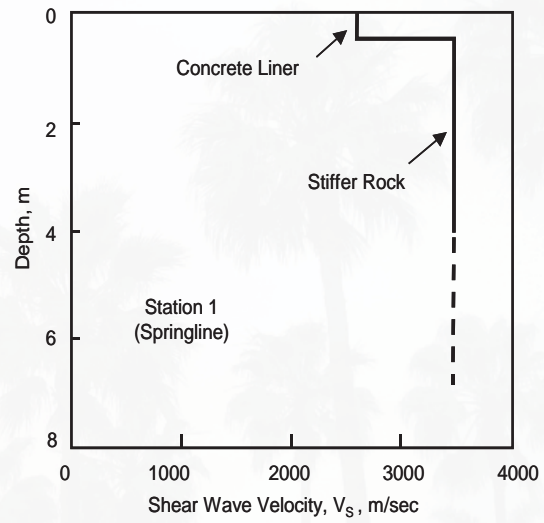
Short course notes: A. Elgamal, Chicago, Illinois, April 29 - 30, 2013

58

Example of the Inversion Process and Resulting V_S Profile from SASW Testing in the Tunnel



a. Matching the Experimental Dispersion Curve with a Theoretical Dispersion Curve



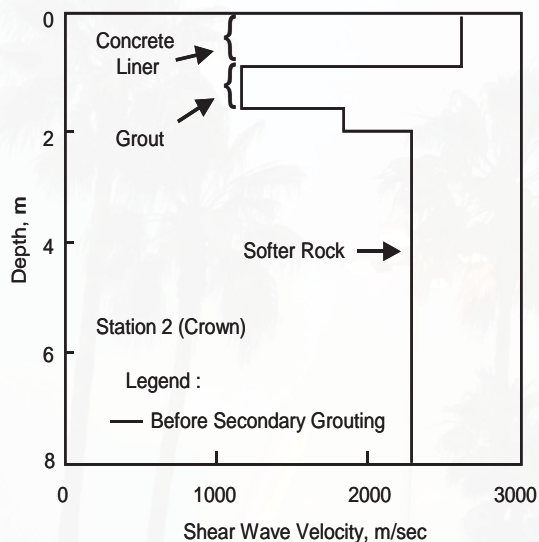
b. V_S Profile from the Inversion (Match) Shown in Figure 43a

Courtesy of K. H. Stokoe II

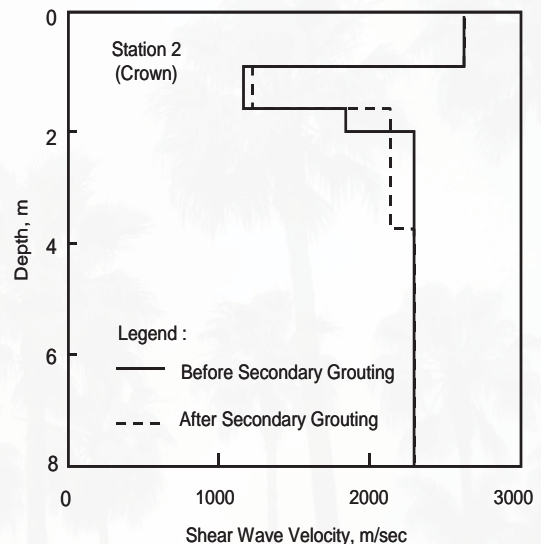
Short course notes: A. Elgamal, Chicago, Illinois, April 29 - 30, 2013

59

Examples of a V_S Profile Measured by SASW Testing near the Tunnel Crown and the Evaluation of the Effect of Secondary Grouting using “before and after” Profiles

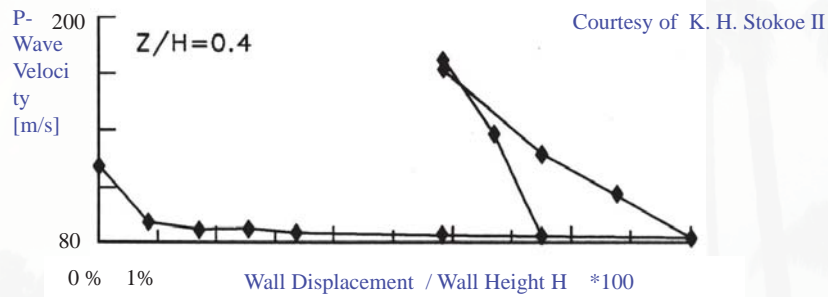
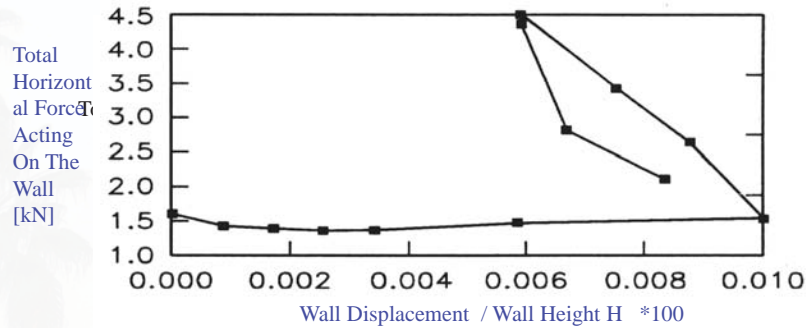


a. Interpreted V_S Profile from SASW Testing



b. Comparison of V_S Profiles before and after Secondary Grouting

Retaining Wall - Monitoring the evolution of internal stresses with P-wave velocities. The top frame shows the force acting against the wall (monitored with 4 load cells). The lower frame shows the evolution of the horizontal P-wave velocity measured in the backfill behind the wall, at depths $z=0.4 H$ from the top of the wall (Santamarina and Potts, 1994).



Site Investigation (SPT and CPT)

The Standard Penetration Test (SPT)



Courtesy of M. Fraser



Short course notes: A. Elgamal, Chicago, Illinois, April 29 - 30, 2013

Standard Penetration Test (SPT)

Courtesy of M. Fraser



- The test uses a split barrel sample tube which is driven into the ground at the bottom of a borehole by blows from a slide hammer with a weight of 140 lb falling through a distance of 30 in.
- The sample tube is driven 6 inches into the ground and then the number of blows needed for the tube to penetrate each 6 inches up to a depth of 18 inches is recorded.
- The sum of the number of blows required for the second and third 6 in. of penetration is termed the “standard penetration resistance,” the “N-value,” or the “blow count.”
- The blow count provides an indication of the density of the ground, and it is used in many empirical geotechnical engineering formulae.
- ASTM D1586 test method provides a disturbed soil sample for moisture content determination, for identification and classification purposes, and for laboratory tests appropriate for soil obtained from a sampler that will produce large shear strain disturbance in the sample.
- Sample quality is generally not suitable for advanced laboratory testing for engineering properties.

Short course notes: A. Elgamal, Chicago, Illinois, April 29 - 30, 2013

The Standard Penetration Test (SPT)



Courtesy of M. Fraser

Short course notes: A. Elgamal, Chicago, Illinois, April 29 - 30, 2013

The Standard Penetration Test (SPT)

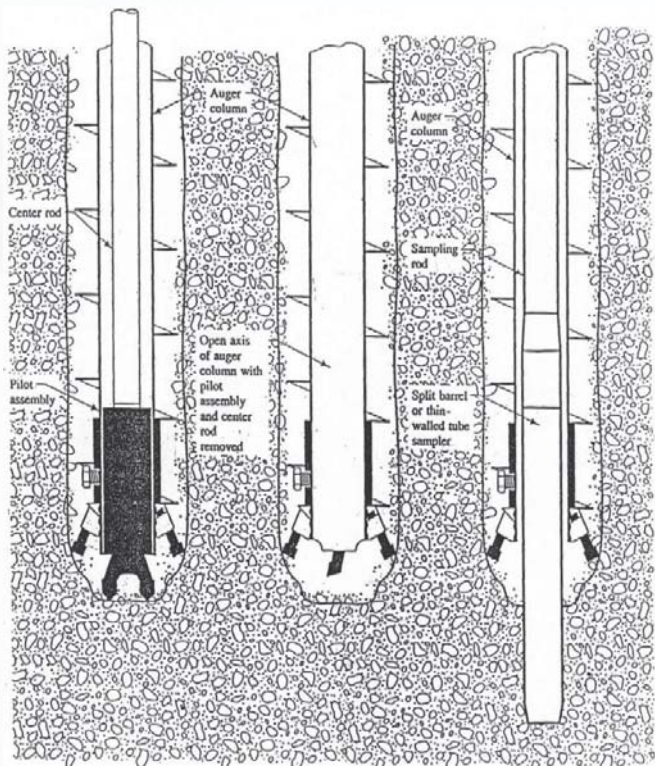


Illustration of the SPT process with pilot assembly and collection of a formation sample (after Riggs, 1963).



Courtesy of M. Fraser

Short course notes: A. Elgamal, Chicago, Illinois, April 29 - 30, 2013

The sum of the number of blows required for the second and third 6 in. of penetration is termed the “standard penetration resistance,” the “N-value,” or the “blow count.”

$(N_1)_{60}$ is the SPT blow count number normalized to an overburden pressure of 1 ton/ft² (96 kPa) and corrected to an energy ratio of 60%.

$$(N_1)_{60} = C_N N_{60} \text{ (see figure)}$$

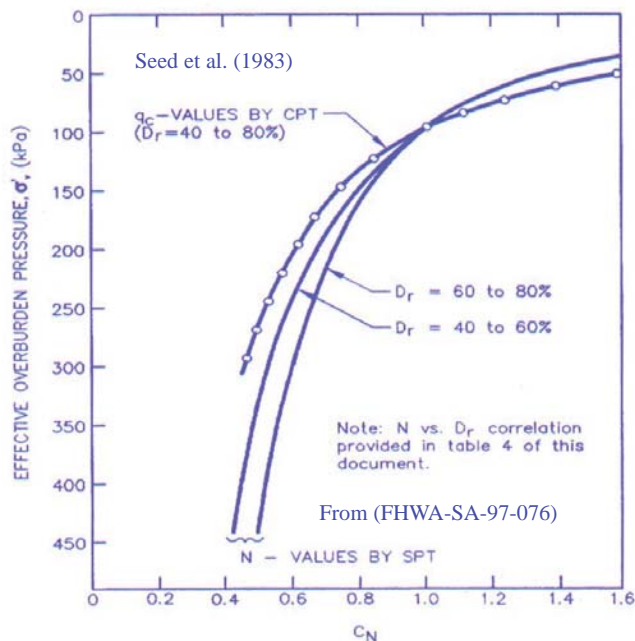
$$N_{60} = N C_{60} \text{ (see next page)}$$

Alternatively, just use:

$$C_N = (P_a / \sigma'_{vo})^{0.5} < \text{or} = 1.7$$

σ'_{vo} = Effective vertical stress

P_a = Atmospheric pressure
(e.g., 2116 psf)



Short course notes: A. Elgamal, Chicago, Illinois, April 29 - 30, 2013

Correction for	Correction Factor	Reference
Nonstandard Hammer Type (DH = doughnut hammer; ER = energy ratio)	$C_{HT} = 0.75$ for DH with rope and pulley $C_{HT} = 1.33$ for DH with trip/auto & ER=80	Seed et al. (1985)
Nonstandard Hammer Weight or Height of Fall (H = height of fall in mm; W = hammer weight in kg)	$C_{HW} = \frac{H \cdot W}{63.5 \cdot 762}$	calculated per Seed et al. (1985)
Nonstandard Sampler Setup (standard samples with room for liners, but used without liners)	$C_{SS} = 1.10$ for loose sand $C_{SS} = 1.20$ for dense sand	Seed et al. (1985)
Nonstandard Sampler Setup (standard samples with room for liners, and liners are used)	$C_{SS} = 0.90$ for loose sand $C_{SS} = 0.80$ for dense sand	Skempton (1986)
Short Rod Length	$C_{RL} = 0.75$ for rod length 0-3 m	Seed et al. (1983)
Nonstandard Borehole Diameter	$C_{BD} = 1.05$ for 150 mm borehole diameter $C_{BD} = 1.15$ for 200 mm borehole diameter	Skempton (1986)

Notes: N = Uncorrected SPT blow count.

$$C_{60} = C_{HT} \cdot C_{HW} \cdot C_{SS} \cdot C_{RL} \cdot C_{BD}$$

$$N_{60} = N \cdot C_{60}$$

C_N = Correction factor for overburden pressure.

$$(N_1)_{60} = C_N \cdot N_{60} = C_N \cdot C_{60} \cdot N$$

C_{60} from Richardson et al. (1995)

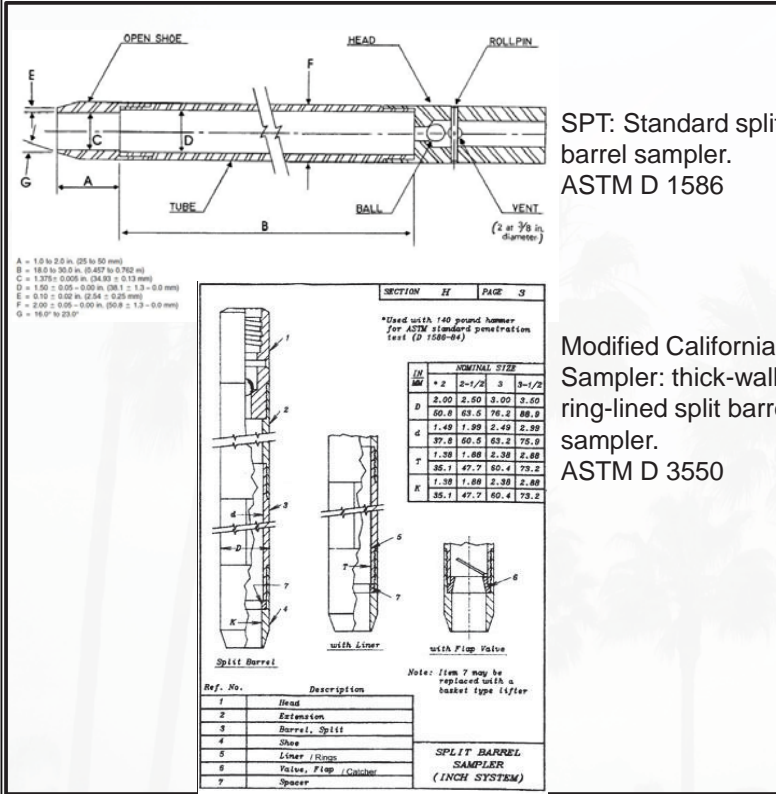
From (FHWA-SA-97-076)

Short course notes: A. Elgamal, Chicago, Illinois, April 29 - 30, 2013

Standard Penetration Test (SPT)

Not all penetration resistance (blow counts) are the same

Courtesy of M. Fraser



Bott et al. compared penetration resistance values taken from the California versus standard penetration test Samples.

SPT: ID-1.375" & OD-2.0"

MCS: ID-2.4/2.5" & OD-3.0"

Due to difference in diameter, the energy required to drive the MCS is much higher.

Conversion factor for MCS to SPT-equivalent blows:

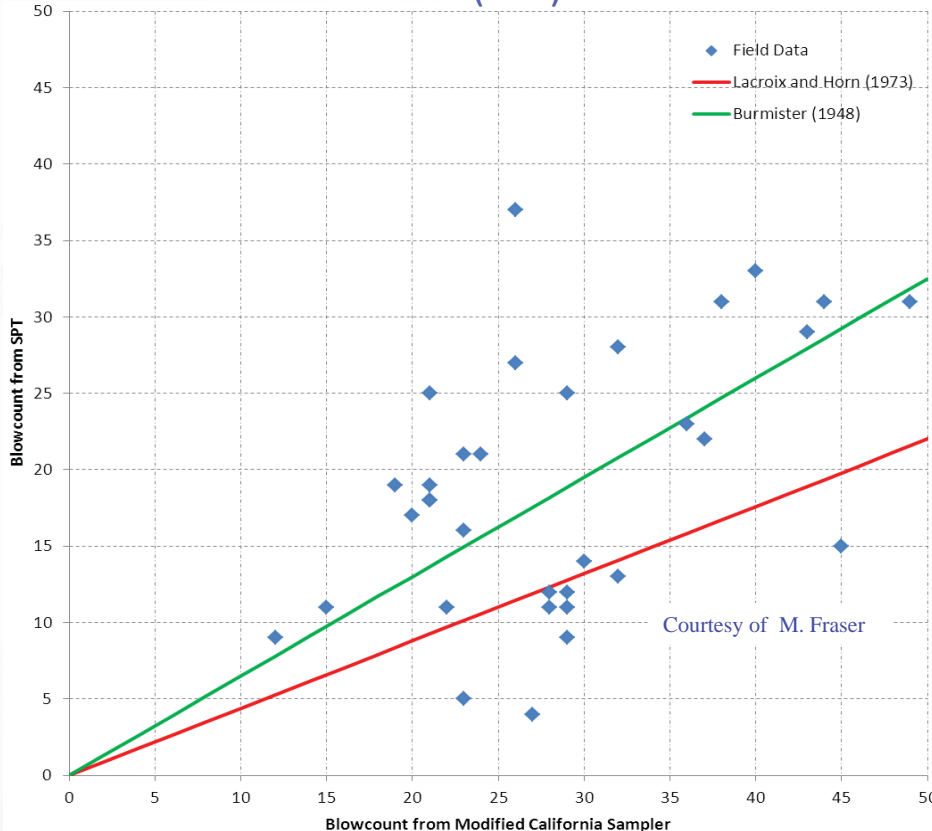
Burmister, 1948: 0.65

LaCroix & Horn, 1973: 0.44

MCS blow counts should not be used in liquefaction analysis

Short course notes: A. Elgamal, Chicago, Illinois, April 29 - 30, 2013

Standard Penetration Test (SPT)



4 borings were advanced through alluvium, each to a depth of 50 feet using an 8-inch Diameter Hollow-stem- auger.

Samples were obtained every 5 feet.

At each sampling interval, a sample was obtained from a Modified California Sampler followed immediately afterwards by an Standard sampler (SPT).

Blowcounts for both samplers are plotted on the figure to the left.

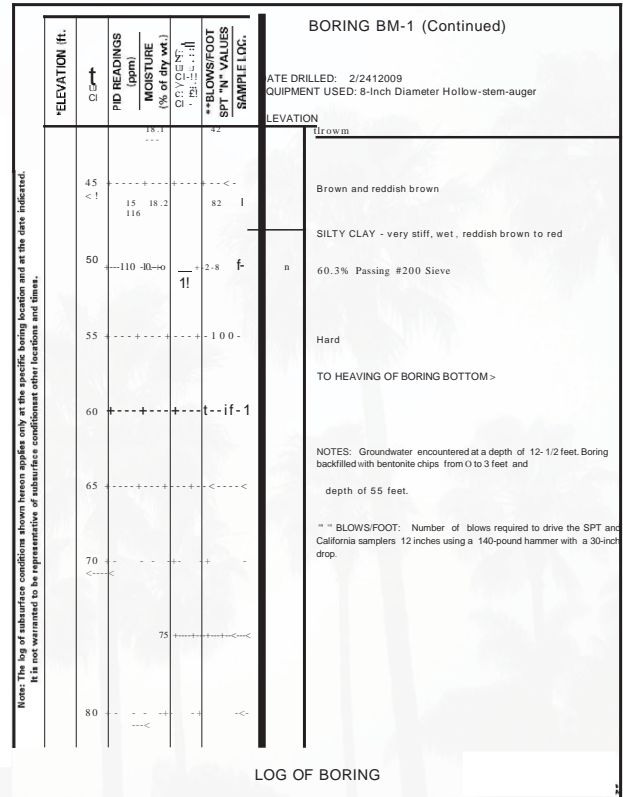
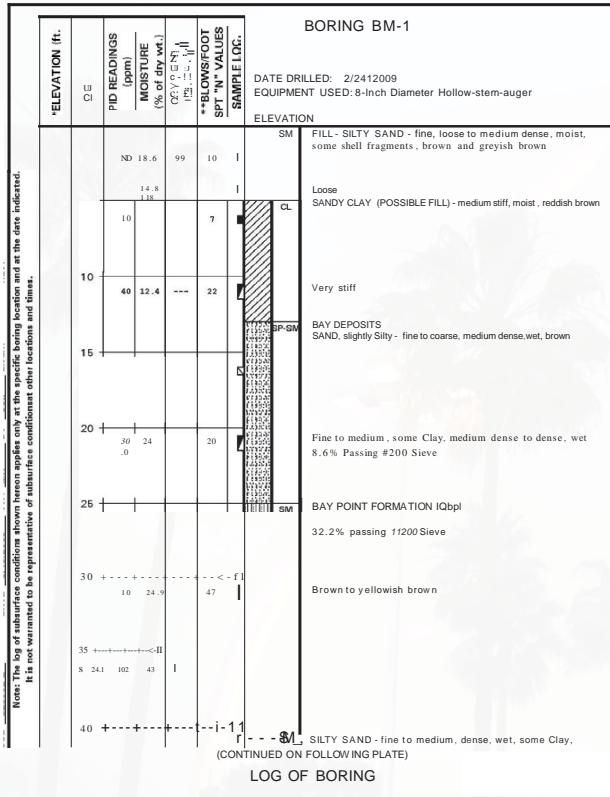
Only samples obtained where the material type (i.e., SM, SP- SM, CL, etc.) was constant are included.

Correlations suggested by Burmister (1948) and Lacroix and Horn (1973) are included.

Short course notes: A. Elgamal, Chicago, Illinois, April 29 - 30, 2013

Standard Penetration Test (SPT)

Courtesy of M. Fraser



Short course notes: A. Elgamal, Chicago, Illinois, April 29 - 30, 2013

Courtesy of M. Fraser

Cone Penetration Test (CPT)

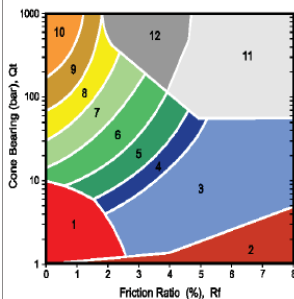
- A CPT sounding is made by pushing a small probe (cone) into the ground.
- The cone is advanced downward at a constant velocity of 2 centimeters per second, using hydraulic rams that apply the full 23-ton weight of the CPT truck to push the probe rods to depth.
- In typical CPT soundings, the resistance to penetration is measured.
- Continuous measurements are made of the resistance to penetration of the tip and the frictional sliding resistance of the sleeve of the cone.
- The penetration resistance, which is digitized at 5-centimeter depth intervals, permits detailed inferences about stratigraphy and lithology.



q_c = Cone tip stress (force/area)
 f_s = Sleeve friction stress (force/area)
 $R_f = f_s/q_t$ = friction ratio
 u = Excess pore water pressure



(After Robertson, et al., 1996)



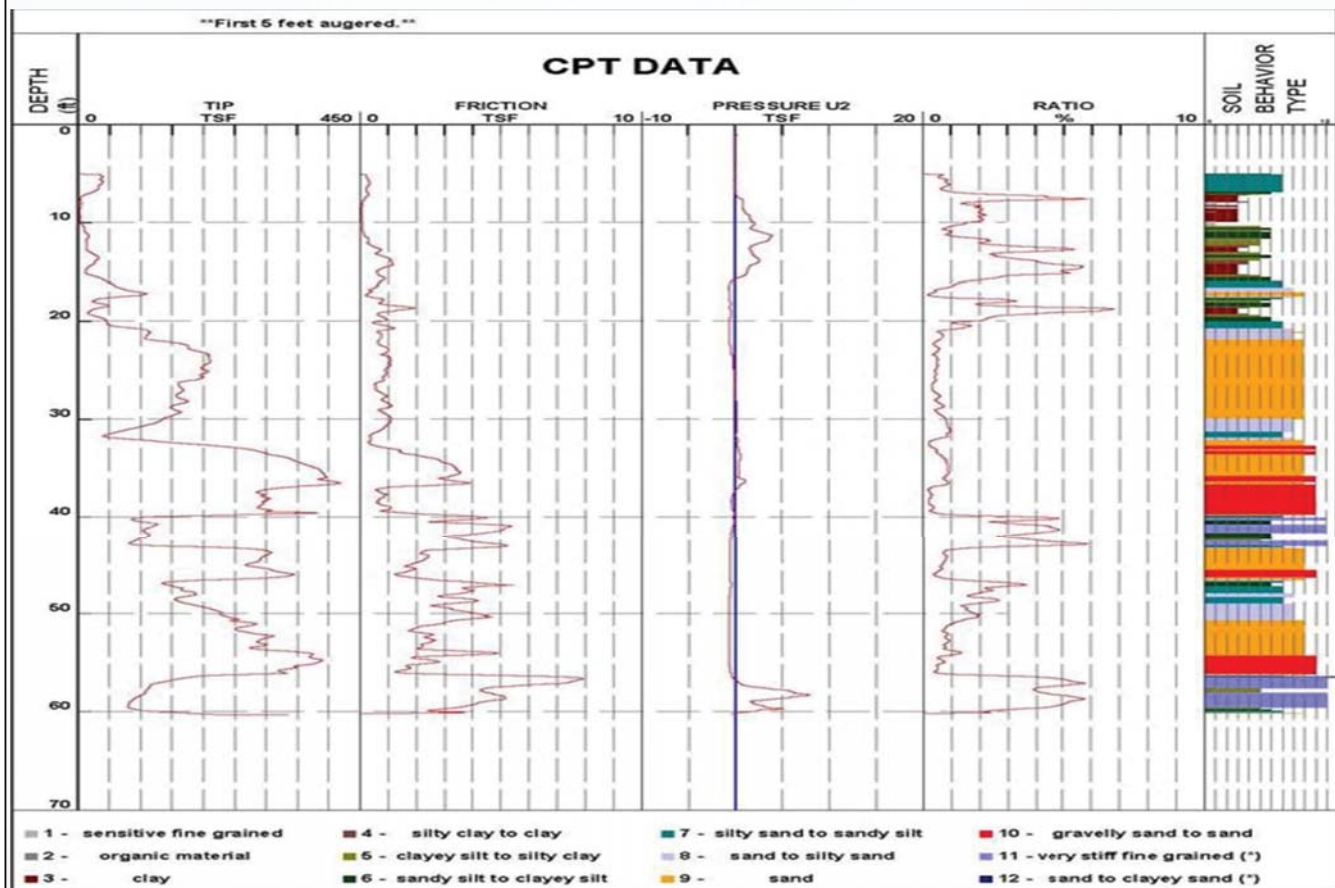
ZONE	SBT
1	Sensitive, fine grained
2	Organic materials
3	Clay
4	Silty clay to clay
5	Clayey silt to silty clay
6	Sandy silt to clayey silt
7	Silty sand to sandy silt
8	Sand to silty sand
9	Sand
10	Gravelly sand to sand
11	Very stiff fine grained*
12	Sand to clayey sand*

*over consolidated or cemented

- Soil type is inferred from a chart that compares these two measurements with the known physical properties of various soils.

Note: Tip resistance can be normalized in the form:
 $q_{c1N} = C_Q(q_c/P_a)$, in which $C_Q = (P_a/\sigma'_{v0})^n$, P_a = atmospheric pressure, σ'_{v0} = Effective vertical stress, $n = 0.5$ for course soils (sands), $n = 1.0$ for fine soils (clays) and, and $n = 0.7$ for intermediate soils

Short course notes: A. Elgamal, Chicago, Illinois, April 29 - 30, 2013



Short course notes: A. Elgamal, Chicago, Illinois, April 29 - 30, 2013

Laboratory Testing of Soil Samples

Laboratory testing of collected soil samples is often required to identify non-liquefiable layers.

- The vast majority of liquefaction hazards are associated with sandy soils and silty soils of low plasticity (and relatively high water content).
- Cohesive soils are generally not considered susceptible to soil liquefaction.
- Analysis of fine-grained soils affected by the 1999 earthquakes in Taiwan and Turkey contributed to the eventual rejection of the so-called —Chinese Criteria, particularly grain size (or percent fines), as an indicator of potential soil susceptibility to liquefaction.



Material reproduced/compiled from: CDMG SP 117A (<http://www.conservation.ca.gov/cgs/shzp/webdocs/sp117.pdf>) & NEHRP Recommended Seismic Provisions for New Buildings and Other Structures. 2009 Edition.

Short course notes: A. Elgamal, Chicago, Illinois, April 29 - 30, 2013

Laboratory Testing of Soil Samples (*continued*)

Laboratory testing of collected soil samples is often required to identify non-liquefiable layers.

- Although soils having a plasticity index (PI) greater than 7 have generally been expected to behave like clays (Boulanger and Idriss, 2006), Bray and Sancio (2006) found loose soils with a PI < 12 and moisture content > 85% of the liquid limit are susceptible to liquefaction.
- Moreover, sensitive soils having PI > 18 can undergo severe strength loss, so engineering judgment must be applied when using screening criteria.
- It is recommended that both PI and moisture content criteria be considered for screening purposes.



Material reproduced/compiled from: CDMG SP 117A <http://www.conservation.ca.gov/cgs/shzp/webdocs/sp117.pdf> & NEHRP Recommended Seismic Provisions for New Buildings and Other Structures. 2009 Edition.

Short course notes: A. Elgamal, Chicago, Illinois, April 29 - 30, 2013

SPT and CPT correlations to Friction angle ϕ and Relative Density D_r

References include:

Caltrans, GEOTECHNICAL SERVICES DESIGN MANUAL VERSION 1.0 , August 2009 ([http:// http://dap3.dot.ca.gov/shake_stable/references/GS_Design_Manual_081209.pdf](http://dap3.dot.ca.gov/shake_stable/references/GS_Design_Manual_081209.pdf))

Idriss, I.M., and Boulanger, R.W., Soil Liquefaction During Earthquakes, EERI Monograph, 2008.

Kramer, S. L., Geotechnical Earthquake Engineering, Publ. Prentice Hall, 1996.

Sabatini, P.J., Bachus, R.C., Mayne, P.W., Schneider, T. E., Zettler, T. E., FHWA-IF-02-034, 2002, Evaluation of soil and rock properties, Geotechnical Engineering Circular No. 5.

Short course notes: A. Elgamal, Chicago, Illinois, April 29 - 30, 2013

Some additional practical considerations

Use of Cal Sampler versus use of SPT

Use of Hollow Stem Auger below water table and possible use mud drilling to prevent blow-up

CPT correlation with Borings logs (soil types in general and fines content)

Sampling for I_c materials GT 2.4 (sampling and lab testing for PI and w_d)

Energy ratio of Hammers on Drill Rigs (check that calibration is made) ... the 60% Energy ratio assumption.

Sufficient borings to draw soil profile over the site (small project 2-4 borings at least per 2-3 story building/addition footprint..)

Boring sufficiently deep (e.g., 30 ft versus 50 ft or more for liquefaction assessment or pile design..)

SEISMIC-WAVE-BASED TESTING IN GEOTECHNICAL ENGINEERING

Kenneth H. Stokoe, II¹ and J. Carlos Santamarina²

ABSTRACT

As the geotechnical engineering profession moves forward into the twenty-first century, the role of seismic testing, as well as other geophysical testing methods, will increase. Geophysical methods present unique advantages, including a strong theoretical basis, the ability to perform the same basic measurement in the laboratory and field, and the noninvasive nature of many of the tests. A brief review of the fundamental concepts of seismic wave testing as applied in geotechnical engineering is presented. Determination of engineering design information (subsurface conditions and design parameters) is illustrated through case histories, which also highlight some of the strengths and inherent limitations of the methods. Suggestions for future directions, applications and potential developments are offered.

INTRODUCTION

New demands in civil engineering require advanced characterization techniques to assess in-situ conditions and to monitor processes. Challenges include aging infrastructure, construction in critical/sensitive zones, restrictions created by the urban environment, trenchless construction, installation of new infrastructure, and environmental demands and protection.

Near-surface geophysical methods can play a critical role in satisfying these needs. This situation resembles the role played by wave-based diagnostic technology in revolutionizing the medical practice during the 20th century, starting with X-ray plates and later including CAT-scan, PET-scan, ultrasound, and magnetic resonance imaging, among others.

Geophysical methods (e.g., gravity, magnetic seismic and electromagnetic) offer the geotechnical/geoenvironmental engineer unique opportunities in characterizing sites, materials and processes. These opportunities arise from the strong theoretical bases upon which geophysical methods are founded, the complementary physical principles that support various field tests, and the ability to perform the same basic measurement in the laboratory and in the field. Furthermore, many geophysical methods are noninvasive; still, an image of the subsurface can be rendered from the tomographic reconstruction of boundary measurements. Therefore, geophysical testing can be integrated into field and laboratory investigations, as a “road map” for planning and decision making and to gain valuable information.

In this paper, the most relevant concepts behind near-surface geophysical methods based on seismic (stress) waves are reviewed. The physical principles are highlighted. Selected case histories are presented to demonstrate the strengths and limitations of seismic methods. Finally, the increasing importance and future developments in this area are discussed.

EXPLORATION GEOPHYSICS

Exploration geophysics is the study of the subsurface by quantitative physical methods. These methods are based on extensive theoretical, mathematical and experimental foundations, some dating back more than a century. For example, early pioneering studies in the propagation of stress waves were conducted by Rayleigh (1887), Love (1892) and Lamb (1904). Much of the progress in this area has been driven by the

¹ University of Texas, Austin, Texas, USA

² Georgia Institute of Technology, Atlanta, Georgia, USA

petroleum exploration industries and earthquake seismology (e.g., Aki and Richards, 1980; Bourbié, et al., 1987; Mavko, et al., 1998).

In the past three decades, geotechnical, geoenvironmental and earthquake engineering applications in civil engineering have stimulated further development in geophysical exploration methods. The primary goal has been the characterization of near-surface materials and conditions, where the near-surface refers to the upper ~50 m. Numerous conference proceedings (e.g., Annual Proceedings of the Symposium on the Applications of Geophysics to Engineering and Environmental Problems, SAGEEP) textbooks (e.g., Ward, 1990; and Sharma, 1997), and manuals (e.g., Woods, 1994; ASTM, 1997; Department of the Army, 1995; “Seeing into the Earth”, NRC, 2000) have been published. Salient methods in near-surface geophysical exploration are (NRC, 2000 - See Table 1 for typical applications):

- gravity (assesses variations in density and is used to determine localized features),
- magnetic (detects variations in earth's magnetic field caused by local variations in magnetic properties of localized subsurface features),
- seismic (propagating elastic waves are used to identify changes in stiffness and density),
- resistivity (detects variation in electrical resistivity which may be related to changes in pore fluid characteristics of soil composition - if electromagnetic induction is used, changes in magnetic susceptibility may be detected as well).
- ground penetrating radar (propagating electromagnetic waves detect changes in electromagnetic impedance, which depends on permittivity, conductivity and permeability)

Table 1 General Applicability of Selected Noninvasive Geophysical Methods to Typical Sites Assessments and Monitoring Objectives (from NRC, 2000)

Example Objectives	Seismic Refraction	Seismic Reflection	Ground-Penetrating Radar	Electrical Resistivity	Electromagnetics	Induced Polarization	Microgravity	Airborne Sensing	Magnetics
Geologic mapping	①	①	①	①	①	②	②	②	②
Hydrogeology characteristics	①	②	①	①	①	②	②	②	na
Water table depth	①	②	②	①	①	③	na	②	na
Top of bedrock	①	①	③	①	①	③	②	③	na
Cavity detection	②	②	①	①	①	③	①	③	③
Disposal trench mapping	③	②	①	①	①	na	②	②	②
Nature of trench fill	③	na	①	①	①	?	①	na	①
Inorganic contaminant plume	na	na	①	①	①	①	na	②	na
Organic contaminant plume	na	na	②	?	?	?	na	②	na
Disposal container (metal drum)	na	na	①	②	①	③	③	na	①
Underground storage tanks	③	③	①	②	①	③	②	na	①
UXO detection	na	na	①	①	①	na	na	③	①

KEY: ① = primary applicability; ② = secondary supporting applicability; ③ = limited applicability; na = no general applicability or not widely used; and ? = area of active research and rapidly evolving technology or questionable application.

(Note: UXO stands for unexploded ordinance)

Wave-based methods play a preponderant role in near surface characterization. Both elastic and electromagnetic waves share most of the inherent characteristics in wave phenomena, which are summarized in Table 2. Such phenomenological richness provides valuable information to the analyst; however, it adds complexity to the interpretation of field and laboratory tests as discussed herein.

Table 2 Wave phenomena: complexity and richness *

<i>Assumption</i>	<i>Consequences</i>	
Infinite medium	P waves (requires a material: fluid or solid) S waves (requires shear stiffness)	*
Finite medium		
Propagation modes	R-waves, L-waves, S-waves Rod waves, Tube waves	* *
Interfaces	Reflection, transmission and refraction Mode conversion	
Heterogeneous		
Gradual	Curved rays and deformed wavefronts (Fermat)	
Anomalies	Diffraction, scattering (Huygens)	
Lossy	Attenuation and dispersion Relaxation	
Anisotropic	Quasi-propagation S-wave splitting and birefringence	*
Non-Linear	Shock waves	*
Discrete	Dispersion Low-pass filtering	
Multiphase medium	Slow and fast P-waves	*
Coda	A signal tail captures information about boundaries and heterogeneity	

* Examples are specific to elastic waves

Geophysical methods can be used to infer engineering design parameters. For example, strong interrelation exists between the following engineering parameters and wave-related measurements (physical justifications and correlations based on first order physical relations are presented in Santamarina et. al., 2000),

Specific surface (leading to soil classification)	electrical conductivity
Electrolytes / organics	conductivity
Void ratio	permittivity
Stiffness: unsaturated soil	V _p and V _s
Stiffness: saturated soil	V _s
Degree of saturation (near 100% saturation)	V _p
Cyclic liquefaction: unsaturated soil	V _p and V _s
Cyclic liquefaction: saturated soil	V _s
Residual shear strength	permittivity (through void ratio)
State of stress	V _s
Degree of cementation / diagenesis	V _s , Q

This list highlights the complementary nature of elastic and electromagnetic waves in near-surface characterization. The goal of geophysical surveys is to assess these parameters and their spatial distribution (e.g., stratigraphy, layering, the presence of anomalies).

FUNDAMENTAL STRESS-WAVE CONCEPTS APPLIED TO GEOTECHNICAL MATERIALS

A wave is a perturbation that propagates across a medium, varying both in time and space. Therefore, a wave has a characteristic time and spatial scale, these being the period T and the wavelength λ . Both scales are related for a given medium through the phase velocity V ,

$$V = \frac{\lambda}{T} \quad (1)$$

The wavelength λ impacts the spatial resolution that can be attained: if the wavelength is much larger than the size of an anomaly, the anomaly will not be detected. In a layered medium, with layer thickness "a", the velocity of wave propagation across the layers becomes wavelength dependent; as the wavelength decreases, attenuation increases until the wavelength reaches $\lambda=2a$. Therefore, a layered medium acts as a low-pass filter.

The wavelength must be taken into consideration when designing field or laboratory experiments. (1) The size of the receivers that are used to monitor wave motions should be much smaller than the wavelength. (2) Receivers should be in the far field to facilitate interpretation, therefore, receivers should be at least two to four wavelengths from the source. (3) The separation between receivers in an array should be small enough to avoid aliasing, yet large enough to provide independent information; both criteria are wavelength dependent.

While the wavelength must be compared to internal spatial scales such as the size of anomalies, the period T is compared to internal temporal scales such as the rate of excess pore pressure dissipation. It follows from Biot-type analysis that wave propagation in saturated soils in the low frequency range used in near surface characterization takes place under undrained conditions (Ishihara, 1967).

Mode of propagation – Particle Motion

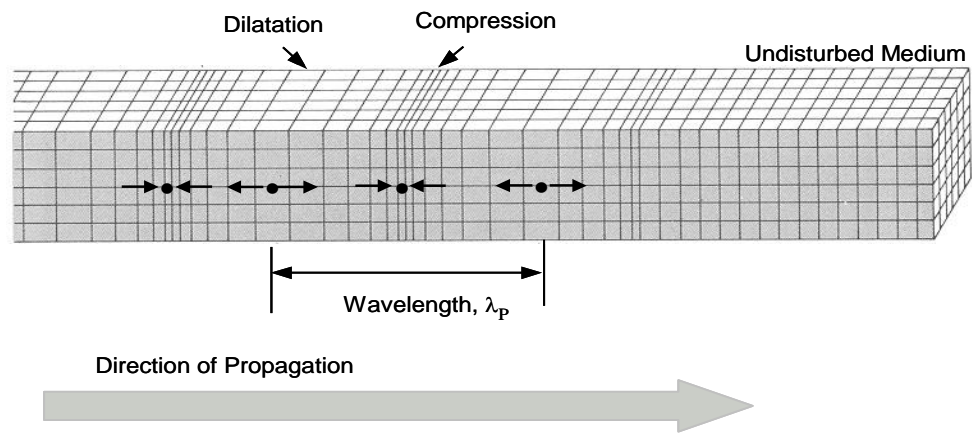
When a mechanical disturbance is initiated in any kind of solid medium, a stress wave field is generated, and energy propagates away from the disturbance. The complexity of the wave field depends upon the characteristics of the disturbance (called the "source" in seismic testing) and the uniformity of the medium. The simplest solid medium is a single-phase, linear, elastic homogeneous, isotropic, continuum material. This medium is often used as a first approximation of either: 1. a uniform soil or rock deposit, or 2. uniform layers within soil or rock deposits. Transient mechanical perturbations created in such a medium during in situ seismic testing propagate as small-strain stress waves. The maximum strain amplitude under these conditions is generally less than 0.0001%. The term "elastic" is also used to describe these waves in geotechnical materials, because the propagation behavior is independent of strain amplitude and the waves exhibit a minor amount of energy dissipation due to material damping.

Different modes of propagation can be identified by observing the particle motion relative to the propagation direction.

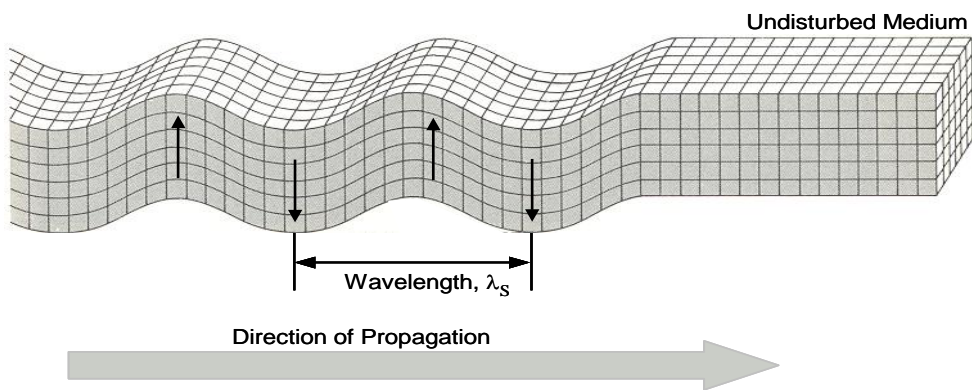
Body Waves

For stress waves propagating far from any boundaries in a uniform medium, two fundamental modes of propagation exist (Figure 1): compression waves, also called P-waves (particle motion parallel to the direction of propagation), and shear waves, also called S-waves (particle motion perpendicular to the direction of propagation). Since they propagate within the mass or body of the medium, the waves are known as body waves.

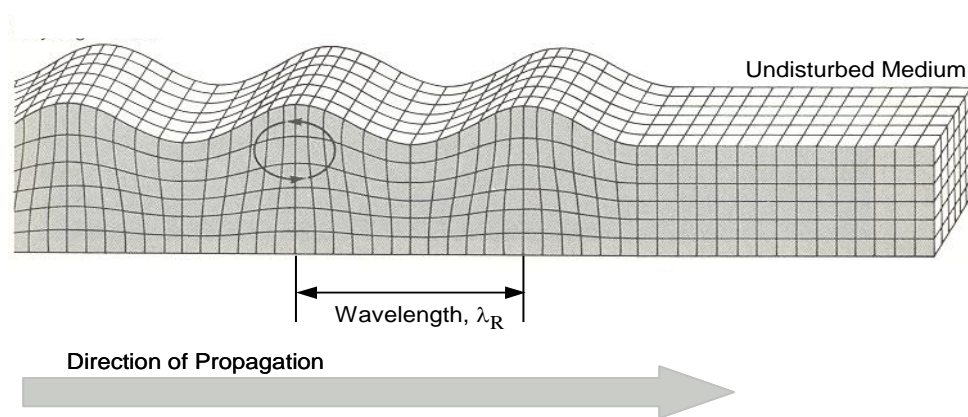
Near a typical three-dimensional (3-D) source used in seismic testing, P- and S-wave particle motions are quite complex, with each wave containing "additional near-field" (often simply termed "near-field") and "far-field" components (Sanchez-Salinero et al., 1986). As the waves propagate away from the source, the additional near-field components decay rapidly, leaving only the far-field components. Nearly all treatments of wave propagation in geotechnical engineering implicitly ignore the additional near-field components and consider only the far-field components (as in Figure 1 a-and-b). Typically, a propagation distance of two to four wavelengths is necessary before the far-field component is clearly the dominant component.



a. Compression (P) Wave



b. Shear (S) Wave



c. Rayleigh (R) Wave

Figure 1 Wave Propagation Modes. Body Waves within a Uniform, Infinite Medium and Rayleigh (R) Waves Along the Surface of a Uniform Half Space (after Bolt, 1976)

In seismic measurements, both in the field and in the laboratory, the particle motion is monitored with transducers (called “receivers”). Therefore, to monitor the propagation of the body waves shown in Figure 1, only two receivers in a 3-D receiver package would be needed, with the vertically oriented receiver used to monitor S-wave motion and the horizontally oriented receiver used to monitor P-wave motion. In this case, the S wave can also be denoted as an SV wave, with the “V” representing the fact that the particle motion is contained or “polarized” in the vertical plane.

Surface Waves (Rayleigh)

The presence of interfaces alters the particle motion, causing other modes of propagation. In particular, if the medium has an exposed surface, such as the ground surface at a geotechnical site, surface Rayleigh R-waves develop. Rayleigh wave particle motion is a combination of vertical (shear) and horizontal (compression) motions. Near the surface, Rayleigh waves create particle motion that follows a retrograde elliptical pattern as illustrated in Figure 1c. The decay with depth of the vertical and horizontal components of R-wave particle motion is illustrated in Figure 2. The depth axis is normalized by the Rayleigh wavelength, λ_R . It is interesting to see in Figure 2 that the horizontal component changes sign at a normalized depth around 0.15. The meaning of this change in sign is that R-wave particle motion changes from a retrograde ellipse to a prograde ellipse in a uniform half-space.

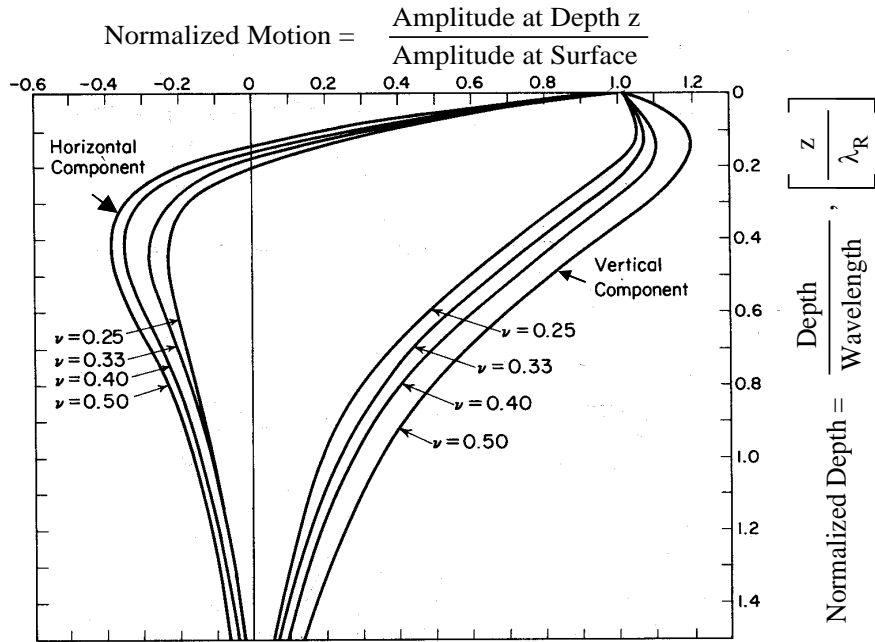


Figure 2 Variation in Normalized Particle Motions with Normalized Depth for Rayleigh Waves Propagating Along a Uniform Half Space (from Richart et al., 1970)

As with body waves, particle motion is the parameter monitored during seismic testing. Typically, the motion at various points along the exposed surface is measured. While, both components can easily be measured simultaneously, only the vertical component is usually captured.

Wave Velocities

Stress waves are non-dispersive in a uniform elastic medium. The term non-dispersive indicates that the propagation velocity is independent of frequency. These waves are also considered non-dispersive in low-loss homogeneous soils at small-strains and low frequencies. However, stratigraphy and other forms of heterogeneity cause frequency-dependent velocity. (This dependency is the fundamental premise on which the SASW seismic technique is based as noted later.) The “far-field” velocities of elastic stress waves depend on the stiffness and mass density of the material as:

$$\text{P-wave velocity} \quad V_P = \sqrt{\frac{M}{\rho}} = \sqrt{\frac{B + \frac{4}{3}G}{\rho}} = \sqrt{\frac{E}{\rho} \frac{(1-\nu)}{(1+\nu)(1-2\nu)}} \quad (2)$$

$$\text{S-wave velocity} \quad V_S = \sqrt{\frac{G}{\rho}} \quad (3)$$

where ρ is the mass density and M , B , G and E are the constrained, bulk, shear, and Young's moduli, respectively, and ν is Poisson's ratio. For a homogeneous, isotropic material, compression and shear wave velocities are related through Poisson's ratio, ν , as:

$$V_P = V_S \sqrt{\frac{1-\nu}{0.5-\nu}} \quad (4)$$

The ("far-field") velocity of the Rayleigh wave, V_R , is related to the velocities of P and S waves as (Achenbach, 1975):

$$\left[2 - \left(\frac{V_R}{V_S} \right)^2 \right]^2 - 4 \cdot \left[1 - \left(\frac{V_R}{V_P} \right)^2 \right]^{1/2} \left[1 - \left(\frac{V_R}{V_S} \right)^2 \right]^{1/2} = 0 \quad (5)$$

A good approximation for the velocity V_R in terms of V_S and Poisson's ratio is (modified from Achenbach, 1975),

$$V_R = \frac{0.874 + 1.117\nu}{1 + \nu} V_S \quad (6)$$

These equations permit computing the relative values of V_P , V_S and V_R as a function of Poisson's ratio, as shown in Figure 3. At $\nu=0$, $V_P=\sqrt{2} V_S$ and $V_R=0.874 V_S$. At $\nu=0.5$ (which theoretically represents an incompressible material; hence, an infinitely stiff material), $V_P=\infty$ so that $V_P/V_S=\infty$. At $\nu=0.5$, $V_R=0.955 V_S$. The ratios of body wave velocities (V_P / V_S) typically determined with small-strain seismic tests on unsaturated soils are around ~ 1.5 , which corresponds to Poisson's ratio ~ 0.10 ; therefore, the small-strain Poisson's ratio is relatively low.

It is important to note that the S-wave velocity is the same in an infinite medium as in a rod (torsional motion). However, the longitudinal P-wave velocity is different, being $V_P=\sqrt{M/\rho}$ in an infinite medium and $V_L=\sqrt{E/\rho}$ in a rod (this is for wavelength λ much greater than the radius of the rod; V_L decreases as the frequency increases).

Material Damping

Particle motions created by stress waves attenuate as the waves propagate away from a source. In a uniform half space of soil or rock, stress wave attenuation is caused by two mechanisms: 1) spreading of wave energy from the source, generally called geometrical or radiational damping, and 2) dissipation of energy due to internal losses in the soil or rock commonly known as intrinsic material attenuation or internal damping.

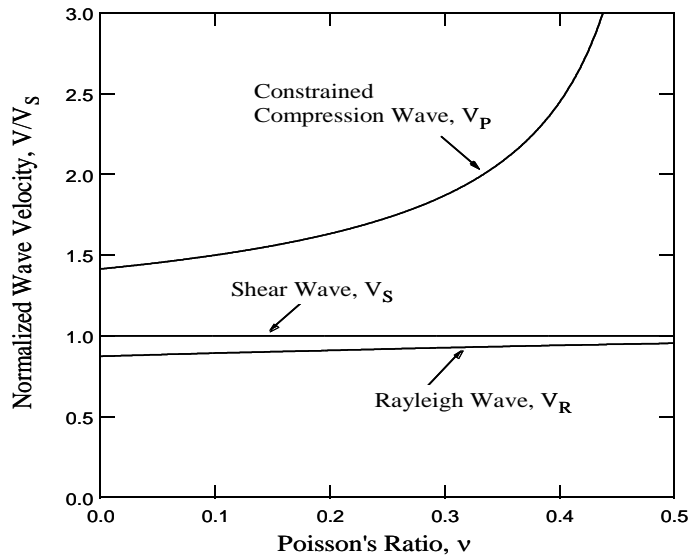


Figure 3 Relationship Between Stress Wave Velocities in a Uniform Half Space and Poisson's Ratio (from Richart et al., 1970)

Geometric spreading depends on the type of propagation and results from the spreading of a given amount of wave energy generated by the source into increasingly larger volumes as the waves propagate away, hence the term geometrical or radiation damping. Figure 4 shows the field radiated from a vertically vibrating circular footing located on the surface of an elastic half space (no material damping). Only the far-field components of particle motion and particle attenuation are illustrated (Sanchez-Salinerio et al., 1986). In this case, body waves (P and S) propagate away from the source on hemispherical wavefronts while the Rayleigh wave propagates on a cylindrical wavefront. Body wave motions decay with increasing distance as $1/r$ within the mass and $1/r^2$ along the surface. Rayleigh wave motions decay as $1/\sqrt{r}$ because of the cylindrically shaped wavefront.

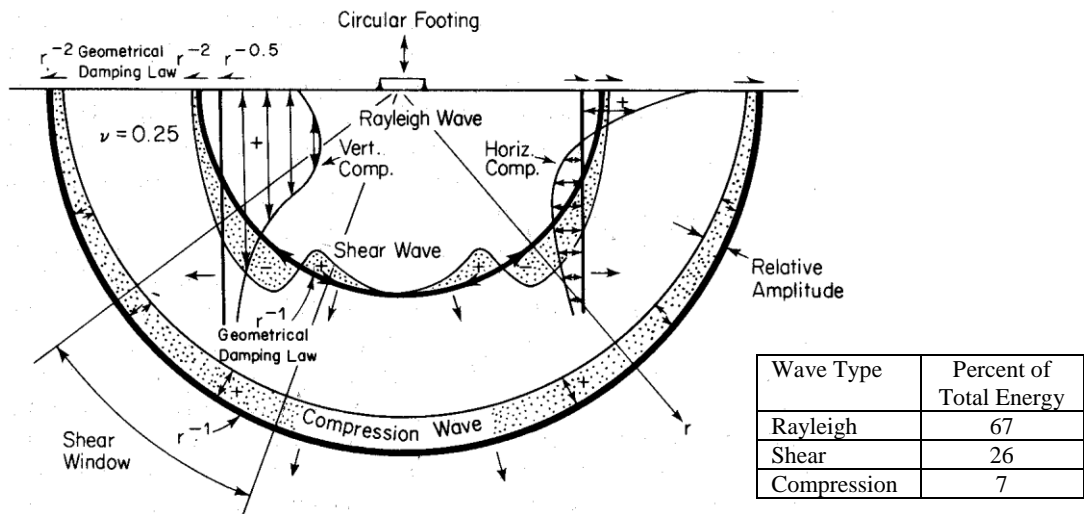


Figure 4 Distribution of Stress Wave Motions from a Vibrating Circular Footing on a Homogeneous, Isotropic, Elastic Half Space (from Woods, 1968)

Intrinsic material loss. There are various internal mechanism that lead to energy losses during wave propagation in soils. If soils are dry, energy losses are due to energy coupling effects such as thermoelasticity, and the breakage of bonds between and within particles. Frictional loss is unlikely during

small-strain wave propagation given that the relative displacement between particles does not reach the atomic dimensions $\sim 10^{-10}\text{m}$ (Winkler and Nur, 1982); however, frictional loss gains relevance when the imposed strain exceeds the threshold strain for the soil, for example, during an earthquake. In wet and saturated soils, hydrodynamic interactions between the fluid and the particles and local fluid flow or "squirting" (Dvorkin and Nur, 1993) are the preponderant energy dissipation mechanisms. Frictional loss is rate independent and strain dependent, however, viscous losses are rate dependent.

Intrinsic material losses in geotechnical materials are characterized through several parameters. Geophysicists and seismologists use the quality factor, Q , and its inverse, Q^{-1} , the dissipation factor (Mok et al., 1988). In wave propagation expressions, the decay in amplitude of a plane wave is captured as an exponential decay $e^{-\alpha x}$, where α is the spatial attenuation coefficient (units of length^{-1}). Laboratory studies determine the logarithmic decrement δ (dimensionless) from the free vibration decay of a specimen or the damping ratio D in resonant tests. The definition of Q and the interrelation among these parameters are captured in the following expression (low damping is assumed),

$$\frac{1}{Q} = \frac{\Delta E}{2\pi E} = 2D = \frac{\alpha V}{\pi f} = \frac{\alpha \lambda}{\pi} = \frac{\delta}{\pi} = \frac{\Delta f}{f_r} \quad (7)$$

where ΔE = the amount of energy dissipated per cycle of harmonic excitation in a certain volume; E = the peak elastic energy stored in the same volume; λ = wavelength (units of length), Δf = resonance width (Hertz), V = propagation velocity (length/time), f = frequency (Hertz), and f_r = resonant frequency (Hertz).

Since both velocity and attenuation are associated with a particular mode of wave propagation, one experimental method may yield a P-wave velocity and dissipation factor Q_p^{-1} , while another may determine the S-wave velocity and Q_s^{-1} . Similarly to the relationship between velocities in different propagation modes, losses are also related through Poisson's ratio as (Winkler and Nur, 1979),

$$\frac{(1-\nu)(1-2\nu)}{Q_p} = \frac{(1+\nu)}{Q_L} - \frac{2\nu(2-\nu)}{Q_s} \quad (8)$$

where subscripts P, L and S indicate P-wave in an infinite medium, longitudinal wave in a rod and S wave, respectively.

Attenuation in soils is much more complex than the elastic aspects of propagation velocity. Both laboratory and field measurements of material damping are difficult to perform and analyze. On the one hand, the exact nature of material damping is often obscure and may result from several concurrent phenomena. On the other hand, the analysis of measurements must take into account geometrical spreading, reflections, refractions, backscattering, mode conversion at interfaces, the coupling of transducers to the medium, and the effects of peripheral electronics. Hence, the analysis of the attenuation of spatially traveling waves, even in a simply layered half space, becomes quite complex. Yet, attenuation conveys information that is complementary to velocity. Thus, improvements in measurement and analysis techniques to determine material damping holds much potential for developing new applications.

Skin depth - Penetration versus Resolution

The penetration of a wave into the medium is an important constraint during the design and implementation of a geophysical survey. This is estimated with the skin depth, S_d , which is the distance the plane wave travels until its amplitude decays to $1/e$ the initial amplitude. For an exponential decay $e^{-\alpha x}$,

$$S_d = \frac{1}{\alpha} \quad (9)$$

In the case of small-strain stress waves, material damping is generally has less than 5%, and the skin depth S_d is several times the wavelength. (In contrast, the skin depth of electromagnetic waves can be quite small in

some soils such as wet clayey soils and soils with high electrolyte concentration in the pore fluid. This is a critical difference in the applicability of elastic and electromagnetic waves in near surface characterization.)

There is a trade-off in the selection of the operating frequency (which determines the wavelength, $\lambda=V/f$) and the minimum size of the object that can be resolved: the higher the frequency, the shorter the wavelength, the higher the resolution, but the shorter the skin depth.

Interfaces, Impedance and Mode Conversion

Only regions with different impedances can be discriminated. Otherwise, the material appears as a uniform medium. The material impedance, z , is:

$$z = V \cdot \rho \tag{10}$$

The detectability of an anomaly or layer is estimated by the reflectivity coefficient, R , which depends on the the relative impedance between the two media 1 and 2; for normal incidence,

$$R = \frac{A_{in}}{A_{refl}} = \frac{1 - z_1/z_2}{1 + z_1/z_2} \tag{11}$$

If the wave front reaches the interface at some inclination not normal to it, mode conversion takes place. For example, an incident P-wave generates reflected and refracted P and S waves. Mode conversion also takes place for incident S-waves when the particle motion is not parallel to the interface. The angle of reflection and refraction for each resulting front is governed by the generalized Snell's law, and the energy in each front will depend on the impedance of the layers and the angle of incidence (formulas in Aki and Richards 1980).

Complexity in Recorded Signals

A uniform half space is rarely a reasonable model for a geotechnical site. The model is, however, an excellent starting point in understanding basic wave propagation. A more realistic model of a geotechnical site is a layered system. The complexity of the wave field increases significantly in a layered medium, as illustrated by the reflected and refracted body waves shown in Figure 5. Other wave propagation forms not shown in the figure are also generated in the layered system. For instance, the interaction between reflected and refracted body waves and the surface generates Rayleigh waves. Furthermore, multiple total reflections of horizontally polarized shear waves (termed SH waves) between the surface and underlying stiffer layers can create a Love (L) wave. Particle motions associated with a Love wave are shown in Figure 6.

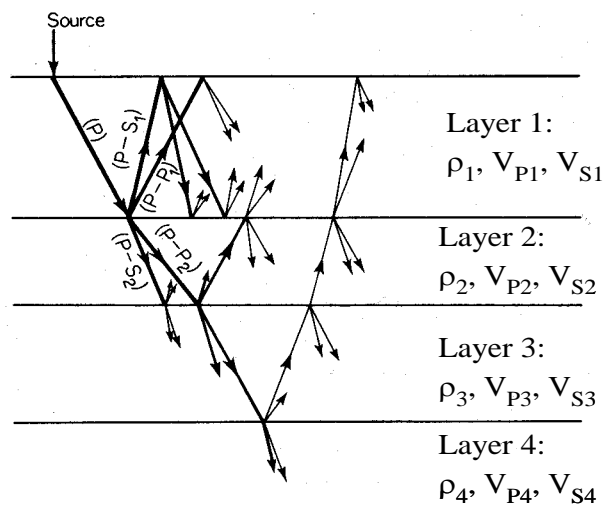


Figure 5 Multiple Wave Reflections and Refractions in a Layered Half-Space and the Resulting Mode Conversions (from Richart et al., 1970)

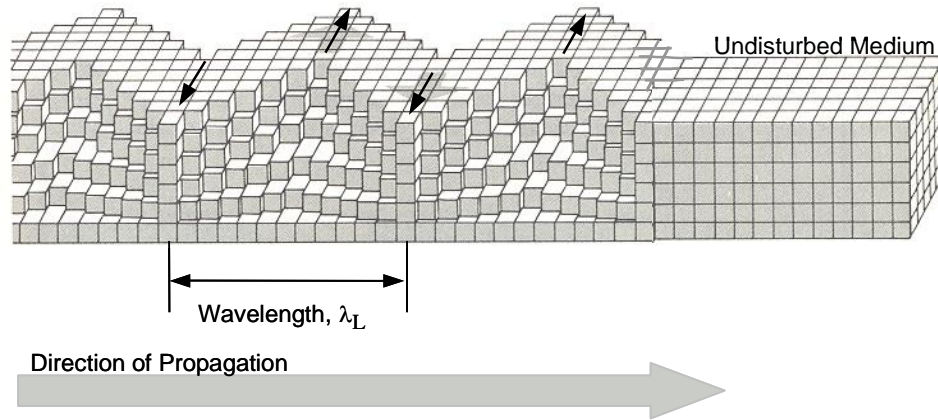


Figure 6 Love (L) Wave Propagating in the Top Layer of a Layered Half Space (after Bolt, 1976)

This example illustrates the complex nature that can exist in recorded waveforms. However, all of this information is contained in field records obtained during seismic testing and is available for data analysis and interpretation. In general, only a fraction of the information in recorded waveforms is used. Current developments are oriented towards extracting more information about the site and the geotechnical materials from the same field tests that are performed today; these developments include advanced signal processing and inversion procedures, such as matching numerically-generated waveforms for assumed subsurface conditions to the measured signals (a form of inversion by successive forward simulations).

SOIL CHARACTERISTICS AND WAVE PROPAGATION

The degree of saturation, the state of effective stress, diagenesis and cementation, inherent anisotropy and stress-induced anisotropy impact body wave velocities in soils. These factors are discussed below.

Velocity and Degree of Saturation

The shear wave velocity is related to the shear stiffness of the soil mass, which is determined by the skeleton. However, P-wave velocity is controlled by the constrained modulus, $M=B+4G/3$, therefore, the fluid and the granular skeleton contribute to V_p . Details follow.

S-wave Velocity

In clean coarse sands, where capillary effects are negligible, the effective stress controls the shear stiffness and the effect of saturation on shear wave velocity is only related to changes in mass density ρ , through $V_s = \sqrt{G/\rho}$. The relevance of capillary forces at interparticle contacts on shear stiffness increases with fines content. Furthermore, the lower the degree of saturation, the higher G and V_s become (Cho and Santamarina, 2000). This is shown in Figure 7, where V_s is determined for a granite powder specimen ($d_{50}=89 \mu\text{m}$) during drying. The finer the material the higher the effect of contact-level capillary forces. Even a small percentage of clay can play a critical role on stiffness: as drying proceeds, fine clay grains migrate towards the contacts between sand and silt-size particles and form clay buttresses and bridges adding significant stiffness to the soil mass. Loess is a typical example.

P-wave Velocity

For degrees of saturation, S_r , less than about 99 percent, compression wave velocity is controlled by the stiffness of the soil skeleton, in constrained compression in the same fashion as discussed above for shear waves; that is, the main influence of water on V_p over this range in S_r comes from unsaturated conditions which impact the soil skeleton stiffness.

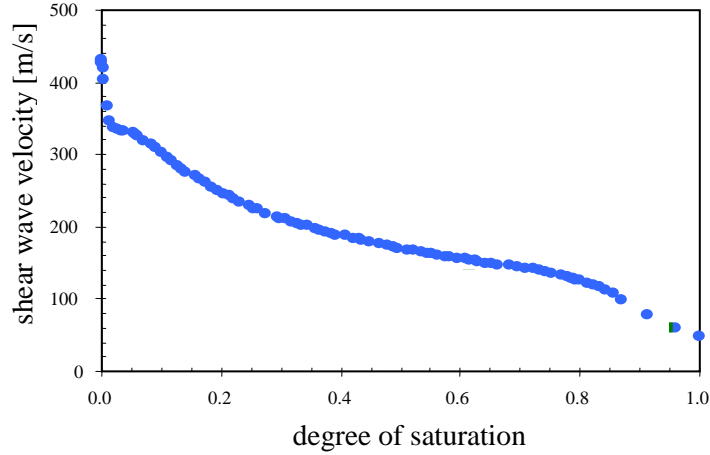


Figure 7 Shear wave velocity versus degree of saturation (granite powder, $d_{50}=89 \mu\text{m}$, applied $\sigma_v=1.5 \text{ kPa}$; Cho and Santamarina, 2000).

However, if the degree of saturation equals 100 percent, the constrained modulus of this two-phase medium is dominated by the relative incompressibility of the water in comparison to the soil skeleton. The resulting value of V_p varies with the void ratio or porosity n , the bulk stiffness of the material that makes the grains B_g and the bulk stiffness of the fluid B_f as predicted by the Biot-Gassmann relation adapted for soils (it is assumed that the stiffness of the skeleton is much smaller than the stiffness of the material that makes the particles),

$$V_{Po} = \sqrt{\frac{B_f}{\rho_f}} \sqrt{\frac{1}{\left[(1-n) \frac{B_g}{B_f} + n \right] \left[(1-n) \frac{\rho_g}{\rho_f} + n \right]}} \quad (12)$$

Typical field values for V_p in saturated soils range from about 1350 to 2000 m/s.

The bulk stiffness of the fluid phase B_f in Equation 12, is very sensitive to the presence of air (the bulk stiffness of water is $B_w=2.18 \text{ GPa}$, while the bulk stiffness of air at 1 atm is $B_{air} \sim 140 \text{ kPa}$)

$$B_f = \frac{1}{\frac{S_r}{B_w} + \frac{1-S_r}{B_a}} \quad (13)$$

Therefore, when the degree of saturation S_r is about 99.5 to 100 percent, the value of V_p is very sensitive to S_r . Figure 8 shows the typical influence of degree of saturation on V_p over this very small change in degree of saturation (the shear wave velocity remains unaffected by such a small change in saturation). For completeness, it is noted that the impact of S_r on V_s and V_p of rock is very small (only a few percent change) for S_r going from zero to 100%.

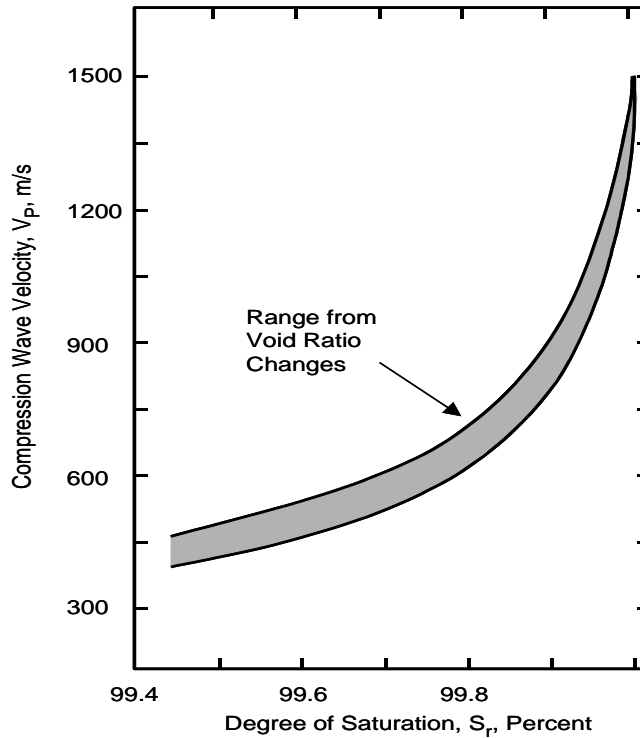


Figure 8 Typical Variation in Compression Wave Velocity with Degree of Saturation Changing from 99.4 to 100 % for Sand (after Allen et al., 1980)

Effective Stress State

Early studies in which the small-strain stiffness of the soil skeleton was investigated often involved torsional resonant column testing. The soil specimens, typically composed of reconstituted or freshly remolded dry sandy soils, were confined isotropically. The generalized relationship between V_S and effective isotropic stress, σ'_0 , was found to be (Hardin and Richart, 1963; Hardin, 1978):

$$V_S = C_S \sqrt{F(e)} \left(\frac{\sigma'_0}{P_a} \right)^n \quad (14)$$

where C_S and n are material constants associated with the type of grains, the nature of contacts and the stability of the soil skeleton. $F(e)$ is a void ratio homogeneity function, so that when the proper relation is used for a given soil, velocity-stress data gathered with specimens of the same soil at different void ratios collapse onto a single trend. P_a is atmospheric pressure in the same units as σ'_0 . Material constants C_S and n are the intercept and the slope of the measured trend plotted in $\log V_S - \log \sigma'_0$. Typically, the constrained compression wave velocity, V_P , was assumed to have the same functional relationship in an unsaturated soil, with the only change occurring in C_P , the material constant.

More recent studies have been performed with reconstituted soils subjected to anisotropic stress states (e.g., Roesler, 1979; Stokoe, et al., 1991; and Bellotti et al., 1996). These studies have shown that the relationship between body wave velocities and effective state of stress is more complex than expressed by Equation 14. For body waves with their directions of wave propagation and particle motion polarized along principal stress directions, P- and S-wave velocities can be expressed by the following functional relationships:

$$V_P = C_P \sqrt{F(e)} \left(\frac{\sigma'_a}{P_a} \right)^{ma} \quad (15)$$

$$V_S = C_S \sqrt{F(e)} \left(\frac{\sigma'_a}{P_a} \right)^{na} \left(\frac{\sigma'_b}{P_a} \right)^{nb} \quad (16)$$

in which σ'_a is the principal effective stress in the direction of wave propagation, σ'_b is the principal effective stress in the direction of particle motion. For sandy and gravelly soils which exhibit minor void ratio changes with confining pressure, ma is about 0.25 and $na = nb \cong 0.125$. Hence, $ma \cong na + nb$. An alternative expression for the shear wave propagation is to relate the velocity to the mean state of stress on the plane of particle motion.

$$V_S = C_S \sqrt{F(e)} \left(\frac{\sigma'_x + \sigma'_y}{2P_a} \right)^n \quad (17)$$

Equations 16 and 17 fit experimental data with similar statistics, and apply within the tested stress range.

The material constants C and exponents m and n are affected by similar internal processes, and are inversely correlated: the looser and the finer the soil is, the lower the value of C and the higher the exponent are (Santamarina et al., 2000).

It should be noted that the functional velocity-stress relationships can have additional stress terms when they are presented in their most general form. For S waves, there is one term which represents the out-of-plane principal effective stress, $\sigma'_c{}^{nc}$; that is, the stress on a plane perpendicular to the plane on which σ'_a and σ'_b act. For P waves, there are two terms which represent the two principal stress orthogonal to $\bar{\sigma}_a$ (remembering that $\bar{\sigma}_b = \bar{\sigma}_a$ for P waves; hence the reason $ma \cong na + nb$). Several studies have shown that $nc \approx 0$ (Roesler, 1979; Lee, 1993 and Belloti, et al., 1996). Therefore, these terms were deleted for simplicity. Likewise, Equation 17 can include another factor that takes into consideration the deviatoric stress on the polarization plane; once again, experimental data show that the exponent for this term approaches zero (Santamarina and Cascante, 1996).

Velocity-stress equations presented above show that for body waves polarized along principal stress directions, the value of V_P only depends on the state of stress in the direction of wave propagation, while the value of V_S depends on the states of stress in the directions of wave propagation and particle motion. These findings apply for principal effective stresses ratios between 0.5 to 2.0. For body waves with directions of propagation and particle motion oriented obliquely to the principal stress directions, wave propagation velocities will vary from those predicted by the previous equations as discussed below.

Inherent and Stress Induced Anisotropy

Soils exhibit small-strain stiffnesses that vary with direction under isotropic loading. This type of anisotropy is called inherent or structural anisotropy and results from the depositional process and grain characteristics (Arthur and Menzies, 1972; and Oda, 1972). This characteristic is manifested in the variation of C_P and C_S with direction. In calibration chamber tests, structural anisotropy in soil under isotropic loading has been shown to be well represented by a transversely isotropic model, also termed a cross-anisotropic model (Lee and Stokoe, 1986; Lee, 1993; Stokoe et al., 1991; and Belloti et al., 1996). In the case of a granular sample constructed by dry pluviation, the horizontal plane acts as the plane of isotropy and the vertical planes exhibit equal stiffnesses which are slightly less than the stiffnesses on the horizontal plane. This condition is expressed by the following general relationships in terms of velocities of compression and shear wave polarized along principal stress directions:

$$V_{Px} = V_{Py} > V_{Pz1} = V_{Pz2} \quad \text{and} \quad (18)$$

$$V_{Sxy} = V_{Syx} > V_{Sxz} = V_{Szx} = V_{Syz} = V_{Szy} \quad (19)$$

in which V_{Px} , V_{Py} and V_{Pz} are the P-wave velocities in the x, y and z directions, respectively, and V_{Sxy} , and V_{Syx} are the S-wave velocities in the x-y plane, V_{Sxz} and V_{Szx} are the S-waves velocities in the x-z plane, and V_{Syz} and V_{Szy} are the S-wave velocities in the y-z plane. The principal planes and associated wave velocities are shown in Figure 9. The relative order in wave velocities has been exhibited by both sand and gravel specimens (Lee, 1993; Belloti, et al., 1996; and Brignoli et al., 1997). In fact, when quantified in terms of overall averages, the P- and S-wave velocities in the x-y plane (V_{Px} , V_{Py} , V_{Sxy} , and V_{Syx}) under isotropic conditions are on the order of 10% higher than the respective velocities in the x-z and y-z planes.

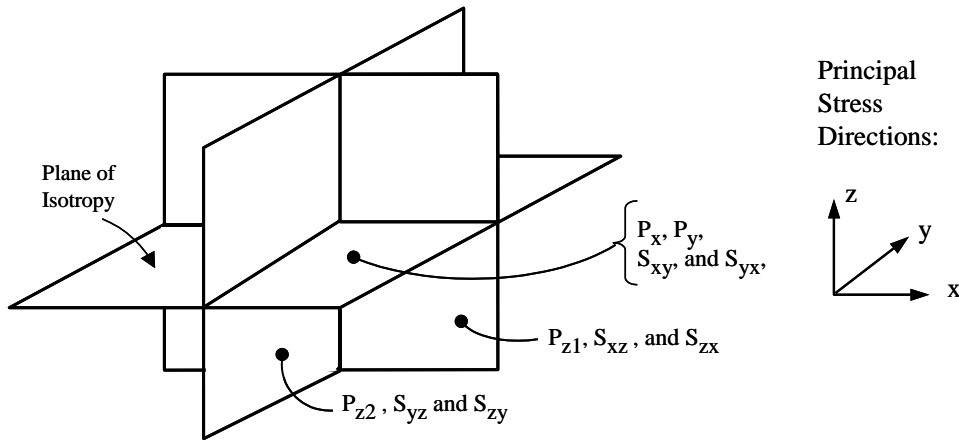


Figure 9 Principal Planes and Associated Polarized Body Waves in a Cross-Anisotropic Model with the Plane of Isotropy Oriented Horizontally

Anisotropy in soil stiffness can also be created by the stress state, as predicted by the velocity-stress expressions listed above. This type of anisotropy is termed stress-induced anisotropy and a biaxial ($\sigma'_1 = \sigma'_2 > \sigma'_3$ or $\sigma'_1 > \sigma'_2 = \sigma'_3$) or true triaxial ($\sigma'_1 > \sigma'_2 > \sigma'_3$) stress state is required to create this condition (where σ'_1 , σ'_2 and σ'_3 represent the major, intermediate and minor principal effective stresses, respectively).

To illustrate the impact of anisotropy on stress wave propagation, consider a point source generating a seismic wave in an infinite space. If the material is isotropic, the wavefront after a unit time is circular as shown in Figure 10a, and the phase velocity equals the wave velocity (also called ray velocity). The phase velocity is the velocity of the wave normal to the wavefront. It is important to realize that the phase velocity is the velocity required to calculate the elastic constants. In an anisotropic medium, the wavefront is no longer circular as shown in Figure 10b. The velocity that is obtained experimentally is the ray velocity. Therefore, for obliquely propagating waves, depending upon the degree of anisotropy, it may be necessary to convert the ray velocity to the phase velocity by the following relationship:

$$\text{Phase velocity} = \text{Ray velocity} \cdot \cos\psi \quad (20)$$

with ψ defined in Figure 10b.

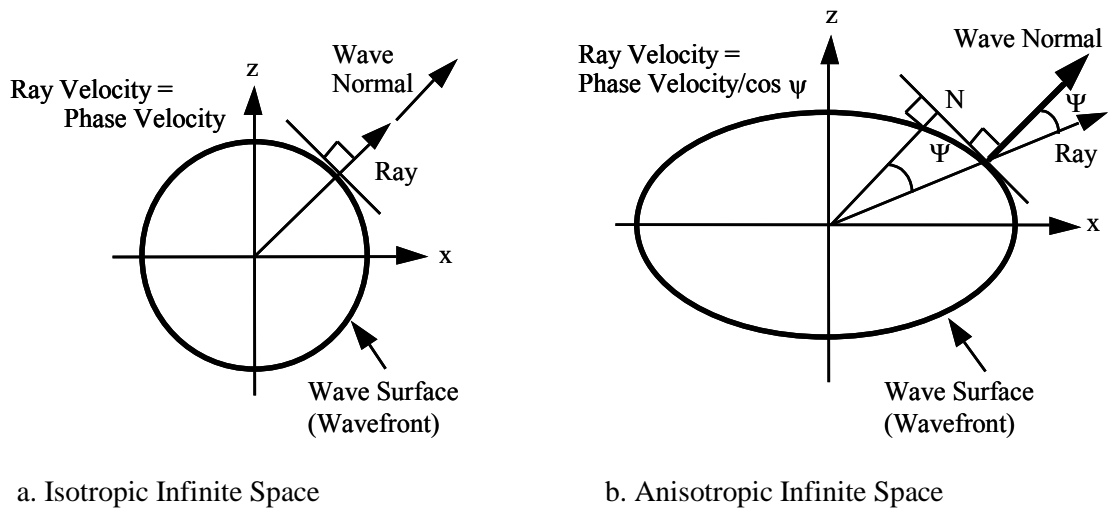


Figure 10 Direction of Ray and Wave Normals on Wavefronts Generated by a Point Source in Isotropic and Anisotropic Infinite Spaces

Implications

To illustrate the impact of anisotropy on wave velocities that could be measured in seismic testing (e.g., traditional crosshole or downhole tests), consider a level soil sites under various biaxial states of stress. In this example, wave velocity surfaces (not wavefronts) in the horizontal and vertical planes have been calculated for a soil in which structural anisotropy causes the ratio of V_{P_x} to V_{P_z} to be 1.10. Wave velocity surfaces are presented so that phase velocities in all ray directions can be discussed. Also, structural anisotropy and stress-induced anisotropy are assumed to coincide; that is, the horizontal plane is the isotropic plane under each anisotropic condition. Hence, a cross-anisotropic model can be used to represent the soil. Two examples from Stokoe et al. (1994a) are presented. The first example simulates a normally consolidated soil in which the coefficient of earth pressure at-rest, K_0 , is 0.5 (Figure 11a). The second example simulates a mildly overconsolidated soil where K_0 is 1.0 (Figure 11b).

For ease of comparison, vertical and horizontal wave velocity surfaces are normalized in terms of the P-wave velocity in the vertical direction in each example. Three wave surfaces (P-wave, SH-wave and SV-wave) exist in the horizontal and the vertical planes for each K_0 condition as shown in Figure 11. In the horizontal plane, the three wave velocity surfaces form concentric circles in both examples because the horizontal plane is the plane of isotropy. The P-wave has the highest velocity and, hence, is represented by the outermost circle in the velocity surfaces. The SV-wave has the lowest velocity and, hence, is represented by the inner most circle in the horizontal plane. The SH-wave has a velocity slightly greater than the SV-wave in both examples.

In the vertical plane, the three velocity surfaces are more complex, and they no longer form three concentric circles as shown in Figure 11. For the same wave type (i.e. P, SV or SH), velocities are different in different propagation directions. The SH-wave velocity surface forms an ellipse in the vertical plane. The P- and SV-wave surfaces are neither circular nor elliptical as shown in the figure. The P-wave velocity surface always occupies the outermost surface because it has the highest velocity. The S-wave velocities in the vertical direction are more complicated. One cannot say that the SH-wave velocity is always higher than the SV-wave velocity. The ratio varies with direction. In the vertical direction, the SV- and SH-wave velocities are the same. In the horizontal direction, the SH-wave velocity is higher than the SV-wave velocity. In an oblique direction, the SH-wave velocity is higher than the SV-wave velocity at some vertical angles, but, at other angles, the SV-wave velocity is higher than the SH-wave.

For $K_o = 0.5$, the P-wave velocity in the vertical direction is slightly higher than in the horizontal direction. When $K_o = 1.0$, the relative values reverse, and the P-wave velocity in the vertical direction is slightly smaller than in the horizontal direction (Figure 11b). This relationship simply illustrates the combined effect of structural and stress-induced anisotropy in soil. As K_o increases, the difference in SH- and SV-wave velocities increases in the horizontal plane. However, this difference is less than the difference exhibited by the P-wave velocities in the horizontal and vertical directions.

Lastly, triaxial states of stress cannot be modeled by this cross-anisotropic model. In this situation, use of an orthotropic model is required (Love, 1892). In this model, nine elastic constants are needed rather than the five elastic constants needed in a cross-anisotropic model. Six elastic constants can be obtained from the three principal stress directions (three P-wave velocities and three S-wave velocities). The other three elastic constants can be obtained from measurements in three oblique directions (Podio, 1968).

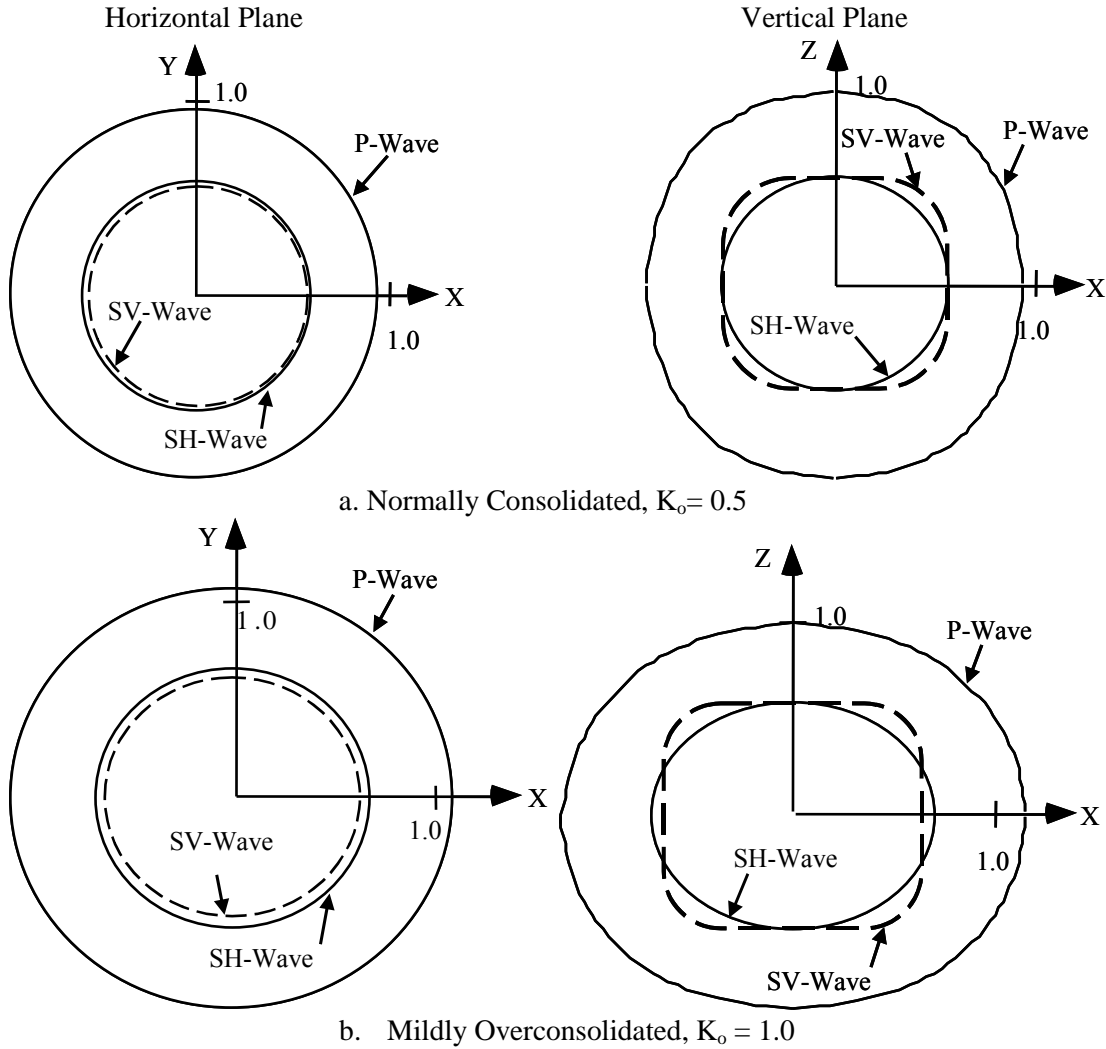


Figure 11 Theoretical Wave Velocity Surfaces in the Horizontal and Vertical Planes for a Cross-Anisotropic Material Under Normally Consolidated (a) and Mildly Overconsolidated (b) States (from Stokoe et al., 1994a)

Relationship to In Situ Seismic Testing

The wave velocity surfaces shown in Figure 11 offer significant insight into the relationships between body wave velocities measured during traditional downhole and crosshole seismic testing. This insight is correct to the extent that the assumptions made in the cross-anisotropic model represent the soil in each layer at the site which is assumed to be horizontally layered. In this discussion, the wave paths are idealized as horizontal in the crosshole test and vertical in the downhole test. The relationships are easily seen by viewing the wave velocity surfaces in the vertical plane and comparing wave velocities in the horizontal (X) and vertical (Z) directions. These velocity surfaces are assumed to represent those within each layer.

First, the P-wave velocity measured in the downhole test (V_{PZ}) does not equal the P-wave velocity measured in the crosshole test (V_{PX} or V_{PY} and $V_{PX} = V_{PY}$) in unsaturated soil ($S_r < 99\%$). The difference in these two velocities is controlled by structural anisotropy combined with stress-induced anisotropy. In the normally consolidated state, V_{PZ} is greater than V_{PX} or V_{PY} . For the other stress state shown, the P-wave velocity measured in the crosshole test is higher than the P-wave velocity measured in the downhole test.

Second, the SV-wave velocity (V_{SXZ}) measured in the crosshole test is the same as the SH-wave velocity (V_{SZX}) measured in the downhole test in all cases. This result is shown by the SV- and SH-wave velocity surfaces coinciding in the Z- direction combined with the fact that the SV-wave velocity is equal in the X- and Z-directions. Finally, the SH-wave velocity is different from the SV-wave velocity for waves propagating in the horizontal direction. Therefore, different shear wave velocities would be measured in the crosshole test using SH- and SV-waves (V_{SXY} and V_{SXZ} , respectively) as noted by Fuhrman (1993) and Roblee et al. (1994). Of course, these differences in wave velocities also lead to the potential use of in situ seismic wave velocities to evaluate stress state (Lee and Stokoe, 1986 and Lee, 1993). In such an application, use of electrical resistivity measurements to evaluate structural anisotropy could significantly enhance the accuracy of the stress state measurement.

Cementation - Diagenesis

While the state of effective stress determines velocity in freshly remolded specimens, various diagenetic processes can alter the stiffness of a soil with time. These include secondary consolidation, thixotropy, aging, and internal mechanism such as contract creep, changes in pore fluid characteristics, colloid migration, and cementation. In general, any process that renders an increase in the number of interparticle contacts or an increase in the area of contacts will cause an increase in velocity and a decrease in damping.

Cementation is particularly important. Figure 12 shows the evolution in shear wave velocity for two identical sand specimens mixed with 2% cement, but subjected to different effective confining pressures. At the beginning, V_s is determined by the effective stress, but as cementation progresses, stiffness becomes cementation-controlled, and both specimens approach the same velocity which is significantly higher than the initial velocity in the freshly remolded specimens.

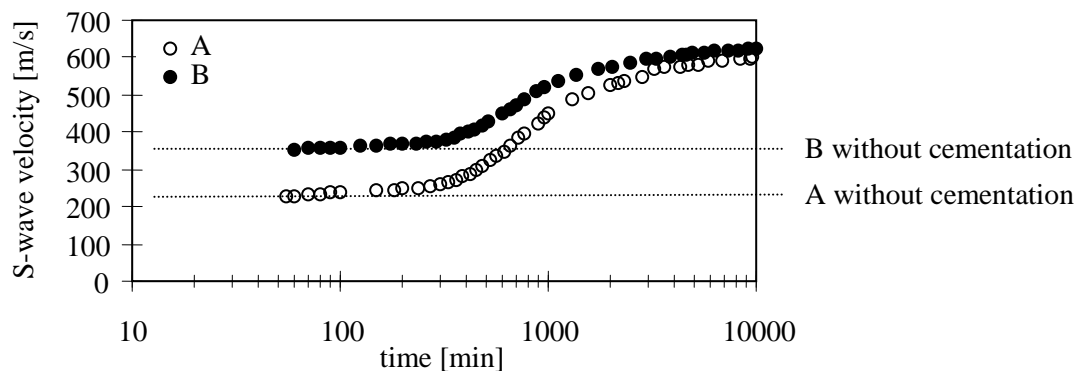


Figure 12 The effect of cementation on shear wave velocity. Sand specimens with 2% Portland cement by weight. In specimen A, the fresh mixture is isotropically confined to 70 kPa and allowed to harden. The level of confinement for specimen B is 415 kPa. (Fernandez and Santamarina, 2000).

It is important to highlight that diagenetic effects such as cementation, can be readily lost upon unloading, for example, during sampling. (Implications are discussed in the section on case histories).

FIELD TESTING

Most wave-based geophysical methods are used to measure propagation velocities. Attenuation-based measurements are infrequently used because of difficulties in analyzing these measurements as noted earlier in the discussion on material damping. Yet, attenuation-based measurements have the potential to be very valuable, especially in combination with wave velocity measurements.

Field testing methods can be classified as active or passive. Active-type methods are generally employed, whereby a wave is radiated into the medium from a source that is energized as part of the test. Passive-type methods are used less frequently. However, a passive system can be selected when the background noise can be used as the excitation or “illumination” source. Field testing methods can also be classified as nonintrusive if all instrumentation is mounted on the surface, or intrusive when boreholes or penetrometers are used. The most common stress-wave based methods in field use today are briefly reviewed below.

Nonintrusive, Active Methods

Nonintrusive methods eliminate the time and cost of drilling are eliminated, avoid the potential environmental consequences of drilling permit effectively covering large areas.

Surface Reflection Method

One of the oldest and most common seismic methods is the surface reflection method. This method is well documented in numerous textbooks in geophysics (e.g., Dobrin and Savit, 1988; and Burger, 1992). The main principle of the seismic reflection method is illustrated in Figure 13a. Both the active source and receivers are placed on the ground surface. Typically, compression wave measurements are performed using either mechanical sources that are vertically oriented or explosive sources. Waves reflected from interfaces at depth are monitored with vertically-sensitive geophones.

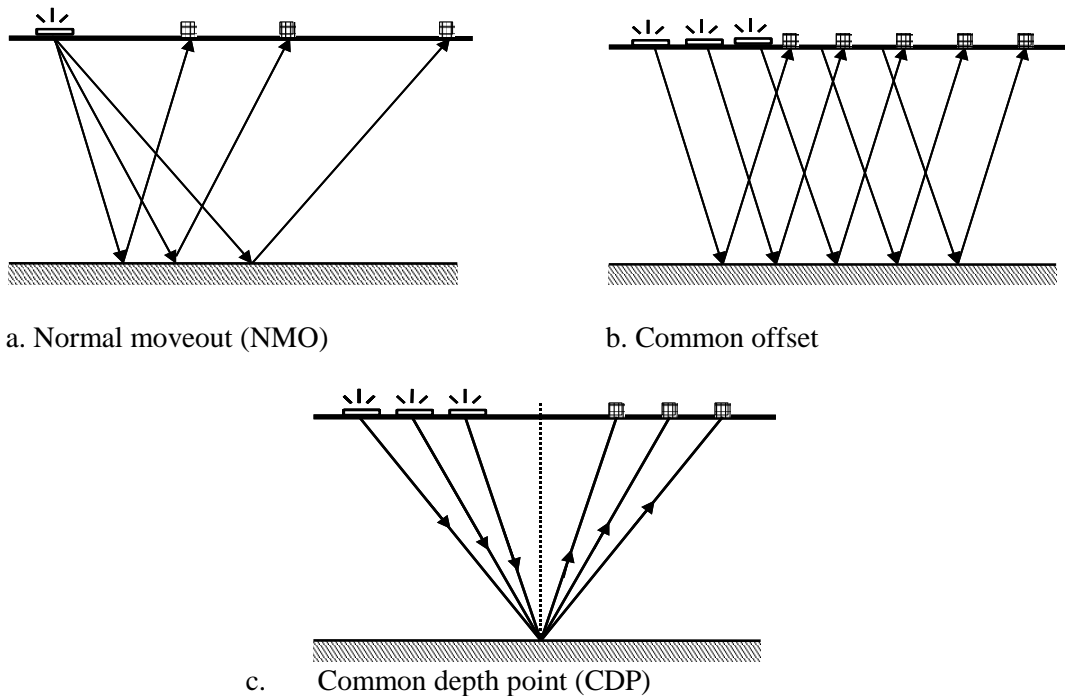


Figure 13 Field Arrangements Used in Surface Reflection Testing. (a) Normal moveout. (b) Common offset. (c) Common depth point

Interference between reflected waves and surface waves requires careful signal processing and it may restrict the applicability of the reflection method in some shallow-depths applications.

Different patterns of the source-receiver layout can be used in the reflection method to optimize the measurements, depending on the specific application. The normal moveout NMO pattern (Figure 13a) is used to estimate the average velocity of the formation. Detection of reflectors is usually obtained using the common offset pattern (Figure 13a). The common depth point CDP pattern is used to enhance the signal-to-noise ratio at a specific location (Figure 13c). Advanced signal processing capabilities, mostly developed by the petroleum industry, are available and becoming more widely used in geotechnical engineering.

One example of the results found with reflection testing is presented in Figure 14. This work was conducted by D. Steeples (NRC, 2000) to locate the deepest alluvium-bedrock contact. The location was then used to drill and place a monitoring well. The reflection technique was effective because of the significant impedance contrast at the reflector, the favorable depth of the reflector, and the lack of disturbance/anomalies in the alluvium above the reflector.

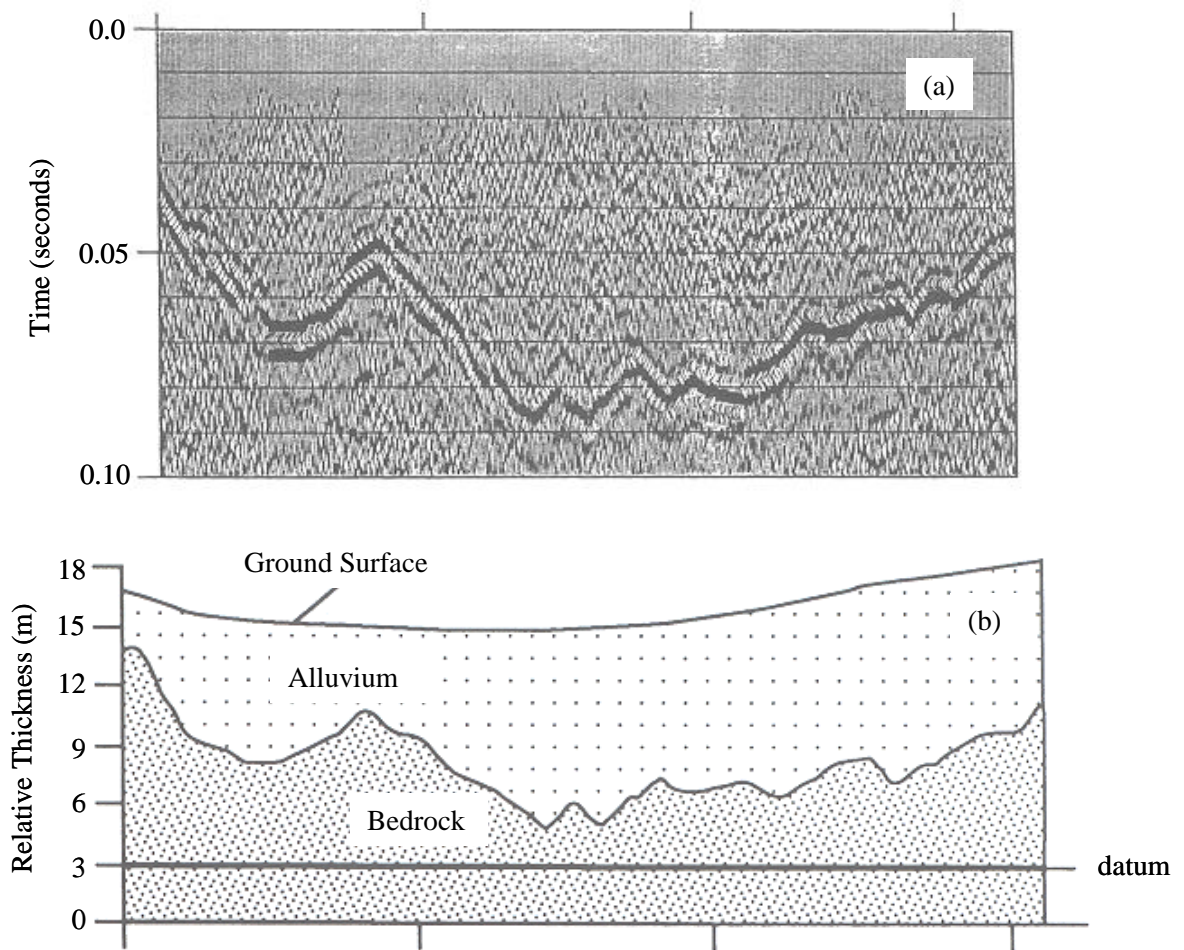


Figure 14 Seismic Reflection Cross Section (a) and Interpreted Geotechnical Cross Section (b) Used to Locate the Alluvium-Bedrock Contact (from NRC, 2000)

Surface Refraction Method

The surface refraction method is an established geophysical method for nonintrusively identifying sediment stiffnesses and layer interfaces at depth. The method is based on the ability to detect the arrival of wave energy that is critically refracted from a higher velocity layer which underlies lower velocity sediment.

Seismic signals are generated with an active source, and wave arrivals are detected on the surface with an array of receivers as shown in Figure 15. As with the surface reflection method, compression wave measurements are typically performed using vertical mechanical sources or explosives. The arrivals of refracted waves on the ground surface are monitored with vertically-sensitive geophones. Seismic refraction testing is appropriate to detect boundaries and dipping layers at shallow depths. Reflection and refraction methods are compared in Table 3.

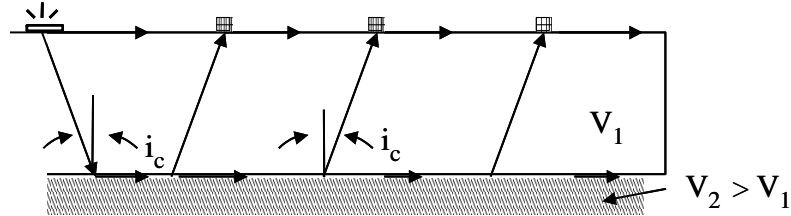


Figure 15 Field Arrangement Used in Surface Refraction Testing

Table 3 Advantages and Disadvantage of Seismic Refraction and Seismic Reflection Methods (from NRC, 2000)

Refraction Method		Reflection Method	
Advantage	Disadvantage	Advantage	Disadvantage
Observation generally use fewer source and receiver locations: relatively cheap to acquire	Observation require relatively large source-receiver offset	Observations are collected at small source-receiver offsets	Many source and receiver locations must be used to produce meaningful images; expensive to acquire
Little processing is needed except for trace scaling or filtering to help pick arrival times of the initial ground motion	Only works if the speed at which motions propagate increases with depth	Method can work no matter how the propagation speed varies with depth	Processing can be expensive as it is very computer intensive, needed sophisticated hardware and high-level of expertise
Modeling and interpretation fairly straightforward	Observation generally interpreted in layers that can be dip and topography; produces simplified models	Reflection observations can be more readily interpreted in terms of complex geology; subsurface directly imaged from observations	Interpretations require more sophistication and knowledge of the reflection process

Surface Wave Methods

Surface wave testing can involve Rayleigh and Love waves, and testing has been conducted on land and offshore (Stokoe et al., 1994b; Stoll et al., 1994; Tokimatsu, 1995; and Luke and Stokoe, 1998). The most common method used on land is called the spectral-analysis-of-surface-waves (SASW) method. This test method involves actively exciting Rayleigh wave energy at one point and measuring the resulting vertical

surface motions at various distances (receiver points) away from the source. A typical field testing arrangement is shown in Figure 16 for one set of source-receiver spacings. Measurements are performed at multiple source-receiver spacings along a linear array placed on the ground surface.

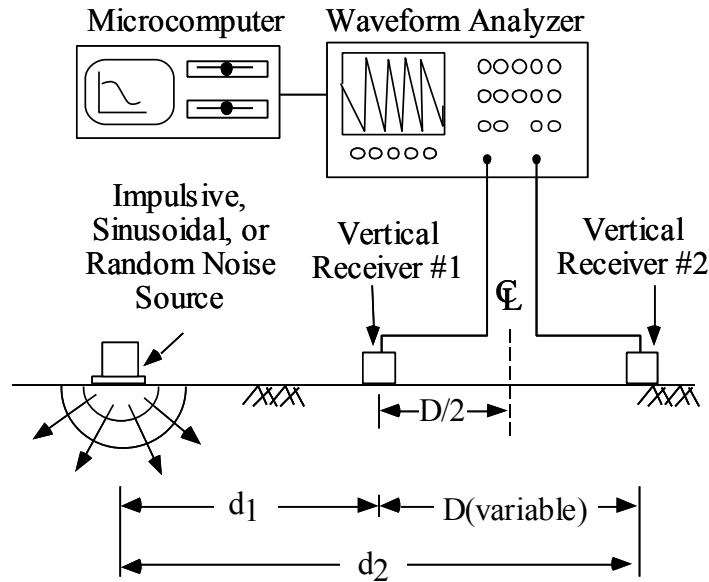


Figure 16 Field Arrangement Used in SASW Testing with a Common-Receivers Midpoint Geometry

The basis of the SASW method is the dispersive characteristics of Rayleigh waves when propagating in a (horizontally) layered system. The phase velocity, V_R , depends primarily on the material properties (shear wave velocity, mass density, and Poisson's ratio or compression wave velocity) over a depth of approximately one wavelength. Waves of different wavelengths, λ , (or frequencies f) sample different depths as illustrated in Figure 17. As a result of the varying shear stiffnesses of the layers, waves with different wavelengths travel at different phase velocities. A surface wave dispersion curve is the variation of V_R with λ or f . It is this characteristic of the site, sometimes called the "signature" of the site, that is evaluated in the field. The dispersion curve is then interpreted to determine the shear wave velocity profile with depth. The simplest interpretation is based on the fact that longer wavelengths sample deeper portions of the near surface. Formal mathematical inversion is now being implemented in practice (Nazarian, et al. 1994; Joh, 1996; Gangi, et al., 1998; Rix, et al., 2000).

From a wave-propagation point of view, the additional advantages of Rayleigh waves are that: 1. a high percentage of the energy generated by a surface source is radiated in the form of Rayleigh waves (see Figure 4); and 2. the geometrical attenuation of Rayleigh waves is low because the wavefront is cylindrical, rather than the higher geometrical attenuation caused by the spherical wavefronts of body waves.

The disadvantages of surface wave methods are that: 1. resolution decreases with depth below the surface, 2. thin layers, that are either much stiffer or much softer than the surrounding material, can be missed, and 3. a portion of each layer adjacent to a large velocity contrast is difficult to resolve. Obviously, the optimum investigative approach is to combine several seismic methods so that strengths and weakness of each method are counter-balanced.

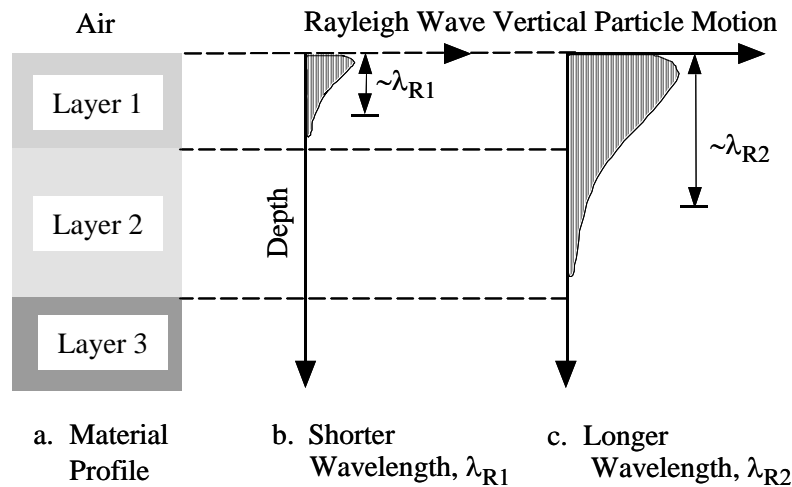


Figure 17 Schematic Representation of Rayleigh Waves of Different Wavelengths Sampling Material to Different Depths

Intrusive, Active Methods Based on Stress Waves

Crosshole Method

Shear and compression wave velocities can be determined from time-of-travel measurements between a source and one or more receivers. The crosshole method is a time-of-travel measurement where the source and receivers are placed at the same depth in adjacent boreholes, as illustrated in Figure 18a. The times of travel from the source to the receivers, called direct travel times, and the times of travel between receivers, called interval travel times, are measured. Examples of these measurements are shown in Figures 19a and b, respectively. In this example, vertically oriented impacts have been applied to the borehole wall using a wedged source. Vertically oriented receivers were used to monitor wave particle motions. This measurement then involves generating and monitoring horizontally propagating shear waves with vertical particle motion; hence SV waves. Shear wave velocities are determined by dividing the borehole spacings at the testing depth by the respective travel times. The test is repeated at multiple depths to compile a complete profile of shear and compression wave velocities versus depth. This method is used extensively on land.

Inclusions and anomalies may not be properly resolved using surface geophysics (reflection, refraction or surface wave techniques). Crosshole testing overcomes some resolution issues by drilling two (or more) boreholes around the target zone. A string of receivers (geophones or hydrophones) is lowered in one of the boreholes. The source is fired and the arrival times at all receivers are recorded. The next step is to change the location of the source and to acquire new arrival times. When multiple-source to multiple-receiver data are obtained, a tomographic inversion can be implemented, similar to applications in the medical field.

There are several strengths associated with crosshole testing. First, the source and receivers are placed close to the material/target to be evaluated, thus enhancing resolution. Second, measurements can be gathered along multiple inclined ray paths which can be processed together to render a tomographic image of the cross section (Menke, 1989; Santamarina and Fratta, 1998). Third, P, SV and SH waves can be generated and measured. The main disadvantage in crosshole testing is the time and cost associated with drilling boreholes; however, ongoing developments in cone-source combined with effectively deployed receivers promise efficient crosshole implementations (e.g., Fernandez, 2000).

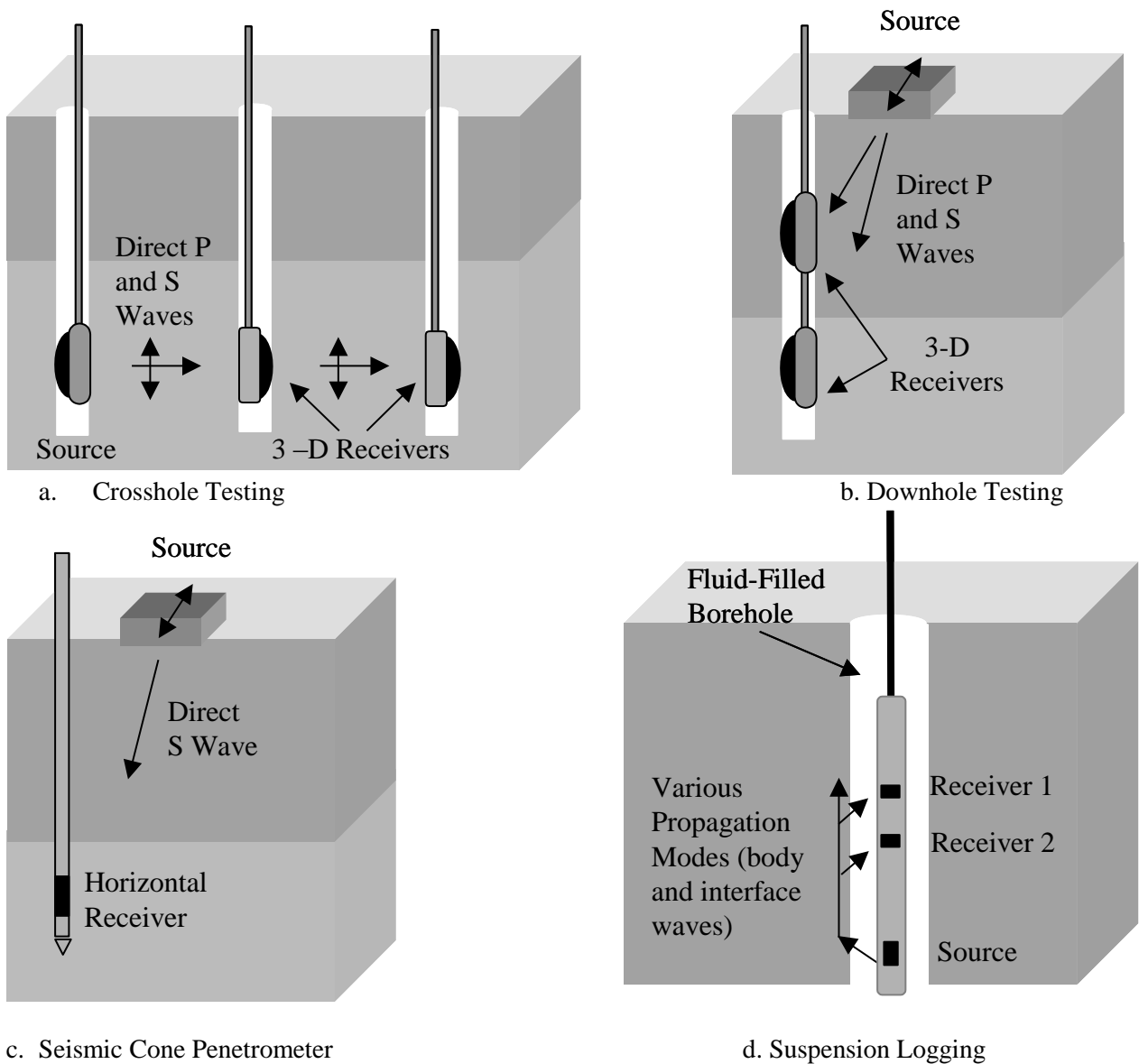
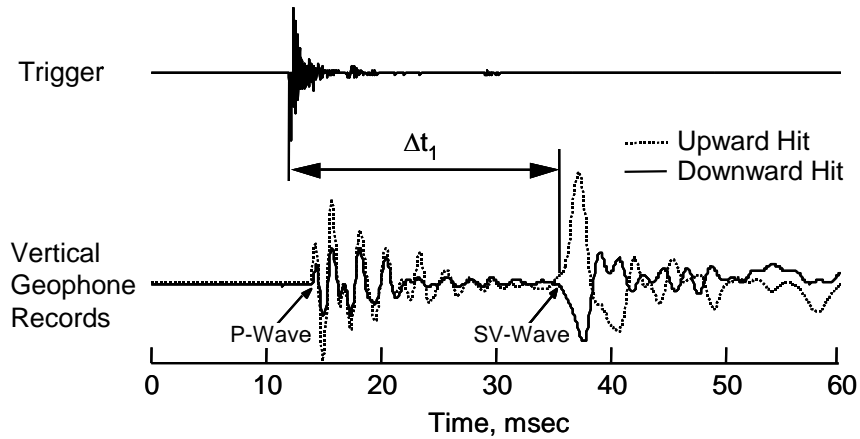


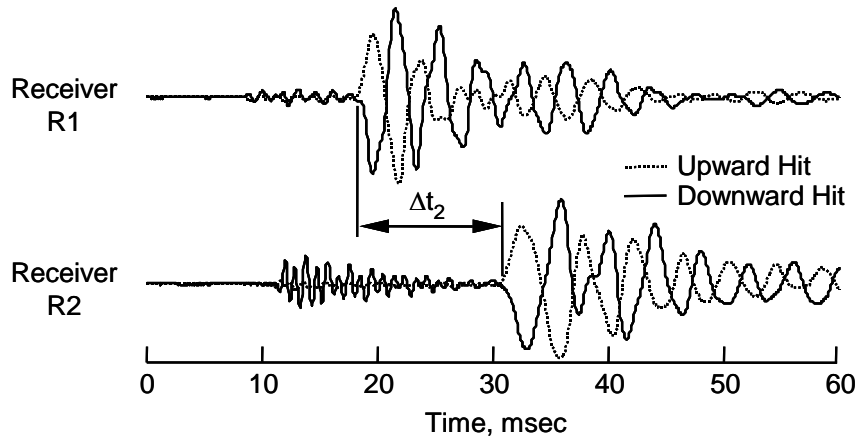
Figure 18 Field Arrangements Used to Perform Intrusive Seismic Tests

Downhole Method

In the downhole method, the times for compression and shear waves to travel between a source on the surface and points within the soil mass are measured. Wave velocities are then calculated from the corresponding travel times after travel distances have been determined. Travel distances are typically based on assuming straight ray paths between the source and receivers, although the analysis may sometimes account for refracted travel paths. Figure 18b shows a conventional setup which requires the drilling of only one borehole. One of the main advantages of the downhole method in comparison to the crosshole method is the need for only one borehole, so the cost is less. However, the disadvantage is that wave energy has to travel increasingly larger distances as the depth of testing increases. In the writers' experience, the optimum testing depths range from about 10 m to 50 m. This depth is, of course, very dependent on the energy developed by the source (various high-energy, mechanical sources have been constructed, e.g., Liu et al., 1988).



a. Record Illustrating a Direct Travel Time Measurement of an SV Wave



b. Record Illustrating an Interval Travel Time Measurement of an SV Wave

Figure 19 Example Shear Wave Records Measured in Traditional Crosshole Testing Using Upward and Downward Impacts to Help Identify the Initial SV-Wave Arrival (from Fuhrman, 1993). Note: the P-wave signal may also reverse, depending on the directivity of the source and the relative position of the receiver.

Seismic Cone Penetrometer Testing (SCPT)

The cone penetrometer is a well established tool for characterizing soil properties by measuring tip and side resistances on a probe pushed into the soil (Lunne et al., 1997). The SCPT test is a modification of the cone penetrometer test that allows measurement of shear wave velocities in a downhole testing arrangement (Campanella, et al., 1986). Seismic energy is generated at the surface near the insertion point of the cone. Usually, a horizontal impact on an embedded anvil is used to generate the SH waves. Travel times of the shear wave energy, either direct or interval, are measured at one or more locations above the cone tip as shown in Figure 18c. After testing at one depth, the cone is penetrated further into the soil, and the test is repeated. One of the important benefits of this method is that the seismic data can be combined with the cone resistance values to build a clearer picture of both soil type, strength, stiffness, and layering. This is an excellent example of using multiple techniques to investigate sites.

Borehole Logging

Logging tools can be lowered into borehole to determine material properties with stress waves, electromagnetic waves, gamma radiation, and other physical principles. Gathered data are rendered versus depth to produce a profile of the cross section. The procedure can be implemented while drilling with

“monitoring while drilling”. Borehole logging is a common practice in petroleum engineering. Different parameters can be estimated using borehole logging, including: density, conductivity, acoustic velocity, clay content, degree of fracturing, etc (Daniels and Keys, 1992; Howard 1992; Labo 1992). The main limitations in borehole logging are the effect of casing and drilling fluids on the measured response and the depth scanned by the technique relative to the depth affected by the borehole.

One of the more recent advances in borehole shear wave methods is the suspension logger (Kitsunezaki, 1980; Toksoz and Cheng, 1991; and Nigbor and Inai, 1994). This test is performed in a single, mud-filled borehole. The device is lowered on a wire line into the borehole, and seismic energy is generated and received by a receiver array in the borehole as shown in Figure 18d. The shear wave velocities of the surrounding material can be inverted from the arrival times of the predominately Scholte-type energy. One of the advantages of this method is that the wire-line nature of the test allows for penetration to great depths (hundreds of meters). One drawback of the method is that it generally can not be performed in a steel or thick plastic casing if soft soils are to be tested. This constraint limits application of the test in soft onshore or offshore sediments.

Passive systems: Acoustic and Seismic Emissions

Sudden frictional slips and crack formation and growth, produce acoustic and seismic emissions. These emissions cover a wide range of frequencies, from several Hertz up to MegaHertz. The central frequency of the emission depends on the material and the nature and geometry of the source. There is a general inverse relationship between frequency and source size. Many applications of mechanical emissions in testing and process monitoring exist. Some examples are: nondestructive testing metals and other materials such as concrete (Scott, 1991), determination of pre-stress in clays and granular soils, and assessment of stress levels in rocks using the Kaiser effect (Koerner et al., 1984), characterization of fractures (Glaser and Nelson, 1992), monitoring landslides, avalanches and engineering processes such enhanced oil recovery. Emissions are also involved in special phenomena, for example, the case of "booming sands" (not fully understood yet; Haff, 1986).

Microseismicity is a special case of mechanical emissions. Excavation in mines and tunneling leads to the redistribution of stresses within the rock mass. The redistribution of stress and the presence of dykes, faults and joints trigger the liberation of strain energy in the form of seismic waves (Talabei and Young, 1988). While structural damages are seldom, rockbursts may take place (magnitude between 1.5 to 4.5). Small seismic events or microtremors are frequent, often exceeding, thousands per day (magnitudes smaller than 0). Microtremors permit rapidly sampling the structural properties of mines, by determining the location, the source characteristics, and the properties of the rock mass.

Background noise can also be used as the source or excitation. For example, passive surface wave testing to characterized geotechnical sites (Tokimatsu et al., 1992; and Tokimatsu, 1995)

LABORATORY TESTING

One of the strengths of geophysically-based tests is that the same tests that are performed in the field can be performed in the laboratory as well. Both intact and reconstituted specimens are used in the laboratory, with the choice often controlled by the ability to obtain intact specimens. Laboratory tests provide the opportunity to conduct parametric studies which can greatly enhance the analysis of field data. Additionally, these studies contribute to the development of new field applications. Laboratory testing has, however, the shortcomings associated with testing small samples of material under imposed boundary conditions.

Because of the prevailing effect of the state of effective stress on wave propagation parameters, specimens in laboratory studies must be placed within pressure cells. Typical cell designs include rod specimens subjected to axi-symmetric stresses, oedometer cells that impose zero-lateral strain conditions (K_0 state of stress), and true-triaxial configurations whereby the three principal stresses can be independently controlled. The type of excitation can include short wavelets, single frequency sinusoid or frequency sweep, steady state sinusoidal excitation, random noise, or a step function (release from an imposed quasi-static displacement). For small-strain propagation, linear time invariant conditions can be assumed and time signals can be interpreted in the frequency domain to compute the frequency response of the soil mass (such

analyses are detailed in Orfanidis, 1996 and in Santamarina and Fratta, 1998). Most commonly used measurement techniques are briefly discussed below.

Resonant Column Testing

Resonant column (RC) testing is the most widely used stress-wave based technique in the laboratory. The testing configuration involves either fixed-free or free-free boundary conditions (Drnevich et al., 1978 - The fixed-free torsional resonant column is the most widely used method in testing soils). The test consists of exciting the cylindrical specimen to identify first-mode resonance. Both longitudinal and torsional modes are used. One of the important advantages of RC testing is that measurements can be performed in the small-strain range, just as done in field seismic testing.

A typical fixed-free, torsional device is shown in Figure 20. Sinusoidal torsional excitation is applied to the top of the specimen over a range in frequencies, and the acceleration amplitude at the top of the specimen is measured for the different frequencies. A typical data set is shown in Figure 21. Determinations of the resonant frequency and maximum amplitude of vibration are then made from the response curve. These values are combined with equipment and specimen characteristics to calculate shear wave velocity, V_s , shear modulus, G , and shearing strain amplitude.

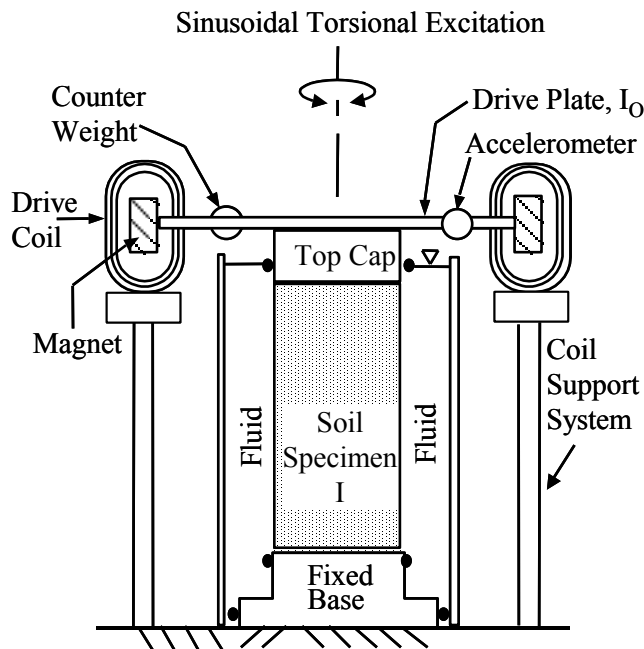


Figure 20 Simplified Diagram of a Fixed-Free, Torsional Resonant Column (Confining chamber not Shown)

Material damping is evaluated from the dynamic response using any of the following: 1. the free-vibration decay curve, 2. the half-power bandwidth method, or 3. phase shift measurements between the input force and the output displacement. As an example, consider measurements with the free-vibration decay curve. This curve is recorded by shutting off the driving force after the specimen is vibrating in steady-state resonant motion, or by releasing the specimen from an imposed quasistatic torque (i.e., negative step). Figure 22 shows a data set. The logarithmic decrement, δ , is defined from the decay curve as:

$$\delta = \ln(z_1/z_2) \tag{21}$$

where z_1 and z_2 are the amplitudes of two successive cycles. Material damping ratio, D , can then be determined from δ as prescribed in Equation 7.

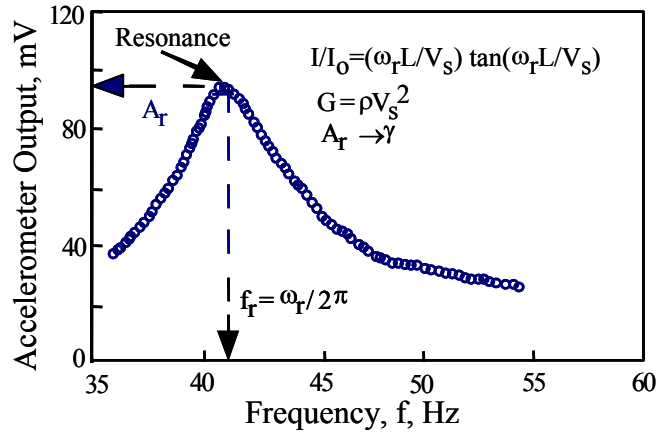


Figure 21 Dynamic Response Curve Measured with a Fixed-Free Torsional Resonant Column

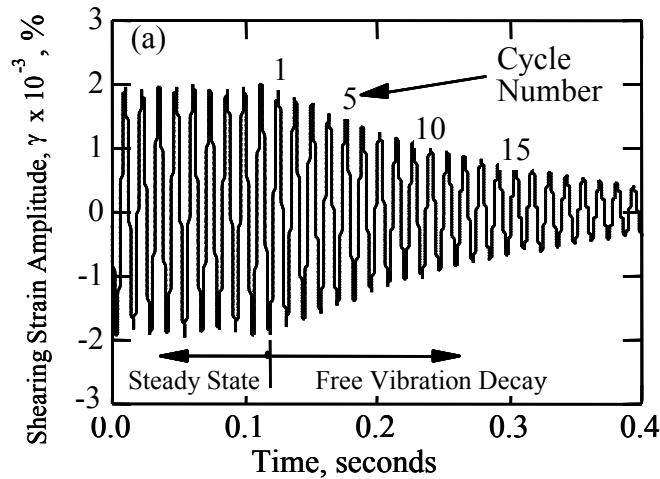


Figure 22 Material Damping Measurement with a Fixed-Free Torsional Resonant Column Test Using the Free-Vibration Decay Curve

Hardin and Drnevich (1972) studied the relative effects of many parameters such as shearing strain amplitude, effective mean principal stress, and void ratio, on V_s and D_s . They observed that the frequency of loading (also termed excitation frequency herein) is relatively unimportant in measurements of small-strain shear modulus (hence, V_s) for all soils and only somewhat important in the measurement of material damping of clayey soils. A recent study by Stokoe et al. (1999) confirms the observations by Hardin and Drnevich (1972) and provides the following quantitative trends (see Figure 23): (1) for excitation frequencies changing from 1 to about 100 Hz, G_{max} increases by about 5 to 30 %, with the effect generally increasing with increasing PI. (2) Over the same frequency range, D_s is affected much more, with the value of D_s easily doubling. (In fact, factors in excess of three were measured on a few specimens.)

Thus, it is not surprising that excitation frequency has been relatively unimportant in general comparisons between field and laboratory values of V_s . On the other hand, depending on the fines content (material passing the #200 sieve), it may be very important to account for excitation frequency in comparing D_s values determined by different stress wave techniques.

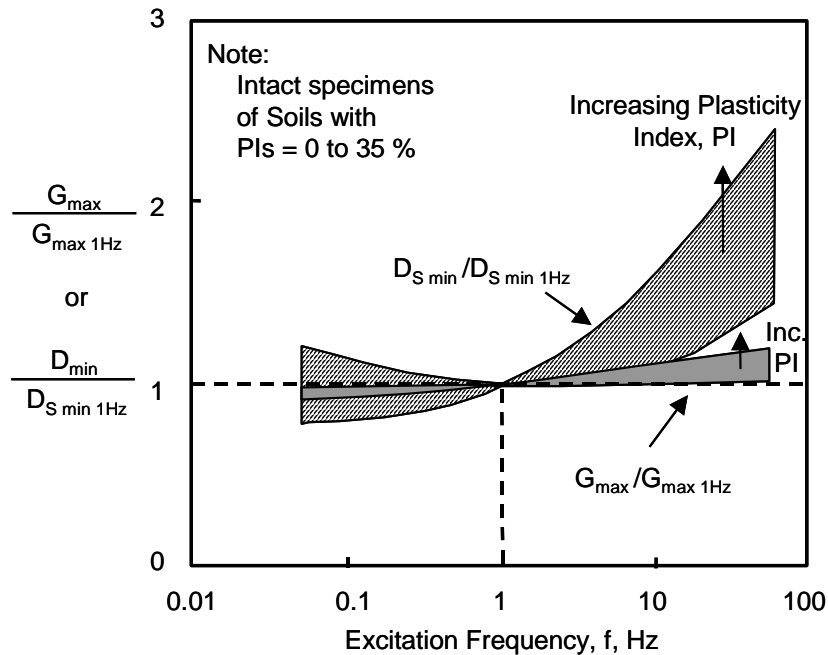


Figure 23 General Effect of Excitation Frequency on Small-Strain Shear Modulus, G_{\max} , and Small-Strain Material Damping Ratio in Shear, $D_{S \min}$ (After Stokoe, et al., 1999).

Piezoelectric Transducers

While standard resonance columns are driven by coil-magneti systems, the instrumentation of laboratory devices commonly used in geotechnical engineering is effectively implemented with piezoelectric transducers. Typical installations include two piezo-transducers, one acting as the source and the other as the receiver. In this configuration, measurements are based on the propagation of short wavelets and require the peripheral electronic devices such as those shown in Figure 24.

Piezoelectric transducers can be designed and mounted to generate and detect P- or S-waves. A particularly convenient design consists of two piezoelectric plates glued together forming a bimorph that bends when a potential difference is applied (and generates a voltage when bent). These bimorphs or "bender elements" are mounted as cantilever beams on end-plattens and cell boundaries, and partly protrude into the soil mass, providing robust coupling (mounting details are shown in Figure 25). Therefore, bender elements are excellent sources and receivers of shear waves.

Installations based on piezoelectric transducers permit accurate travel time determinations. However, attenuation measurements are affected by geometric spreading, coupling between the transducers and the soil mass, installation characteristics, and peripheral electronics. In this case, proper experimental design (such as wave-guide configuration) and careful signal processing (e.g., spectral ratios) are required to compute attenuation (Sachse and Pao, 1978; Pialucha et al., 1989; Fratta and Santamarina, 1996).

Calibration Chambers and True-triaxial Cell

Many calibration chambers (CC) are in use today. The chambers are generally used to load carefully constructed samples of soil with known boundary conditions. Models or prototype systems are then inserted into the soil to evaluate their performance in a known geotechnical environment. Evaluation of the performance of in situ devices are typical uses of these chambers. An overview of the history of many chambers is given in Lunne, et al., (1997). Well known results include the Gibbs and Holtz (1957) standard penetration test (SPT) relationships, the Schmertmann (1976) cone penetration test (CPT) relationships and numerous studies conducted by the Norwegian Geotechnical Institute, and ENEL and ISMES in Italy (e.g., Baldi et al., 1981).

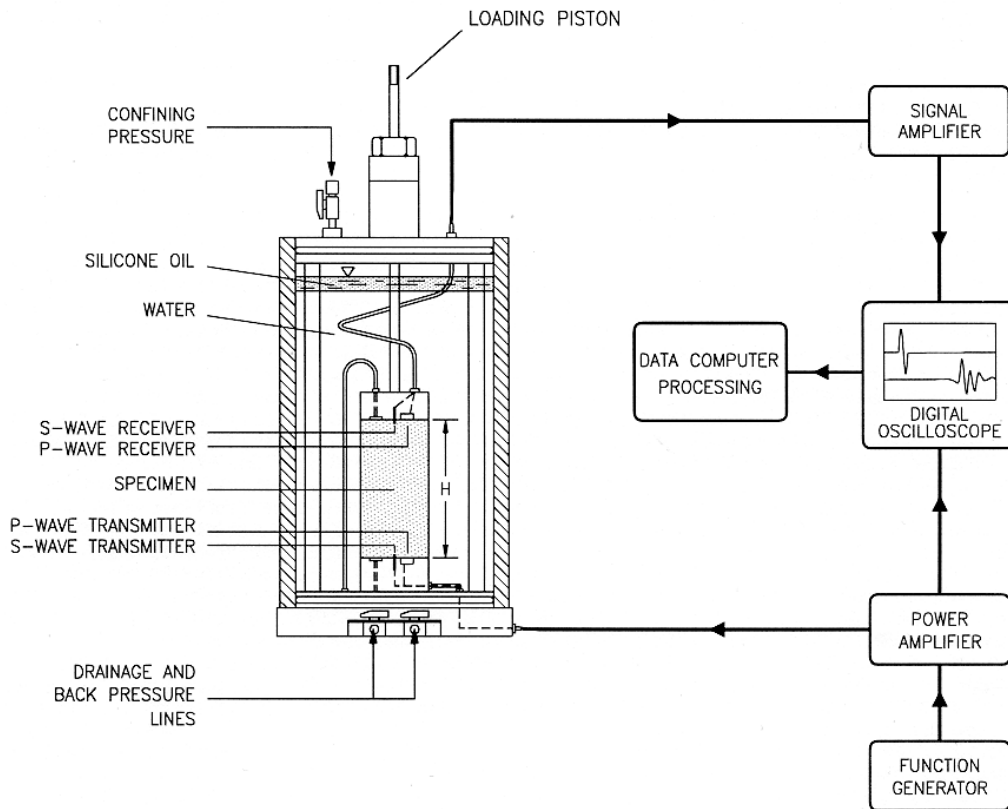


Figure 24 Schematic of Piezoelectric Transducers and Associated Electronics Used During Triaxial Testing (from Brignoli, et al., 1996)

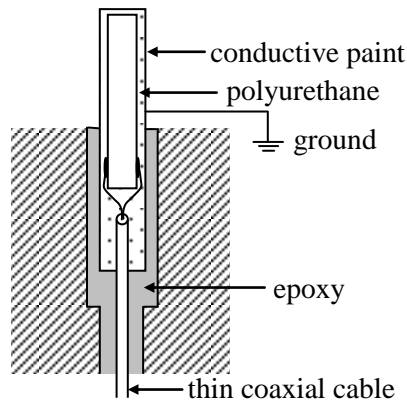


Figure 25 Mounting bender elements. The element is coated with polyurethane to prevent moisture and with conductive paint and grounded to avoid cross-talk and antenna-effects (see details in Dyvik and Madshus, 1985; Santamarina et al., 2000).

In terms of stress wave measurements, calibration chambers have been used for the past 20 years to investigate the impact of state of stress and structural anisotropy on V_S and V_P of sandy and gravelly soils (e.g., Knox, et al., 1982). Most of these chambers have the shape of a right circular cylinder and thus have been used to load the soil isotropically ($\bar{\sigma}_1 = \bar{\sigma}_2 = \bar{\sigma}_3$) and biaxially ($\bar{\sigma}_1 > \bar{\sigma}_2 = \bar{\sigma}_3$ or $\bar{\sigma}_1 = \bar{\sigma}_2 > \bar{\sigma}_3$). There are a few cubical calibration chambers in use (e.g., Stokoe, et al., 1991). Cubical chambers have the advantage of being able to load soil under true triaxial ($\bar{\sigma}_1 > \bar{\sigma}_2 > \bar{\sigma}_3$) states of stress as well as isotropically and biaxially. Generally, stress-controlled boundaries are used, although a few devices also have strain-controlled boundaries (Baldi et al., 1981; and Parkin and Lunne, 1982).

Seismic testing in calibration chambers is usually performed with embedded arrays of sources and receivers. Two such arrays are shown in Figure 26, one for generating and measuring vertically propagating P waves and the other for vertically propagating SH waves. Geophones can be used to function as a source or as a receiver. Each geophone array is arranged in a linear pattern, with the axis of the array and the sensing axis of each geophone oriented parallel to a principal stress direction in the test specimen. Compression waves are generated and monitored with geophones oriented so that their axis of sensitivity coincides with the array axis. Shear waves are generated and monitored with geophones oriented so that their axis of sensitivity is perpendicular to the array axis. Numerous arrays of three geophones each can be placed in the test specimens. Measurements with each three-geophone array involves using the geophone located at one end of the array as the source and the other two geophones as receivers. Typical spacings between adjacent geophones range from 40 to 60 mm. The source geophone is typically excited with one input cycle of a given frequency (often 1 to 2 kHz), and the resulting outputs generated by the stress waves passing the receiver geophones are recorded. The electronics used are shown in Figure 26.

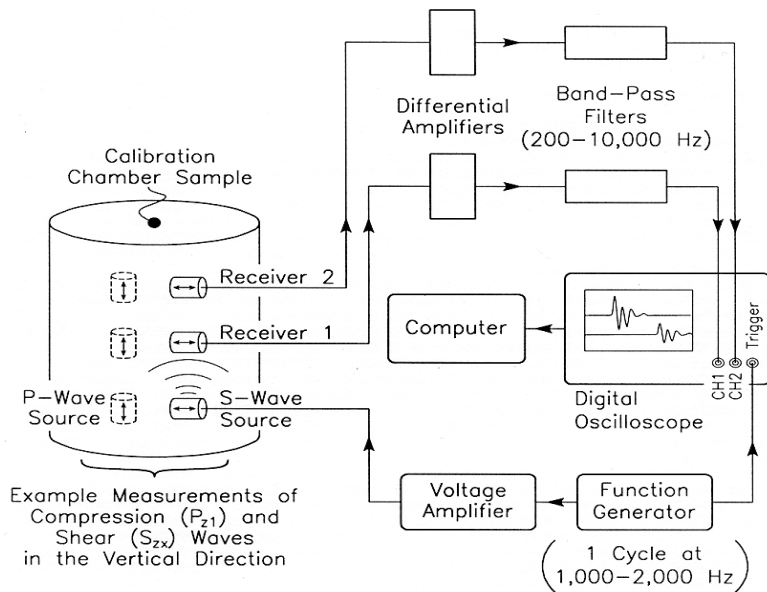


Figure 26 Schematic Diagram of Embedded Geophones and Electronics Used in Seismic Measurements in Calibration Chamber (from Brignoli et al., 1997)

A typical seismic record is shown in Figure 27. In this record, only true-interval velocities are evaluated; that is, for the same source input, the travel time, Δt , between the receivers is measured. Then, with the distance between receivers known from array construction, the particular wave velocity is determined simply by dividing the receiver distance by travel time. Additional details on this type of seismic testing in calibration chambers can be found in Stokoe et al. (1991) and Bellotti et al. (1996).

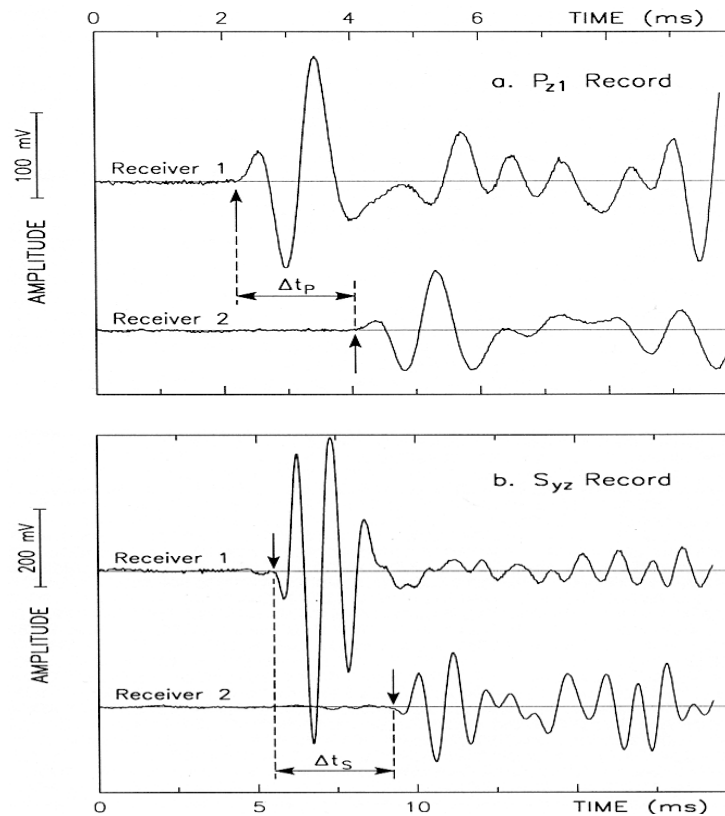


Figure 27 Example Compression Wave (a) and Shear Wave (b) Records Measured in a Calibration Chamber Test (from Brignoli et al., 1997)

The records shown in Figure 27 could have come from one of the field seismic tests noted earlier. The only difference is the somewhat higher excitation frequencies are used in CC tests. These higher frequencies are necessary so that an appropriate number of wavelengths exist between the source and receivers (hence, the additional near-field terms are significantly attenuated). Higher frequencies also provide a sharper break at the time of the initial wave arrival.

CASE HISTORIES

The previous sections showed that the propagation of elastic waves through geomaterials provides valuable information about critical engineering material properties (e.g., saturation, state of stress, stiffness, diagenesis, and even soil type) and their spatial distribution (e.g., layers, anomalies, inclusions, water table). Field characterization and laboratory tests were also reviewed. The purpose of this section is to present selected case histories, and to highlight some unique aspects of the application of seismic-wave based technology to engineering practice.

Case History No. 1 – Comparison of Field and Laboratory V_S Values

In civil engineering, the initial impetus for developing stress-wave based methods was to evaluate the dynamic properties of near-surface geotechnical materials, with emphasis on two areas of application. The first was soil dynamics, specifically, for designing dynamically loaded foundations where small-strain shear stiffness G_{\max} or G_0 is the key soil property. The second area was geotechnical earthquake engineering for site response analyses. In this case, measurements in the small-strain and nonlinear-strain ranges were required. This requirement necessitated the combined use of field (small-strain) and laboratory (small- to large-strain) measurements.

Invariably, when field and laboratory values of V_S are compared, values of $V_{S \text{ lab}}$ range from slightly less to considerably less than the in situ values, $V_{S \text{ field}}$ (Anderson and Woods, 1975). An on-going study dealing with the resolution of site response issues in the 1994 Northridge earthquake, called the ROSRINE study, involves numerous field and laboratory investigations. At this time, about 40 intact samples have been recovered and tested in the laboratory. Additionally, in situ seismic measurements have been conducted during the field investigation phase. Therefore, the ROSRINE study offers an excellent opportunity to investigate further the relationship between field and laboratory values of V_S .

When comparing field and laboratory data, the following issues must be addressed. First, have high-quality intact samples been recovered? Second, are any of the samples cemented and has the cementation been damaged? Third, what stress path should be followed and what final stress state should be applied during sample confinement? Fourth, what drainage conditions should be used? Finally, fifth, what confinement time should be associated with the laboratory measurement?

In order to attain observations relevant to engineering practice, good judgment was exercised in the ROSRINE study, proper procedures were followed, and state-of-the-art (or at least high-quality state-of-the-art) results were obtained. An example field V_S profile measured in this study is presented in Figure 28. At this site, called La Cienega, in situ seismic tests (crosshole testing and suspension logger) were performed to a depth of nearly 300 m. Intact samples were recovered from depths ranging from 4 to about 240 m. The laboratory values of V_S , shown by the solid circular symbols, are plotted at the corresponding sample depths. There is considerable variability in the field V_S profile. The “average” field values associated with the laboratory values are shown by the short vertical lines through the field V_S profile in the vicinity of the sample depth.

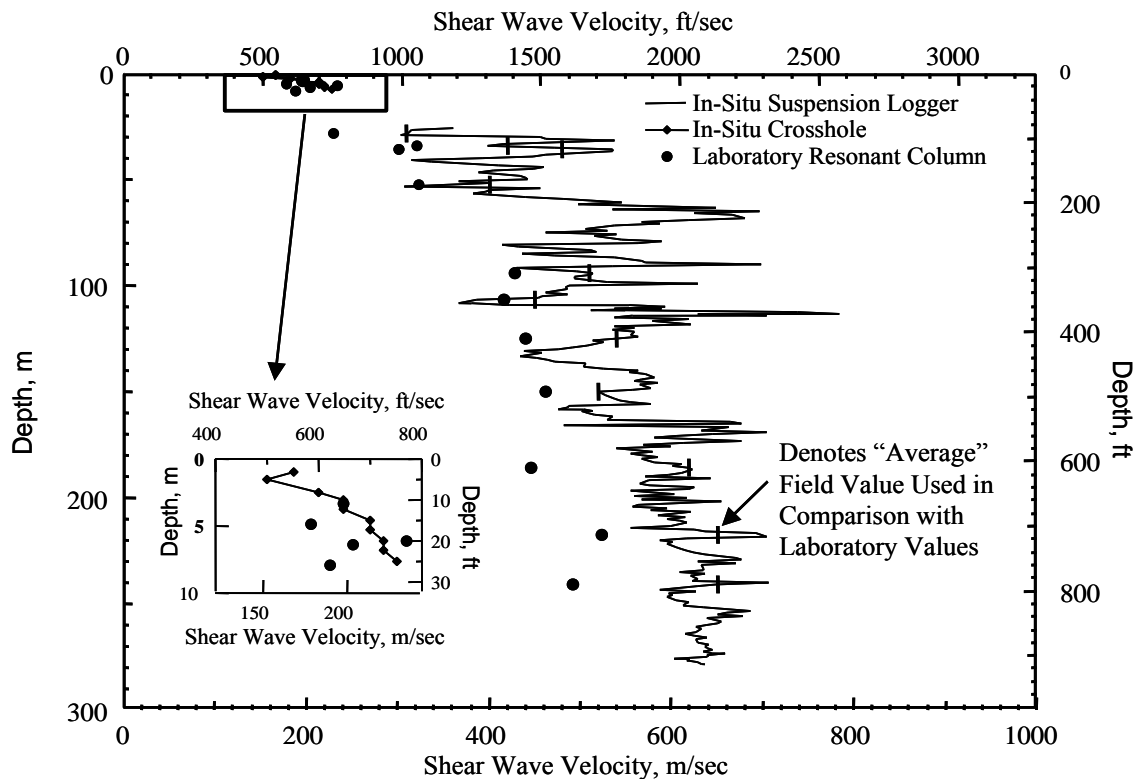


Figure 28 Example Profile of Field and Laboratory Shear Wave Velocities Evaluated at a Strong-Motion Earthquake Site on the ROSRINE Study

A summary of all 40 comparisons from the ROSRINE study is presented in Figure 29. There is a general trend in the data, with the velocity ratio ($V_{S, \text{lab}} / V_{S, \text{field}}$) decreasing as the in situ V_S increases. (There is essentially no correlation with sample depth.) The velocity ratio is around one at $V_S \cong 200$ m/s. However, at $V_S \cong 650$ m/s, the velocity ratio is about 0.6, which means that the small-strain shear modulus from laboratory testing is on the order of 1/3 of the value in the field. This comparison strongly supports the need to perform field seismic tests, certainly in studies dealing with siting and retrofitting of critical facilities.

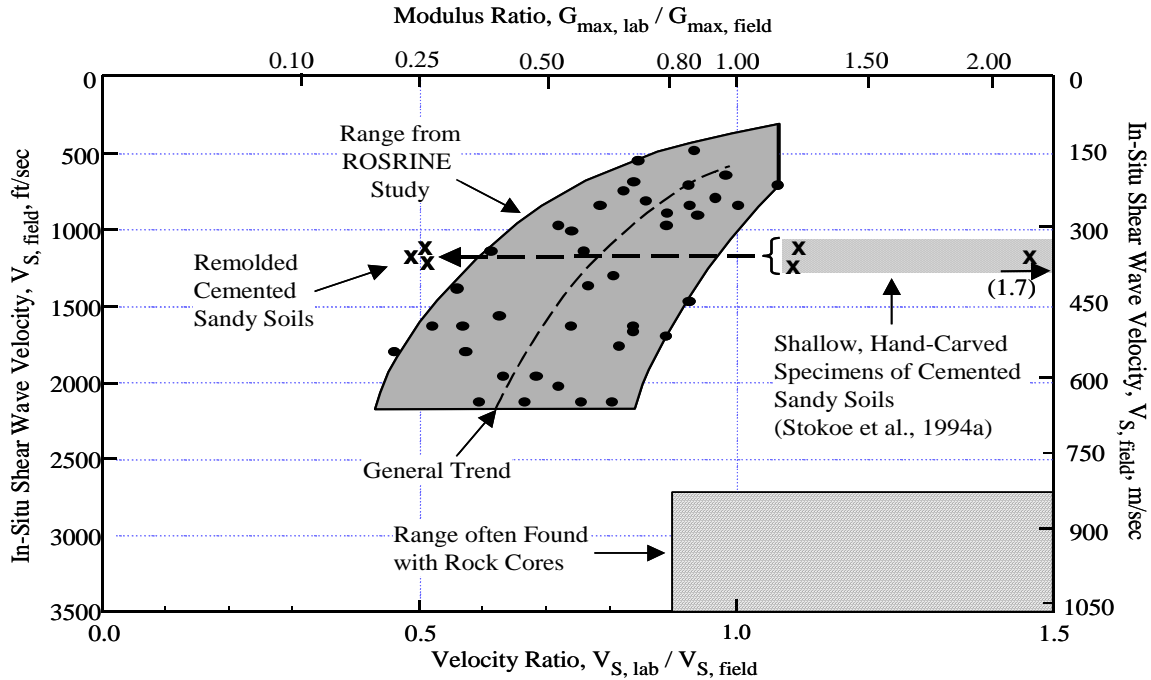


Figure 29 Variation in the Ratio of Laboratory-to-Field Stiffness ($V_{S, \text{lab}} / V_{S, \text{field}}$) with respect to the In Situ Value of V_S

Figure 29 also shows results from three tests with hand-carved samples of cemented soils (Stokoe et al., 1994a). Clearly, in the vicinity of the in situ seismic tests, the stiffer samples were recovered and tested in the laboratory (because $V_{S, \text{lab}} / V_{S, \text{field}} > 1.1$). Importantly, when these intact specimens were remolded, the velocity ratio decreased to about 0.5 where they behaved like an uncemented sand during handling and sample preparation. This comparison suggests that some, if not most, of the loss in stiffness in the laboratory samples tested in the ROSRINE study results from irrecoverable damage at interparticle contacts. This is in line with the previous discussion on the effect of cementation and diagenesis on wave velocity, and the implications of sampling.

Case History No. 2 – Prediction of Earthquake Site Response

The importance of field V_S measurements in dynamic response analyses is illustrated by considering the prediction of earthquake ground motion for an idealized geotechnical site. The site is shown in Figure 30a. It is composed of four 12.5 –m thick layers of clay over bedrock. Other characteristics of the site are given in the figure. The key point in this example is that two different V_S profiles are used in the site response calculation. The first profile is shown as the “field” profile in Figure 30b and is assumed to represent the results from in situ seismic tests. The second profile is shown as the “laboratory” profile in Figure 30b. The laboratory profile was estimated using the general trend line from the ROSRINE study in Figure 29 combined with the field profile. The shear wave velocity ratios, $V_{S, \text{lab}} / V_{S, \text{field}}$, from the trend line are shown in Figure 30c. Any changes in the bedrock were ignored for simplicity.

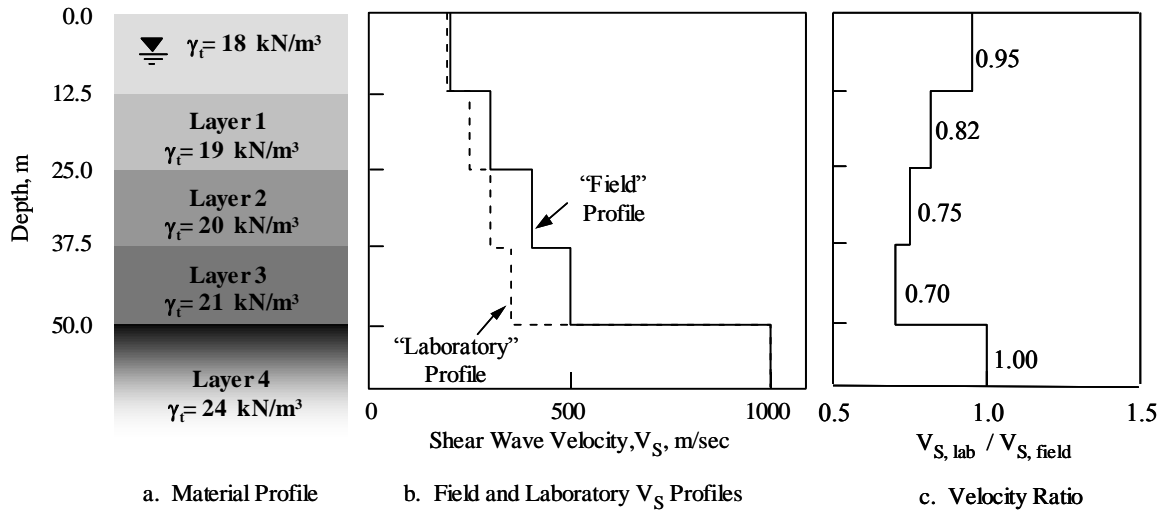


Figure 30 Idealized Geotechnical Site Used to Illustrate the Importance of In Situ Seismic Testing

Once the V_S profile of the site has been defined, the next step is to determine the nonlinear characteristics of the soil. At high-risk sites, this step involves cyclic and/or dynamic laboratory testing of intact specimens. These results are presented in terms of the variations in normalized modulus, G/G_{max} , and material damping in shear, D_S , with shearing strain amplitude, γ . The Idriss (1991) normalized modulus and material damping curves for clay have been selected to represent this step. These curves are shown in Figure 31. For simplicity, these curves are assumed to be the same for each layer.

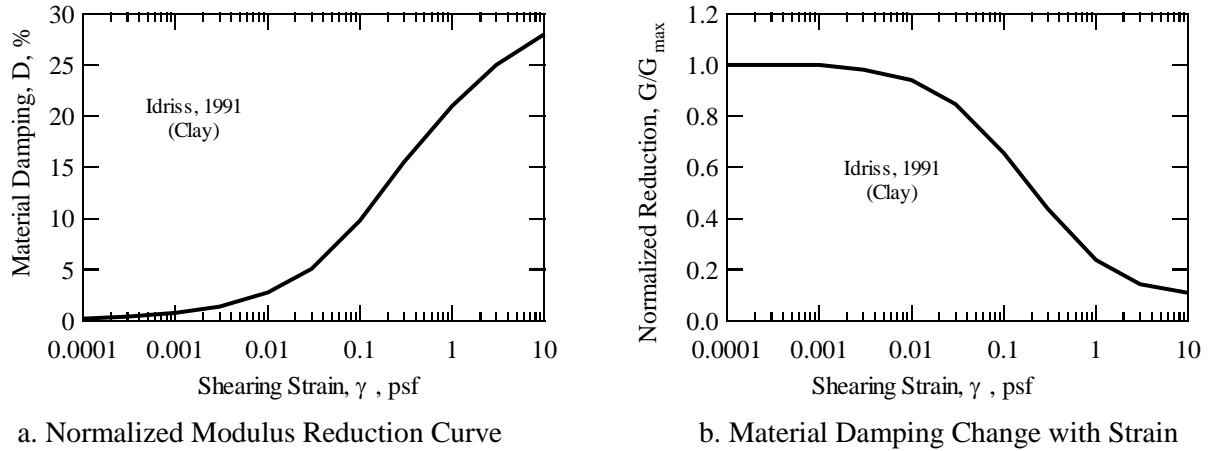


Figure 31 Nonlinear Soil Characteristics Used to Represent Each Layer

The in-situ nonlinear behavior of each soil layer is then estimated in terms of the $G - \log \gamma$ and $D_S - \log \gamma$ relationships. In equivalent linear analyses, (ProShake - 1998) as used in this example, the $D - \log \gamma$ relationship determined from laboratory testing or estimated from empirical relationships is used directly. To determine, the field $G - \log \gamma$ curve, the laboratory curve is scaled using G_{max} determined from the field seismic tests as :

$$G_{\gamma, \text{field}} = \left(\frac{G_{\gamma, \text{lab}}}{G_{\text{max, lab}}} \right) G_{\text{max, field}} \quad (22)$$

where,

$G_{\gamma, \text{field}}$ = in situ shear modulus at a shearing strain of γ ,

$G_{\gamma, \text{lab}}$ = shear modulus determine in the laboratory with an intact specimen at a shearing strain of γ ,

$G_{\text{max, lab}}$ = small-strain shear modulus determined in the laboratory, and

$G_{\text{max, field}}$ = in situ shear modulus measured by seismic testing.

The relationships between the field and laboratory G - $\log \gamma$ curves and the corresponding field and laboratory $\tau - \gamma$ curves are shown in Figure 32. (If samples are not obtained, $G/G_{\text{max}} - \log \gamma$ relationships that exist in the literature for various soil types are used in place of the laboratory normalized modulus in Equation 22.) The importance of the field V_S profile in this procedure is clearly shown in Figure 32. Also, this adjustment procedure is possible because of the link between the field and laboratory measurements created by V_S .

The final step is to subject the site to the design earthquake shaking and predict the resulting response. In this example, the rock outcrop motion shown in Figure 33 was used. An equivalent linear analysis was performed using 1.25-m thick sublayers. The outcrop motion presented in Figure 33 was transferred to the bedrock of the site, and the response at the surface was calculated using the two V_S profiles shown in Figure 30b as the initial small-strain stiffness. The results are presented in Figure 34 in terms of spectral accelerations at the ground surface. The results show that using field stiffness instead of laboratory stiffness may be more conservative (predicts higher accelerations), depending on the characteristics of the base motion (such as frequency content and intensity) and characteristics of the soil deposit (such as depth, stiffness and nonlinearity). Similar conclusions are presented by Darendeli et al. (2001). It is important to note that using lower V_S values for a soil layer results in increased of straining of the layers. In the nonlinear range, increased γ may cause a significant increase in material damping. Therefore, the energy dissipation is over-predicted.

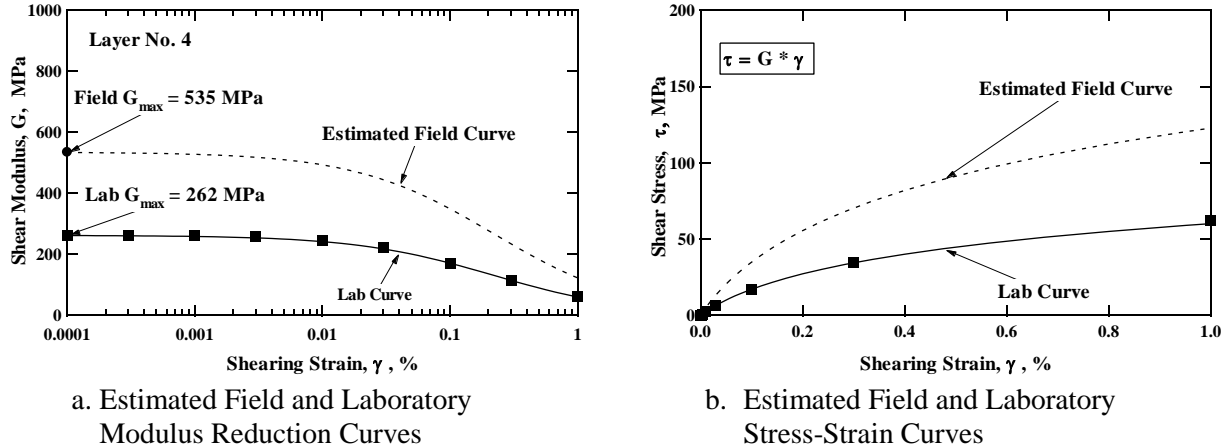


Figure 32 Comparison of the Estimated Field and Laboratory Nonlinear Stiffness Characteristics

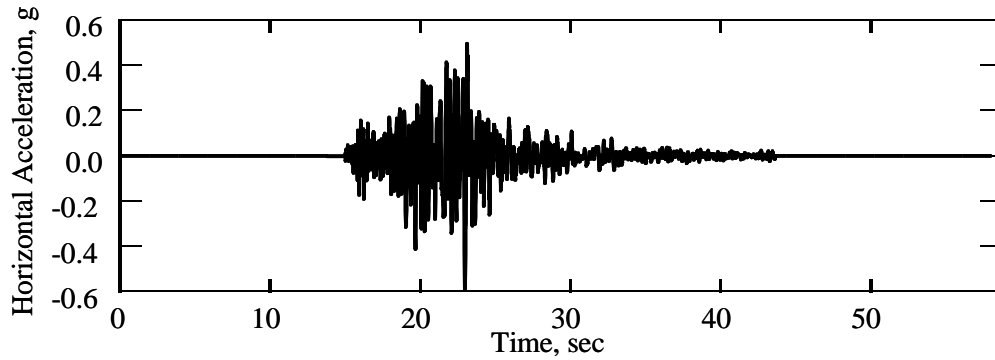


Figure 33 Rock Outcrop Motion from the Topanga 1994 Strong-Motion Record Scaled to 0.6 g

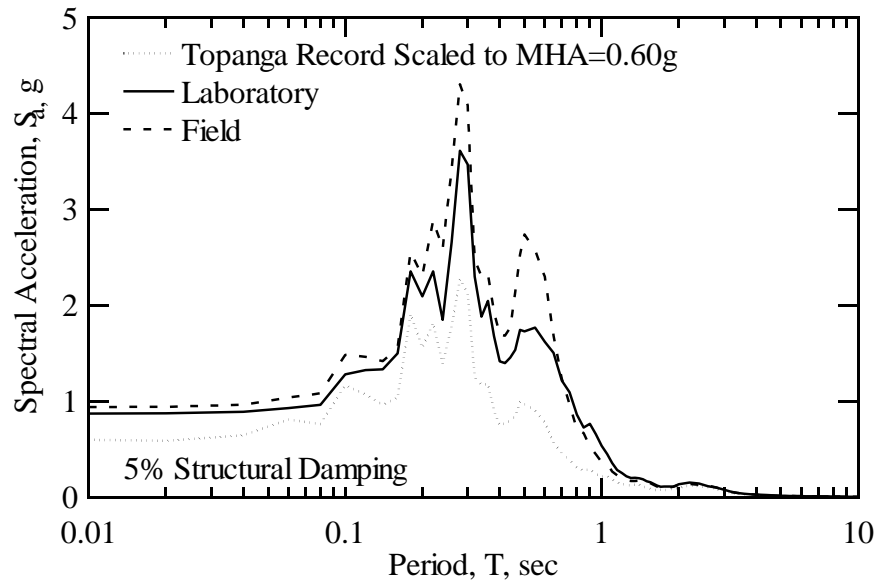


Figure 34 Comparison of Surface Spectral Accelerations Predicted for the Clay Deposit in Figure 30 Using Laboratory and Field V_S Profiles

Case History No. 3 – Evaluation of Liquefaction Resistance

The field procedure originally developed by Seed and Idriss (1971) is used around the world to evaluate the liquefaction resistance of granular soils. This procedure, termed the simplified procedure, uses blow count from the standard penetration test (SPT) correlated with a parameter representing the seismic loading on the soil, called the cyclic stress ratio. During the past two decades, various simplified procedures for evaluating liquefaction resistance based on shear wave velocity have been proposed (e.g., Dobry et al., 1981; Seed et al., 1983; Bierschwale and Stokoe, 1984; Stokoe and Nazarian, 1985; Tokimatsu and Uchida, 1990; Robertson et al., 1992; and Andrus et al., 1999) Several of these procedures follow the general format of the Seed-Idriss simplified procedure, with V_S corrected to a reference overburden stress and correlated with the cyclic stress ratio. However, nearly all of the simplified procedures have been developed with limited or no field performance data.

The procedure proposed by Andrus et al. (1999) uses field performance data from 26 earthquakes and in situ V_S measurements at over 70 sites. The case history data from this procedure, adjusted to an earthquake moment magnitude (M_w) of 7.5, is shown in Figure 35. Of the 90 liquefaction case histories shown in the figure, only two incorrectly lie in the no-liquefaction region. These two points are, however, very near the boundary. Clearly, the procedure based on field V_S measurements can be used as a supplement or in lieu of SPT and CPT procedures.

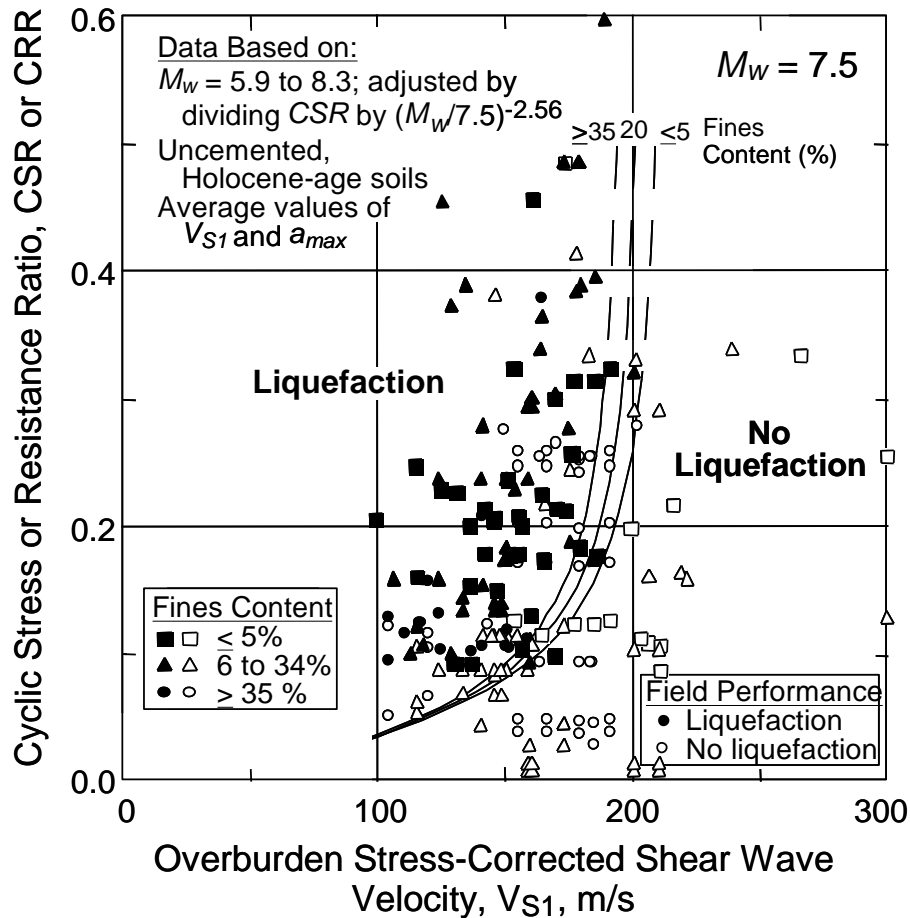


Figure 35 Curves Proposed by Andrus et al. (1999) for Delineating Liquefiable and Nonliquefiable Granular Soils Based on Field V_s Measurements

The main concerns expressed by the profession are: 1. the relative precision with which V_s must be measured since it only varies from about 100 m/s for very soft liquefiable soils to above 300 m/s for stiff soils that are not liquefiable, 2. the lack of a physical sample for identifying non-liquefiable clayey soils, and 3. the possibility of missing thin liquefiable strata sandwiched between stiffer materials (Andrus et al., 1999). In part, these objections are minimized by today's ability to measure shear wave velocity with a precision greater than 2-5%, the use seismic CPT to characterize layering and estimate soil type, and the complementary usage of other geophysical principles, such as electromagnetic properties to enhance the characterization of the soils.

The critical question is: Why does a small-strain measurement provide such a robust predictive criterion for the large-strain liquefaction phenomenon? or, in other words, to what extent does the high sensitivity of V_s to weak interparticle bonding affect the criterion captured in Figure 35? The build up in pore pressure during cyclic loading depends on the shear strain the soil mass experiences. Therefore, stiff, high shear wave velocity soils, because of density and/or cementation, will experience a lower rate of pore pressure build up and will be less likely to liquefy.

Furthermore, there are two the important unique advantages of V_s measurements for liquefaction assessment. First, the same field technique can be used to test soils containing large gravel particles and cobbles. And second, V_s measurements can also be performed in the laboratory during liquefaction studies to form a link between the field and laboratory.

Case History No. 4 – Evaluation of Soil Improvement from Blasting

In terms of process monitoring, V_S measurements offer the opportunity to track changes in material stiffness from planned or unplanned processes. In this case history, a pilot study of blast densification was conducted. The target layer was a loose fine silty sand that was approximately 7 to 11 m below the ground surface. The water table at the time of blasting was about 0.8 m below the surface. SASW testing was employed in the monitoring program. Results were also available from seismic CPT tests that were conducted before blasting.

The results of the monitoring program are shown in Figure 36. The before-blast measurements indicate a relative loose layer (average $V_S \cong 180$ m/s), with good agreement between the V_S profiles from SASW and SCPT testing (Figure 36a). A significant reduction in V_S was measured one day after blasting, as shown in Figure 36b. This reduction reflects the residual excess pore water pressure (i.e., lower effective stress) and the disturbance of the medium which leads to a loss in the stiffening effects of aging and diagenesis. The sand stiffness, and the stiffness of the overlying soil layers, increased with time after blasting, as the excess pore water pressure dissipated (Figure 36c). Interestingly, 10 months after blasting, the loose sand had not regained the stiffness it had before-blasting (Figure 36d - average $V_S \cong 160$ m/s). However, the material in the top 1.4 m at the site was stiffer than before blasting (This change is largely justified by the water table being approximately 2 m below the ground surface at the 10-month measurement time).

Based on the V_S measurements, blasting was ineffective. One possible reason is that the energy level was too high. The liquefaction resistance of the loose sand can be estimated with the after-blasting values of V_S . An earthquake with $M_W = 7.5$ would have to create a cyclic stress ratio in excess of ~ 0.1 in the lower portion of the layer to cause the loose sand to liquefy.

Case History No. 5 – Evaluation of a Concrete-Lined Tunnel and the Surrounding Host Rock

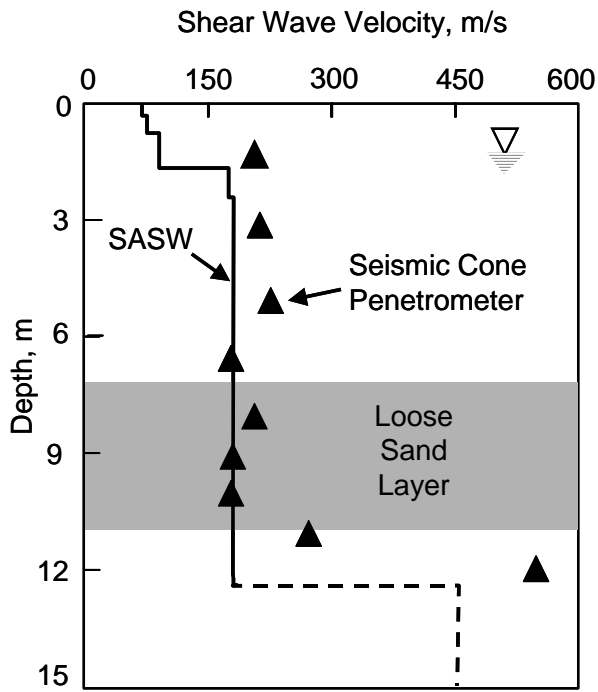
Many uses of V_S measurements involve profiling constructed systems and their geotechnical foundation materials to assist in engineering analyses and forensic studies. Pavement investigations with the seismic pavement analyzer (SPA) are one example (Nazarian et al., 1995). A forensic study of a concrete-lined tunnel in rock is described next. A generalized cross section of the tunnel is shown in Figure 37a. The tunnel is approximately 3 m in diameter, with a concrete liner that has a nominal thickness of 30 cm.

An extensive investigation was conducted in which SASW testing was performed at more than 100 locations along the longitudinal axis of the tunnel. SASW testing was performed with hand-held hammers as sources and accelerometers as receivers. The accelerometers were held magnetically to metal disks attached to the liner. This general configuration is shown in Figure 37b. Testing was conducted to profile along two planes into the liner-rock system. One profile was along the springline, and the other profile was near the crown as illustrated in Figure 37b.

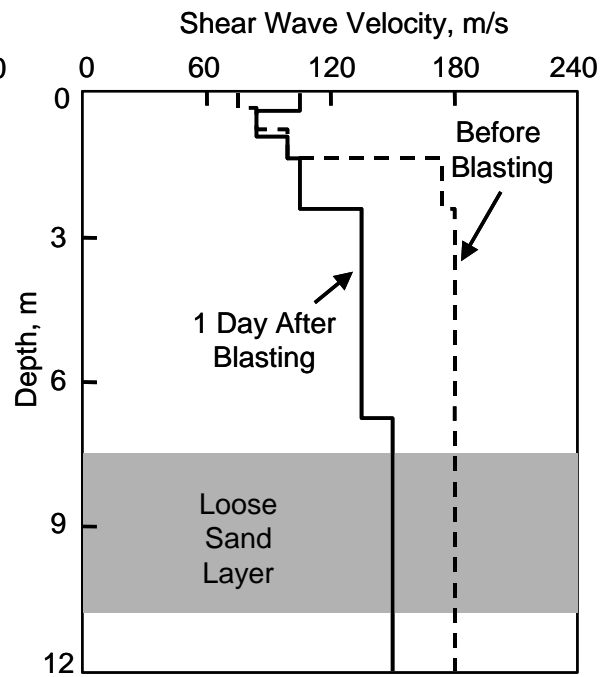
The SASW testing program was designed to investigate the following: 1. the thickness and quality of the concrete liner in the springline and crown areas, 2. the thickness and quality of any grout in the area of the crown, 3. the identification of any voids in the crown area, and 4. the stiffness and variability of the rock behind the liner. (Grouting in the crown area was done some time after construction of the liner.) The program successfully answered these questions. Examples are given below.

The results of one field measurement with a pair of receivers spaced 1.2 m apart are shown in Figure 38a. The results are excellent, as shown by the continuous “sawtooth” phase relationship (shown as wrapped phase). These results were possible mainly because the high wave velocities of both the concrete and surrounding rock allowed a significant amount of high-frequency energy to be transmitted along the tunnel axis. (These results are viewed in the field during testing, so that one can immediately judge how well the test is being conducted and determine if any adjustments to the testing procedure should be made.)

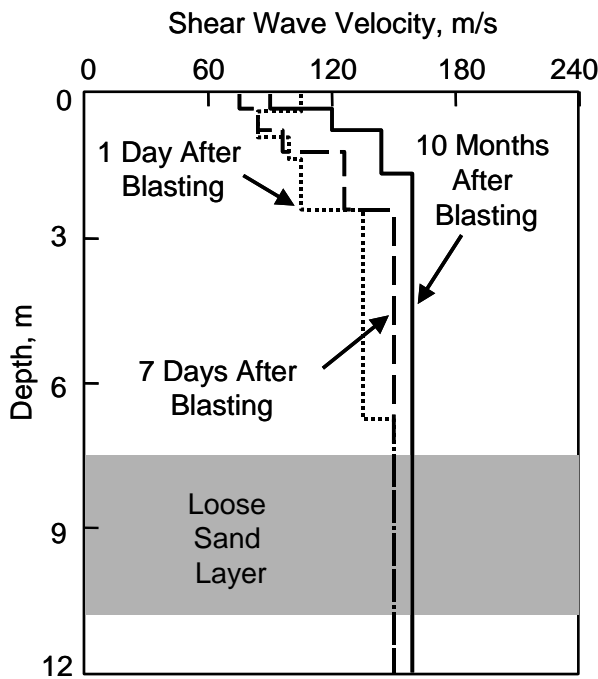
The composite dispersion curve at this location is shown in Figure 38b, with each portion of the curve identified according to receiver spacing. The theoretical match to the experimental dispersion curve is shown in Figure 39a, and the resulting stiffness profile is shown in Figure 39b. The inversion model used in these preliminary analyses was based on a flat, horizontally-layered model. (Subsequently, the analysis for a circular cavity with concentric layers was developed, but is not shown in these figures.) The profile in Figure 39b shows a high-quality concrete liner ($V_S > 2500$ m/s) that is about 30 cm thick. At this location, the liner is in direct contact with the rock, and the rock is stiffer (and presumably stronger) than the concrete.



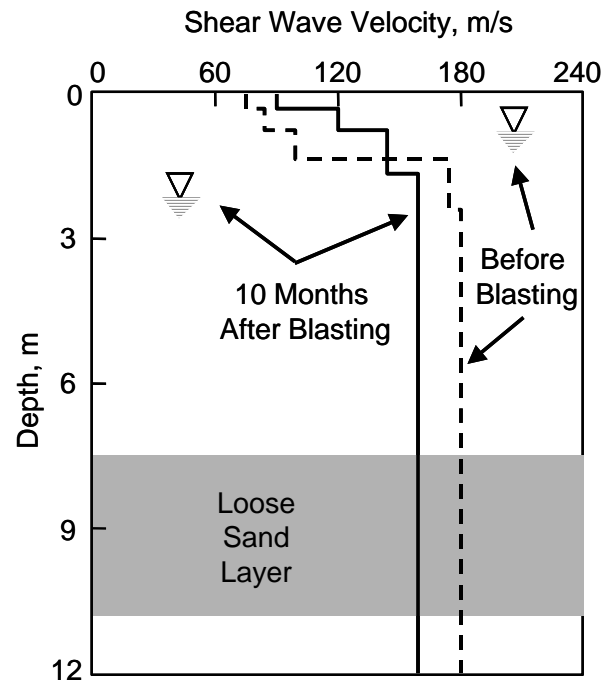
a. V_S Profile before Blasting



b. Comparison of V_S Profiles before and after Blasting



c. Change in V_S Profiles with Time after Blasting



d. Comparison of V_S Profiles before and 10 Months after Blasting

Figure 36 Evaluation of the Effectiveness of Blast Densification of a Loose Sand Layer with Field V_S Measurements

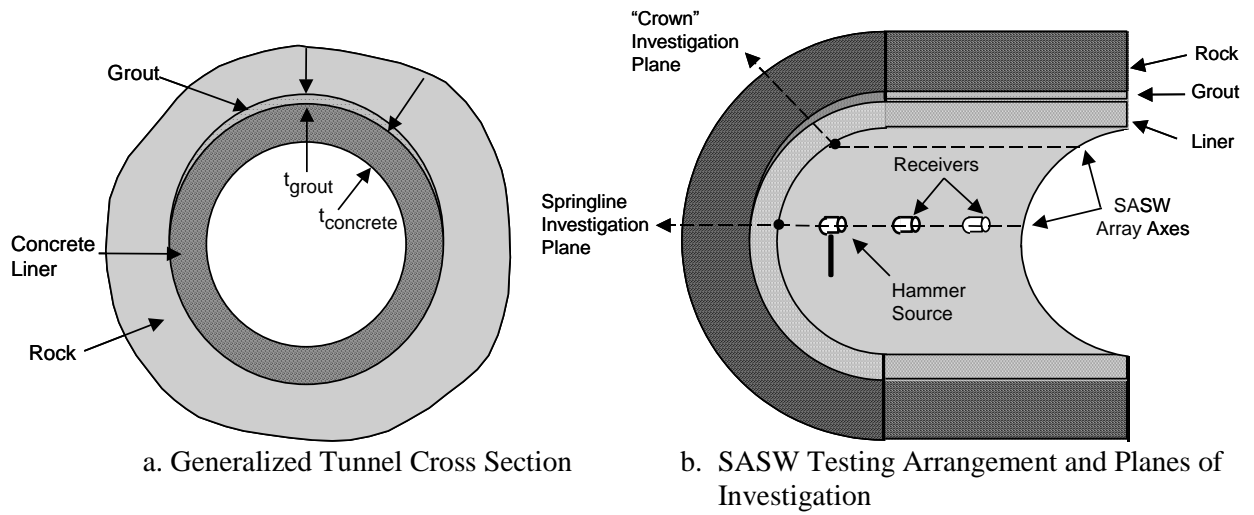
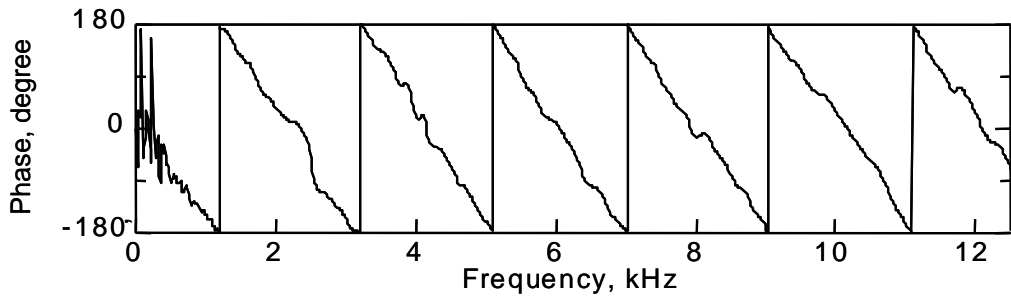
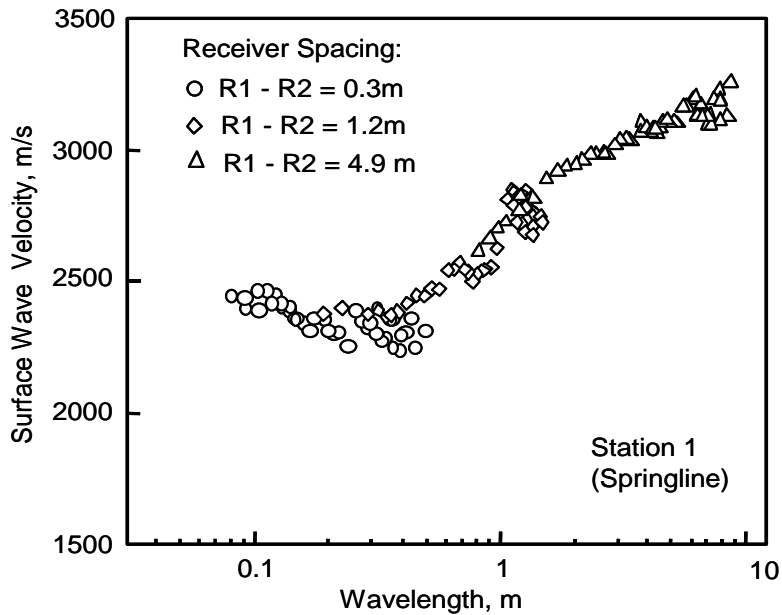


Figure 37 SASW Testing Performed Inside a Concrete-Lined Tunnel



a. Wrapped Phase from Tests with $R1-R2 = 1.2$ m



b. Composite Dispersion Curve from Three Receiver Spacings

Figure 38 Example of the Phase-Shift Measurements and Composite Dispersion Curve from SASW Testing in the Concrete-Lined Tunnel

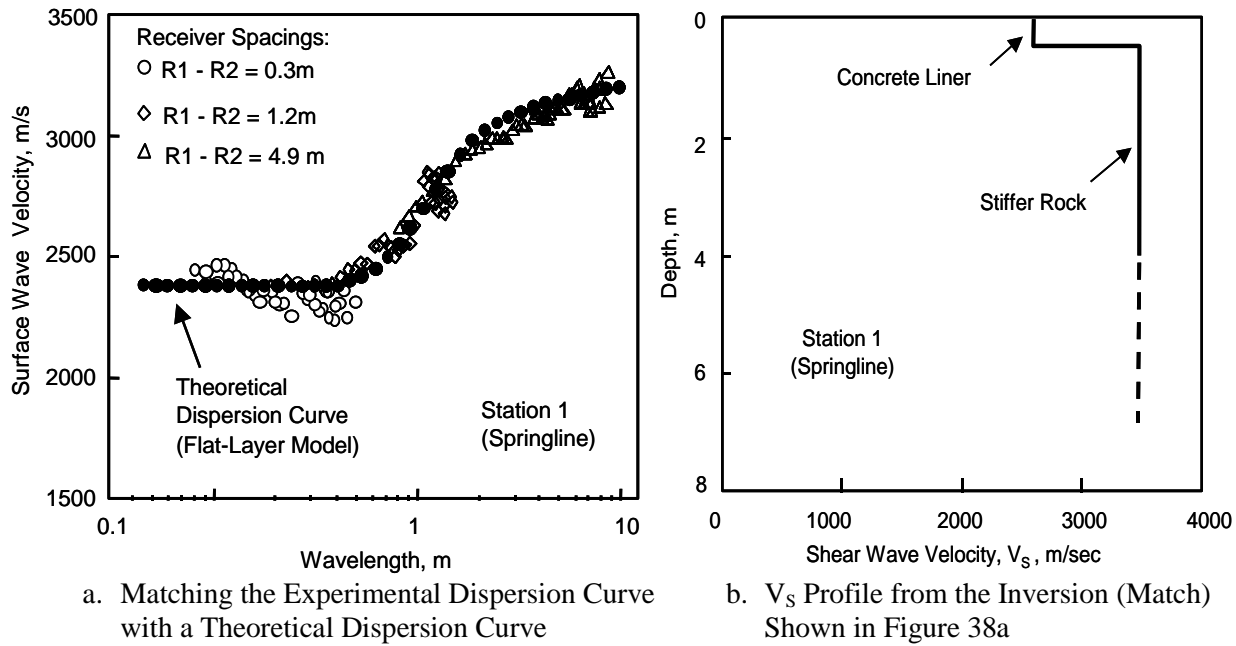


Figure 39 Example of the Inversion Process and Resulting V_S Profile from SASW Testing in the Tunnel

Results from one crown location is shown in Figure 40a. In this case, the liner is thicker than 30 cm, and there is grout between the liner and the rock. Based on the V_S values, both the concrete and grout are high quality. The concrete-grout-rock interfaces have intimate contact. Also, the rock is less stiff than the concrete at this location. Finally, some secondary grouting was attempted at this location. SASW measurements were performed before and after the secondary grouting process. A comparison of these measurements is shown in Figure 40b. They reveal that the grouting had essentially no effect.

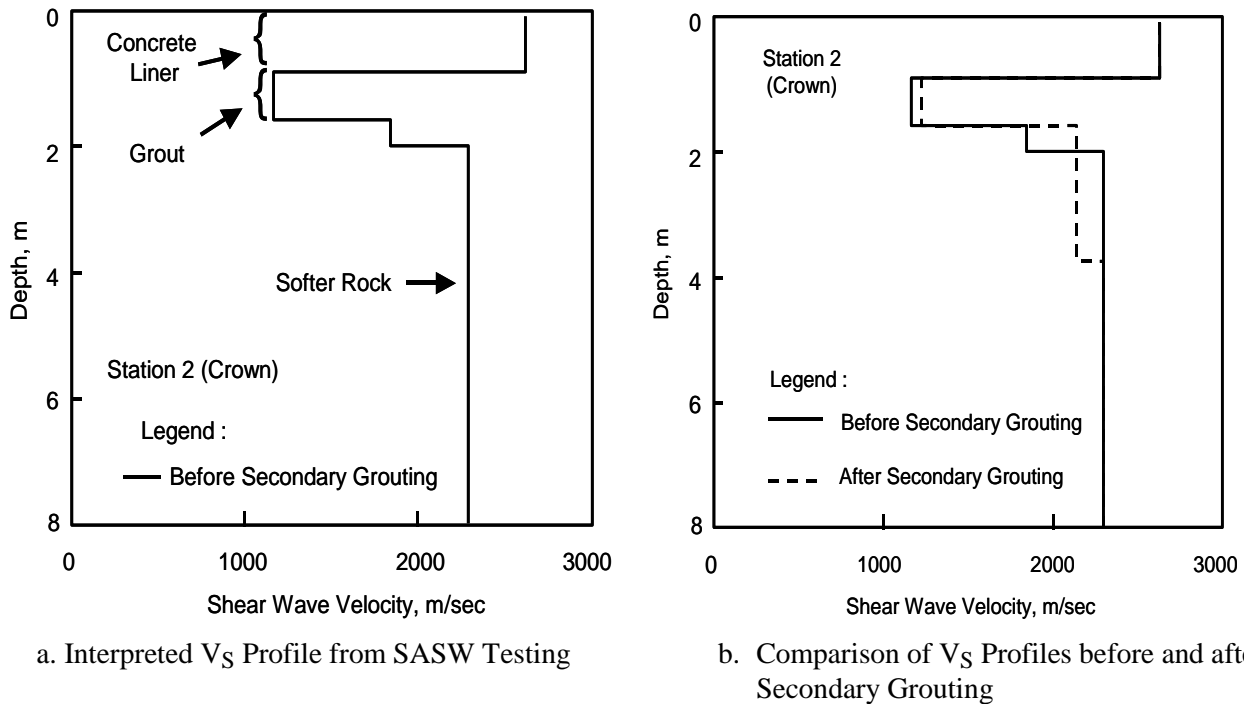


Figure 40 Examples of a V_S Profile Measured by SASW Testing near the Tunnel Crown and the Evaluation of the Effect of Secondary Grouting using “before and after” Profiles

Case History No. 6 – Process Monitoring Changes in Effective Stress (Stress Tomography)

A very important application of geophysical testing is monitoring the evolution of subsurface processes. Given the dependency between soil characteristics and elastic wave parameters discussed earlier, elastic waves can be used to monitor processes such as: changes in effective stress due to loading, unloading or pore pressure changes (as predicted in Equations 14 through 17); changes in stiffness due to stress relaxation and de-cementation (e.g., during excavation), the evolution of stiffness in creeping granular materials (e.g., cavities filled with granular salt and grains in silos); and cementation is stabilized soil systems, among others.

Monitoring the evolution of the state of effective stress is of particular interest in soils, because soil behavior is determined by the state of stress, including strength, stiffness, and contractive-dilatative tendency. Figure 41 shows the evolution of P-wave velocity within the backfill behind a retaining wall. The model wall is $H=0.8$ m high, and filled with sand. The wall acts on 4 load cells that permit measuring the force applied by the backfill onto the wall as the wall is moved relative to the backfill. The P-wave velocity normal to the wall is determined with piezoelectric transducers buried in the backfill at different depths z from the top of the wall. The measured horizontal force and horizontal P-wave velocity at $z=0.4H$ are plotted versus wall displacement in Figure 41. As the wall is moved away from the retained fill, the force decreases relaxing the state of stress towards Rankine's k -active condition, reaching 1% wall displacement. Then, the wall is pushed against the retained fill and removed again.

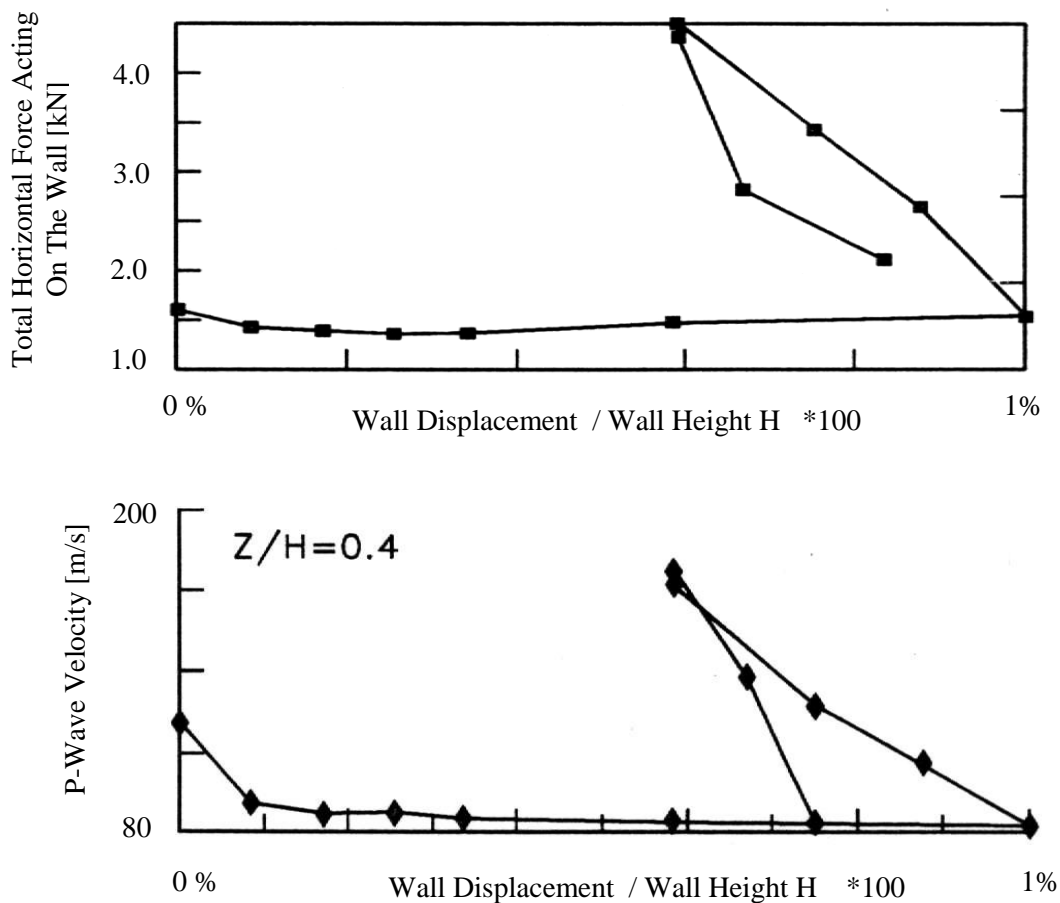


Figure 41 Retaining Wall - Monitoring the evolution of internal stresses with P-wave velocities. The top frame shows the force acting against the wall (monitored with 4 load cells). The lower frame shows the evolution of the horizontal P-wave velocity measured in the backfill behind the wall, at depths $z=0.4 H$ from the top of the wall (Santamarina and Potts, 1994).

The methodology can be applied to monitor various geotechnical systems such as stress changes in piling projects, underpinning, scouring effects on foundation stability, soil improvement, tunnels, dam foundations, load distribution under complex structural systems (Fernandez et al., 2001). Furthermore, it can be complemented with tomographic imaging to render a picture of the spatial distribution of the state of stress in the soil mass (Santamarina, et al., 1994).

SPECULATION ON FUTURE DEVELOPMENTS

The acceptance and credibility of geophysical testing within civil engineering has changed significantly in the last 40 years. In the 1960's, the prevailing sentiment was that geophysical measurements were obscure and dubious, reminiscent of the rabadomantes (water diviners) whose predictions were random or would satisfy the known expectations. Improvements in the credibility of geophysical testing have been led by seismic testing, which is becoming firmly embedded in all types of non-destructive investigations and evaluations in civil engineering. (Among the most outstanding early successes was the application of common depth point seismics in petroleum exploration in the 1960's; major developments in petroleum geophysics followed.)

It can be stated without hesitation that the role of geophysical testing in near-surface characterization will continue to grow. This activity will likely evolve into a geophysical engineering discipline, where engineering needs and concepts will dominate.

The growth of geophysical engineering needs to involve four areas: Instruction, Industrialization (automation), Integration, and Innovation.

1. **Instruction.** Innovation and growth in geophysical testing, its implementation in practice, and its proper utilization will remain hampered by lack of proper understanding and training. Therefore, geophysical principles, testing and interpretation (non-destructive evaluation included) must be incorporated in civil engineering undergraduate and graduate curricula.
2. **Industrialization** or automation is critically needed to facilitate the widespread use of geophysical testing by the profession. Automation will lead to the generation of subsurface images that can be visualized quickly and efficiently. This is a major advantage in itself, as it will allow modifying the testing program during the execution of the measurements to obtain the needed resolution and certainty in the results.
3. **Integration** implies the fusion of data from multiple testing techniques. Data fusion will provide more comprehensive subsurface information, improve diagnostic capabilities, and support optimal engineering decision making.
4. **Innovation.** The availability and usage of new and powerful tools for subsurface characterization will open the doors to alternative construction practices. But innovation must also take place from within the geophysical community, for example, by exploring new physical phenomena as well as processing/interpretation paradigms.

Numerous improvements and exciting new applications will result. Several examples, again centered around seismic testing, are listed below:

- *Enhanced Analysis.* Full waveform analysis to improve today's ability to determine material parameters (such as velocity and attenuation), and their spatial distribution (including layers, inclusions and anomalies). The increased application of successive forward modeling in today's analyses is a step in the right direction. Advanced signal processing and involved inversion algorithms will follow.
- *Integration.* (1) Implementation of multiple, complementary geophysical tests (e.g., stress-wave and electromagnetic-wave based methods), followed by data integration (taking into consideration classical geomechanical field and laboratory test results as well) through physically-based data fusion. (2) Identification of soil type from combined use of V_s and D_s spectral measurements (augmented with other complementary measurements). (3) Determination of engineering design parameters including constitutive parameters in design tools.
- *Enhanced field testing and analysis:* (1) Fast deployment of transducers (which may involve low-cost, high-response microelectronics in use-and-lose fashion), complemented with automation and smart analysis and interpretation. (2) On-the-fly measurements of V_s profiles by rolling SASW equipment. (3)

Continued improvement in near-surface logging techniques for rapid vertical profiling. (4) Large strain field testing to determine non-linear properties in situ. (5) Improved modeling, recording and interpretation of near-field motions to assess soil parameters, including damping, through effective "local" tests. (6) Innovative test procedures, advanced signal processing, and inversion algorithms to overcome some of the inherent limitations in near-surface testing (e.g., noisy environment, poor coupling, energy-frequency trade-off in seismic sources in soils, limited access to the boundaries of the unknown region for tomographic imaging).

- *Imaging.* (1) Spatial distribution of material properties and identification of anomalies through robust tomographic images. (2) Continued improvement in state of stress evaluation from seismic measurements leading to stress tomography. (3) Eventually, non-intrusive, 3D subsurface imaging capabilities will be developed, as well as forward visualization in directionally driven penetrometers for high resolution studies.
- *New/unexplored physical principles.* Possible examples include dynamic energy coupling (e.g., electroseismic and seimoelectric effects) and non-linear dynamic effects (e.g., stochastic resonance).

SUMMARY AND CONCLUSIONS

New engineering demands require advanced characterization techniques. Geophysical testing present unique advantages to satisfy these needs. The role of geophysical testing in civil engineering has increased steadily over the past several decades, primarily through the development of a wide range of nondestructive tests procedures. These developments resemble those in medical diagnosis in the twentieth century, which led to unprecedented growth in medicine and medical practice. It is speculated that the role of geophysical testing in near-surface characterization will continue to grow, and the field will evolve into a geophysical engineering discipline where engineering needs and concepts will dominate. Yet, further growth will require Instruction, Industrialization (automation), Integration, and Innovation.

Geophysical tests are based on fundamental physical principles and phenomena, such as stress and electromagnetic wave propagation, gravity, magnetism, electricity, and gamma radiation. Some of the measured parameters are relevant engineering soil parameters (e.g., mass density, stiffness). Others maintain first order physical relation to engineering parameters (e.g., permittivity and volumetric moisture content, which is the void ratio in saturated soils from which the undrained critical state strength can be determined). There are some weaker relations that are still most valuable to the geotechnical profession; this is particularly true for the dependency between S-wave velocity to state of effective stress in freshly remolded soils.

Geophysical tests are supported by robust analysis and interpretation tools (signal processing and inverse problem solving). Many of these tools have been developed for petroleum exploration. Recent developments and current efforts focus on the special characteristics and needs in near-surface geophysical testing to address geotechnical and geoenvironmental engineering requirements. An important advantage of geophysical studies is the ability to perform the same test both in the laboratory and in the field, allowing for parametric studies to enhance field interpretation.

This article centered on stress-wave based methods, in the context of geotechnical materials. Salient observations follow:

- Body waves within the medium can be either compression and shear waves. Interfaces allow other types of particle motion causing other propagation modes such as surface Rayleigh waves and Love waves.
- The wavelength is the spatial scale of a propagating wave. It determines the ability of a wave to detect an anomaly or layer, affects the near-field distance to a source, and must be carefully considered in experimental design (both field and laboratory studies). The period is the temporal scale of the wave; for all practical purposes in relation to near surface characterization, stress wave propagation in saturated soils is an undrained phenomenon.
- Stress wave measurements are small-strain perturbations, with strain levels lower than 0.001%. Therefore, inferred geomaterial properties are "elastic", small-strain properties (the shear modulus is G_{max} , and Poisson's ratio can be lower than 0.1 in unsaturated soils).
- Stress wave parameters (velocity and attenuation) reflect the saturation of a soil, the state of effective stress, inherent and stress induced anisotropy, cementation and other diagenetic effects. The presence of

finer and soil plasticity leads to frequency dependent damping. The stiffening effects of cementation and diagenesis can be readily lost during stress relaxation, such as sampling.

- Field testing can be intrusive or nonintrusive, active or passive. While nonintrusive methods avoid the cost and potential environmental consequences of drilling or penetration, intrusive techniques reduce the difficulties associated with non-unique interpretation and allow for enhanced resolution.
- Laboratory testing soils with stress waves requires pressure cells to attain the proper state of effective stress. Standard geotechnical test devices can be readily adapted to measure P- and S-wave velocity with piezoelectric transducers. The measurement of attenuation is more challenging. The resonant column remains the most convenient device for this purpose.

The selected case histories illustrate some uses of stress waves in geotechnical engineering. Traditional field and laboratory measurements in geotechnical earthquake engineering are shown and the effect of sampling leading to lower stiffness is highlighted; therefore, proper dynamic response predictions require adequate field testing. It is shown that while stress-wave velocity depends on the small-strain stiffness, it can be utilized to predict liquefiable conditions because early pore pressure buildup is related to the stability of the granular skeleton (which is related to its small-strain stiffness). Newer applications are also presented, including forensic studies (tunnel investigation), and process monitoring (blast densification and evolution of the state of stress).

ACKNOWLEDGEMENTS

The writers sincerely appreciate the opportunity given by the organizers of this conference to present these results. The patience and understanding of Mr. Max Ervin is especially appreciated.

Support from the California Department of Transportation, the National Science Foundation, NSERC-Canada, the National Institute of Standards and Technology, the United States Geological Survey, INTEVEP-Venezuela, and the ROSRINE project is gratefully acknowledged. Interaction, encouragement and guidance from Dr. Donald Anderson, Mr. Enrico Brignoli, Prof. I.M. Idriss, Prof. Michele Jamialkowski, Dr. Robert Nigbor, Dr. Robert Pyke, Dr. Clifford Roblee, Dr. Walter Silva, and Prof. T. Leslie Youd are appreciated. Finally, the assistance of colleagues and graduate students at the University of Texas and at Georgia Tech is greatly appreciated. In particular, Prof. Ronald D Andrus, Dr. James Bay, Prof. Giovanni Cascante, Mr. Mehmet Darendeli, Prof. Moheb Fam, Dr. Americo Fernandez, Prof. Dante Frata, Prof. Katherine Klein, Dr. Sung-Ho Joh, Prof. Young-Jin Mok, Prof. Soheil Nazarian, Prof. Glenn Rix, Prof. Jose M. Roesset, Mr. Brent Rosenblad, and Dr. Ignacio Sanchez-Salinero made significant contributions in support of this work.

Several of the case histories involved work with geotechnical consulting firms and their clients. Permission to publish the results is appreciated. Sincere thanks are extended to Dr. Edward Kavazanjian of GeoSyntec Consultants in Huntington Beach, California and Mr. Syed Ahmed of Law Engineering and Environmental Services in Houston, Texas for their stimulation, guidance and foresight on some very interesting projects.

REFERENCES

- Achenbach, J. D. (1975), *Wave Propagation in Elastic Solids*, North Holland, 425p.
- Aki, K., and Richards, P.G. (1980). *Quantitative Seismology Theory and Methods*, W.H. Freeman and Company, Vol. I.
- Allen, N. F., Richart, F.E., Jr. and Woods, R.D. (1980). "Fluid wave propagation in saturated and nearly saturated sands," *Journal of Geotechnical Engineering*, ASCE, Vol. 106, No. GT3, March, pp. 235-254.
- American Society for Testing and Materials (ASTM) (1997). "Provisional standard guide for expedited site characterization of hazardous waste contaminated sites", ASTM PS 85-96.
- Anderson, D.G., and Woods, R.D. (1975). "Comparison of field and laboratory shear moduli," *Proceedings In Situ Measurement of Soil Properties*, ASCE, Vol. I, Raleigh, N.C., pp 66-92.

- Andrus, R.D., Stokoe, K.H., II and Chung, R.M. (1999), "Draft Guidelines for Evaluating Liquefaction Resistance Using Shear Wave Velocity Measurements and Simplified Procedures," NISTIR 6277, National Institute of Standard and Technology, Gaithersburg, MD, 121p.
- Arthur, J.R.F. and Menzies, B.K. (1972). "Inherent anisotropy in a sand," *Geotechnique* 22, No. 1, pp. 115-128.
- Baldi, G., Bellotti, R., Ghionna, V., Jamiolkowski, M. and Pasqualini, E. (1981). "Cone resistance of a dry medium sand," X ICSMFE, Stockholm.
- Bellotti, R., Jamiolkowski, M., Lo Presti, D.C.F. and O'Neill, D.A. (1996). "Anisotropy of small strain stiffness of ticino sand," *Geotechnique*, Vol. 46, No. 1, pp. 115-131.
- Bierschwale, J.G. and Stokoe, K.H., II (1984), "Analytical Evaluation of Liquefaction Potential of Sands Subjected to the 1981 Westmorland Earthquake," Geotechnical Engineering Report GR-84-15, University of Texas at Austin, 231p.
- Bolt, B.A. (1976). Nuclear Explosions and Earthquakes, W.H. Freeman and Company.
- Bourbié, T., Coussy, O. and Zinszner, B. (1987), Acoustics of Porous Media, Gulf Publishing Company, Houston, 334p.
- Brignoli, E.G., Gotti, M. and Stokoe, K.H., II (1996). "Measurements of shear waves in laboratory specimens by means of piezoelectric transducers," *Geotechnical Testing Journal*, GTJODJ, Vol. 19, No. 4, December, pp. 384-397.
- Brignoli, E.G., Fretti, C., Jamiolkowski, M., Pedroni, S. and Stokoe, K.H., II (1997). "Stiffness of gravelly soils at small strains," XIVth International Conference on Soil Mechanics & Foundation Engineering, Hamburg, Germany, September 6-12.
- Burger, H.R. (1992). Exploration Geophysics of the shallow subsurface, Prentice Hall, Englewood Cliffs, New Jersey.
- Campanella, R.G., Robertson, P.K., and Gillespie, D. (1986). "Sesimic cone penetration test," Use of in Situ Tests in Geotechnical Engineering, Proceedings, In Situ '86, ASCE Geotechnical Specialty Publication No. 6, Samuel P. Clemence (ed.), Balcksburg, VA, June, pp. 116-130.
- Cho, G. C., and Santamarina, J. C. (2000), "Partially saturated particulate materials - particle level studies, *ASCE Geotechnical Journal* (in print).
- Daniels, J. I. and Keys, W.S. (1992). "Geophysical well logging for evaluating hazardous waste sites," Investigations in Geophysics No. 5, Geotechnical and Environmental Geophysics. S. H. Ward (ed.), Vol. 1, pp. 263-286.
- Darendeli, M.B., Stokoe, K.H., II, and Rathje, E.M. (2001). "Importance of confining pressure on nonlinear soil behavior and its impact on earthquake response predictions of deep sites," Fifteen International Conference on Soil Mechanics and Geotechnical Engineering, August 27-31, 2001, Istabul, Turkey (accepted for publication).
- Department of the Army (1995). "Engineering and Design: Geophysical Exploration for Engineering and Environmental Applications, Engineer Manuel EM 1110-1-1802 (31 August 19915), U.S. Army Corps of Engineers, Washington, D.C. Internet: www.usace.army.mil/linet/usace-docs/eng-manuals/em1110-1802/toc.htm.
- Dobrin, M.B. and Savit, C.H. (1988). Introduction to Geophysical Prospecting, Fourth Edition, McGraw-Hill Book Company.
- Dobry, R., Stokoe, K.H., II, Ladd, R.S., and Youd, T.L. (1981). "liquefaction susceptibility from s-wave velocity," Proceedings, In Situ Tests to Evaluate Liquefaction Susceptibility, ASCE Nat. Convention, held 27 Oct., St. Louis, MO.
- Drnevich, V.P., Hardin, B.O., and Shippy, D.J. (1978). "Modulus and damping of soils by the resonant-column method," Dynamic Geotechnical Testing, ASTM STP 654, American Society of Testing and Materials, pp. 91-125.
- Dvorkin, J. and Nur, A. (1993), "Dynamic poroelasticity: A unified model with the squirt and the Biot mechanisms", *Geophysics*, Vol. 58, pp. 524-533.
- Fernandez, A. (2000), Tomographic Imaging Stress Fields in Discrete Media, Ph.D. Dissertation, Georgia Institute of Technology, Atlanta.

- Fernandez, A. and Santamarina, J. C. (2000), "The effect of cementation on the small strain parameters of sands", *Canadian Geotechnical Journal* (accepted for publication).
- Fernandez, A., Gonzalez, M., Malave, G., Alvarelos, J., and Santamarina, J.C. (2001), Stress Tomographic: Monitoring Dam foundations, Geo-Institute Conference 2001, Blacksburg.
- Fratta, D. and Santamarina, J. C. (1996), "Waveguide device for multi-mode, wideband testing wave propagation in soils", *ASTM Geotechnical Testing J.*, Vol. 19, pp. 130-140.
- Fuhriman, Mark, D. (1993). "Crosshole seismic tests at two northern california sites affected by the 1989 loma prieta earthquake," M.S. Thesis, University of Texas at Austin, May.
- Glaser, S. and Nelson, P. (1992), Acoustic emissions produced by discrete fracture in rocks, *International Journal of Rock Mechanics, Mining Science and Geomechanics Abstracts*, Vol. 29, no. 3, pp. 253-265.
- Ganji, V., and Gucunski, N. (1998). "Automated inversion procedure for spectral analysis of surface waves," *ASCE, Journal of Geotechnical and Geoenvironmental Engineering*, pp757-770.
- Haff, P. (1986). Booming Sands, *Scientific American*, Vol. 74, no. 4, pp. 367-381.
- Hardin, B.O. and Richart, F.E., Jr. (1963). "Elastic wave velocities in granular soils," *Journal of Soil Mechanics and Foundation Division*, Vol. 89, No. SM 1, February, pp. 33-65.
- Hardin, B. O. and Drnevich, V.P. (1972), "Shear Modulus and Damping in Soils: Measurement and Parameter Effects," *Journal of Soil Mechanics and Foundation Engineering Div.*, ASCE, Vol. 98 No. SM6, June, pp 603-624.
- Hardin, B.O. (1978). "The nature of stress-strain behavior for soils," Proceedings of the ASCE Geotechnical Engineering Division Specialty Conference, Earthquake Engineering and Soil Dynamics, Vol. 1, pp. 3-91.
- Howard, W. F. (1992). "Geophysical well logging methods for detection and characterization of fractures in hard rocks," Investigations in Geophysics No. 5, Geotechnical and Environmental Geophysics. S. H. Ward (ed.), Vol. 1, pp. 287-308.
- Idriss, I.M. (1990), "Response of Soft Soil Sites during Earthquakes," Proceedings, H. Bolton Seed Memorial Symposium, Vol. 2, pp. 273-289.
- Ishihara, K. (1967), "Propagation of compressional waves in a saturated soil", International Symposium on Wave Propagation and Dynamic Properties of Earth Materials, Albuquerque, pp. 451-467
- Joh, Sung-Ho, (1996). "Advances in interpretation and analysis techniques for spectral-analysis-of-surface-waves (SASW) Measurements," Ph.D. Dissertation, Univeristy of Texas at Austin, December.
- Kitsunozaki, C. (1980), "A New Method for Shear Wave Logging," *Geophysics*, Vol. 45, pp. 1489-1506.
- Koerner, R. Lord, A., and Deutsch, W. (1984), Determination of Prestress in Granular Soils Using AE, *Journal of Geotechnical Engineering*, Vol. 110, no. 3, pp. 346-358.
- Labo, J. (1992). A Practical introduction to borehole geophysics, Society of Exploration Geophysics.
- Lamb, H. (1904). "On the propagation of tremors over the surface of a an elastic solid," *Philosophical Transaction of the Royal Society of London* A203: 1-42.
- Lee, N.-K. J. (1993). "Experimental study of body waves velocities in sand under anisotropic conditions," Ph.D., Univeristy of Texas at Austin, May, 503 pp.
- Lee, S.H.H., and Stokoe K.H., II (1986). "Investigation of low-amplitude shear wave velocity in anistoropic material," Report GR86-6, Univeristy of Texas at Austin, 34 pp.
- Liu, H.-P., Warrick, R.E., Westerlund, R.E., Fletcher, J.B., and Maxwell, G.L. (1988). "An air-powered impulsive shear-wave source with repeatable signals," *Bulletin Seismological Society of America*, Vol. 78, No. 1, pp 355-369.
- Love, A.E.H. (1892). Mathematical Theory of Elasticity, Cambridge Univeristy, 643 pp.
- Luke, B.A. and Stokoe, K.H., II (1998), "Application of SASW Method Underwater," *Journal of Geotechnical and Geoenvironmental Engineering*, Vol. 124, No. 6, June, pp. 523-531
- Lunne, T., Robertson, P.K., and Powell, J.M. (1997), *Cone Penetrometer Testing in Geotechnical Practice*, 1st Edition, London, NY, Blackie Academic & Professional Press, 312 pp .
- Mavko, G. M., Mukerji, T. and Dvorkin, J. (1998), The Rock Physics Handbook, Cambridge University Press, New York, 329p.
- Menke, W. (1989), Geophysical Data Analysis: Discrete Inverse Theory, Academic Press, 289 p.

- Mok, Y.J., Stokoe, K.H., II and Wilson, C.R. (1988). "Analysis of downhole seismic data using inverse theory," Proceedings, Ninth World Conference on Earthquake Engineering, Vol. III, Tokyo, Japan, pp. 65-60
- NRC (2000). "Seeing into the Earth," Committee for Noninvasive Characterization of the Shallow Subsurface for Environmental and Engineering Applications, P.R. Romig, Chair, 129 pp.
- Nazarian, S., Yuan, D., and Baker M.R. (1994). "Automation of spectral analysis of surface waves method," Dynamic Geotechnical Testing II, ASTM STP1213, pp 88-100.
- Nazarian, S., Baker, M., and Crain, K. (1995). "Use of seismic pavement analyzer in pavement evaluation," *Transportation Research Record* 1505, pp.1-8.
- Nigbor R.L. and Imai T. (1994). "The suspension P-S velocity logging method," Geophysical Characteristics of Sites, ISSMFE, Technical Committee 10 for XIII ICSMFE, International Science Publishers, New York, pp. 57-63.
- Oda, M. (1972). "Initial fabric and their relationships to mechanical properties of granular material," *Soils and Foundation*, 12, No. 2, pp. 1-28.
- Orfanidis, S. J. (1996), Signal Processing, Prentice-Hall, Upper Saddle River, 798 p.
- Parkin, A.K. and Lunne, T. (1982). "Boundary effects in the laboratory calibration of a cone penetrometer for sand," Proceedings, Second European Symposium on Penetration Testing, Amsterdam.
- Pialucha, T., Guyott, C. C. H. Guyott and Cawley, P. (1989), "Amplitude spectrum method for the measurement of phase velocity", *Ultrasonics*, Vol. 27, pp. 270-279.
- Podio, A.L. (1968). "Experimental determination of the dynamic elastic properties of anisotropic rocks, ultrasonic pulse method," Ph.D. Dissertation, Univeristy of Texas at Austin, 181 pp.
- Rayleigh, L. (1887). "On waves propagated along the plane surface of an elastic solid," *Proceedings of the London Mathematical Society*, Vol. 17, pp 4-11.
- Richart, F. E., Hall, J. R., and Woods, R. D. (1970), Vibrations of Soils and Foundations, Prentice Hall, Englewood Cliffs, 414p.
- Rix, G. J., C. G. Lai, and A.W. Spang, "In Situ Measurement of Damping Ratio Using Surface Waves," *Journal of Geotechnical and Geoenvironmental Engineering*, ASCE, 126, Vol. 5, 472-480, 2000.
- Robertson, P.K., Woeller, D.J., and Finn, W.D. L. (1992). "Seismic cone penetration test for evaluating liquefaction potential under cyclic loading," *Canadian Geotech. Journal*, Vol. 29, pp. 686-695.
- Roble, C.J., Stokoe, K.H., II, Fuhrman, M.D., and Nelson, P.P. (1994). "Crosshole SH-wave measurements in rock and soil," Dynamic Geotechnical Testing II, ASTM STP1213, pp 58-72.
- Roesler, S. (1979). "Anisotropic Shear Modulus Due to Stress Anisotropy," *Journal of Geotechnical Engineering Division*, ASCE, Vol. 105, GT7, pp. 871-880.
- Sachse, W. and Pao, Y. H. (1978), "On the determination of phase and group velocities of dispersive waves in solids", *Journal of Applied Physics*, Vol. 49, pp. 4320-4327.
- Sanchez-Salinerro, I., Roesset, J.M. and Stokoe, K.H., II (1986). "Analytical Studies of Body Wave Propagation and Attenuation," Geotechnical Engineering Report GR86-15, Department of Civil Engineering, The University of Texas at Austin.
- Santamarina, J.C. and Potts, B. (1994), "On the Imaging of Stress Changes in Particulate Media -An Experimental Study-", *Canadian Geotechnical Journal*, Vol. 31, n. 2, pp 215-222.
- Santamarina, J.C., Graham, J., MacDougall, C., and Roy, V. (1994), "Tomographic Imaging Changes in Effective Stress in Granular Media (Simulation Study)", *Transportation Research Record*, no. 1415, pp. 95-99.
- Santamarina, J. C. and Cascante, G. (1996), "Stress anisotropy and wave propagation – A micromechanical view", *Canadian Geotechnical Journal*, Vol. 33, pp. 770-782.
- Santamarina, J. C. and Fratta, D. (1998), Introduction to Discrete Signals and Inverse Problems in Civil Engineering, ASCE Press, Reston, 327p.
- Santamarina, J.C., Klein, K. and Fam, M. (2000). Soils and Waves, John Wiley and Sons, In Print, Chichester, 530 p.
- Scott, R. D., (1991), Basic Acoustic Emission. Gordon and Breach Science Publishers, New York.
- Seed, H. B. and Idriss, I. M. (1971). "Simplified procedure for evaluating soil liquefaction potential," *Journal of the Soil Mechanics and Foundations Div.*, ASCE, Vol. 97, SM9, pp. 1249-1273.

- Seed, H. B., Idriss, I. M., and Arango, I. (1983). "Evaluation of liquefaction potential using field performance data," *Journal of Geotech. Engrg.*, ASCE, Vol. 109, No. 3, pp. 458-482.
- Sharma, P.V. (1997). Environmental and Engineering Geophysics, Cambridge Univeristy Press, Cambridge, U.K., 475 pp.
- Stokoe, K.H., II and Nazarian, S. (1985), "Use of Rayleigh Waves in Liquefaction Studies," Proceedings, Measurement and Use of Shear Wave Velocity for Evaluating Dynamic Soil Properties, *J. Geotechnical Engineering Division*, ASCE, May, pp. 1-17.
- Stokoe, K.H., II, Lee, J.N.-K. and Lee, S.H.-H, (1991). "Characterization of Soil in Calibration Chambers with Seismic Waves," Proceedings, 1st Int. Symposium on Calibration Chamber Testing, Potsdam, New York.
- Stokoe, K.H., II, Hwang, S.K., Lee J.N.K, and Andrus, R.D. (1994a) "Effects of various parameters on the stiffness and damping of soils at small to medium strains," by , International Symposium on Pre-failure Deformation Characteristics of Geomaterials, Shibuya, Mitachi and Miura, eds., Sapporo, Japan, September 12-14, pp. 785-816.
- Stokoe, K.H., II, Wright, S.G., Bay,J.A. and J.M. Roesset (1994b), "Characterization of geotechnical sites by SASW method," Geophysical Characteristics of Sites, ISSMFE, Technical Committee 10 for XIII ICSMFE, International Science Publishers, New York, pp. 15-25.
- Stokoe, K. H., II, Darendeli, M. B., Andrus, R. D. and Brown, L. T. (1999) "Dynamic soil properties: laboratory, field and correlation studies," Proceedings, Second International Conference on Earthquake Geotechnical Engineering, Sêco e Pinto, Editor, A.A. Balkema Publishers/Rotterdam & Brookfield, Netherlands, Vol. 3, pp. 811-845.
- Stoll, R.D., Bryan, G.M., and Bautista, E.O. (1994). "Measuring lateral variability of sediment geoaoustic properties," *J Acoustical Soc. Of Am.*, 96 (1), pp 427-438.
- Talabei, S. and Young, R. (1988), Characterizing Microseismicity associated with stope development, Second Int. Symp. Rockbursts and Seismicity in Mines, June, Mineapolis.
- Tokimatsu, K. and Uchida, A. (1990). "Correlation between liquefaction resistance and shear wave velocity," *Soils and Foundations*, Vol. 30, No. 2, pp. 33-42.
- Tokimatsu, K., Shinzawa, K., and Kuwayama, S. (1992). "Use of short-period microtremors for V_s profiling," *Journal of Geotechnical Engineering*, ASCE, 118 (10), pp. 1544-1558.
- Tokimatsu, K. (1995). "Geotechnical site characterization using surface waves," First International Conference on Earthquake Geotechnical Engineering, Vol. 3, Kenji Ishihara, editor, Tokyo, pp. 1333-13368.
- Toksoz, M.N., and Cheng, C.H. (1991), "Wave Propagation in a Borehole," in J.M. Hovem, M.D. Richardson, and R.D. Stoll (eds.), *Shear Waves in Marine Sediments*, Kluwer Academic Publishers, Dordrecht, The Netherlands.
- Ward, S. H. (1990). *Geotechnical and Environmental Geophysics, Investigations in Geophysics No. 5*, Society of Exploration Geophysics, 3 volumes.
- Winkler, K. and Nur, A. (1979), "Pore fluids and seismic attenuation on rocks", *Geophysical Research Letters*, Vol. 6, pp. 1-4.
- Winkler, K., and Nur, A. (1982), "Seismic attenuation: Effects of pore fluids and frictional sliding", *Geophysics*, Vol. 47, pp. 1-15.
- Woods, R.D. (1968). Screening of Surface Waves in Soils, *J. Soil Mechanics and Foundation Division*, Vol. 94, no 4, pp. 951-979.
- Woods, R.D. (1994). "Borehole methods in shallow seismic exploration," Geophysical Characteristics of Sites, ISSMFE, Technical Committee 10 for XIII ICSMFE, International Science Publishers, New York, pp. 91-100.

Seismic Site Response (Site Amplification)

An Introduction to Shear Beam Analysis

(Initial version prepared in 2006 in collaboration with Drs. Liangcai He and Zhaohui Yang)

Short course notes: A. Elgamal, Chicago, Illinois, April 29 – 30, 2013

1

Source of seismic disturbance:

Earthquake **Fault** slips suddenly (sideways/vertical relative motion) sending a shear-dominated string of pulses that propagate away from the fault-plane and reach the ground surface.

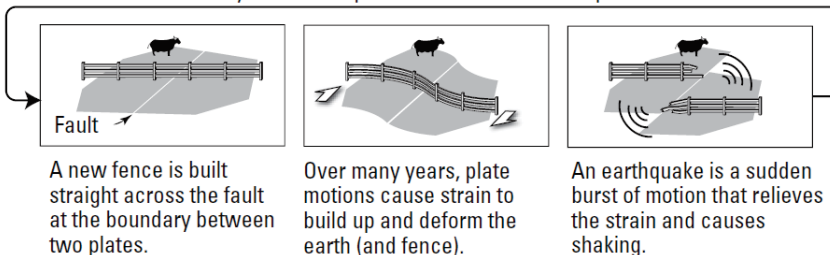
How Earthquakes Happen



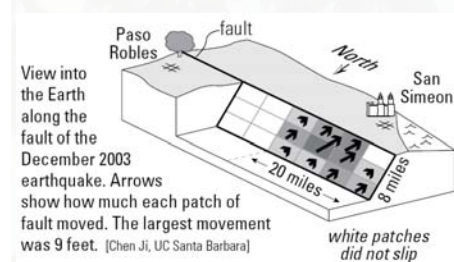
An aerial view of the San Andreas fault in the Carrizo Plain, Central California.

From: <http://pubs.usgs.gov/gip/earthq1/how.html>

Plate tectonics: The cycle of earthquakes continues because plates motions continue.



From: <http://pubs.usgs.gov/gip/2006/21/gip-21.pdf>



Short course notes: A. Elgamal, Chicago, Illinois, April 29 – 30, 2013

2

Seismic Site Response (Site Amplification)

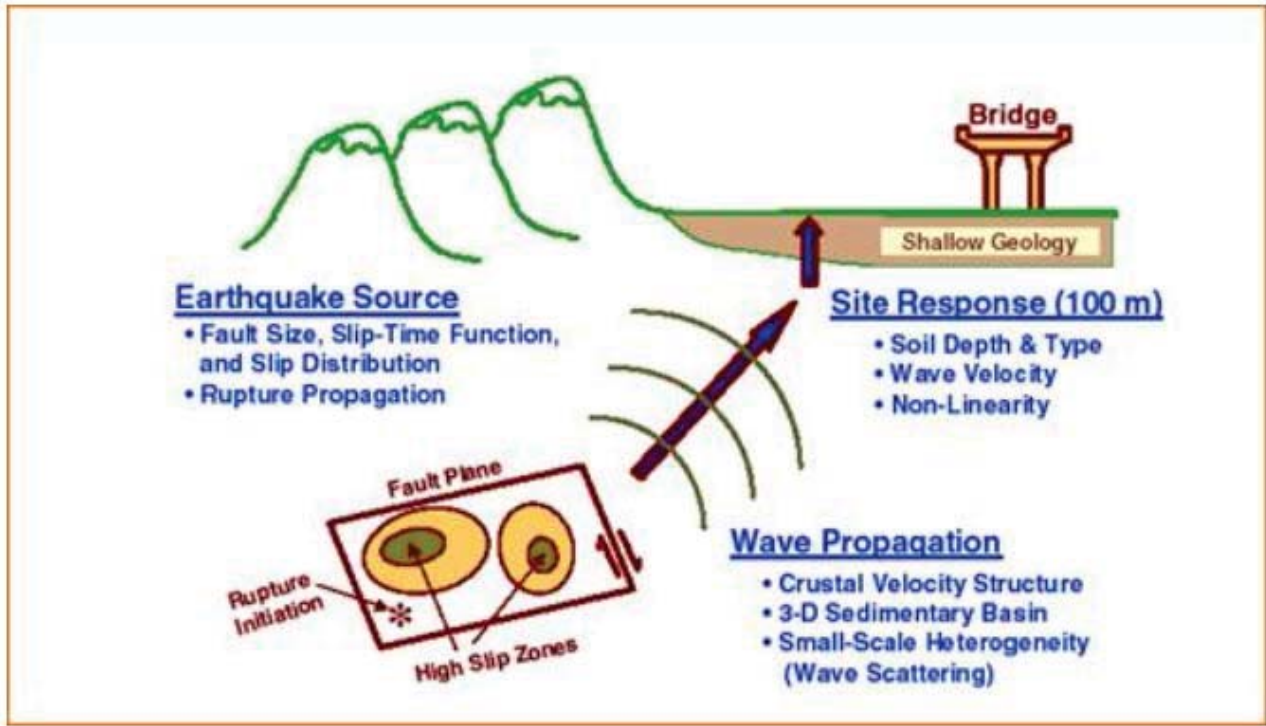
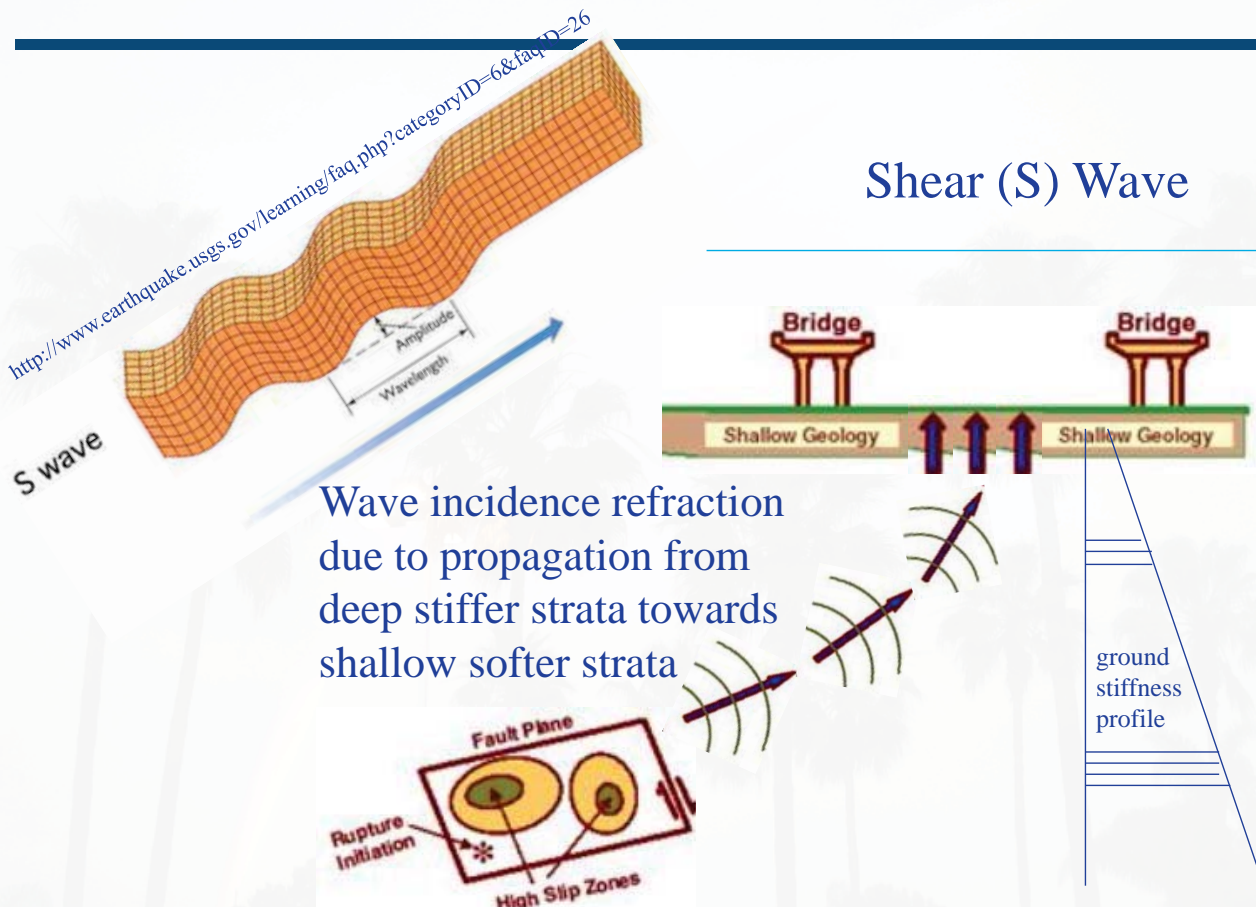


Illustration from: <http://www.uky.edu/KGS/geologichazards/risks.htm>

3

Short course notes: A. Elgamal, Chicago, Illinois, April 29 – 30, 2013

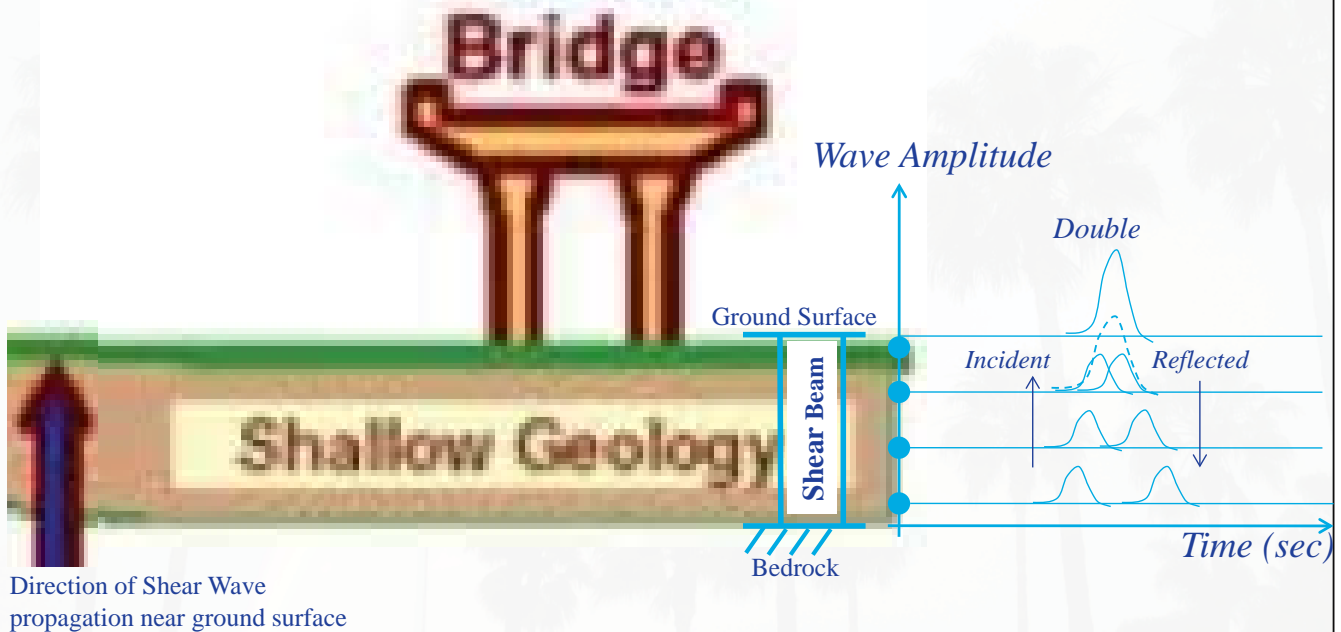


Near-surface shear-wave vertical incidence implies one-dimensional shear beam response

4

Short course notes: A. Elgamal, Chicago, Illinois, April 29 – 30, 2013

Site Amplification due to wave reflection at the ground surface

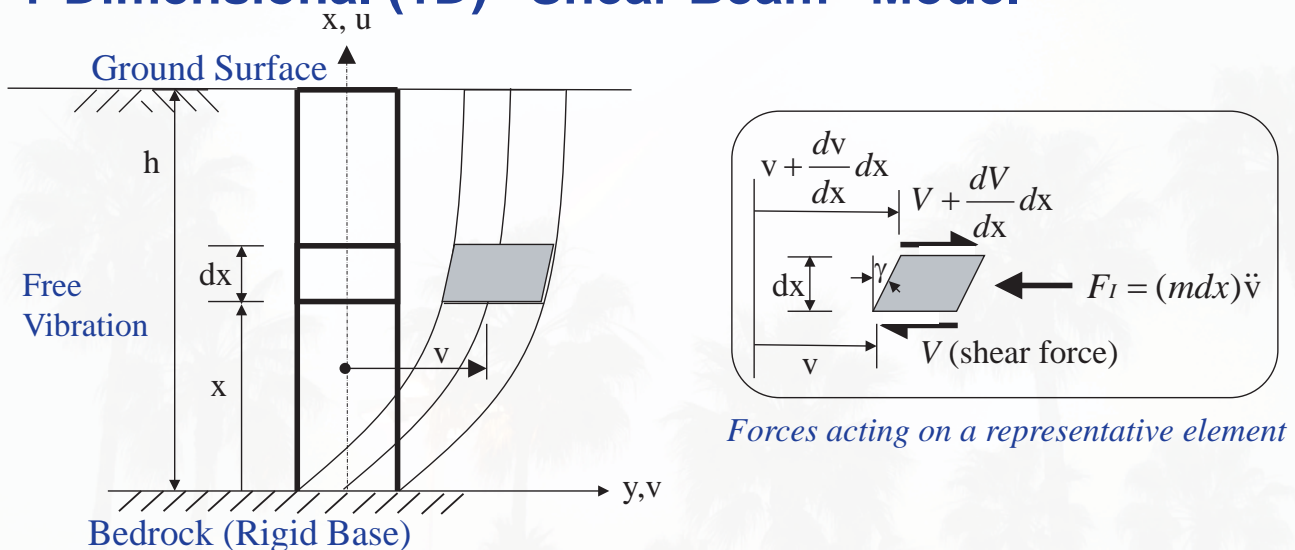


Schematic of amplification (sum of incident + reflected waves). An arbitrary train of actual seismic waves experiences similar phases of constructive wave amplification.

Short course notes: A. Elgamal, Chicago, Illinois, April 29 – 30, 2013

5

1-Dimensional (1D) “Shear Beam” Model



v = lateral displacement, $\gamma = dv/dx$ (shear strain), m = mass per unit height

V = shear force, F_I = inertia Force

- Continuous model useful for illustrating basic concepts
- Uniform shear across the section is assumed
- Represents seismic response of near-surface ground strata
- Represents first order approximation for tall framed structures

6

Short course notes: A. Elgamal, Chicago, Illinois, April 29 – 30, 2013

Equation of Motion

Shear Force $V = \tau A_r = G\gamma A_r = GA_r \frac{\partial v}{\partial x}$

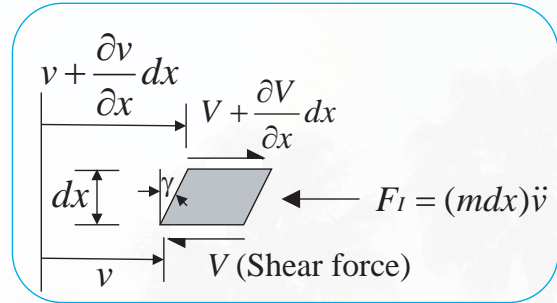
τ : shear stress, and γ : shear strain = $\partial v / \partial x$

G : shear modulus (constant with depth)

A_r : reduced cross sectional area = $k'A$

k' : coefficient of shear (1.0 for soil shear beam)

A : total cross-sectional area



Inertial Force $F_I = mdx \frac{\partial^2 v}{\partial t^2} = \rho A dx \frac{\partial^2 v}{\partial t^2}$

m : mass per unit height

ρ : mass density

$\Sigma F=0$ results in the Free Vibration Equation of Motion:

$$\rho A dx \frac{\partial^2 v}{\partial t^2} = \frac{\partial V}{\partial x} dx = GA_r \frac{\partial^2 v}{\partial x^2} dx \quad \text{or} \quad \frac{\partial^2 v}{\partial t^2} = \frac{G}{\rho} \frac{\partial^2 v}{\partial x^2} = V_s^2 \frac{\partial^2 v}{\partial x^2}$$

where $V_s = \sqrt{\frac{G}{\rho}}$ = shear wave velocity

7

Short course notes: A. Elgamal, Chicago, Illinois, April 29 – 30, 2013

Solution (by separation of variables)

$$v(x, t) = X(x) \cdot T(t) \quad \longrightarrow \quad \frac{\ddot{T}}{T} = \frac{GA_r}{m} \frac{X''}{X} = -\omega^2$$

$$\frac{d^2 T}{dt^2} + \omega^2 \cdot T(t) = 0 \quad \longrightarrow \quad T(t) = A \sin \omega t + B \cos \omega t \quad (\text{i.e., harmonic free-vibration})$$

$$\frac{d^2 X}{dx^2} + \frac{m}{GA_r} \omega^2 X = 0 \quad \longrightarrow \quad X(x) = A^* \sin \sqrt{\frac{m}{GA_r}} \omega x + B^* \cos \sqrt{\frac{m}{GA_r}} \omega x$$

Boundary Conditions

(i) at $x = 0$, $v(0, t) = 0$ "Fixed Base", so $B^* = 0$, or $X(x) = A^* \sin \sqrt{\frac{m}{GA_r}} \omega x$

(ii) at $x = h$, $V = GA_r \frac{\partial v}{\partial x} = 0$ "No shear at Ground Surface; stress - free"

$$X'(h) = 0 = A^* \sqrt{\frac{m}{GA_r}} \omega \cos \sqrt{\frac{m}{GA_r}} \omega h = 0 \quad \longrightarrow \quad \cos \sqrt{\frac{m}{GA_r}} \omega h = 0 \quad \longrightarrow \quad \sqrt{\frac{m}{GA_r}} \omega_n \cdot h = \left(\frac{2n-1}{2} \right) \pi, \quad n = 1, 2, 3, \dots$$

Frequencies

$$\omega_n = \sqrt{\frac{GA_r}{m}} \frac{(2n-1) \cdot \pi}{2h} = 0 \quad \omega_n = \sqrt{\frac{G}{\rho}} \frac{(2n-1) \cdot \pi}{2h} = 0 \quad \omega_n = V_s \frac{(2n-1) \cdot \pi}{2h} = 0 \quad n = 1, 2, 3, \dots$$

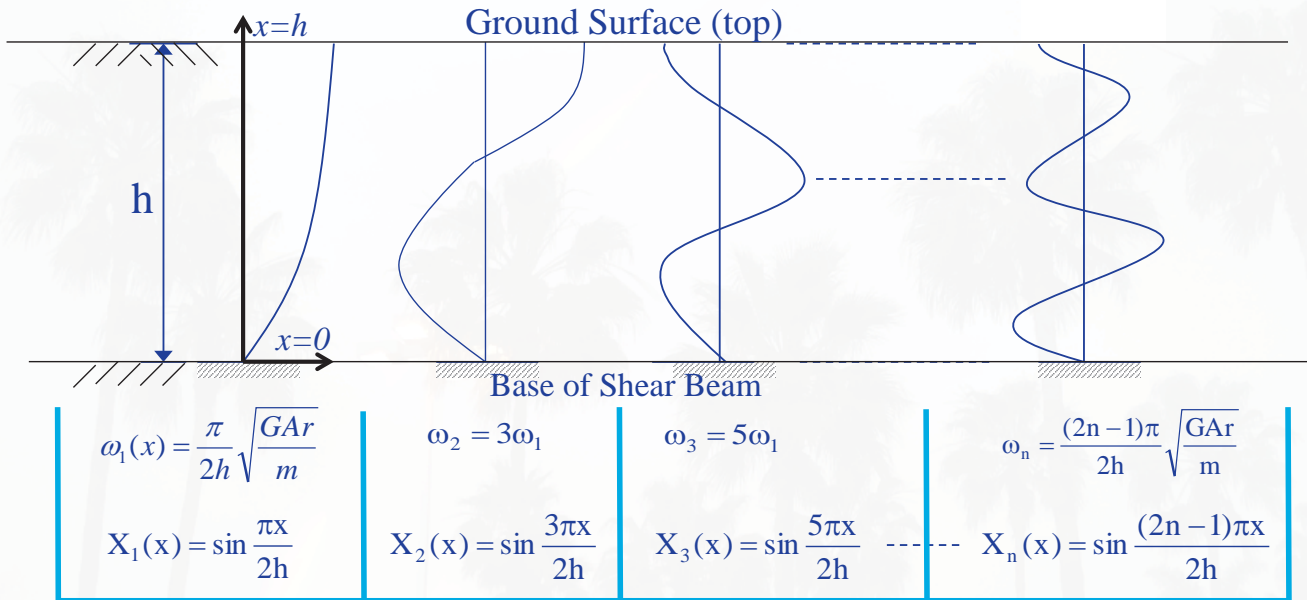
$$V_s = \sqrt{\frac{G}{\rho}}, \quad \text{where } V_s \text{ is the shear wave velocity, and } f_1 = V_s / 4h \text{ (Hz), } f_2 = 3f_1, f_3 = 5f_1$$

8

Short course notes: A. Elgamal, Chicago, Illinois, April 29 – 30, 2013

Mode Shapes

$$X_n(x) = \sin \frac{(2n-1)\pi x}{2h}, \quad n = 1, 2, 3, \dots$$



Notes:

1. The ratios of the natural frequencies go as 1, 3, 5, 7, ...
2. Modes can be normalized such that $X_n(h) = \pm 1$

9

Short course notes: A. Elgamal, Chicago, Illinois, April 29 – 30, 2013

General Solution (Free Vibration)

$$v(x, t) = \sum_{n=1}^{\infty} \sin \frac{(2n-1)\pi x}{2h} (A_n \sin \omega_n t + B_n \cos \omega_n t)$$

Initial Conditions

$$v(x, 0) = v_0(x) = \sum_{n=1}^{\infty} B_n \sin \frac{(2n-1)\pi x}{2h}$$

$$\text{Therefore } B_n = \frac{2}{h} \int_0^h v_0(x) \sin \frac{(2n-1)\pi x}{2h} dx$$

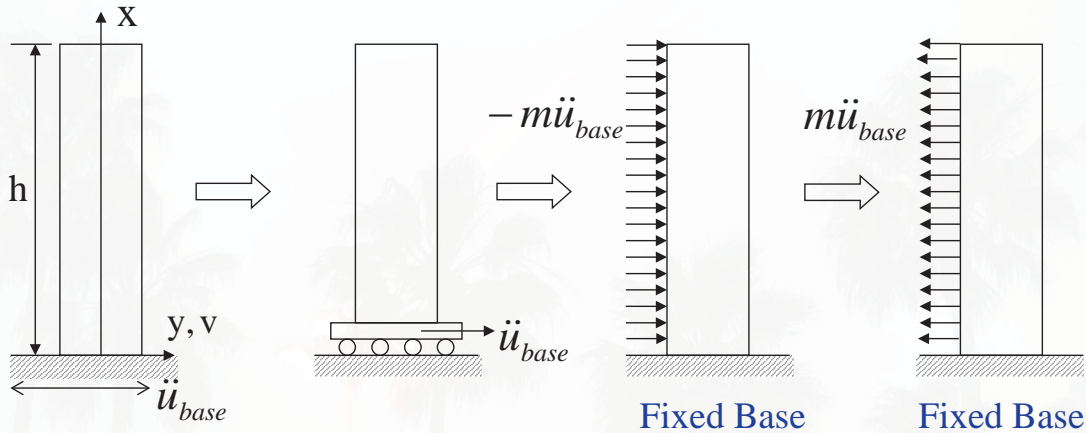
$$\dot{v}(x, 0) = \dot{v}_0(x) = \frac{(2n-1)\pi}{2h} \sqrt{\frac{GA_r}{m}} \sin \frac{(2n-1)\pi x}{2h} A_n$$

$$\text{Therefore } A_n = \frac{4}{(2n-1)\pi} \sqrt{\frac{m}{GA_r}} \int_0^h \dot{v}_0(x) \sin \frac{(2n-1)\pi x}{2h} dx$$

10

Short course notes: A. Elgamal, Chicago, Illinois, April 29 – 30, 2013

For an earthquake base motion at some depth



$$p(t) = -m\ddot{u}_{base}(t)$$

$$v(x,t) = -\frac{4}{\pi} \sum_{n=1}^{\infty} \frac{1}{(2n-1)} \sin \frac{(2n-1)x}{2h} \left[\frac{1}{\omega_n} \int_0^t \ddot{u}_{base}(\tau) \sin \omega_n(t-\tau) d\tau \right]$$

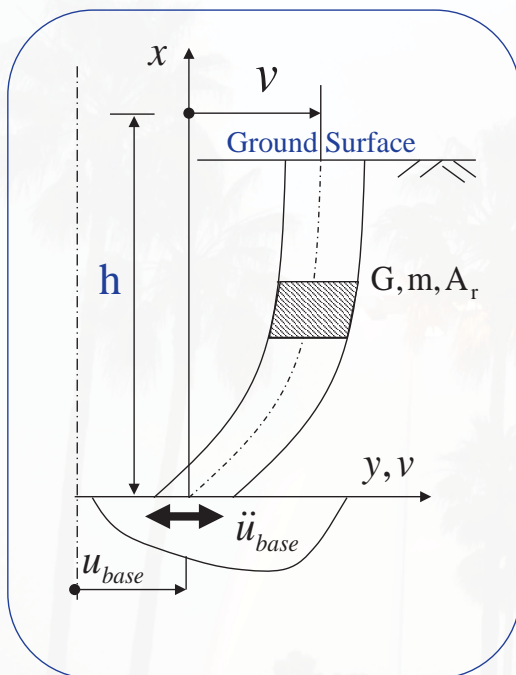
Let $\lambda_n = \frac{2h}{(2n-1)\pi}$, then

$$v(x,t) = -\frac{2}{\pi} \sum_{n=1}^{\infty} \lambda_n \sin \frac{x}{\lambda_n} \left[\frac{1}{\omega_n} \int_0^t \ddot{u}_{base}(\tau) \sin \omega_n(t-\tau) d\tau \right]$$

11

Short course notes: A. Elgamal, Chicago, Illinois, April 29 – 30, 2013

Earthquake Response Analysis Modal Solution



Dynamic Equilibrium

$$\begin{aligned} & V + dV \\ & dx \left[\gamma \right] \left[\leftarrow m \cdot dx \cdot (\ddot{v} + \ddot{u}_{base}) \right] \\ & \downarrow V = \tau A_r = A_r G \frac{\partial v}{\partial x} \end{aligned}$$

$$GA_r \frac{\partial^2 v}{\partial x^2} = m \left(\frac{\partial^2 v}{\partial t^2} + \ddot{u}_{base}(t) \right)$$

$$-GA_r \frac{\partial^2 v}{\partial x^2} + m \frac{\partial^2 v}{\partial t^2} = -m\ddot{u}_{base}(t)$$

12

Short course notes: A. Elgamal, Chicago, Illinois, April 29 – 30, 2013

Modal Solution

$$v(x,t) = \sum_{n=1}^{\infty} X_n(x)q_n(t)$$

$q_n(t)$: Generalized coordinates

$$X_n(x) = \sin \frac{(2n-1)\pi x}{2h}$$

$$\sum_{n=1}^{\infty} [\ddot{q}_n(t) + \omega_n^2 q_n(t)] X_n = -\ddot{u}_{base}(t)$$

Multiplying by any mode, for instance $X_l(x)$ and integrating leads to

$$\sum_{n=1}^{\infty} [\ddot{q}_n(t) + \omega_n^2 q_n(t)] \int_0^h X_n(x)X_l(x) dx = -\int_0^h \ddot{u}_{base}(t)X_l(x) dx$$

13

Short course notes: A. Elgamal, Chicago, Illinois, April 29 – 30, 2013

From the condition of modal orthogonality

$$\int_0^h X_n(x)X_l(x) dx = 0 \quad n \neq l$$

$$\ddot{q}_n(t) + \omega_n^2 q_n(t) = -\alpha_n \ddot{u}_{base}(t) \quad \text{SDOF - type Equation}$$

where,

$$\alpha_n = \frac{\int_0^h X_n(x) dx}{\int_0^h X_n^2(x) dx} \quad \text{Modal Participation Factor}$$

$$= \frac{4}{(2n-1)\pi} \quad \left[\frac{4}{\pi}, \frac{4}{3\pi}, \frac{4}{5\pi}, \frac{4}{7\pi}, \dots \right]$$

Now, viscous modal damping can be conveniently included:

$$\ddot{q}_n(t) + 2\xi_n \omega_n \dot{q}_n(t) + \omega_n^2 q_n(t) = -\alpha_n \ddot{u}_{base}(t) \quad \text{where } n = 1, 2, 3, \dots$$

14

Short course notes: A. Elgamal, Chicago, Illinois, April 29 – 30, 2013

For any value of n , the modal equation above can now be solved numerically as a single degree of freedom system, resulting in the modal “amplitudes” (variation of each q_n with time during the Earthquake), and the relative displacement along the beam depth is defined by:

$$v(x,t) = \sum_{n=1}^{\infty} X_n(x)q_n(t) \quad \text{and} \quad X_n(x) = \sin \frac{(2n-1)\pi x}{2h}$$

Note: Relative velocity is obtained by replacing $q_n(t)$ by $\dot{q}_n(t)$

Note: Relative acceleration is obtained by replacing $q_n(t)$ by \ddot{q}_n

with the total or absolute acceleration at any depth equal to the relative + $\ddot{u}_{base}(t)$

Note: In the above, $x=h$ corresponds to the ground surface and $x=0$ is at the shear beam base (where the input base shaking acceleration is imparted).

Note: We typically get a very good approximation of shear beam response just by including the contribution of the first few modes (i.e., $n=1$ or $n=1$ and 2 or $n=1$ and 2 and 3 for instance):

As such, a first mode solution would be: $v(x,t) = X_1(x)q_1(t)$

A second mode solution would be: $v(x,t) = X_2(x)q_2(t)$

and a solution based on the first 2 modes would be: $v(x,t) = X_1(x)q_1(t) + X_2(x)q_2(t)$

(with velocity and acceleration calculated as described above)

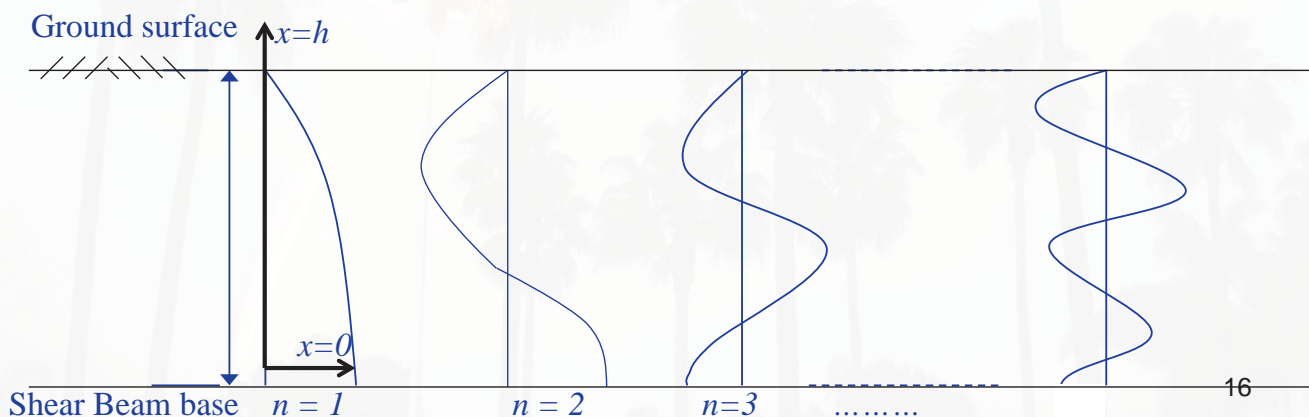
Short course notes: A. Elgamal, Chicago, Illinois, April 29 – 30, 2013

In the above, shear strain $\gamma(x,t)$ anywhere along the depth can be evaluated by differentiating the mode shapes to give:

$$\partial v(x,t) / \partial x = \left(\sum_{n=1}^{\infty} \partial X_n(x) / \partial x \right) q_n(t)$$

in which: $\partial X_n(x) / \partial x = \frac{(2n-1)\pi}{2h} \cos \frac{(2n-1)\pi x}{2h}$ (see Fig. below)

and shear stress $\tau(x,t) = G \gamma(x,t)$



Damping in Continuous Systems

1. Fundamental Approach

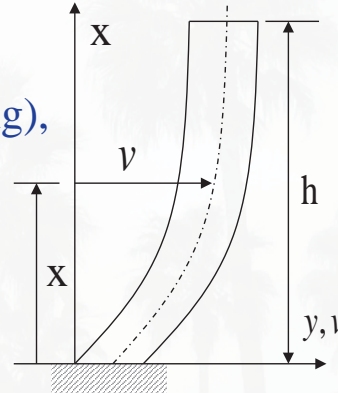
Postulate material behavior and/or mechanism and investigate the consequences

2. Ad Hoc Approach (Modal Damping), where

$$v(x,t) = \sum_{n=1}^{\infty} V_n(x) q_n(t)$$

and

$$\ddot{q}_n(t) + 2\xi_n \omega_n \dot{q}_n(t) + \omega_n^2 q_n(t) = p_n(t) \quad \text{where } n = 1, 2, 3, \dots$$



17

Short course notes: A. Elgamal, Chicago, Illinois, April 29 – 30, 2013

Damping in a Shear Beam

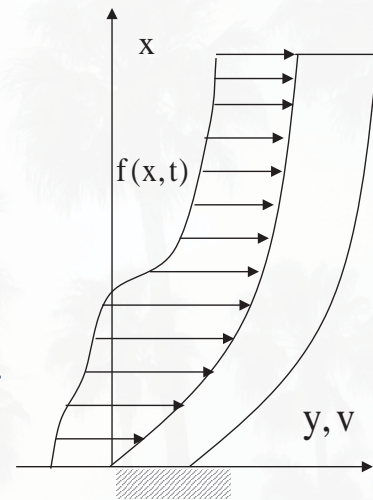
1. Equation of Motion for Forced Vibration

$$k'GA \frac{\partial^2 v}{\partial x^2} + f(x,t) = m \frac{\partial^2 v}{\partial t^2} = \rho A \frac{\partial^2 v}{\partial t^2}$$

$$\text{let } v(x,t) = \sum_{n=1}^{\infty} V_n(x) q_n(t)$$

$$\text{where } V_n(x) = \sin \frac{(2n-1)\pi x}{2h}, \quad n = 1, 2, 3, \dots$$

$$\text{and } \omega_n = \frac{(2n-1)\pi}{2h} \sqrt{\frac{k'G}{\rho}}, \quad n = 1, 2, 3, \dots$$



18

Short course notes: A. Elgamal, Chicago, Illinois, April 29 – 30, 2013

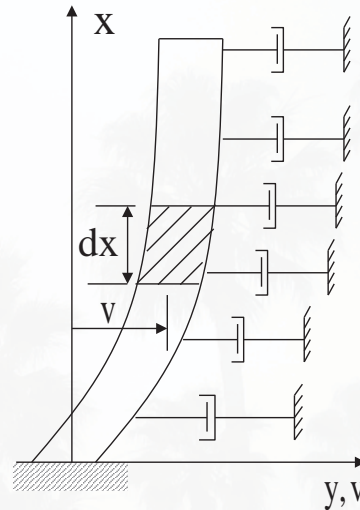
I. For External or Absolute Damping (Mass proportional)

$$f(x, t) = -F_D$$



$$F_D = -c_1 A \frac{\partial v}{\partial t} dx$$

Force per unit length



Thus, the equation of motion becomes

$$k'GA \frac{\partial^2 v}{\partial x^2} - c_1 A \frac{\partial v}{\partial t} - \rho A \frac{\partial^2 v}{\partial t^2} = 0$$

19

Short course notes: A. Elgamal, Chicago, Illinois, April 29 – 30, 2013

Solution can be obtained by: $v(x, t) = \sum_{n=1}^{\infty} V_n(x) q_n(t)$

Substituting the above results in:

$$\sum_{n=1}^{\infty} -\frac{(2n-1)^2 \pi^2}{(2h)^2} q_n(t) \frac{G}{\rho} \sin \frac{(2n-1)\pi x}{2h} - \sum_{n=1}^{\infty} \frac{c_1}{\rho} \sin \frac{(2n-1)\pi x}{2h} \dot{q}_n(t) - \sum_{n=1}^{\infty} \sin \frac{(2n-1)\pi x}{2h} \ddot{q}_n(t) = 0$$

$$\sum_{n=1}^{\infty} \left(\ddot{q}_n(t) + \frac{c_1}{\rho} \dot{q}_n(t) + \omega_n^2 q_n(t) \right) \sin \frac{(2n-1)\pi x}{2h} = 0$$

$$\text{or } \ddot{q}_n(t) + \frac{c_1}{\rho} \dot{q}_n(t) + \omega_n^2 q_n(t) = 0, \quad n = 1, 2, 3, \dots$$

Now replacing $\frac{c_1}{\rho}$ by $2\omega_n \xi_n$, $\xi_n = n^{\text{th}}$ damping ratio

$$\text{or } \xi_n = \frac{c_1}{2\rho} \frac{2h}{(2n-1)\pi} \sqrt{\frac{\rho}{G}} = \frac{c_1 h}{\sqrt{\rho G}} \frac{1}{(2n-1)}, \quad n = 1, 2, 3, \dots$$

Thus, the “absolute” damping factors go to zero as n increases. If $\xi_1 = \xi$, $\xi_2 = \xi/3$, $\xi_3 = \xi/5$

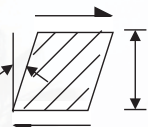
“This is not so good for many physical systems”

20

Short course notes: A. Elgamal, Chicago, Illinois, April 29 – 30, 2013

II. Strain Rate or Relative Damping (stiffness proportional)

$$F_D + dF_D = c_2 A_r \frac{\partial^2 v}{\partial x \partial t} + c_2 A_r \frac{\partial v}{\partial x} \left(\frac{\partial^2 v}{\partial x \partial t} \right) dx$$

$$\gamma_{xy} = \frac{\partial v}{\partial x}$$


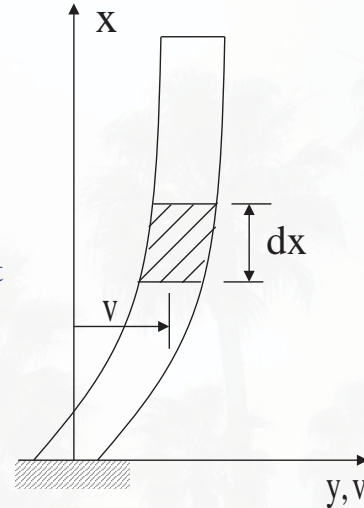
$$F_D = c_2 A_r \frac{\partial}{\partial t} \left(\frac{\partial v}{\partial x} \right)$$

$c_2 = \text{damping constant}$
 $A_r = k' A$

Thus, $f(x, t) dx = c_2 A_r \frac{\partial^3 v}{\partial t \partial x^3} dx$

Equation of Motion:

$$k' GA \frac{\partial^2 v}{\partial x^2} + c_2 A_r \frac{\partial^3 v}{\partial t \partial x^2} - \rho A \frac{\partial^2 v}{\partial t^2} = 0$$



21

Short course notes: A. Elgamal, Chicago, Illinois, April 29 – 30, 2013

$$v(x, t) = \sum_{n=1}^{\infty} \sin \frac{(2n-1)\pi x}{2h} q_n(t)$$

$$\sum_{n=1}^{\infty} \left[-\frac{(2n-1)^2 \pi^2}{(2h)^2} \frac{G}{\rho} q_n(t) - \frac{c_2}{\rho} \frac{(2n-1)^2 \pi^2}{(2h)^2} \dot{q}_n(t) - \ddot{q}_n(t) \right] \sin \frac{(2n-1)\pi x}{2h} = 0$$

$$\sum_{n=1}^{\infty} \left(\ddot{q}_n(t) + \frac{c_2}{G} \omega_n^2 \dot{q}_n(t) + \omega_n^2 q_n(t) \right) \sin \frac{(2n-1)\pi x}{2h} = 0$$

$$\therefore \ddot{q}_n(t) + \frac{c_2}{G} \omega_n^2 \dot{q}_n(t) + \omega_n^2 q_n(t) = 0, \quad n = 1, 2, 3, \dots$$

Let $\frac{c_2}{G} \omega_n^2 = 2\omega_n \xi_n$

$$\Rightarrow \xi_n = \frac{c_2}{2G} \frac{(2n-1)\pi}{2h} \sqrt{\frac{G}{\rho}} = \frac{c_2 \pi}{4h \sqrt{G\rho}} (2n-1), \quad n = 1, 2, 3, \dots \quad \text{"Relative Damping"}$$

if $\xi_1 = \xi$, $\xi_2 = 3\xi$, $\xi_3 = 5\xi$,

- i.e., "Damping increases rapidly"
- Rayleigh Damping \rightarrow a combination of both.

22

Short course notes: A. Elgamal, Chicago, Illinois, April 29 – 30, 2013

III. Arbitrary Damping

Take the damping ratio ξ_n = a set of arbitrary constants. Then substitute in the equation of motion:

$$\ddot{q}_n(t) + 2\xi_n \omega_n \dot{q}_n(t) + \omega_n^2 q_n(t) = -\alpha_n \ddot{u}_g(t)$$

Summary “Damping”

1. Absolute Mass Proportional Damping $\xi_n = \frac{c_1}{2\omega_n \rho}, \quad n = 1, 2, 3, \dots$
2. Relative Stiffness Proportional Damping $\xi_n = \frac{c_2 \omega_n}{2G}, \quad n = 1, 2, 3, \dots$
3. Rayleigh Damping $\xi_n = \frac{c_1}{2\omega_n \rho} + \frac{c_2 \omega_n}{2G}, \quad n = 1, 2, 3, \dots$
4. Constant Damping in all Modes $\xi_n = \text{const.}, \quad n = 1, 2, 3, \dots$
5. Damping as a set of Arbitrary Constants $\xi_n = \text{Arbitrary const.}, \quad n = 1, 2, 3, \dots$

23

Short course notes: A. Elgamal, Chicago, Illinois, April 29 – 30, 2013

Earthquake “Response Spectrum Technique”

$$v(x, t) = \sum_{n=1}^{\infty} V_n(x) q_n(t), \quad \ddot{q}_n(t) + 2\xi_n \omega_n \dot{q}_n(t) + \omega_n^2 q_n(t) = -\alpha_n \ddot{u}_g(t)$$

Solution “Duhamel Integral”

$$q_n(t) = -\frac{\alpha_n}{\omega_n} \left[\int_0^t \ddot{u}_g(\tau) e^{\xi_n \omega_n (t-\tau)} \sin \omega_n \sqrt{1-\xi_n^2} (t-\tau) d\tau \right]$$

Denoting the integral by the symbol $V_n(t)$, i.e.,

$$V_n(t) = \int_0^t \ddot{u}_g(\tau) e^{\xi_n \omega_n (t-\tau)} \sin \omega_n \sqrt{1-\xi_n^2} (t-\tau) d\tau \quad \text{Thus} \quad q_n(t) = -\frac{\alpha_n}{\omega_n} V_n(t)$$

$$q_n(t)|_{\max} = -\frac{\alpha_n}{\omega_n} V_n(t)|_{\max} = -\frac{\alpha_n}{\omega_n} S_v, \quad S_v \text{ is the spectral velocity}$$

Note that the spectral displacement $S_d = \frac{S_v}{\omega_n}$ and the spectral acceleration $S_a = S_v \omega_n$

$$q_n(t)|_{\max} = -\alpha_n S_d, \quad \text{and}$$

$$v_i(x, t)|_{\max} = -X_i(x) q_i(t)|_{\max}, \quad i = 1, 2, 3, \dots$$

24

Short course notes: A. Elgamal, Chicago, Illinois, April 29 – 30, 2013

Displacement at the Top

At the top of the beam, i.e., at $x=h$, $v_i(h, t) = |X_i(h)| \frac{\alpha_i}{\omega_i} S_v$, $i = 1, 2, 3, \dots$

Thus for a single mode, $v_i(h, t) = \frac{\alpha_i}{\omega_i} S_v = \frac{4S_v}{\pi(2i-1)\omega_1(2i-1)} = \frac{4S_v}{\pi(2i-1)^2 \omega_1}$

Combine according to sum of absolute values

$$v(h, t)_{\max} \leq v_1(h, t)_{\max} + v_2(h, t)_{\max} + v_3(h, t)_{\max} + v_4(h, t)_{\max} + \dots$$

Combine according to the root mean square (RMS)

$$v(h, t)_{\max} \cong \sqrt{v_1^2(h, t)_{\max} + v_2^2(h, t)_{\max} + v_3^2(h, t)_{\max} + v_4^2(h, t)_{\max} + \dots}$$

Substituting the above values (and simply just assuming the same S_v for all frequencies)

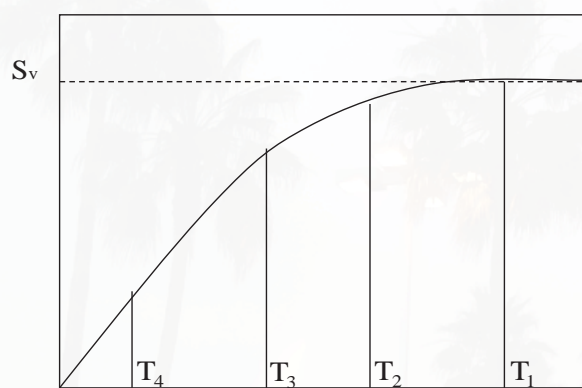
$$v(h, t)_{\max} \leq \frac{4S_v}{\pi \omega_1} \left(1 + \frac{1}{9} + \frac{1}{25} + \frac{1}{49} + \dots \right) = \frac{1.575}{\omega_1} S_v$$

$$v(h, t)_{\max} \cong \frac{4S_v}{\pi \omega_1} \left(1 + \frac{1}{81} + \frac{1}{625} + \dots \right)^{1/2} = \frac{1.280}{\omega_1} S_v$$

25

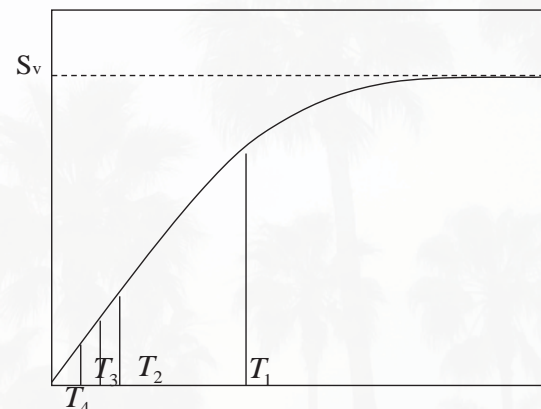
Short course notes: A. Elgamal, Chicago, Illinois, April 29 – 30, 2013

The first mode contributes significantly to the displacement response (on the average, with S_v assumed to be constant for all modes)



Period

Tall System



Period

Short System

26

Short course notes: A. Elgamal, Chicago, Illinois, April 29 – 30, 2013

Acceleration at the Top

$$\ddot{v}(x,t) = \sum_{i=1}^{\infty} X_i(x) \ddot{q}_i(t)$$

Total acceleration $a(x,t) = \ddot{v}(x,t) + \ddot{u}_{base}(t)$

But (see next slide) $\ddot{u}_{base}(t) = \sum_{i=1}^{\infty} \alpha_i \ddot{u}_{base}(t) X_i(x)$

So $a(x,t) = \sum_{i=1}^{\infty} (\ddot{q}_i(t) + \alpha_i \ddot{u}_{base}(t)) X_i(x)$

For the i^{th} mode $a_i(x,t) = (\ddot{q}_i(t) + \alpha_i \ddot{u}_{base}(t)) X_i(x) = (-\omega_i^2 q_i(t)) X_i(x)$

$$a_i(h,t)|_{\max} = \alpha_i \omega_i S_v = \frac{4}{(2i-1)\pi} \omega_i (2i-1) S_v = \frac{4\omega_i S_v}{\pi}$$

Combining as before $a(h,t)|_{\max} \leq \frac{4\omega_1 S_v}{\pi} [1+1+1+1+\dots]$

$$a(h,t)|_{\max} \cong \frac{4\omega_1 S_v}{\pi} [1+1+1+1+\dots]^{1/2}$$

Thus, with the assumed constant S_v , the modes on the average, tend to contribute equally to the acceleration at the top.

27

Short course notes: A. Elgamal, Chicago, Illinois, April 29 – 30, 2013

Section to show that $\sum_{i=1}^{\infty} \alpha_i X_i(x) = 1$

Let $\sum_{n=1}^{\infty} b_n X_n(x) = 1$ where b_n are constants to be identified

multiply by X_l and integrate over the height

$$\sum_{n=1}^{\infty} b_n \int_0^h X_n(x) X_l(x) dx = \int_0^h X_l(x) dx$$

Therefore, on account of modal orthogonality

$$b_n = \frac{\int_0^h X_n(x) dx}{\int_0^h X_n^2(x) dx} = \alpha_n \quad (\text{the Modal Participation Factor})$$

where $\alpha_n = \frac{4}{(2n-1)\pi} \left[\frac{4}{\pi}, \frac{4}{3\pi}, \frac{4}{5\pi}, \frac{4}{7\pi}, \dots \right]$

Short course notes: A. Elgamal, Chicago, Illinois, April 29 – 30, 2013

28

Numerical Implementation of Shear Beam Model

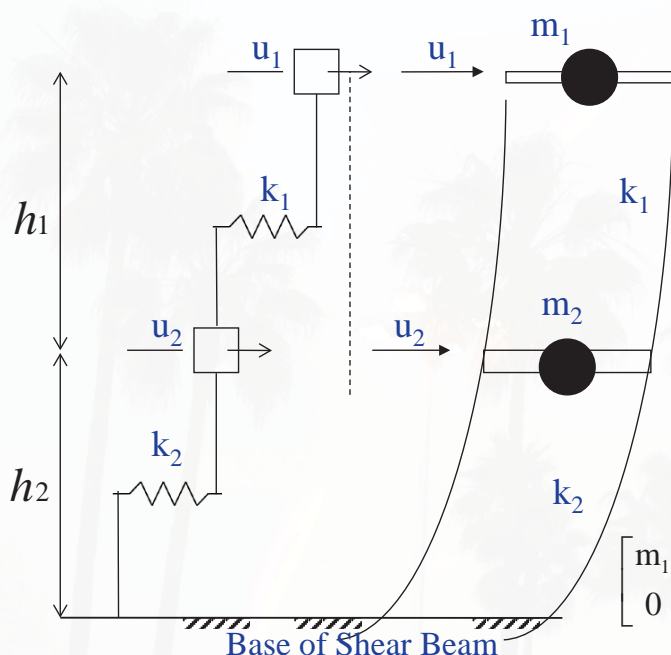
Allows for handling of Stratified soil profiles (i.e., layers of different stiffness/damping properties)

Allows for implementation of nonlinear hysteretic soil shear stress-strain properties

29

Short course notes: A. Elgamal, Chicago, Illinois, April 29 – 30, 2013

Example: 2-DOF Soil shear beam , with $h_i =$ distance between masses



$$m_1 = \rho_1 h_1 / 2$$

$$m_2 = (\rho_1 h_1 + \rho_2 h_2) / 2$$

$$k_1 = G_1 / h_1$$

$$k_2 = G_2 / h_2$$

$$m_1 \ddot{u}_1 + k_1 (u_1 - u_2) = -m_1 \ddot{u}_{\text{base}}$$

$$m_2 \ddot{u}_2 + k_1 (u_2 - u_1) + k_2 u_2 = -m_2 \ddot{u}_{\text{base}}$$

$$\begin{bmatrix} m_1 & 0 \\ 0 & m_2 \end{bmatrix} \begin{bmatrix} \ddot{u}_1 \\ \ddot{u}_2 \end{bmatrix} + \begin{bmatrix} k_1 & -k_1 \\ -k_1 & (k_1 + k_2) \end{bmatrix} \begin{bmatrix} u_1 \\ u_2 \end{bmatrix} = - \begin{bmatrix} m_1 \\ m_2 \end{bmatrix} \ddot{u}_{\text{base}}$$

or $\underline{M} \ddot{\underline{u}} + \underline{K} \underline{u} = -\underline{M} \ddot{u}_{\text{base}}$ where $\underline{1}$ is the Identity Matrix

30

Short course notes: A. Elgamal, Chicago, Illinois, April 29 – 30, 2013

Numerical Solution of Equation of Motion

Average Acceleration Method (Trapezoidal method)

$$m a + c v + k d = f(t)$$

In the above mass-spring-dashpot (damper) equation of motion:

$f(t)$ is the forcing function defined as given f_i values at (t_i) in which $i = 0, 1, 2, \dots$
NTS (number of time steps), with

the time step between any t_i and t_{i+1} equal to Δt , and
 m, c, k are the mass, damping and stiffness matrices.

Initial Conditions: $d(t=0) = d_0$, and $v(t=0) = v_0$

From these conditions and the known f_0 , one can find $a(t=0) = a_0$ from the Equation above

$$\text{At any time step } t = t_{i+1}: m a_{i+1} + c v_{i+1} + k d_{i+1} = f_{i+1} \quad (\text{Eq. 1})$$

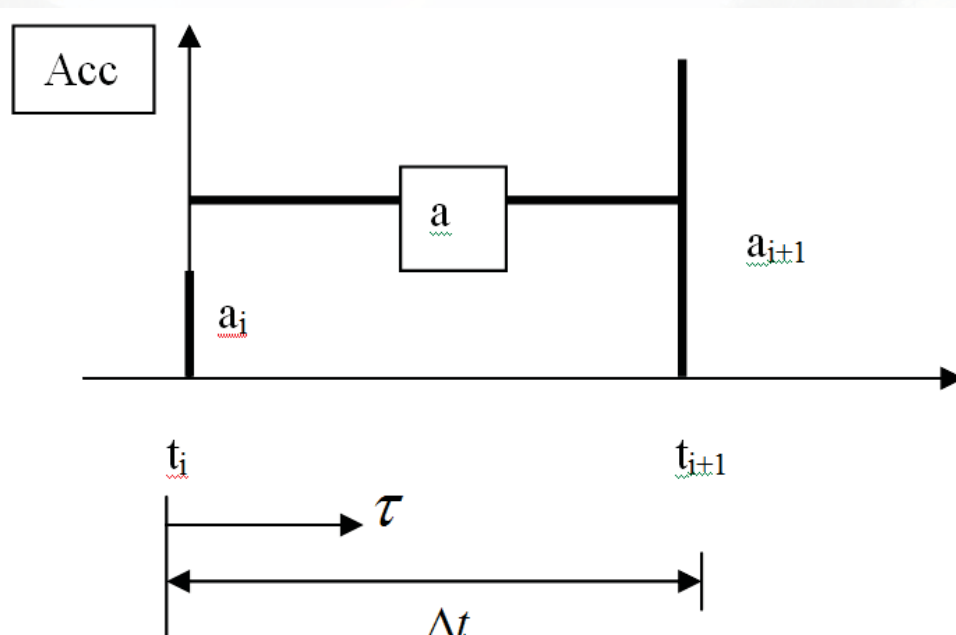
Now, we need to find a_{i+1}, v_{i+1} , and d_{i+1} , using f_{i+1} , and information from the previous time step (i.e., a_i, v_i , and d_i)

35

Short course notes: A. Elgamal, Chicago, Illinois, April 29 – 30, 2013

Average acceleration dictates that (see figure):

$$a = (a_{i+1} + a_i) / 2 \quad (\text{Eq. 2})$$



36

Short course notes: A. Elgamal, Chicago, Illinois, April 29 – 30, 2013

Integrate to get velocity

$$v = v_i + \tau (a_{i+1} + a_i) / 2 \quad (\text{Eq. 3})$$

Integrate above to get displacement:

$$d = d_i + v_i \tau + (\tau^2 / 4) (a_{i+1} + a_i) \quad (\text{Eq. 4})$$

At the end of the Interval, $\tau = \Delta t$ and therefore (using Eqs. 3 and 4)

$$v_{i+1} = v_i + (\Delta t / 2) (a_{i+1} + a_i) \quad (\text{Eq. 5})$$

$$d_{i+1} = d_i + v_i \Delta t + (\Delta t^2 / 4) (a_{i+1} + a_i) \quad (\text{Eq. 6})$$

Now, substitute Equations 5 and 6 into Equation 1 to get

$$m a_{i+1} + c (v_i + (\Delta t / 2) (a_{i+1} + a_i)) + k (d_i + v_i \Delta t + (\Delta t^2 / 4) (a_{i+1} + a_i)) = f_{i+1}$$

or,

$$(m + c (\Delta t / 2) + k (\Delta t^2 / 4)) a_{i+1} = f_{i+1} - c (v_i + (\Delta t / 2) a_i) - k (d_i + v_i \Delta t + (\Delta t^2 / 4) a_i) \quad (\text{Eq. 7})$$

where $[m + c (\Delta t / 2) + k (\Delta t^2 / 4)]$ is known as the effective mass = m^*) and a matrix inversion process is involved for multi-degree-of-freedom cases.

Solve Eq. 7 for a_{i+1} , and (using Eqs. 4 and 5) solve for v_{i+1} , d_{i+1}

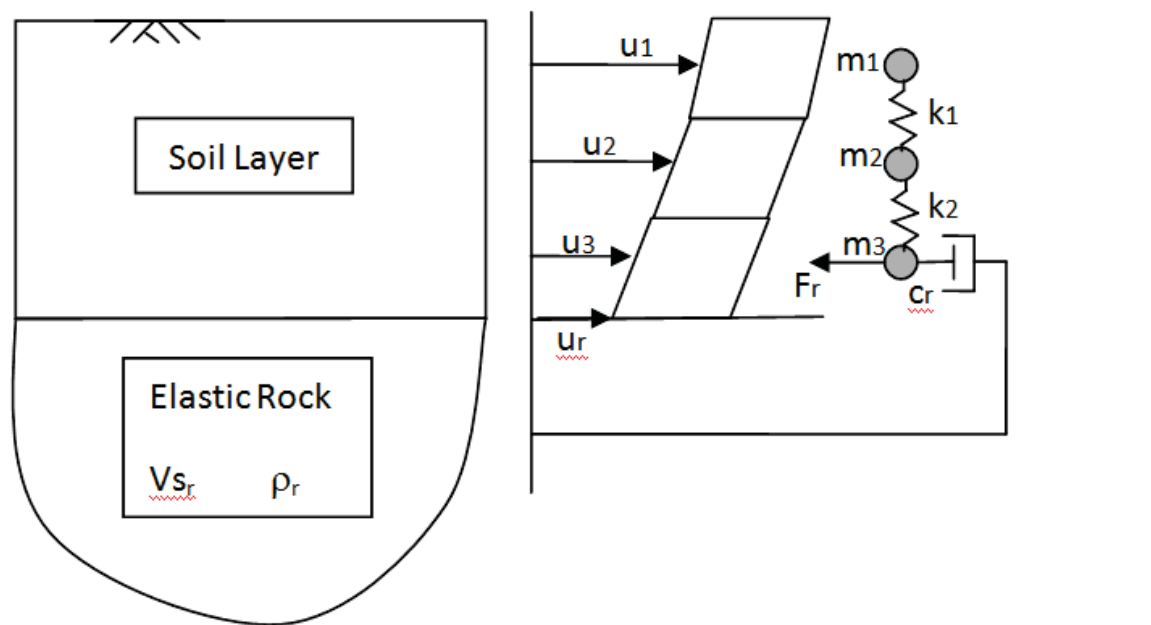
Now all quantities are known at $i + 1$ and we are ready to go to the next time step (repeat the above procedure).

37

Short course notes: A. Elgamal, Chicago, Illinois, April 29 – 30, 2013

Site Amplification: Shear Beam on Elastic Rock (The "Lysmer" Dashpot approach)

Illustration using 3-Degree of freedom model



Lysmer, J. (1978). "Analytical procedures in soil dynamics," Report No. UCB/EERC-78/29, University of California at Berkeley, Earthquake Engineering Research Center, Richmond, CA.

Lysmer, J. and Kuhlemeyer, A.M. (1969). "Finite dynamic model for infinite media," J. of the En Mechanics Division, ASCE, 95, 859-877.

Short course notes: A. Elgamal, Chicago, Illinois, April 29 – 30, 2013

Important note: In this formulation, u^t denotes Total Displacement (i.e. displacement of the rock base u_r + displacement of the soil stratum relative to the rock). As such, the matrix equation of motion can be defined by (for any time step t):

$$\begin{bmatrix} m_1 & 0 & 0 \\ 0 & m_2 & 0 \\ 0 & 0 & m_3 \end{bmatrix} \begin{bmatrix} \ddot{u}_1^t \\ \ddot{u}_2^t \\ \ddot{u}_3^t \end{bmatrix} + \begin{bmatrix} c_{11} & c_{12} & 0 \\ c_{21} & c_{22} & c_{23} \\ 0 & c_{32} & c_{33} + c_r \end{bmatrix} \begin{bmatrix} \dot{u}_1^t \\ \dot{u}_2^t \\ \dot{u}_3^t \end{bmatrix} + \begin{bmatrix} k_1 & -k_1 & 0 \\ k_1 & k_1 + k_2 & -k_2 \\ 0 & -k_2 & k_2 \end{bmatrix} \begin{bmatrix} u_1^t \\ u_2^t \\ u_3^t \end{bmatrix} = \begin{bmatrix} 0 \\ 0 \\ F_r \end{bmatrix}$$

where the c matrix (except for the term c_r) is formed according to the usual Rayleigh damping approach in which $c = a_o m + a_1 k$

The underlying elastic rock stratum introduces the terms c_r and F_r , defined by:

$$c_r = \rho_r V_{s_r} \quad (\text{rock mass density multiplied by rock shear wave velocity})$$

$$F_r = 2 \rho_r V_{s_r} \dot{u}_{ir}$$

In the above, \dot{u}_{ir} is *velocity* of the incident rock motion (often taken for simplicity as $\frac{1}{2}$ that of an available (or assumed) nearby **recorded** rock-outcrop motion).

Implementation notes:

- 1) If needed, filter out the superfluous low frequency components of the input \ddot{u}_g rock-outcrop acceleration time history (say anything below 0.3 Hz). This will help in avoiding superfluous drift upon integrating this motion to get rock velocity \dot{u}_r and double integrating to get rock displacement u_r . After integration, you can plot the rock velocity and displacement to check for drift.
- 2) Divide the rock-outcrop velocity values by $\frac{1}{2}$ throughout to obtain the motion that will be used in the matrix equation above (i.e., $\dot{u}_{ir} = \frac{1}{2} \dot{u}_r$). Using \dot{u}_{ir} , go ahead and define the input time history F_r according to the above equation.
- 3) Solve the matrix equation in time using the usual implicit time integration scheme (average acceleration method, or linear acceleration method for instance), and store the output displacement, velocity, and acceleration vectors.
- 4) The soil absolute (total) acceleration \ddot{u}^t is now already available for plotting. To obtain the soil relative displacement and the soil relative velocity vectors (relative to the rock base motion), you must subtract the corresponding rock motion time histories first (as mentioned in the note above, the matrix equation solves for total motion).

Equivalent Linear Site Response

Short course notes: A. Elgamal, Chicago, Illinois, April 29 - 30, 2013

1

SHAKE / SHAKE 91

A. Elgamal and T. Lai (notes; original version)

References

P. B. Schnabel, J. Lysmer, and H. B. Seed, **Shake: A Computer Program For Earthquake Response Analysis of Horizontally Layered Sites**, Report No. EERC 72-12, University of California at Berkeley, December 1972.

I. M. Idriss, and J. I. Sun, **Shake 91: A Computer Program for Conducting Equivalent Linear Seismic Response Analyses of Horizontally Layered Soil Deposits**, Modified based on Original Program Shake, University of California, Davis, August 1992.

T. Iwasaki, F. Tatsuoka, and Y. Takagi, "Shear Moduli of Sands Under Cyclic Torsional Shear Loading," *Soils And Foundations*, JSSMFE, Vol. 18, No. 1, pp. 39-56.

P. W. Mayne and G. J. Rix (1993), "Gmax-qc Relationships for Clays," *Geotechnical Testing Journal*, ASTM, Vol. 16, No. 1, pp. 54-60.

H. B. Seed, R. T. Wong, I. M. Idriss, and K. Tokimatsu, "Moduli and Damping Factors for Dynamic Analyses of Cohesionless Soils, Report No. UCB/EERC-84/14, Earthquake Engineering Research Center, University of California, Berkeley, Ca, 1984.

M. Jamiolkowski, S. Leroueil, and D. C. F. Lo Presti (1991), "Theme Lecture: Design Parameters from Theory to Practice, Proc. Geo-Coast '91, Yokohama, Japan, pp. 1-41.

Short course notes: A. Elgamal, Chicago, Illinois, April 29 -30, 2013

2

T. Imai and K. Tonouchi, "Correlation of N-Value with S-Wave Velocity and Shear Modulus," Proc. 2nd European Symposium on Penetration Testing, Amsterdam, The Netherlands, pp. 67-72.

E. Kavazanjian, Jr., N. Matasovic, T. Hadj-Hamou, and P. J. Sabatini, Geotechnical Engineering Circular No. 3 – Design Guidance: Geotechnical Earthquake Engineering for Highways, Design Principles, Volume 1, SA-97-076 (NTIS # PB98-11560)

E. Kavazanjian, Jr., N. Matasovic, T. Hadj-Hamou, and P. J. Sabatini, Geotechnical Engineering Circular No. 3 – Design Guidance: Geotechnical Earthquake Engineering for Highways, Design Examples, Volume 2, SA-97-077 (NTIS # PB98-11578)

NRC 2000, Seeing into the Earth, Committee for Noninvasive Characterization of the Shallow Subsurface for Environmental and Engineering Applications, P. R. Roming, Chair, 129 pp.

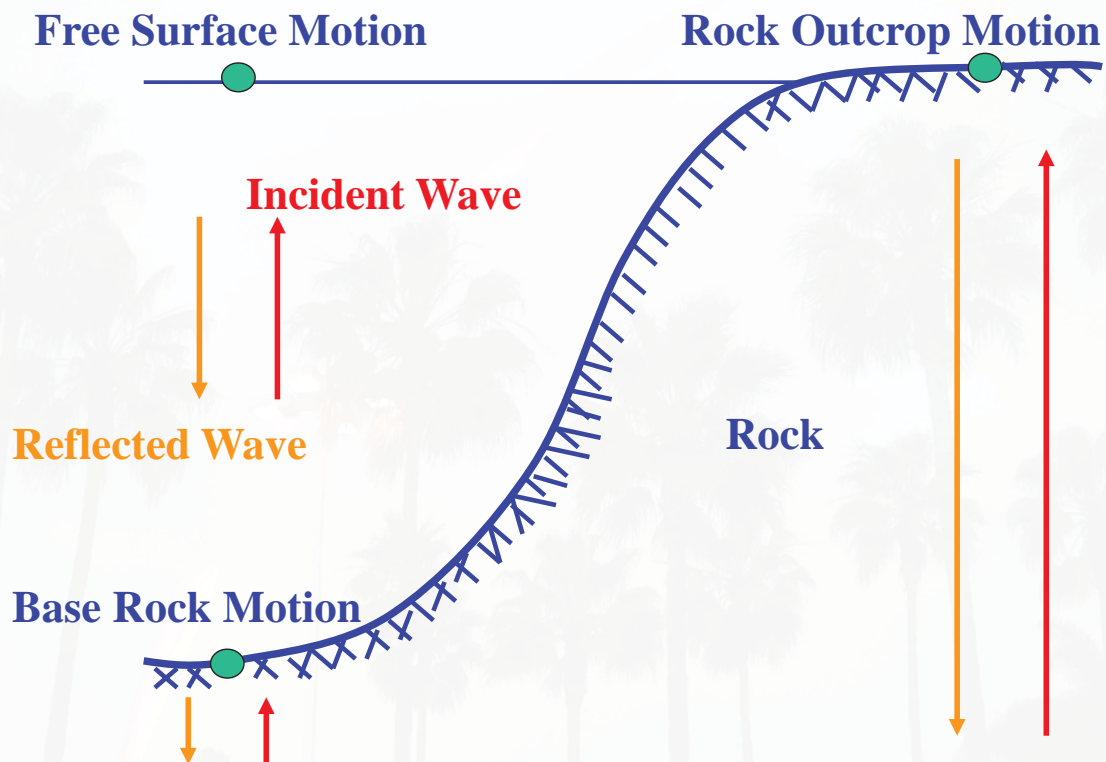
M. Vucetic and Ricardo Dobry, "Effect of Soil Plasticity on Cyclic Response," Journal of Geotechnical Engineering, ASCE, Vol. 117, No. 1, January 1991.

H. B. Seed and I. M. Idriss, "Soil Moduli and Damping Factors for Dynamic Response Analyses," Report No. EERC 70-10, Earthquake Engineering Research Center, University of California, Berkeley, CA, 1970.

H. B. Seed, Robert T. Wong, I. M. Idriss and K. Tokimatsu, "Moduli and Damping Factors for Dynamic Analyses of Cohesionless Soils, Journal of Geotechnical Engineering, ASCE, Vol. 112, No. 11, November, 1986.

Short course notes:A. Elgamal, Chicago, Illinois, April 29 -30, 2013

3



Short course notes:A. Elgamal, Chicago, Illinois, April 29 -30, 2013

4

Wave Equation

$$\rho \frac{\partial^2 u}{\partial t^2} = G \frac{\partial^2 u}{\partial z^2} + \eta \frac{\partial^3 u}{\partial z^2 \partial t}$$

Solution for Homogeneous and Isotropic Soil

$$u(z, t) = \sum_{i=1}^{\infty} \left(E_i e^{ik_i z} + F_i e^{-ik_i z} \right) e^{i\omega_i t}$$

K_i – Wave Number

ω_i – Frequency

E_i – Amplitude of Incident Wave at Frequency ω_i

F_i – Amplitude of Reflected Wave at Frequency ω_i

Short course notes: A. Elgamal, Chicago, Illinois, April 29 -30, 2013

5

Layer No	Coordinates System	Propagation Direction	Properties
1			$G_1 \beta_1 \rho_1 h_1$
...			
i			$G_i \beta_i \rho_i h_i$
i+1			$G_{i+1} \beta_{i+1} \rho_{i+1} h_{i+1}$
...			
N			$G_N \beta_N \rho_N h_N = \infty$

Particle Motion

F_N Reflected Wave **E_N Incident Wave**

Short course notes: A. Elgamal, Chicago, Illinois, April 29 -30, 2013

6

Properties G , β , ρ , h are known

- Unknown in system: $2N (E_i, F_i)$

- **Boundary Conditions:**

Displacement continuity at all interfaces: $N-1$

Stress continuity at all interfaces: $N-1$

Zero stress at free surface: 1

+

Given motion at any one layer: 1

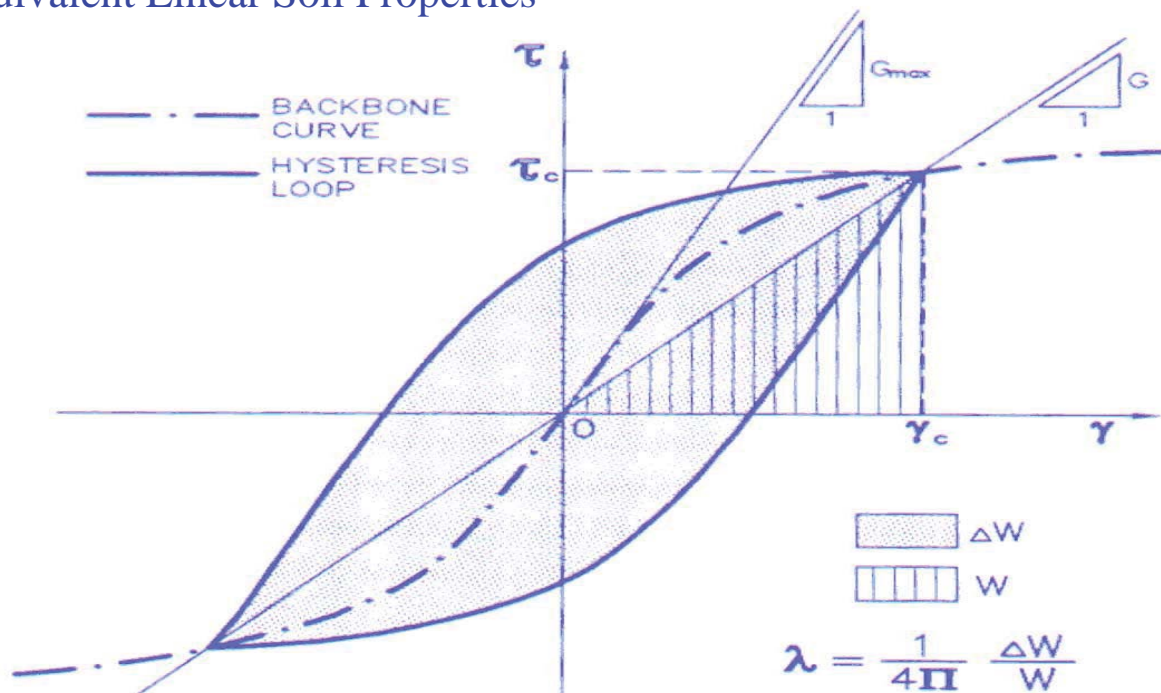


- **Motions at any layer are determined**

Short course notes:A. Elgamal, Chicago, Illinois, April 29 -30, 2013

7

Equivalent Linear Soil Properties

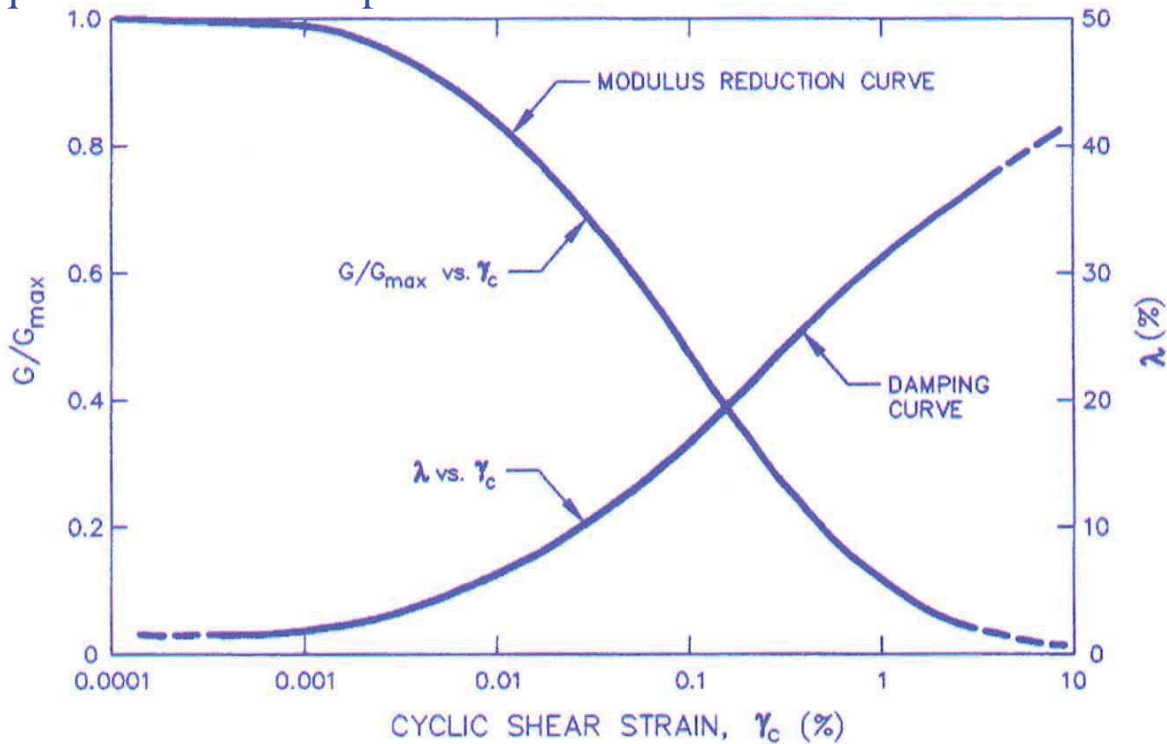


From (FHWA-SA-97-076)

Short course notes:A. Elgamal, Chicago, Illinois, April 29 -30, 2013

8

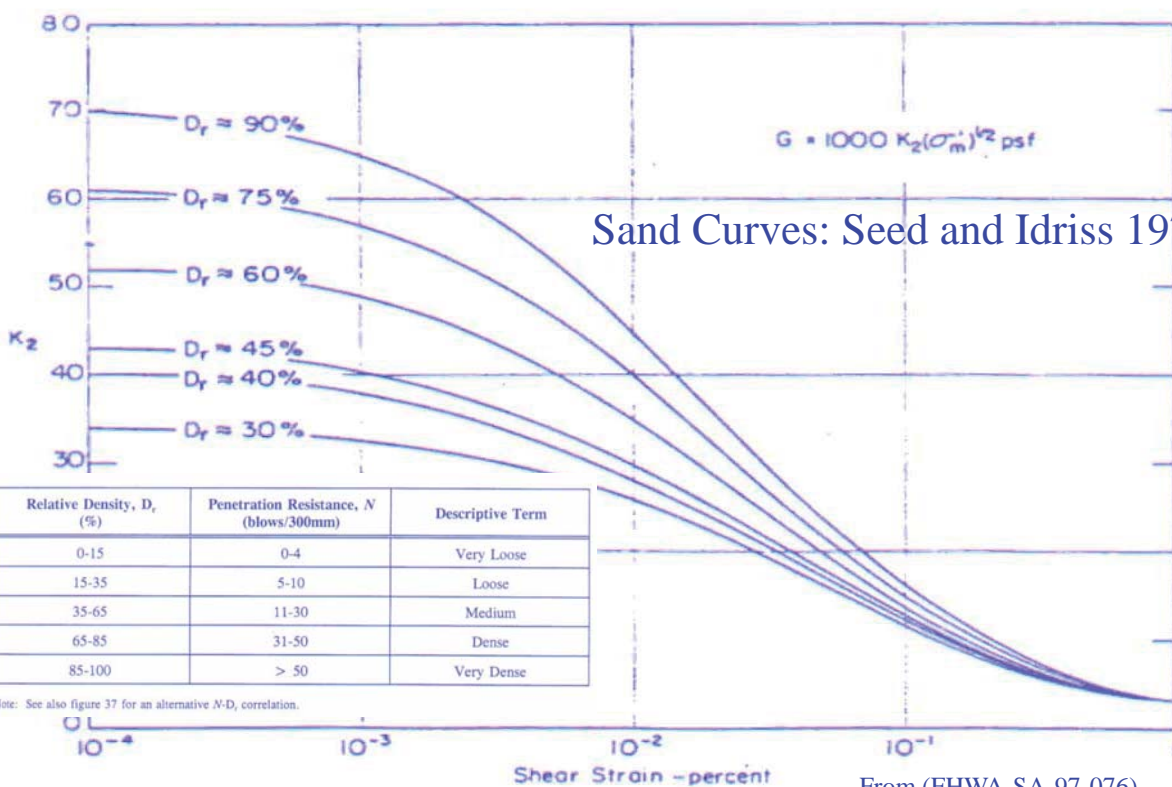
Equivalent Linear Properties



From (FHWA-SA-97-076)

Short course notes: A. Elgamal, Chicago, Illinois, April 29 -30, 2013

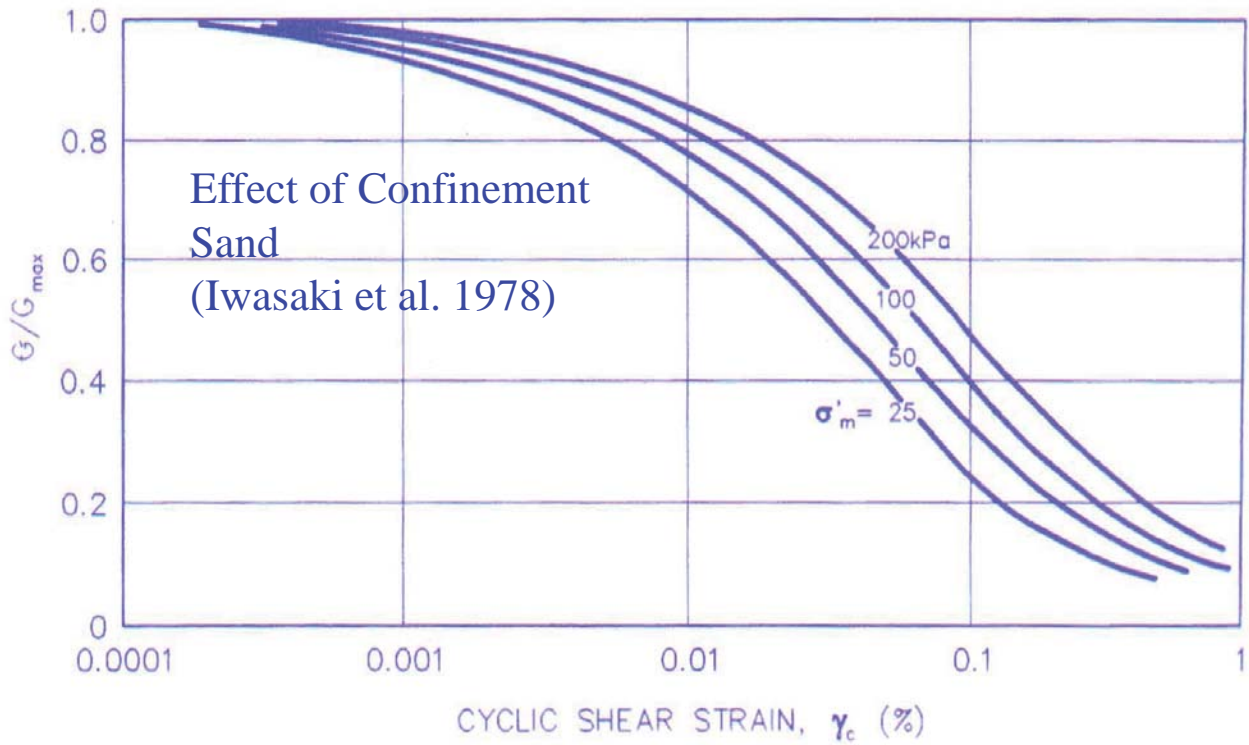
9



From (FHWA-SA-97-076)

Short course notes: A. Elgamal, Chicago, Illinois, April 29 -30, 2013

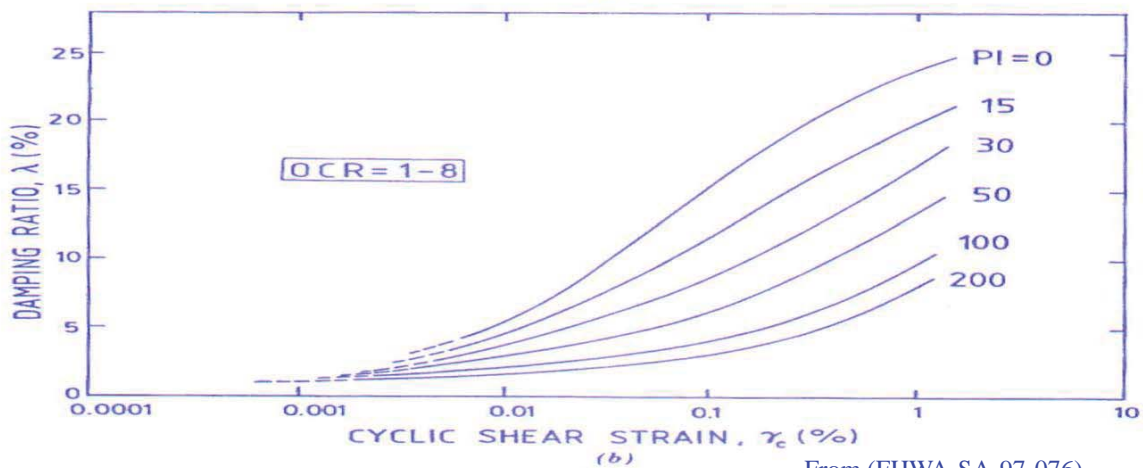
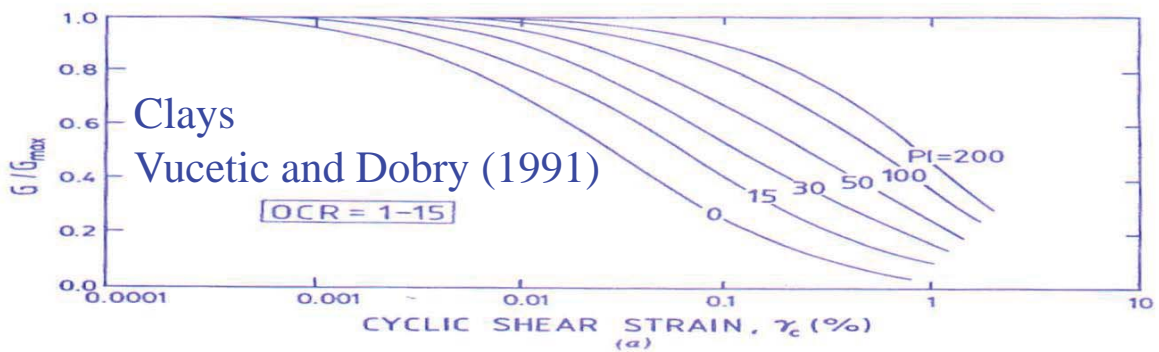
10



From (FHWA-SA-97-076)

Short course notes: A. Elgamal, Chicago, Illinois, April 29 -30, 2013

11



From (FHWA-SA-97-076)

Short course notes: A. Elgamal, Chicago, Illinois, April 29 -30, 2013

12

See also:

Darendeli, M. B. (2001). "Development of a new family of normalized modulus reduction and material damping curves." PhD dissertation, Univ. of Texas at Austin, Austin, Texas.

Darendeli, M.B., and K. H. Stokoe, II (2001). Development of a new family of normalized modulus reduction and material damping curves, *Geotech. Engrg. Rpt. GD01-1, University of Texas, Austin, Texas.*

Menq, F.-Y. (2003). Dynamic Properties of Sandy and Gravelly Soils. PhD Dissertation (supervisor: Prof. Kenneth H. Stokoe), Department of Civil Engineering, The University of Texas at Austin, May.

Reference	Correlation	Units	Limitation
Seed et al. (1984)	$G_{\max} = 220 (K_2)_{\max} (\sigma'_m)^{1/2}$ $(K_2)_{\max} \approx 20(N_1)_{60}^{1/3}$	kPa	$(K_2)_{\max} \approx 30$ for very loose sands and 75 for very dense sands; $\approx 80-180$ for dense well graded gravels; Limited to cohesionless soils
Imai and Tonouchi (1982)	$G_{\max} = 15,560 N_{60}^{0.68}$	kPa	Limited to cohesionless soils
Hardin (1978)	$G_{\max} = \frac{625}{(0.3 + 0.7 e_o^2)} (P_a \cdot \sigma'_m)^{0.5} OCR^k$	kPa ⁽¹⁾	Limited to cohesive soils P_a = atmospheric pressure
Jamiolkowski et al. (1991)	$G_{\max} = \frac{625}{e_o^{1.3}} (P_a \cdot \sigma'_m)^{0.5} OCR^k$	kPa ⁽¹⁾	Limited to cohesive soils P_a = atmospheric pressure
Mayne and Rix (1993)	$G_{\max} = 99.5(P_a)^{0.305}(q_c)^{0.695}/(e_o)^{1.13}$	kPa ⁽²⁾	Limited to cohesive soils P_a = atmospheric pressure

Notes: (1) P_a and σ'_m in kPa
 (2) P_a and q_c in kPa
 σ'_m = mean effective stress, OCR = Overconsolidation ratio
 q_c = CPT tip resistance, $N_1)_{60}$ = SPT corrected resistance (blow count)

Type of Soil	Initial Shear Modulus, G_{\max} (kPa)
Soft Clays	2,750 - 13,750
Firm Clays	6,900 - 34,500
Silty Sands	27,600 - 138,000
Dense Sands and Gravel	69,000 - 345,000

From (FHWA-SA-97-076)

Properties G , β , ρ , h are known

What SHAKE can do?

- **Free Surface Motion Prediction**
When motions at depth are known (either rock outcrop (incident) or total motion)
- **Deconvolution**
When motions at surface are known
(does not work well for nonlinear cases)

Caution when using SHAKE

- **Input motion as outcrop motion (changed to incident motion)**
- **Input motion as inlayer motion (Total motion)**
- **Layer height definition**
- **Units**

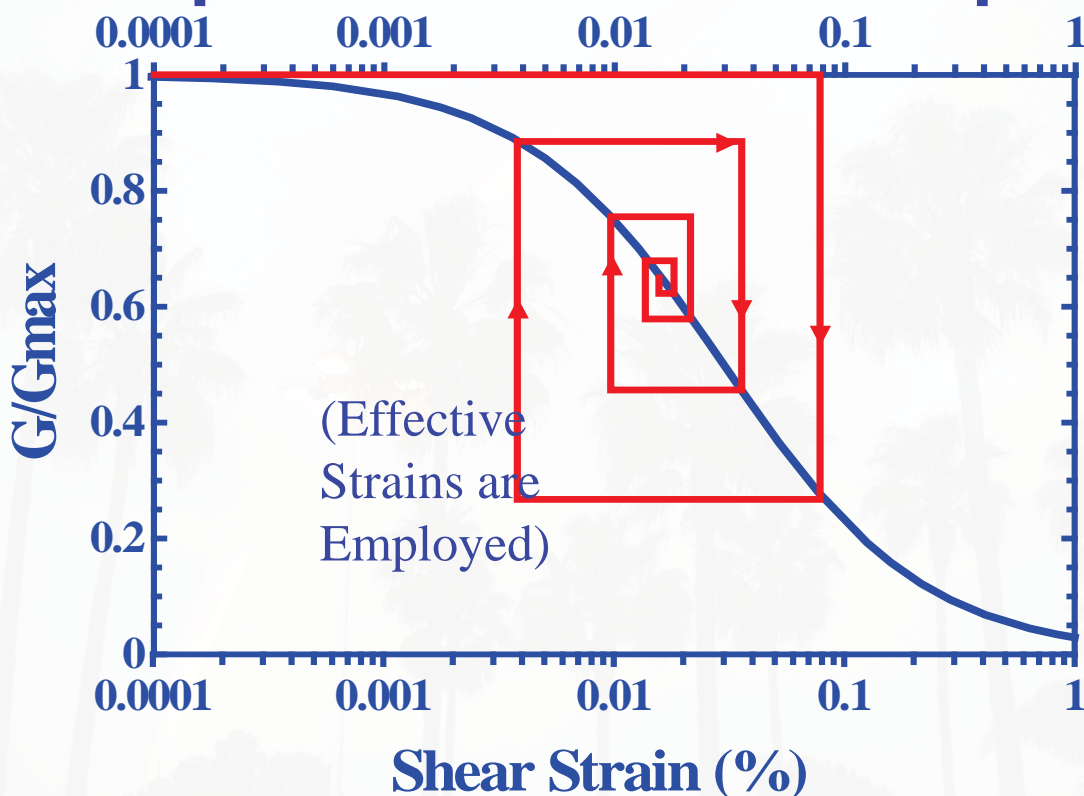
SHAKE Output

- Acceleration Time History
- Strain and Stress History
- Response Spectrum
- Fourier Spectrum
- Amplification Spectrum
- Strain Compatible Soil Properties (Equivalent Linear Option)

Short course notes:A. Elgamal, Chicago, Illinois, April 29 -30, 2013

17

Equivalent Linear Concept



Short course notes:A. Elgamal, Chicago, Illinois, April 29 -30, 2013

18

Caution when using SHAKE (equivalent linear option)

- **Layer Height Definition** (more layers result in additional accuracy, even for constant velocity profile).
- **Ratio of Effective Strain to Maximum** affects the result
- **Deconvolution** (may not work)!

Ratio of Effective Strain to Maximum

Effective Strain Ratio=(Magnitude of EQ -I)/I0

Idriss, [0.4, 0.85]

Ray Seed, as low as 0.35

What can SHAKE do?

See also (General Refs.):

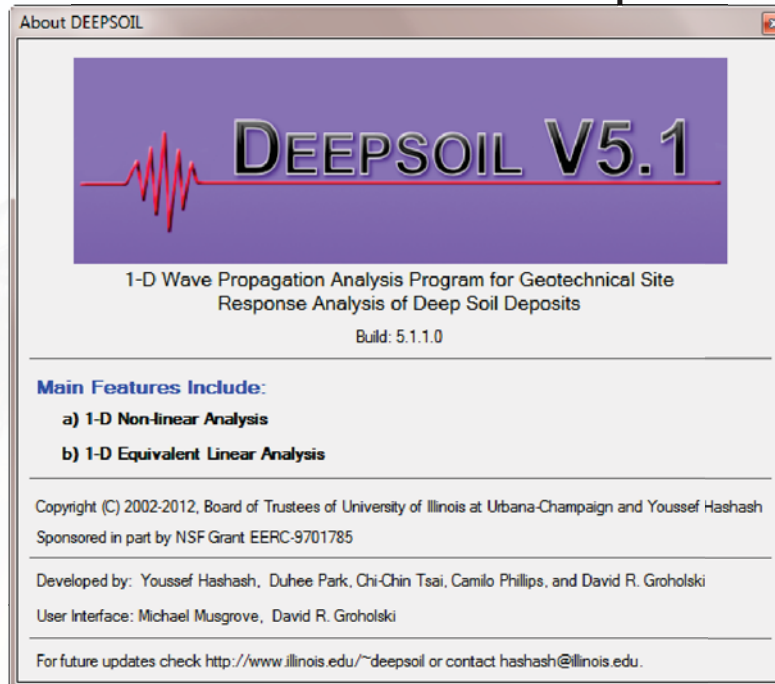
Use of Exact Solutions of Wave Propagation Problems to Guide Implementation of Nonlinear Seismic Ground Response Analysis Procedures, Annie O. L. Kwok, Jonathan P. Stewart, Youssef M. A. Hashash, Neven Matasovic, Robert Pyke, Zhiliang Wang, and Zhaohui Yang, Journal of Geotechnical and Geoenvironmental Engineering, Vol. 133, No. 11, November 1, 2007.

ProShake: Ground Response Analysis Program, Version 1.1 User's Manual, EduPro Civil Systems, Inc. Redmond, Washington .

Examples of User-friendly Computer Programs

DEEPSOIL (For XP and Windows 7)

www.illinois.edu/~deepsoil



CEE 588, Topic 08-P2; © 2013 Y. M. A.
Hashash & Others

This slide contributed by Professor Youssef Hashash

Short course notes: A. Elgamal, Chicago, Illinois, April 29 -30, 2013

23

DEEPSOIL SUMMARY

www.illinois.edu/~deepsoil

Non-linear analysis

- ❑ Hyperbolic hysteretic pressure dependent soil model
- ❑ Flexible sub-incrementation scheme to allow for accurate & efficient analysis
- ❑ Advanced damping formulations to reduce numerically introduced artificial damping

Equivalent Linear Analysis (a.k.a. SHAKE method)

- ❑ Unlimited number of soil layers of varying material properties
- ❑ Unlimited number of input motion data points
- ❑ Two types of complex shear modulus
- ❑ Improved numerical accuracy

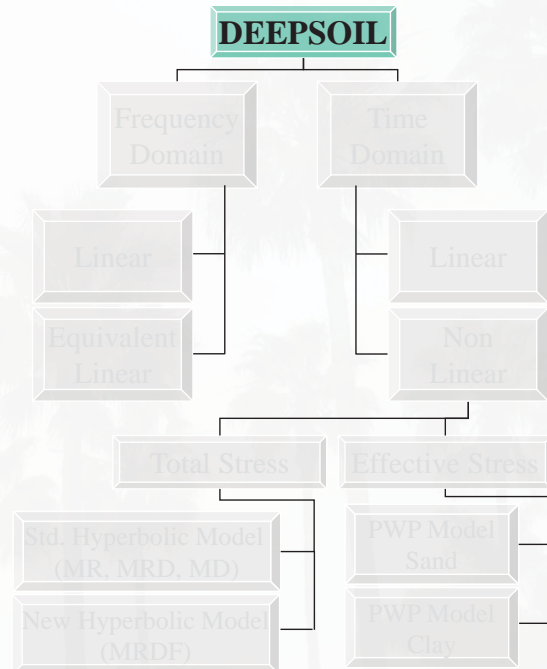
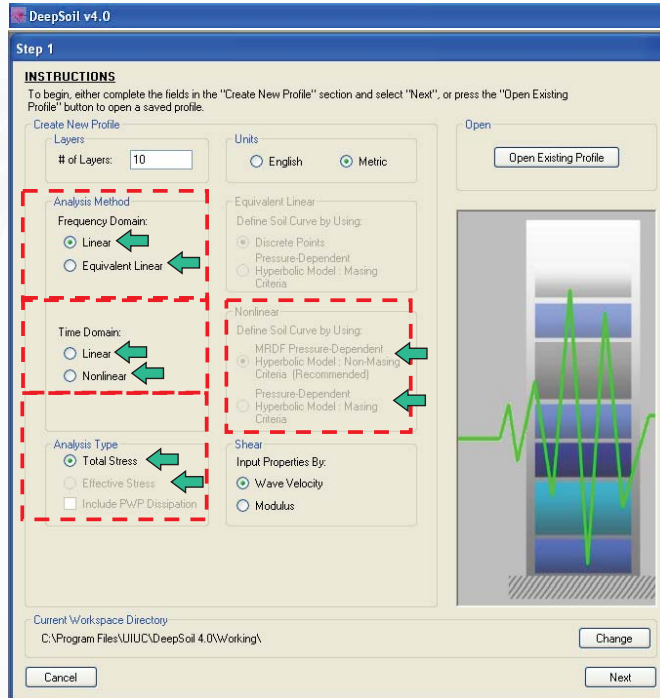
CEE 588, Topic 08-P2; © 2013 Y. M. A.
Hashash & Others

This slide contributed by Professor Youssef Hashash

Short course notes: A. Elgamal, Chicago, Illinois, April 29 -30, 2013

24

DEEPSOIL



CEE 588, Topic 08-P2; © 2013 Y. M. A. Hashash & Others

This slide contributed by Professor Youssef Hashash

Short course notes: A. Elgamal, Chicago, Illinois, April 29 -30, 2013

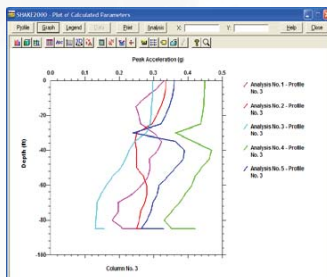
25

GeoMotions Suite

(www.GeoMotions.com)

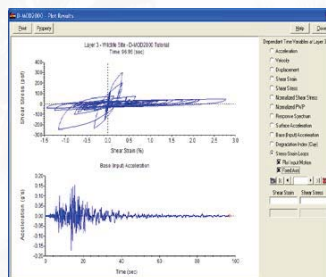
SHAKE2000

Equivalent-Linear
Total-Stress
Analysis



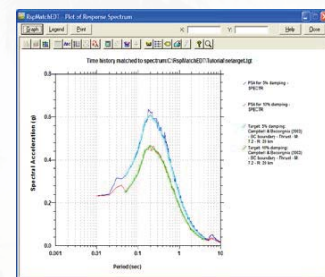
D-MOD2000

Fully Nonlinear Effective-
Stress
w/ PWP Dissipation



RspMatchEDT

Development of Design
Motions by Spectral
Matching



“The *GeoMotions Suite2000* is an essential toolkit for anyone practicing in the field of Geotechnical Earthquake Engineering” (Jonathan D. Bray)

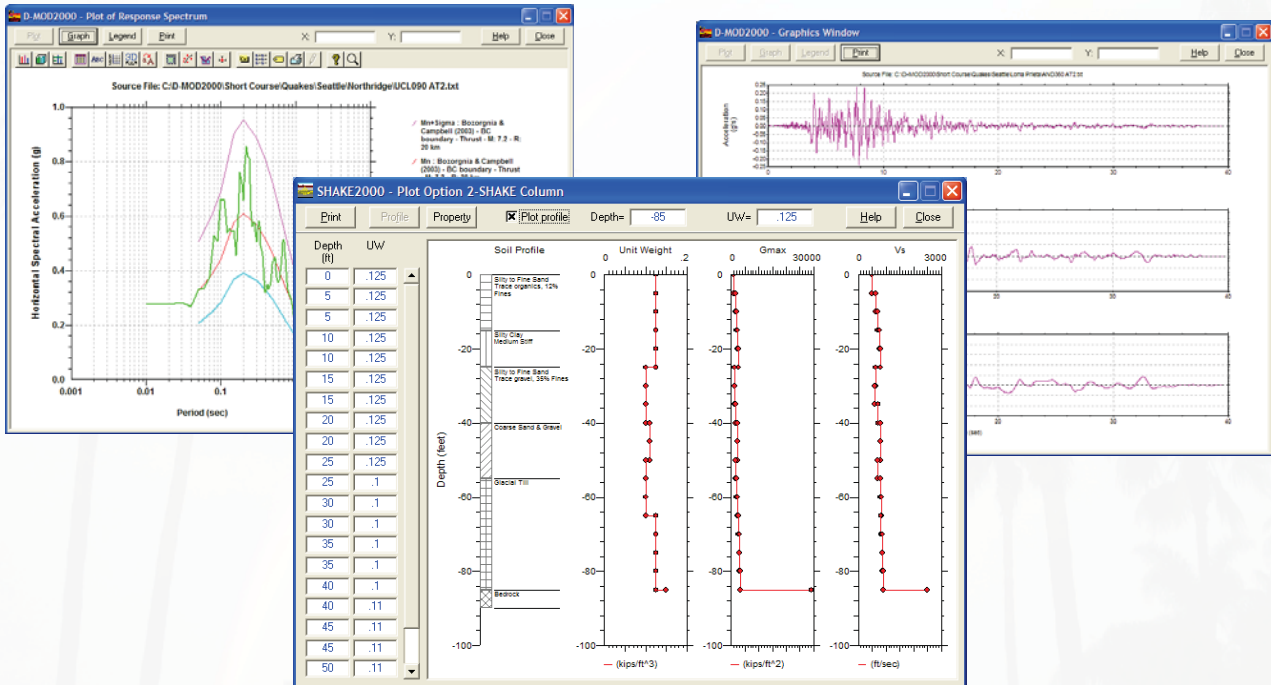
This slide contributed by Dr. Neven Matasovic

Copyright © 2009 GeoMotions, LLC

Short course notes: A. Elgamal, Chicago, Illinois, April 29 -30, 2013

26

Pre-Processing (Target Spectra, Design Motions, Soil Profile, ...)



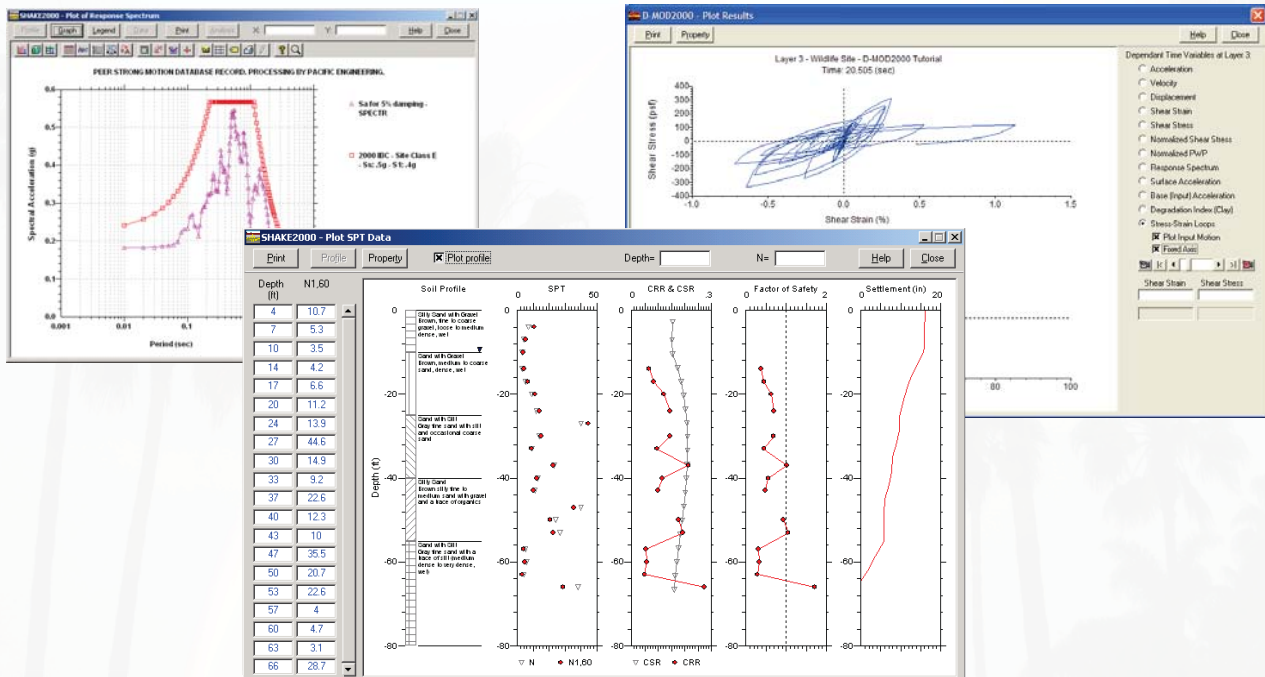
This slide contributed by Dr. Neven Matasovic

Copyright © 2009 GeoMotions, LLC

Short course notes: A. Elgamal, Chicago, Illinois, April 29 -30, 2013

27

Analysis (Total-Stress, Effective Stress, Liquefaction, ...)



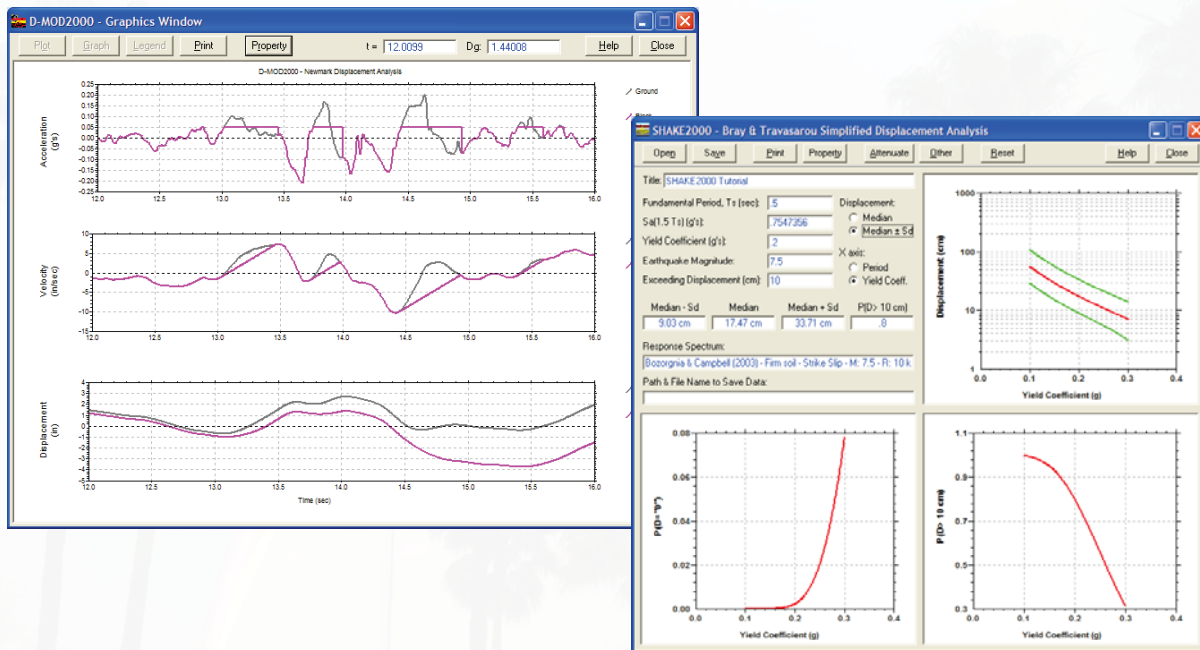
Copyright © 2009 GeoMotions, LLC

This slide contributed by Dr. Neven Matasovic

Short course notes: A. Elgamal, Chicago, Illinois, April 29 -30, 2013

28

Post-Processing (Newmark-type analysis, Animations, ...)



This slide contributed by Dr. Neven Matasovic

Short course notes: A. Elgamal, Chicago, Illinois, April 29 -30, 2013

29

PM4Sand Stress-Strain Model

- PM4Sand (Boulanger 2010, Boulanger & Ziotopoulou 2012) builds on the Dafalias & Manzari (2004) model.
- Modified & calibrated at equation level to improve consistency with body of experimental data & design correlations
 - Added fabric history, including cumulative fabric term
 - Plastic modulus (K_p), elastic modulus (G), and dilatancy (D) depend on fabric and fabric history
 - D constrained by Bolton's (1986) dilatancy relationship
 - Recast in terms of relative state parameter index (ξ_R)
 - Modified logic for updating initial back-stress ratio
 - Neglects Lode Angle dependence
- Implemented as a user-defined material model in FLAC (Itasca 2011) and posted on-line.

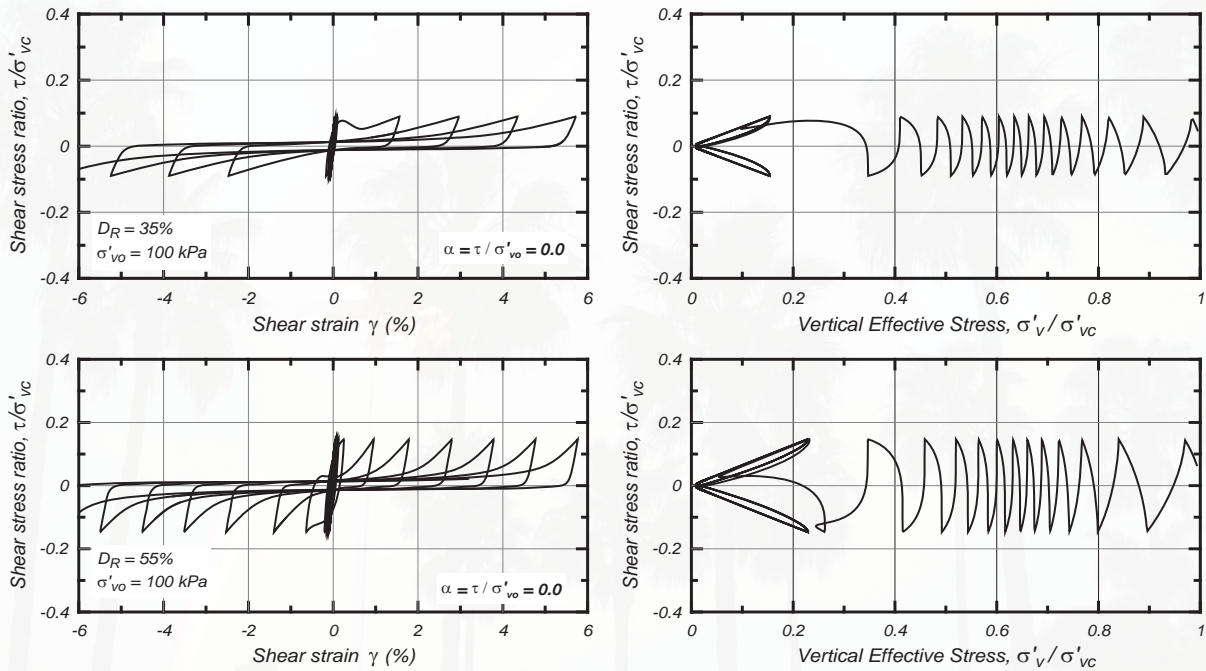
This slide contributed by Professor Ross Boulanger

Short course notes: A. Elgamal, Chicago, Illinois, April 29 -30, 2013

30

PM4SAND: Example – Cyclic undrained loading

- **Fabric damage terms in PM4Sand enable accumulation of shear strains:**



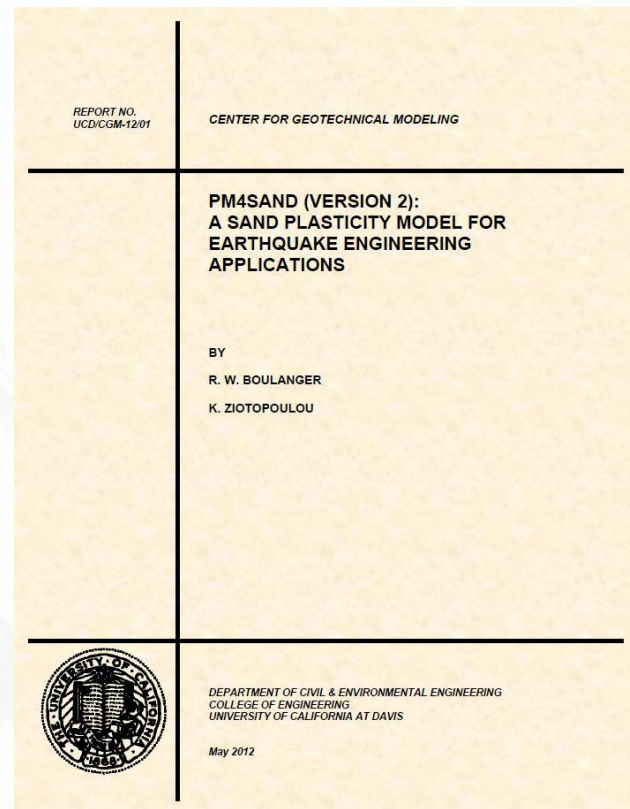
This slide contributed by Professor Ross Boulanger

Short course notes: A. Elgamal, Chicago, Illinois, April 29 -30, 2013

31

PM4SAND

- **Manual and documentation**
- **Element responses illustrated for:**
 - $D_R = 35, 55, 75\%$
 - σ'_v of $\frac{1}{4}, 1, 4, 16, \& 64$ atm
 - **Drained & undrained**
 - **Simple shear & plane-strain loading**
 - **Monotonic, cyclic, and post-cyclic.**
- **Purpose: know what you model can, and cannot, do well.**



This slide contributed by Professor Ross Boulanger

Short course notes: A. Elgamal, Chicago, Illinois, April 29 -30, 2013

32

OpenSees at UC Berkeley

for Earthquake Engineering Simulation - Home Page - Mozilla Firefox

w History Bookmarks ScrapBook Yahoo! Tools Help

http://opensees.berkeley.edu/index.php

OpenSees PEER NEES NEESit

HOME USER DEVELOPER PROJECTS SUPPORT PARALLEL SITE MAP

About News Calendar Registration

HOME

MESSAGE BOARD

USER DOC

DOWNLOAD

SOURCE CODE

BUG REPORT

OpenSees 2.0.0 Released

Version 2.0.0 of the [OpenSees binary](#) is now available for download. Here is the [change log](#).

Parallel Version Released

Register

For information about new releases we encourage you to register with us at the [OpenSees Registration Center](#).

News

2008-04-22 [Version 2.0.0](#)

Short course notes:A. Elgamal, Chicago, Illinois, April 29 -30, 2013

33

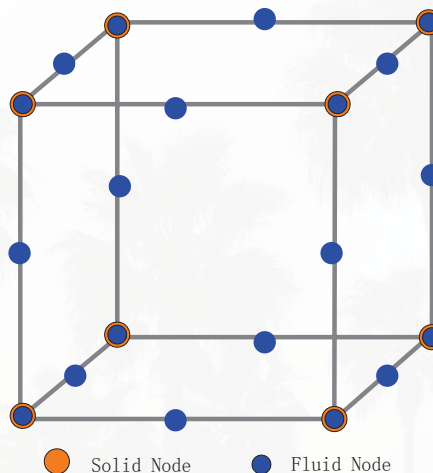
OpenSees

<http://opensees.berkeley.edu/>

PEER Center, UC Berkeley, Prof. Gregory Fenves



Open-source platform



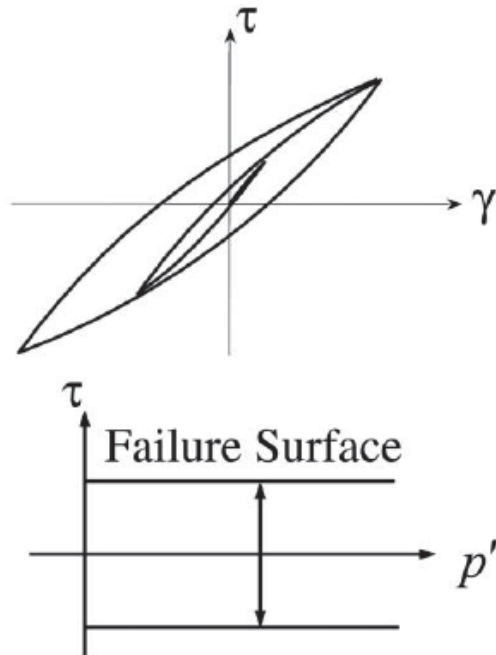
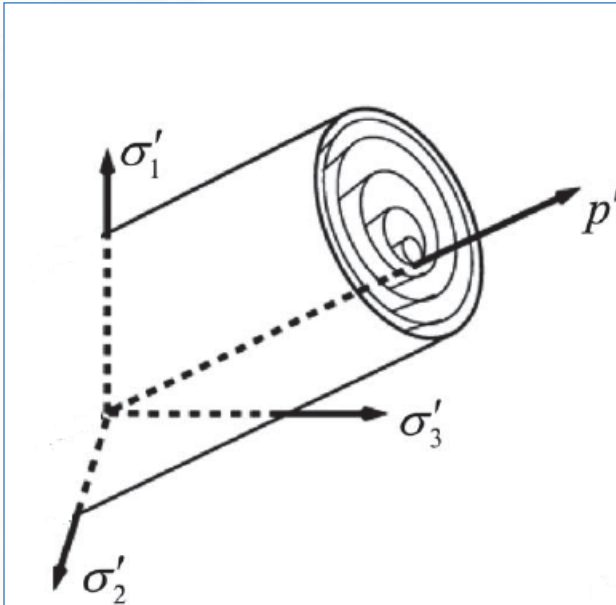
Solid-Fluid Fully Coupled Element for Saturated Soil

Beam Element for Pile

Short course notes:A. Elgamal, Chicago, Illinois, April 29 -30, 2013

34

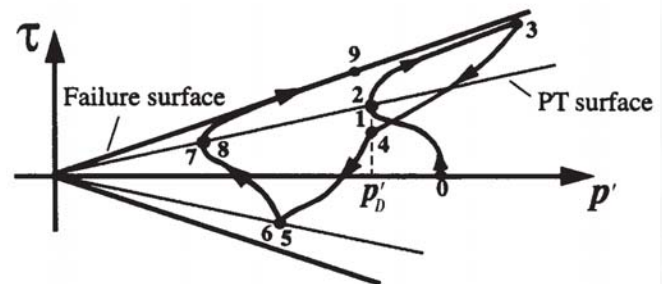
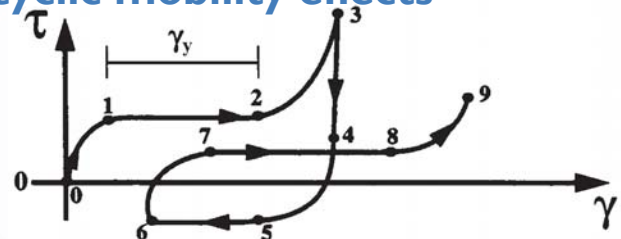
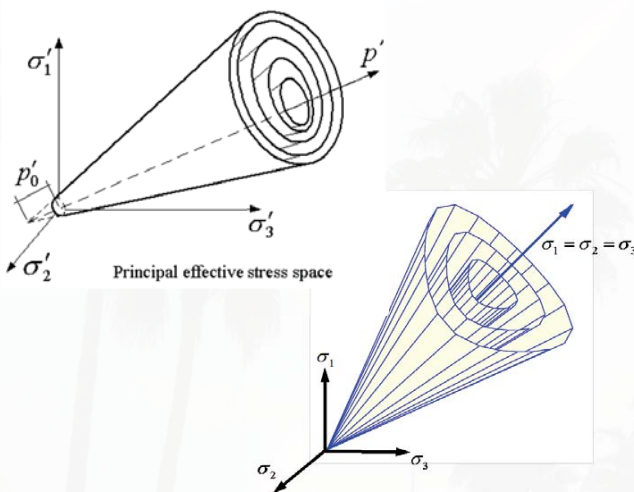
Nonlinear hysteretic Model



Note: Also available with Tension Cut-off for interface between structure and soil

Soil Constitutive Model

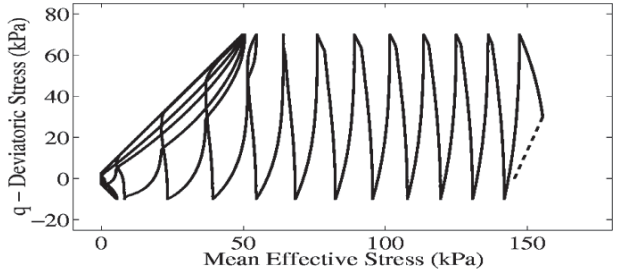
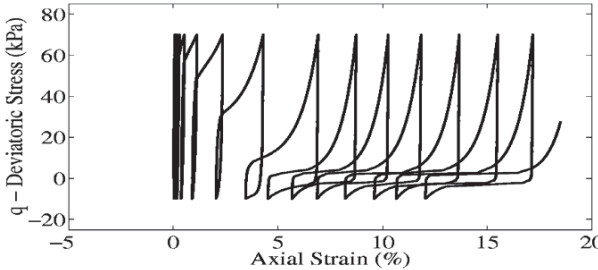
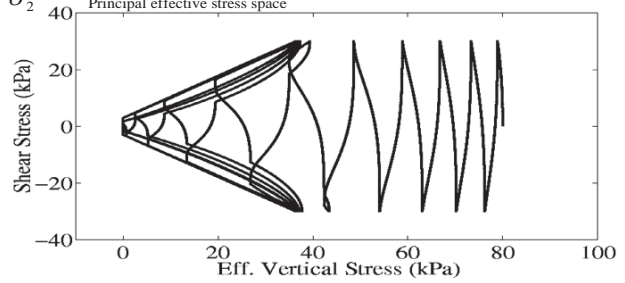
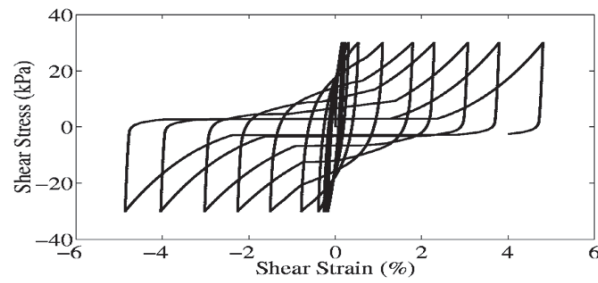
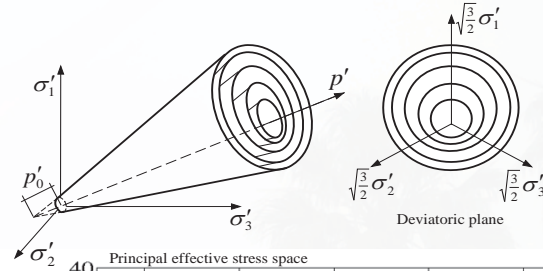
- Multi-yield surface plasticity model (based on Prevost 1985)
- Incorporating dilatancy and cyclic mobility effects



Conical yield surfaces for granular soils (Prevost 1985; Elgamal et al. 2003; Yang and Elgamal 2008)

Shear stress-strain and effective stress path under undrained shear loading condition (Parra 1996, Yang 2000, Yang and Elgamal 2002)

Soil Stress-Strain Model: Multi-surface Plasticity



Short course notes: A. Elgamal, Chicago, Illinois, April 29 -30, 2013

37

OpenSeesPL - Untitled

File Meshing Analyze Display View Options Help

Model Input

Model Definition

File Parameters...

Soil Parameters...

Mesh Parameters...

Analysis Options...

Load

Pushover

Define Pattern...

Base Shaking

Boundary Condition Type

Input Motion

Longitudinal (X) Transverse (Y) Vertical (Z)

X

Y

Z

Frequency (0.5-5Hz)

X Y Z

Number of Cycles (3-30)

X Y Z

Scale Factor (0.01-1)

X Y Z

Model Inclination along Longitudinal Direction

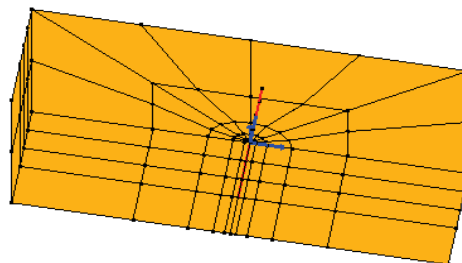
Ground Surface Inclination Angle (0-30 deg)

Whole Model Inclination Angle (0-10 deg)

Finite Element Mesh

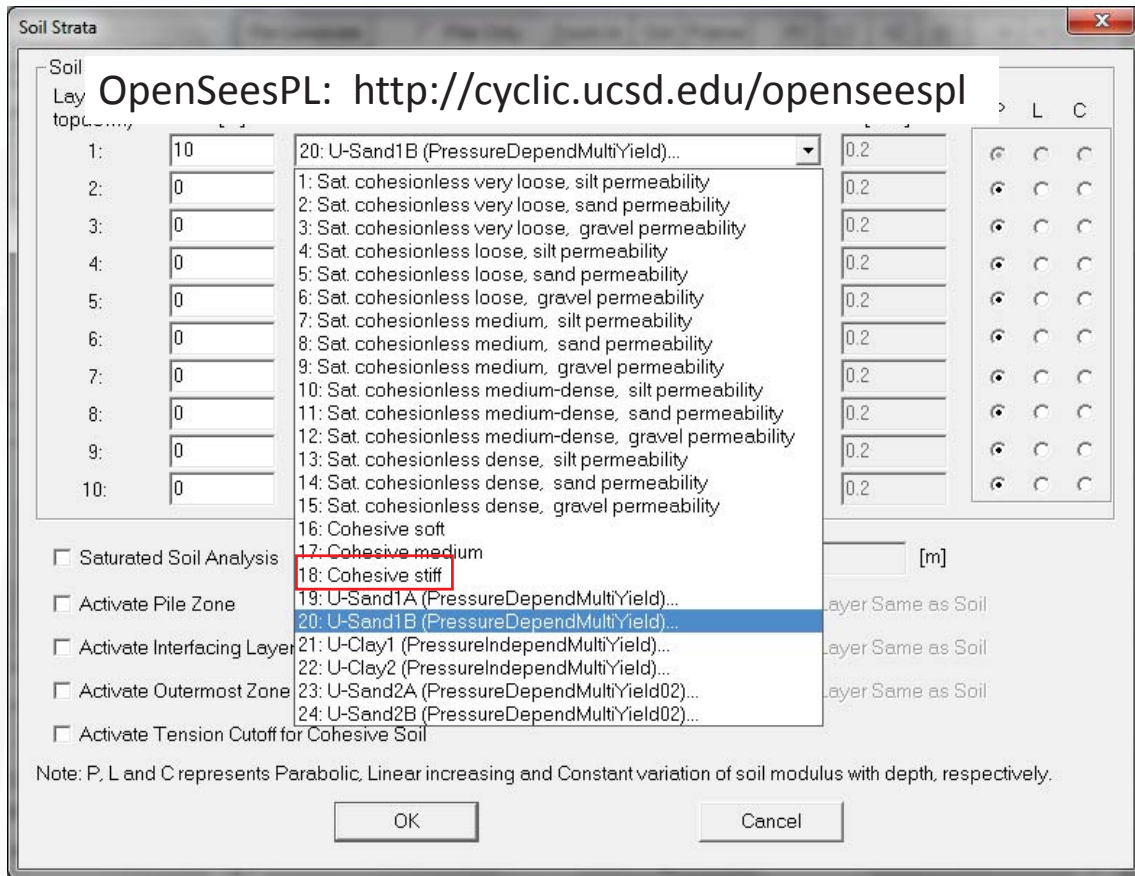
OpenSeesPL Graphical User Interface

<http://cyclic.ucsd.edu/openseespl>



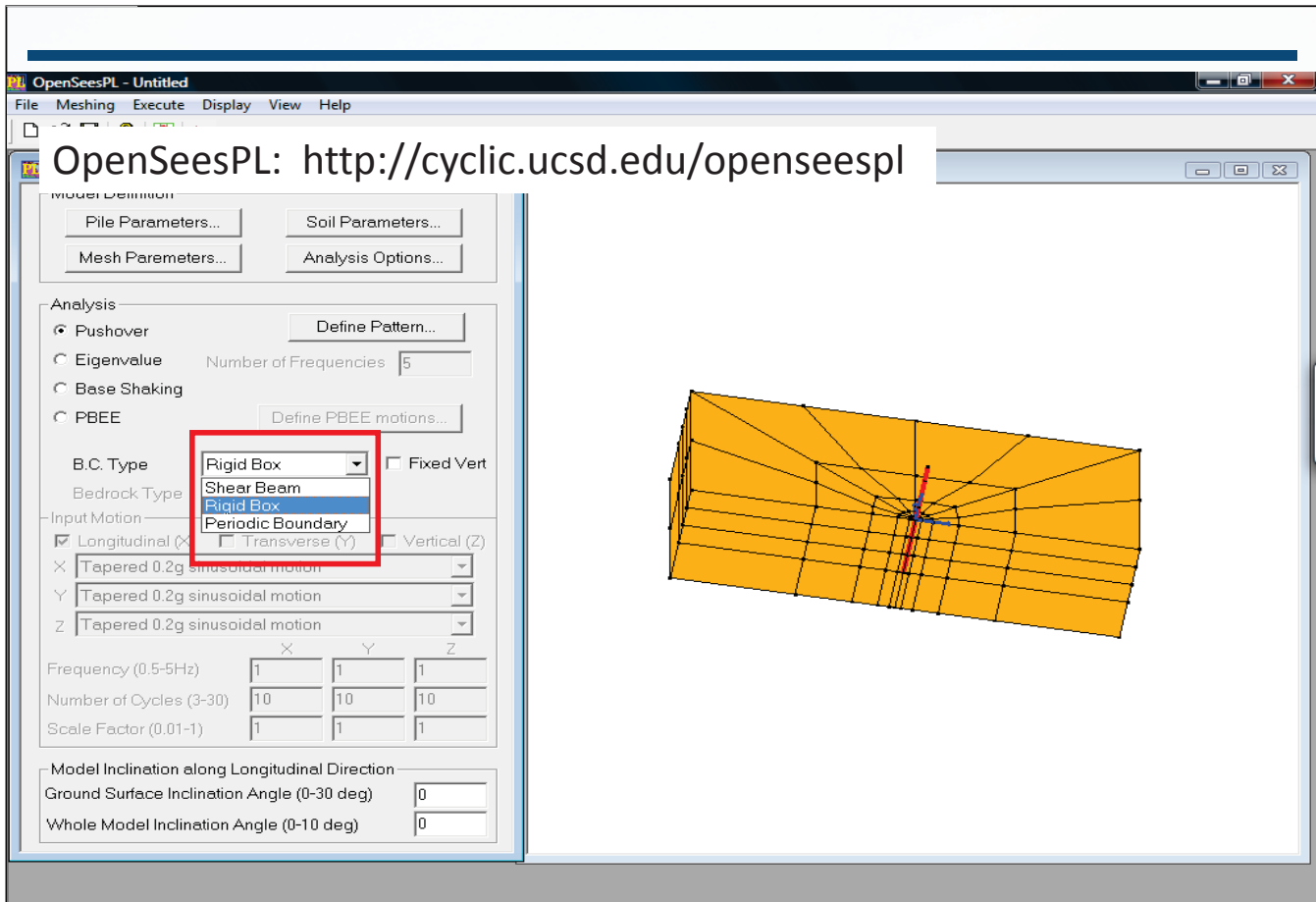
Short course notes: A. Elgamal, Chicago, Illinois, April 29 -30, 2013

38



Short course notes: A. Elgamal, Chicago, Illinois, April 29 -30, 2013

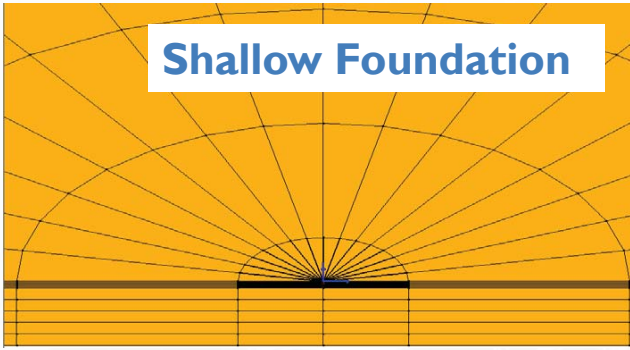
39



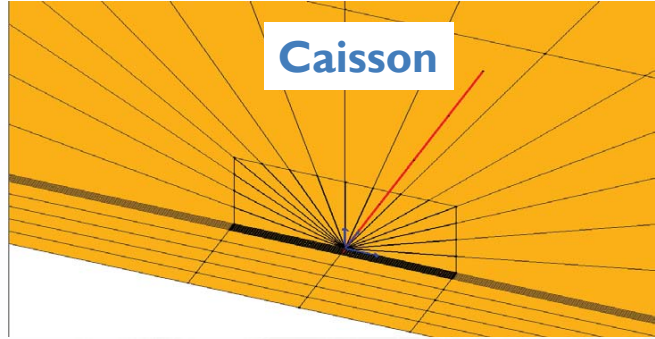
Short course notes: A. Elgamal, Chicago, Illinois, April 29 -30, 2013

40

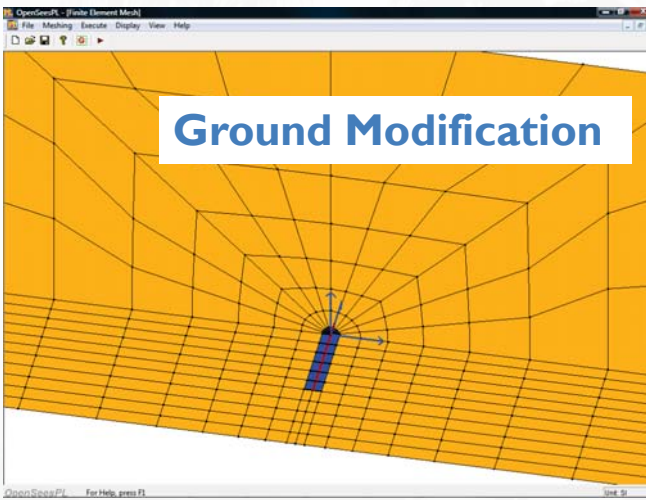
Shallow Foundation



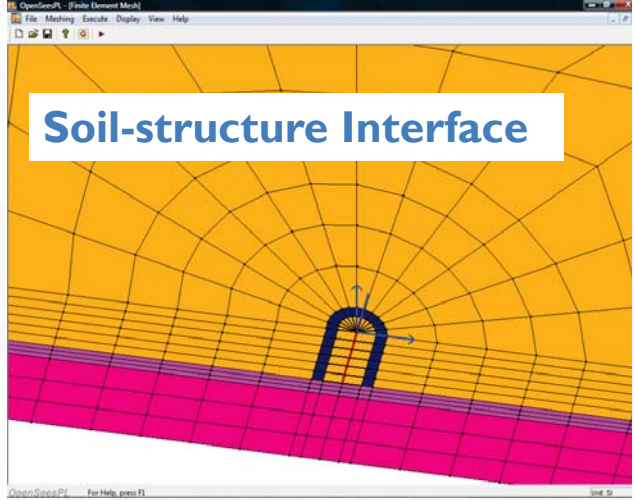
Caisson



Ground Modification

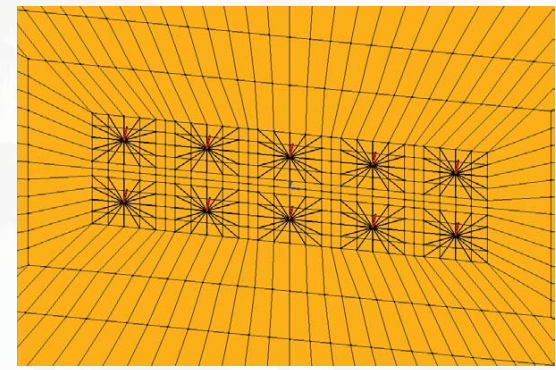
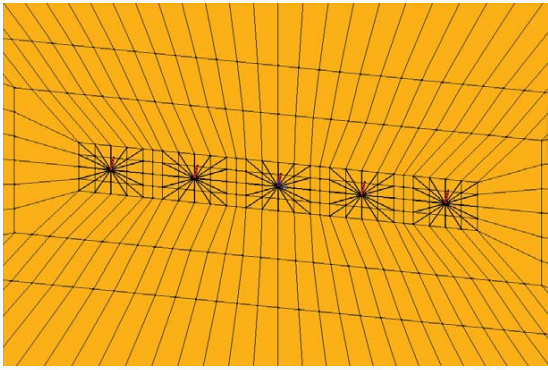
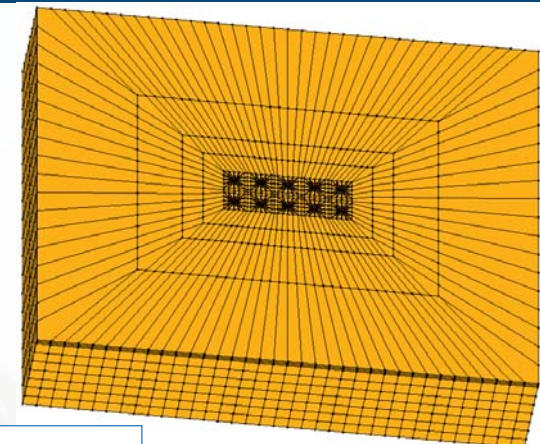
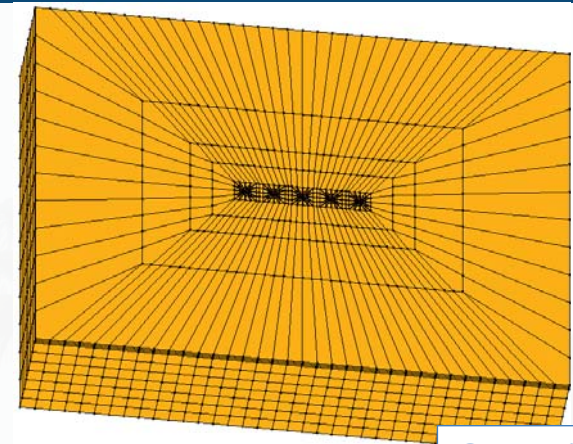


Soil-structure Interface

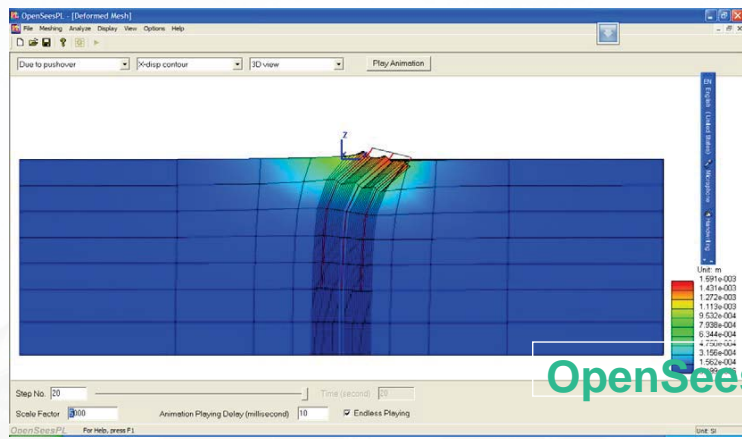


Short course notes:A. Elgamal, Chicago, Illinois, April 29 -30, 2013

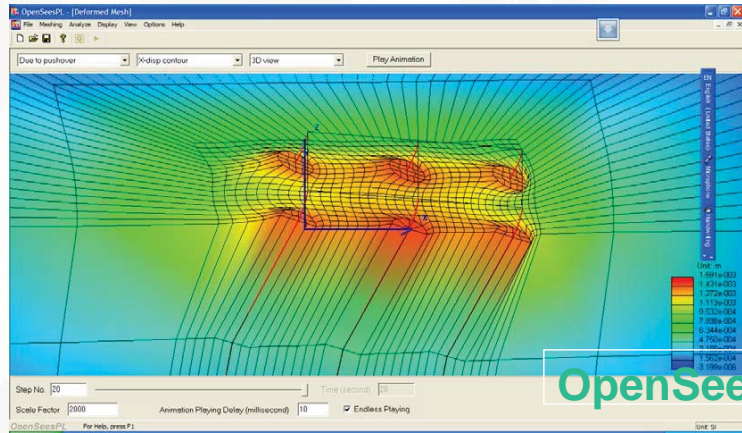
Ongoing Research



Short course notes:A. Elgamal, Chicago, Illinois, April 29 -30, 2013



OpenSeesPL



OpenSeesPL

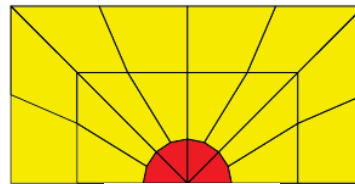
Short course notes:A. Elgamal, Chicago, Illinois, April 29 -30, 2013

43

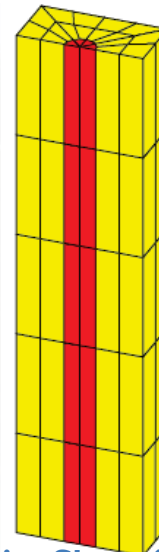
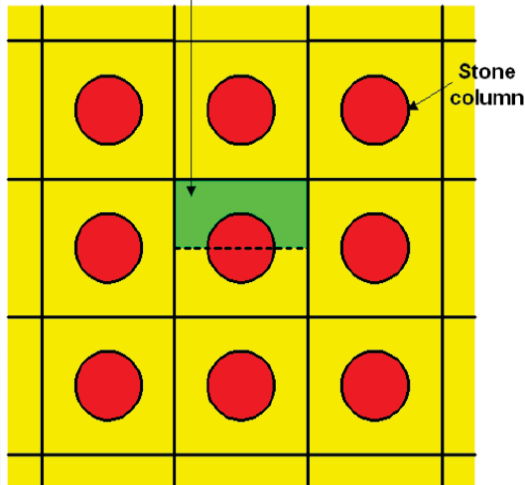


Ground Modification

- Gravel Drain/Stone column
- Pile Pinning



Half mesh within S x S "cell"



Schematic view of stone column or pile-pinning layout

10 m depth Sand Layer (or Silt Layer)

Mild Infinite Slope (4 degrees)

Short course notes:A. Elgamal, Chicago, Illinois, April 29 -30, 2013

44

OpenSeesPL - Untitled

File Meshing Analyze Display View Options Help

Model Input Finite Element Mesh

<http://cyclic.ucsd.edu/openseespl>

Model Definition

Analysis

- Pushover Define Pattern...
- Eigenvalue Number of Frequencies 5
- Base Shaking
 - B.C. Type Laminar Container Fixed Vert
 - Bedrock Type Rigid Bedrock

Input Motion

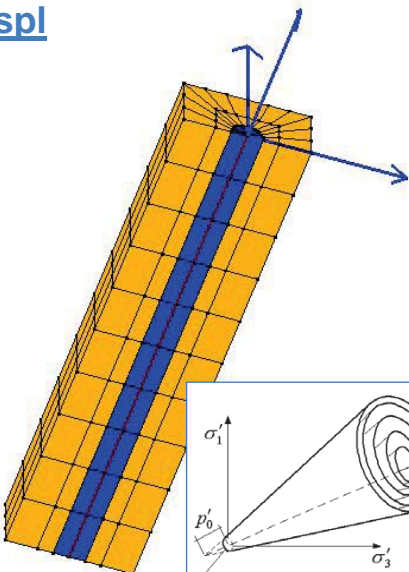
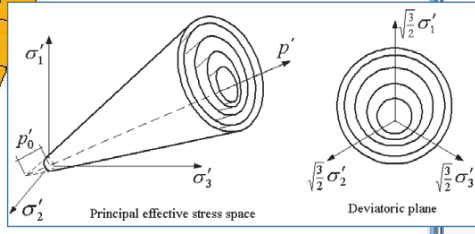
- Longitudinal (X) Transverse (Y) Vertical (Z)
- X Tapered 0.2g sinusoidal motion
- Y Tapered 0.2g sinusoidal motion
- Z Tapered 0.2g sinusoidal motion

Frequency (0.5-5Hz)	1	1	1
Number of Cycles (3-30)	10	10	10
Scale Factor (0.01-1)	1	1	1

Model Inclination along Longitudinal Direction

Ground Surface Inclination Angle (0-30 deg) 0

Whole Model Inclination Angle (0-10 deg) 0

OpenSeesPL For Help, press F1 Unit: SI

Short course notes:A. Elgamal, Chicago, Illinois, April 29 -30, 2013

45

BridgePBEE: PBEE Analysis Framework For Bridge-Abutment-Ground Systems (2-Span Bridge)

Ahmed Elgamal and Jinchi Lu
 University of California, San Diego
 Kevin Mackie
 University of Central Florida



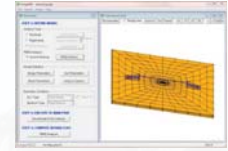
Short course notes:A. Elgamal, Chicago, Illinois, April 29 -30, 2013

46

BridgePBEE: PBEE Analysis Framework For Bridge-Abutment-Ground Systems (2-Span Bridge)

What is BridgePBEE

BridgePBEE* (<http://peer.berkeley.edu/bridgepbee/>)



BridgePBEE is a PC-based graphical pre- and post-processor (user-interface) for conducting Performance-Based Earthquake Engineering (PBEE) studies for bridge-ground systems (2-span single column).

The three-dimensional (3D) finite element computations are conducted using **OpenSees** developed by the Pacific Earthquake Engineering Research Center (PEER).

The analysis options available in BridgePBEE include (SI units in current version): 1) Pushover Analysis, 2) Base Input Acceleration Analysis, and 3) Full Performance-Based Earthquake Engineering (PBEE) Analysis.

*Lu, J., Mackie, K.R., and Elgamal, A. (2011). **BridgePBEE: OpenSees 3D Pushover and Earthquake Analysis of Single-Column 2-span Bridges, User Manual, Beta 1.0.**

Short course notes:A. Elgamal, Chicago, Illinois, April 29 -30, 2013

47

Select PBEE Terminology

IM - Intensity Measure for a given earthquake motion

For any input earthquake motion, the Intensity Measures calculated by BridgePBEE include:

PGA (Peak Ground Acceleration)

PGV (Peak Ground Velocity)

PGD (Peak Ground Displacement)

D₅₋₉₅ (Strong Motion Duration)

CAV (Cumulative Absolute Velocity)

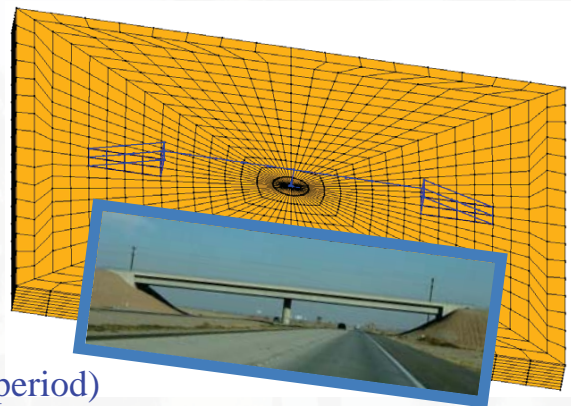
Arias Intensity

SA (Spectral Acceleration; assuming 1 second period)

SV (Spectral Velocity), SD (Spectral Displacement)

PSA (Pseudo-spectral Acceleration)

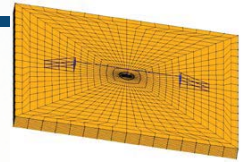
PSV (Pseudo-spectral Velocity)



Short course notes:A. Elgamal, Chicago, Illinois, April 29 -30, 2013

48

The BridgePBEE Framework

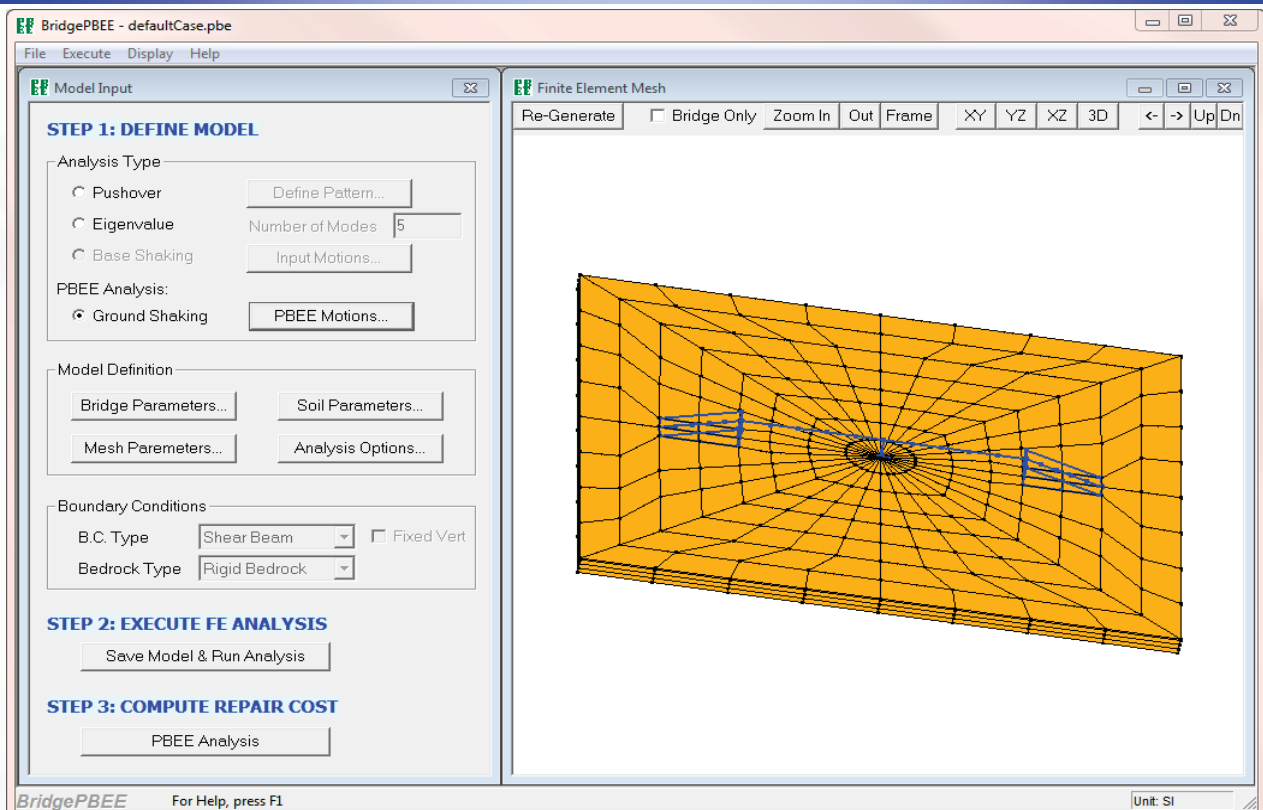


- Define Bridge-abutment-ground geometry and material properties
- Select/Define ensembles of input earthquake ground acceleration (e.g., 100 different ground motions spanning a wide range of Intensities as defined by IM quantities such as Peak ground acceleration (PGA) or Peak Ground Velocity (PGV))
- Conduct individual earthquake shaking simulations for all input motions and View output in terms of Decision Variables (DVs) such as peak column drift and other similar parameters of interest displayed against any desired IM for each employed earthquake input motion.
- View detailed time histories of all responses of interest for any of the individual earthquake simulations (including animations of the deformed mesh, ...).
- Use the DVs (clustered into Performance groups or PGs) variation against the IM to compute repair cost and repair time (based on pre-defined relationships that related the level of each DV to a Damage State (DS) and these Damage states associated with different levels of repair (pre-defined by repair quantities and associated repair times). See contribution to cost for each repair quantity, or for each Performance group as a function of the level of shaking (represented by the IM parameter).
- Compute total cost and repair time shown as a function of level of IM (such as PGV)
- For the bridge geographic location, define the expected seismic hazard.
- Use expected seismic hazard and define expected repair cost and time for this bridge
- For any possible level of shaking, see % contribution of the various performance groups (the DVs) or the Repair quantities to the overall cost or time.

Short course notes:A. Elgamal, Chicago, Illinois, April 29 -30, 2013

49

BridgePBEE Main Window



Short course notes:A. Elgamal, Chicago, Illinois, April 29 -30, 2013

50

Appendix I: Basics of Dynamic Response

Single-Degree-of-Freedom (SDOF) and Response Spectrum

Short course notes: A. Elgamal, Chicago, Illinois, April 29 – 30, 2013

51

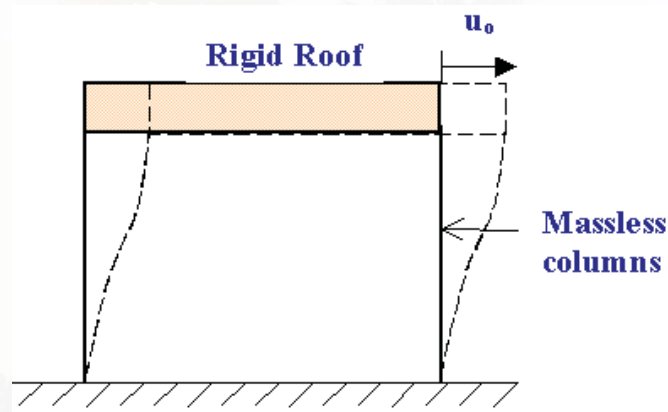
Dynamics of a Simple Structure

The Single-Degree-Of-Freedom (SDOF) Equation

References

Elements Of Earthquake Engineering And Structural Dynamics, André Filiatrault, Polytechnic International Press, Montréal, Canada, ISBN 2-553-00629-4 (Section 4.2.3).

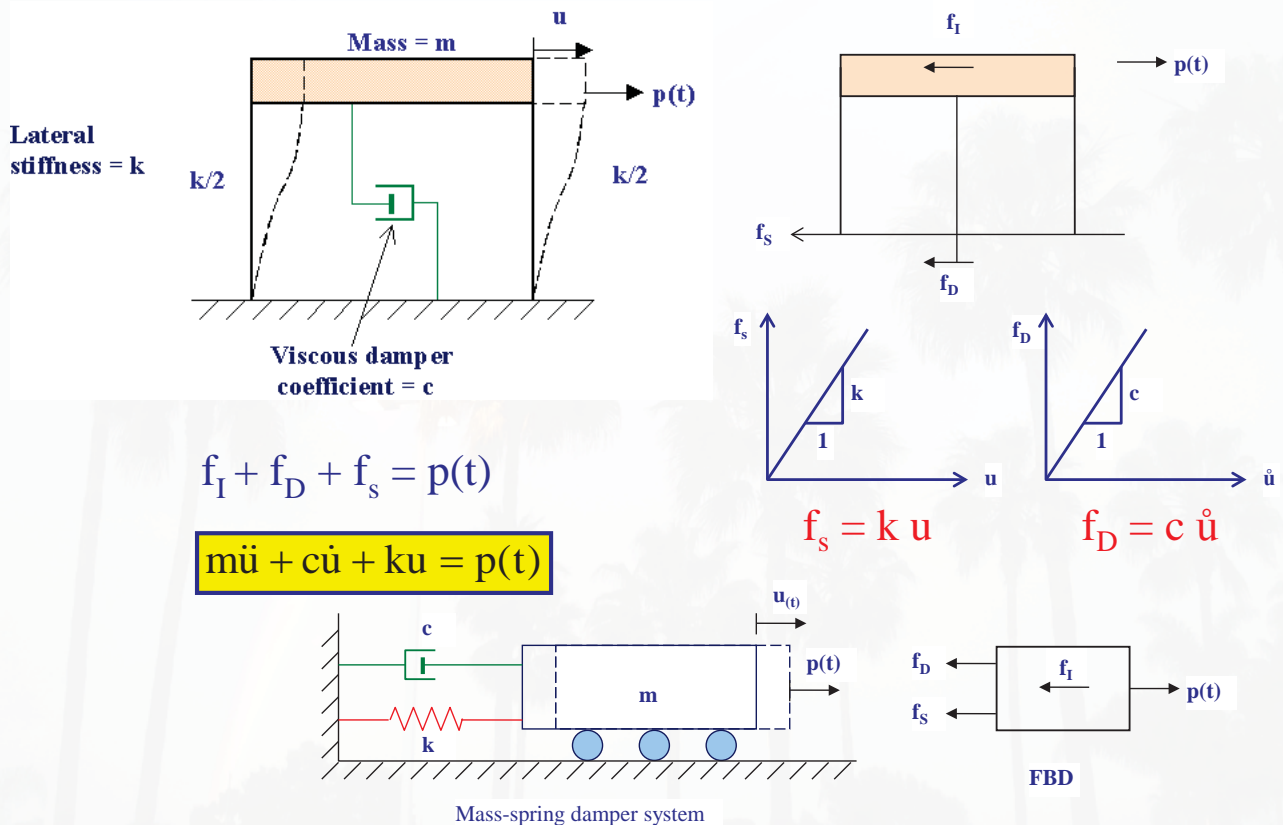
Dynamics of Structures, Anil K. Chopra, Prentice Hall, New Jersey, ISBN 0-13-855214-2 (Chapter 3).



Short course notes: A. Elgamal, Chicago, Illinois, April 29 – 30, 2013

52

Equation of motion (external force)



Short course notes: A. Elgamal, Chicago, Illinois, April 29 – 30, 2013

53

Earthquake Ground Motion

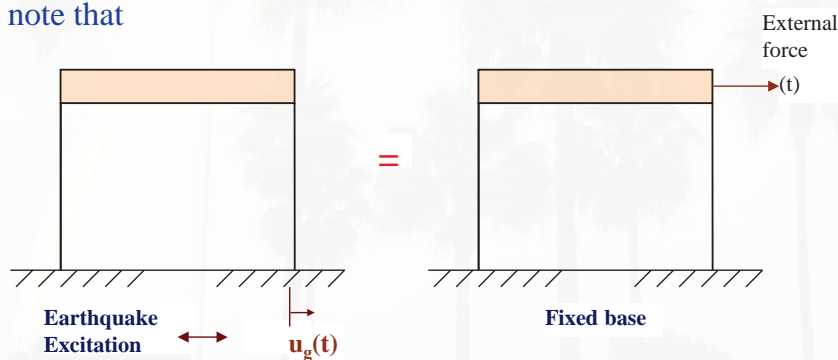
$$f_I + f_D + f_s = 0$$

$$f_I = m \ddot{u}_t = m(\ddot{u}_g + \ddot{u})$$

$$m(\ddot{u} + \ddot{u}_g) + c\dot{u} + ku = 0$$

$$m\ddot{u} + c\dot{u} + ku = -m\ddot{u}_g$$

You may note that



Short course notes: A. Elgamal, Chicago, Illinois, April 29 – 30, 2013

54

Undamped natural frequency

Property of structure when allowed to vibrate freely without external excitation

$$\omega = \sqrt{\frac{k}{m}} \quad \text{Undamped natural circular frequency of vibration (radians/second)}$$

$$f = \frac{\omega}{2\pi} \quad \text{natural cyclic frequency of vibration (cycles/second or 1/second or Hz)}$$

$$T = \frac{1}{f} \quad \text{natural period of vibration (second)}$$

T is the time required for one cycle of free vibration

If damping is present, replace ω by ω_D

where $\omega_D = \omega\sqrt{1-\xi^2}$ natural frequency, and

$$\xi = \frac{c}{2m\omega} \quad \text{fraction of critical damping coefficient}$$

$$= \frac{c}{c_c} \quad (\text{dimensionless measure of damping}) \quad \text{called damping ratio} \quad = \frac{c}{2\sqrt{km}}$$

$$c_c = 2m\omega = 2\sqrt{km}$$

55

Short course notes: A. Elgamal, Chicago, Illinois, April 29 – 30, 2013

in terms of ξ

$$m\ddot{u} + c\dot{u} + ku = -m\ddot{u}_g$$

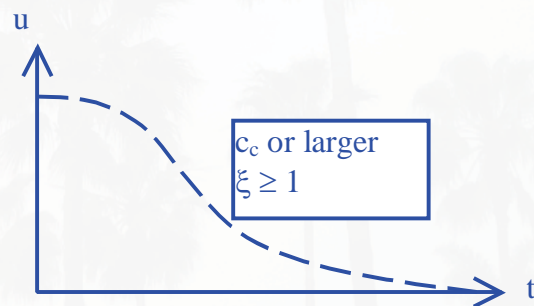
$$\ddot{u} + \frac{c}{m}\dot{u} + \frac{k}{m}u = -\ddot{u}_g$$

$$\ddot{u} + 2\xi\omega\dot{u} + \omega^2u = -\ddot{u}_g$$

In general $\xi < 0.2$, i.e., $\omega_D \approx \omega$, $f_D \approx f$, $T = T_D$

c_c least damping that prevents oscillation

ξ may be in the range of 0.02 – 0.2 or 2% - 20%
5% is sometimes a typical value.



e.g., damper on a swinging door

56

Short course notes: A. Elgamal, Chicago, Illinois, April 29 – 30, 2013

Note: After the phase of forced vibration (due to external force or base excitation, or initial conditions), the structure continues to vibrate in a “free vibration” mode till it stops due to damping. The ratio between amplitude in two successive cycles is

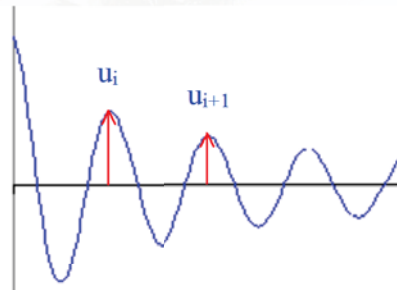
$$\frac{u_i}{u_{i+1}} \approx e^{2\pi\xi}$$

where we define the logarithmic decrement as

$$\delta = 2\pi\xi = \ln\left(\frac{u_i}{u_{i+1}}\right) \text{ if you measure a free vibration response you can find } \xi.$$

Note: for peaks j cycles apart

$$\ln\left(\frac{u_i}{u_{i+j}}\right) = j\delta = 2j\pi\xi$$



Free vibration

Critical viscous damping

The free vibration equation may be written as

$$m\ddot{x} + c\dot{x} + kx = 0$$

and the general solution is

$$x = C_1 e^{\left[\frac{-c}{2m} + \sqrt{\left(\frac{c}{2m}\right)^2 - \left(\frac{k}{m}\right)}\right] t} + C_2 e^{\left[\frac{-c}{2m} - \sqrt{\left(\frac{c}{2m}\right)^2 - \left(\frac{k}{m}\right)}\right] t}$$

if $\left(\frac{c}{2m}\right)^2 = \frac{k}{m}$, the radical part of the exponent will vanish. This will produce aperiodic response (non-oscillatory). In this case

$$\frac{c^2}{(2m)^2} = \frac{k}{m} \text{ or } c = 2\sqrt{km} = c_c$$

since $\omega = \sqrt{\frac{k}{m}}$, c_c is also equal to $2m\omega$ (note that $2\sqrt{km} = 2\sqrt{m\omega^2 m} = 2m\omega$)

$$\text{and also } c_c = 2\sqrt{km} = 2\sqrt{k(k/\omega^2)} = \frac{2k}{\omega}$$

Deformation Response Spectrum

For a given EQ excitation calculate $|u_{max}|$ from SDOF response with a certain ξ and within a range of natural periods or frequencies.

$|u_{max}|$ for each frequency will be found from the computed $u(t)$ history at this frequency.

A plot of $|u_{max}|$ vs. natural period is constructed representing the deformation (or displacement) response spectrum (S_d).

From this figure, one can directly read the maximum relative displacement of any structure of natural period T (and a particular value of ξ as damping)

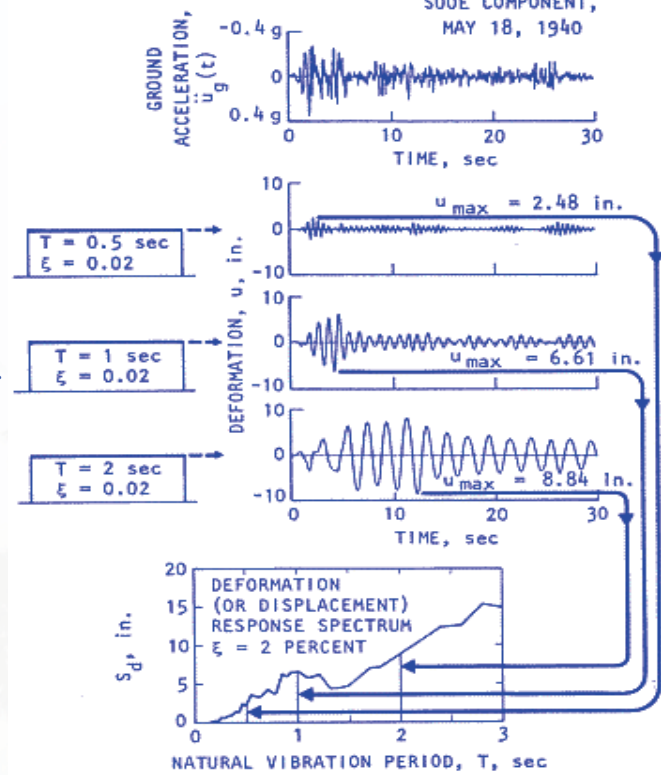


Figure 17. Computation of deformation (or displacement) response spectrum

Concept of Equivalent lateral force f_s

If f_s is applied as a static force, it would cause the deformation u .

Thus at any instant of time:

$$f_s = ku(t), \text{ or in terms of the mass } f_s(t) = m\omega^2 u(t)$$

$$\omega = \sqrt{\frac{k}{m}}$$

The maximum force will be

$$f_{s,max} = m\omega^2 u_{max} = ku_{max} = mS_a = kS_d$$

$$S_a = \frac{k}{m} S_d$$

$$S_a = \omega^2 S_d$$

S_d = deformation or displacement response spectrum

$$S_a = \omega^2 S_d = \text{pseudo-acceleration response spectrum}$$

The maximum strain energy E_{max} stored in the structure during shaking is:

$$E_{max} = \frac{1}{2} k u_{max}^2 = \frac{1}{2} k S_d^2 = \frac{1}{2} \frac{k}{\omega^2} \omega^2 S_d^2 = \frac{1}{2} m \omega^2 S_d^2 = \frac{1}{2} m S_v^2$$

where $S_v = \omega S_d$ = pseudo-velocity response spectrum

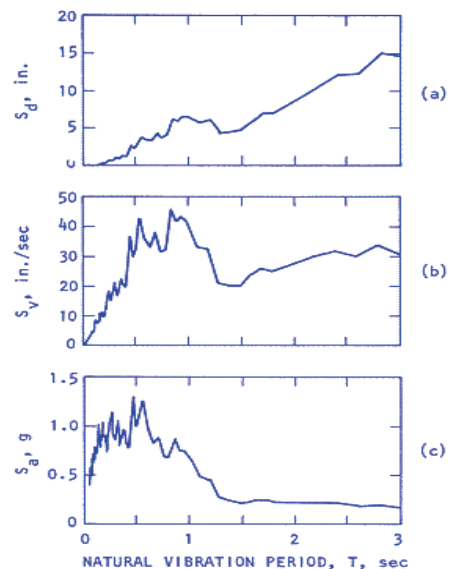


Figure 19. (a) Deformation (or Displacement), (b) pseudo-velocity and (c) pseudoacceleration response spectra. El Centro ground motion—500°E component. Damping ratio $\xi = 2$ percent

From: Chopra, Dynamics of Structures, A Primer

Note that S_d , S_v and S_a are inter-related by

$$S_a = \omega^2 S_d = \omega S_v$$

S_a , S_v are directly related to S_d

by ω^2 and ω respectively or by $(2\pi f)^2$ and $2\pi f$;

or $\left(\frac{2\pi}{T}\right)^2$ and $\left(\frac{2\pi}{T}\right)$ as shown in Figure.

Due to this direct relation, a 4-way plot is usually used to display S_a , S_v and S_d on a single graph as shown in Figure.

In this figure, the logarithm of period T , S_a , S_v and S_d is used.

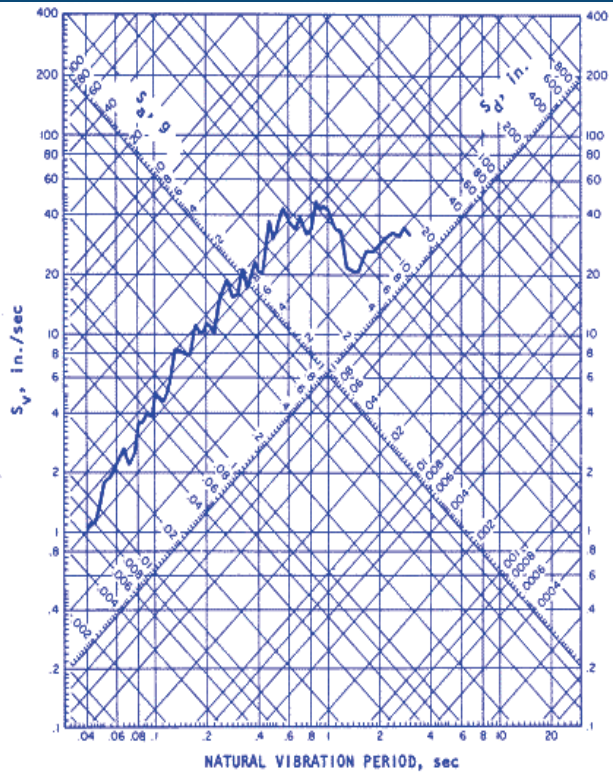


Figure 20. Four-way logarithmic plot of response spectrum, El Centro ground motion—S00°E component. Damping ratio $\xi = 2$ percent

From: Chopra, Dynamics of Structures, A Primer

Short course notes: A. Elgamal, Chicago, Illinois, April 29 – 30, 2013

61

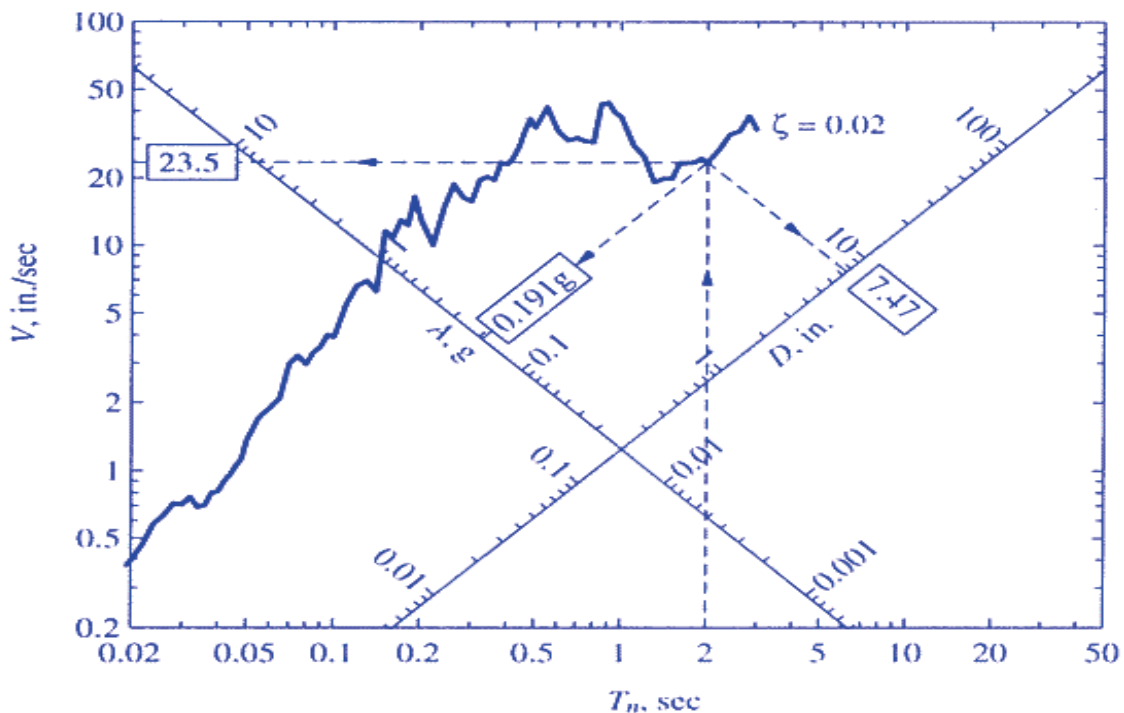


Figure 6.6.3 Combined D - V - A response spectrum for El Centro ground motion; $\zeta = 2\%$.

From: Chopra, Dynamics of Structures

Short course notes: A. Elgamal, Chicago, Illinois, April 29 – 30, 2013

62

In order to cover the damping range of interest, it is common to perform the same calculations for $\xi = 0.0, 0.02, 0.05, 0.10,$ and 0.20 (see Figure)

Typical Notation:

$$S_v \equiv \text{PSV} \equiv V$$

$$S_a \equiv \text{PSA} \equiv A$$

$$S_d \equiv \text{SD} \equiv D$$

Example (El-Centro motion):

Find maximum displacement and base shear of tower with $f = 2 \text{ Hz}$, $\xi = 2\%$ and $k = 1.5 \text{ MN/m}$

$$\text{Period } T = 1/f = 0.5 \text{ second}$$

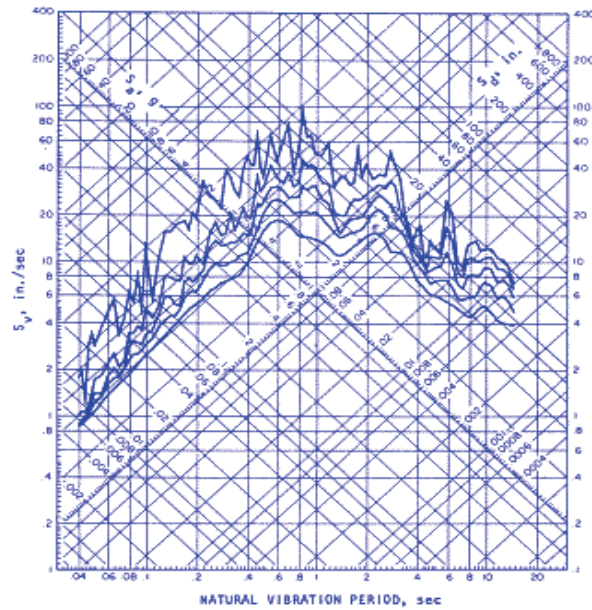
$$S_d = 2.5 \text{ inches} = 0.0635 \text{ m}$$

$$\text{Force}_{\max} = k u_{\max}$$

$$= 1.5 \text{ MN/m} \times 0.0635 \text{ m} = 95.25 \text{ kN}$$

RESPONSE SPECTRUM
IMPERIAL VALLEY EARTHQUAKE
MAY 18, 1940 – 2037 PST

1114001 40.001.0 EL CENTRO SITE
IMPERIAL VALLEY IRRIGATION DISTRICT COMP 500E
DAMPING VALUES ARE 0, 2, 5, 10, AND 20 PERCENT OF CRITICAL



From: Chopra, Dynamics of Structures, A Primer

Figure 21. Four-way logarithmic plot of response spectrum. El Centro ground motion—S00°E component (after Hudson, 1979)

Short course notes: A. Elgamal, Chicago, Illinois, April 29 – 30, 2013

Inspection of this figure shows that the maximum response at short period (high frequency stiff structure) is controlled by the ground acceleration, low frequency (long period) by ground displacement, and intermediate period by ground velocity.

Get copy of El-Centro (May 18, 1940) earthquake record S00E (N-S component) ftp nisee.ce.berkeley.edu (128.32.43.154) login: anonymous password: your_indent cd pub/a.k.chopra get el_centro.data quit

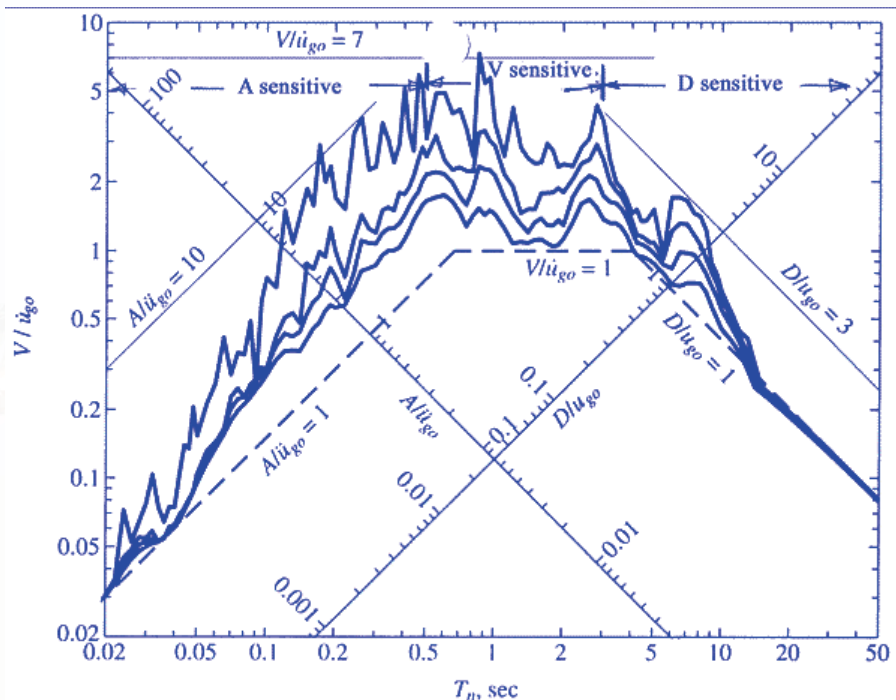


Figure 6.8.2 Response spectrum for El-Centro ground motion plotted with normalized scales A/\ddot{u}_{g0} , V/\dot{u}_{g0} , and D/u_{g0} ; $\zeta = 0, 2, 5,$ and 10% .

From: Chopra, Dynamics of Structures

Short course notes: A. Elgamal, Chicago, Illinois, April 29 – 30, 2013

Note that response spectrum for relative velocity may be obtained from the SDOF response history, and similarly for $\ddot{u}^t = (\ddot{u} + \ddot{u}_g)$. These spectra are known as relative velocity and total acceleration response spectra, and are different from the pseudo velocity and pseudo acceleration spectra S_v and S_a (which are directly related to S_d).

e.g. for $\zeta = 0\%$

$$m(\ddot{u} + \ddot{u}_g) + ku = 0$$

$$\text{or } (\ddot{u} + \ddot{u}_g) + \omega^2 u = 0$$

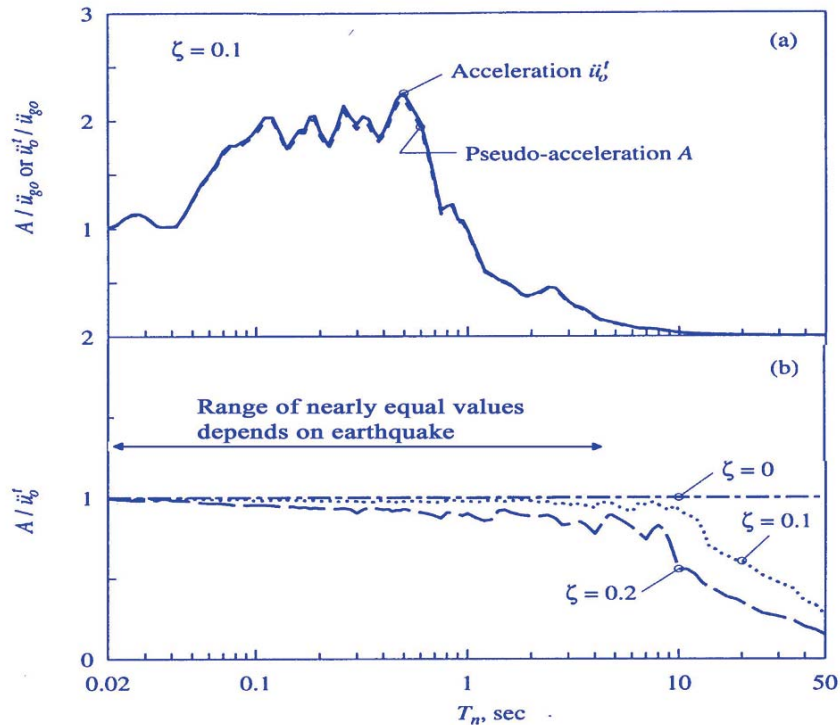


Figure 6.12.2 (a) Comparison between pseudo-acceleration and acceleration response spectra; $\zeta = 10\%$; (b) ratio A/\ddot{u}_o^t for $\zeta = 0, 10,$ and 20% .

From: Chopra, Dynamics of Structures

Short course notes: A. Elgamal, Chicago, Illinois, April 29 – 30, 2013

65

Elastic Design Spectrum

Use recorded ground motions (available)

Use ground motions recorded at similar sites:

Magnitude of earthquake

Distance of site from earthquake fault

Fault mechanism

Local Soil Conditions

Geology/travel path of seismic waves

Motions recorded at the same location. For design, we need an envelope. One way is to take the average (mean) of these values (use statistics to define curves for mean and standard deviation, see next)

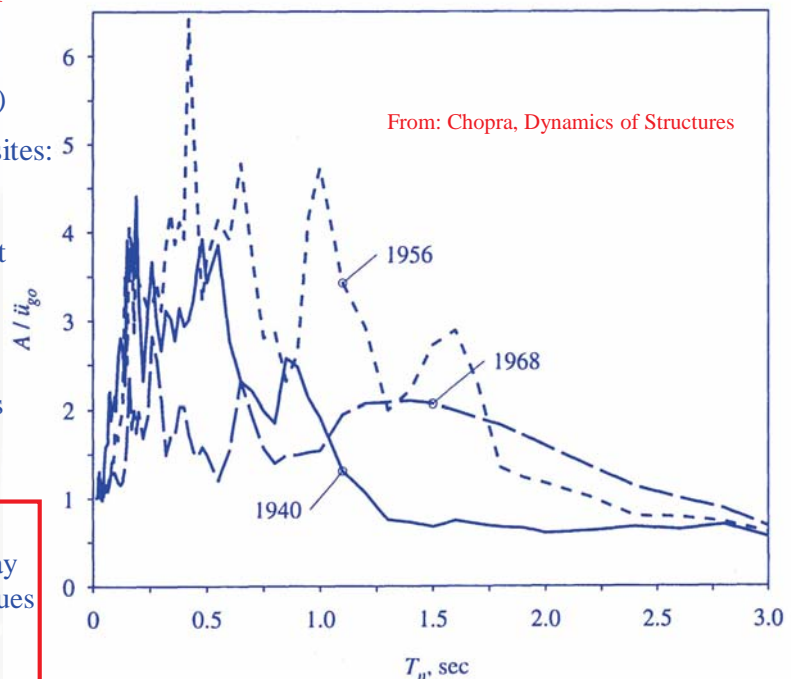


Figure 6.9.1 Response spectra for the north-south component of ground motions recorded at the Imperial Valley Irrigation District substation, El Centro, California, during earthquakes of May 18, 1940; February 9, 1956; and April 8, 1968. $\zeta = 2\%$.

Short course notes: A. Elgamal, Chicago, Illinois, April 29 – 30, 2013

66

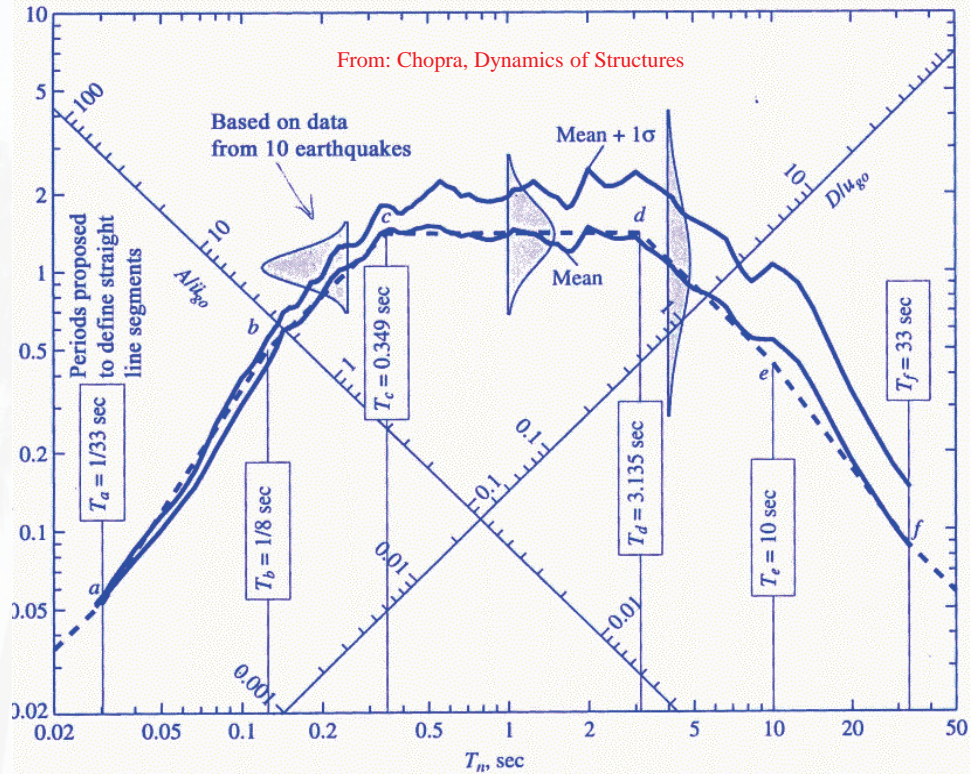


Figure 6.9.2 Mean and mean + 1σ spectra with probability distributions for V at $T_n = 0.25, 1,$ and 4 sec; $\zeta = 5\%$. Dashed lines show an idealized design spectrum. (Based on numerical data from R. Riddell and N. M. Newmark, 1979.)

The periods and values in Table 6.9.1 were selected to give a good match to a statistical curve such as Figure 6.9.2 based on an ensemble of 50 earthquakes on competent soils.

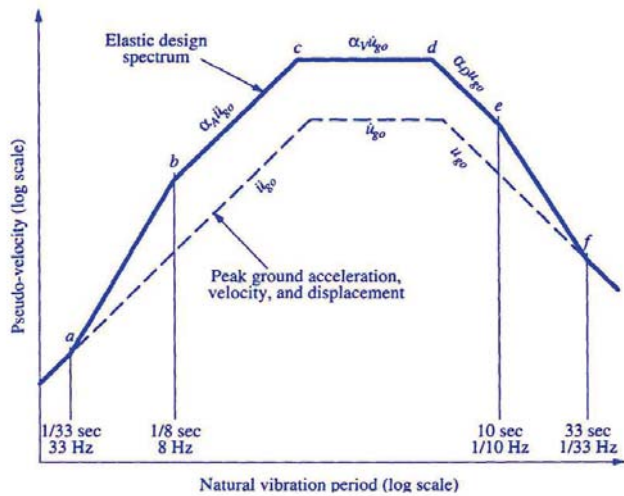


Figure 6.9.3 Construction of elastic design spectrum.

TABLE 6.9.1 AMPLIFICATION FACTORS: ELASTIC DESIGN SPECTRA

Damping, ζ (%)	Median (50 percentile)			One Sigma (84.1 percentile)		
	α_A	α_V	α_D	α_A	α_V	α_D
1	3.21	2.31	1.82	4.38	3.38	2.73
2	2.74	2.03	1.63	3.66	2.92	2.42
5	2.12	1.65	1.59	2.71	2.30	2.01
10	1.64	1.37	1.20	1.99	1.84	1.69
20	1.17	1.08	1.01	1.26	1.37	1.38

Source: N. M. Newmark and W. J. Hall, *Earthquake Spectra and Design*, Earthquake Engineering Research Institute, Berkeley, Calif., 1982, pp. 35 and 36.

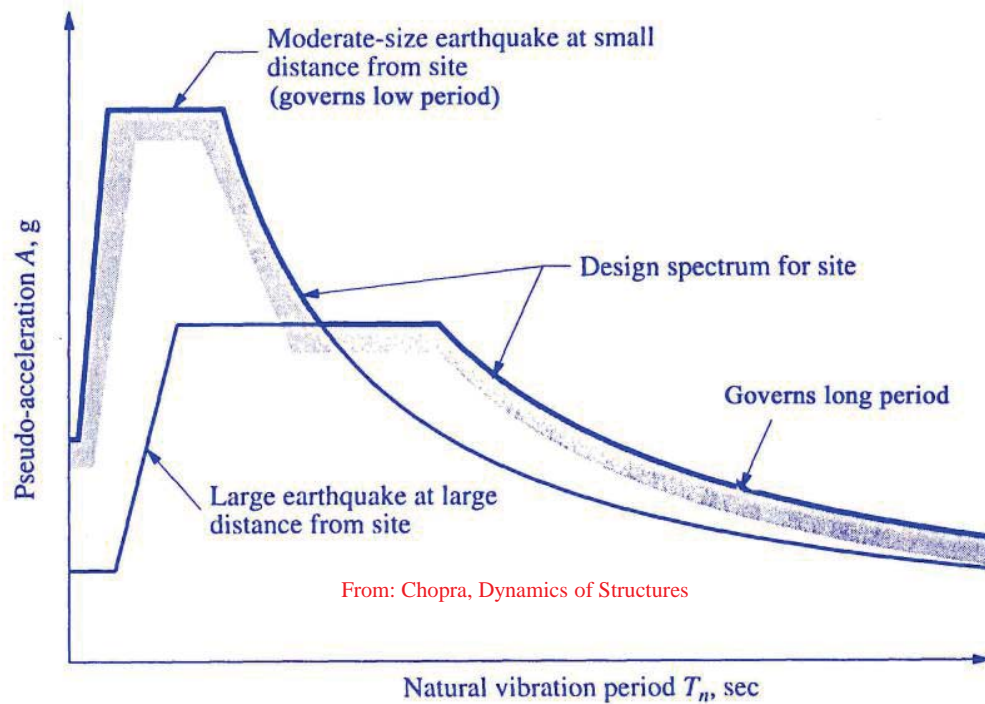
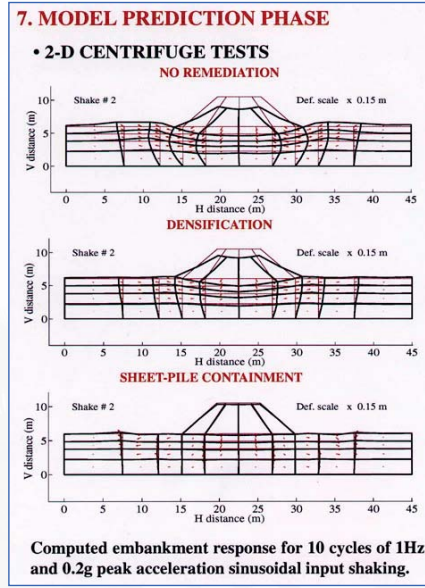
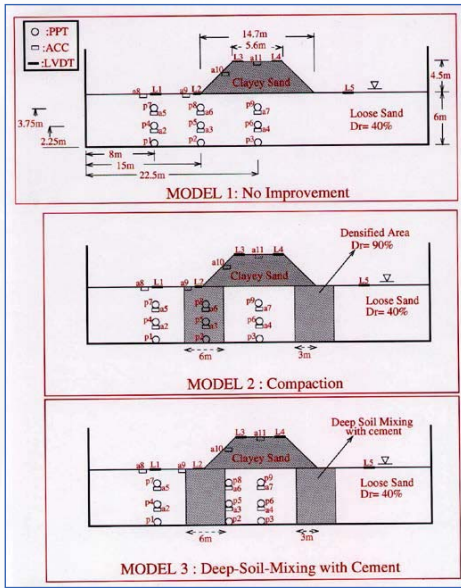


Figure 6.11.1 Design spectrum defined as the envelope of design spectra for earthquakes originating on two different faults.

(Design Spectrum may include more than one earthquake scenario)

Appendix II: Illustrative Examples of Large Scale Numerical Analyses



Adalier, K., A. -W. Elgamal, and G. R. Martin, "Foundation Liquefaction Countermeasures for Earth Embankments," Journal of Geotechnical and Geo-environmental Engineering, ASCE, Vol. 124, No. 6, 500-517, June, 1998.
 Elgamal, Ahmed, Ender Parra, Zhaohui Yang, and Korhan Adalier, "Numerical Analysis of Embankment Foundation Liquefaction Countermeasures," Journal of Earthquake Engineering, Vol. 6, No. 4, pp. 447-471, 2002.
 Yang, Zhaohui, Ahmed Elgamal, Korhan Adalier, and Michael Sharp, "Earth Dam on Liquefiable Foundation: Numerical Prediction of Centrifuge Experiments," Journal of Engineering Mechanics, ASCE, Volume 130, Issue 10, October 2004.

Short course notes: A. Elgamal, Chicago, Illinois, April 29 – 30, 2013

OpenSees 3D FE Model

Three-Dimensional Seismic Response of Humboldt Bay Bridge-Foundation-Ground System, A. Elgamal; L. Yan; Z. Yang; and J. P. Conte, Journal of Structural Engineering, Vol. 134, No. 7, July 1, 2008.

- 30,237 nodes
- 1,140/280 linear/nonlinear beam-column elements
- 81 linear shell elements
- 23,556 solid brick elements
- 1,806 zero-length elements

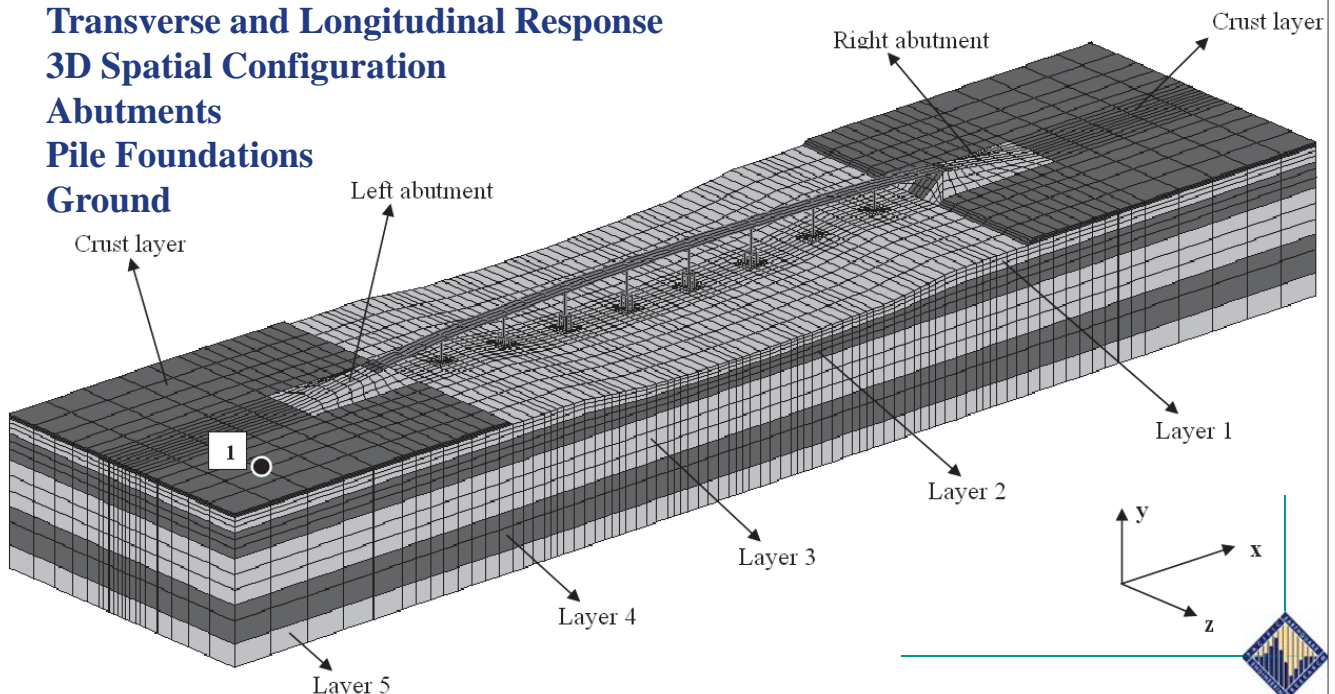
Transverse and Longitudinal Response

3D Spatial Configuration

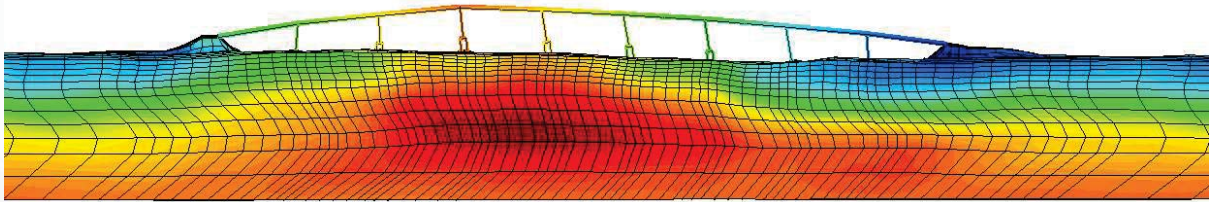
Abutments

Pile Foundations

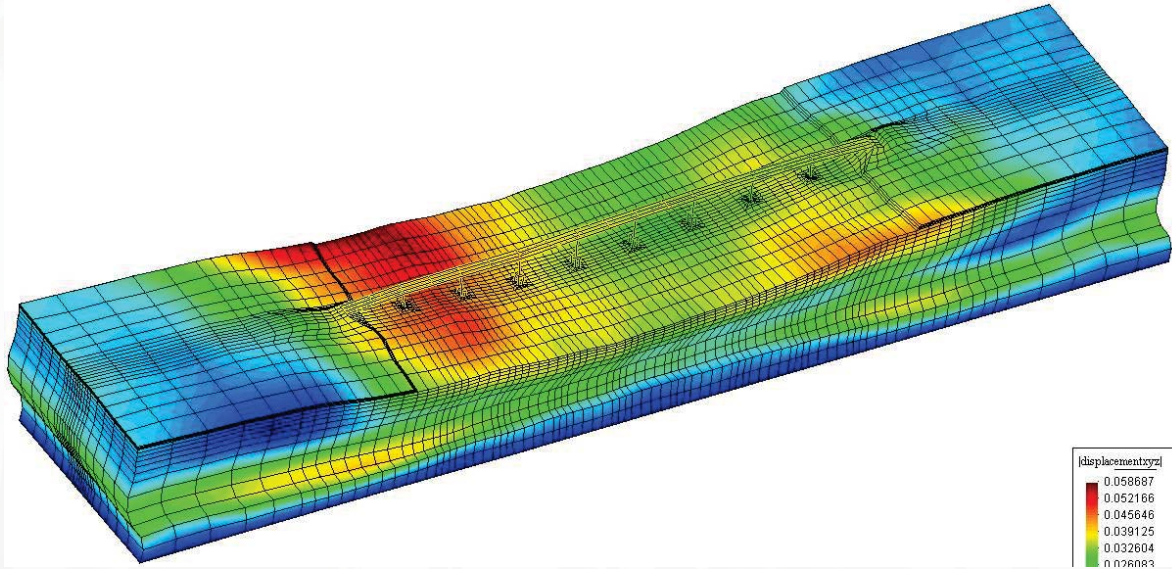
Ground



Short course notes: A. Elgamal, Chicago, Illinois, April 29 – 30, 2013

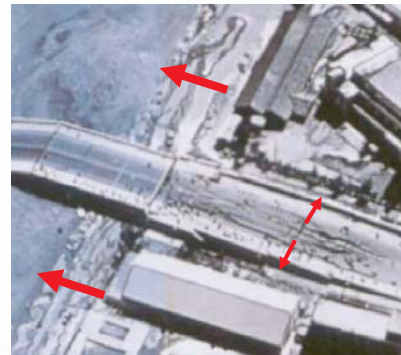
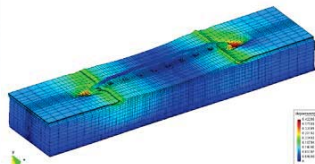


Three-Dimensional Seismic Response of Humboldt Bay Bridge-Foundation-Ground System, A. Elgamal; L. Yan; Z. Yang; and J. P. Conte, Journal of Structural Engineering, Vol. 134, No. 7, July 1, 2008.

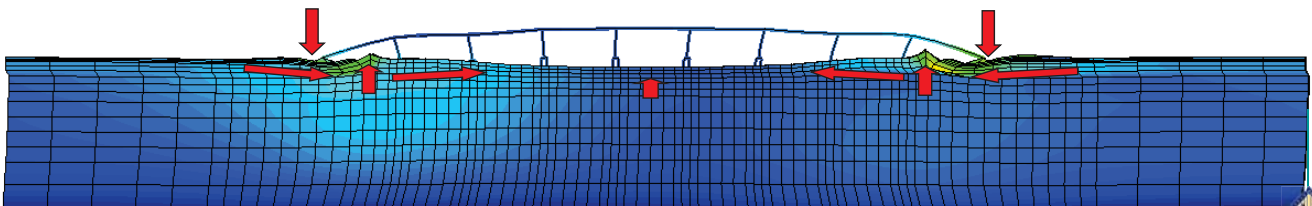
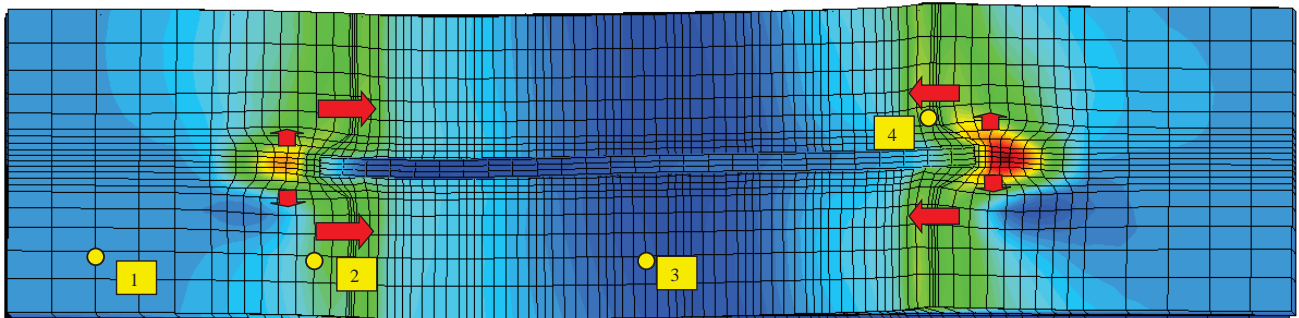


Short course notes: A. Elgamal, Chicago, Illinois, April 29 – 30, 2013

Elevation and plan view of residual deformation (Scale factor = 50)

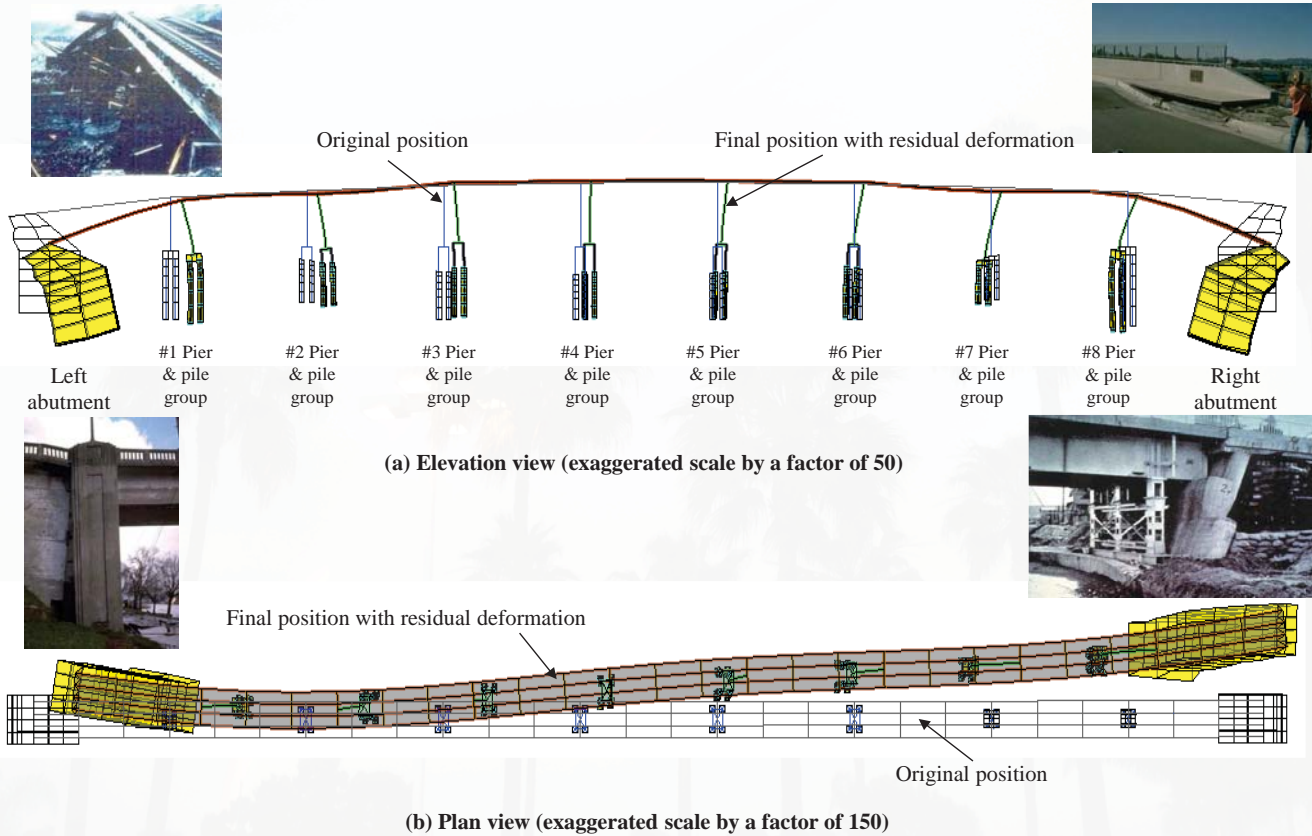


Three-Dimensional Seismic Response of Humboldt Bay Bridge-Foundation-Ground System, A. Elgamal; L. Yan; Z. Yang; and J. P. Conte, Journal of Structural Engineering, Vol. 134, No. 7, July 1, 2008.



Short course notes: A. Elgamal, Chicago, Illinois, April 29 – 30, 2013

Permanent Deformation of Bridge, Foundations, and Abutments



Short course notes: A. Elgamal, Chicago, Illinois, April 29 – 30, 2013

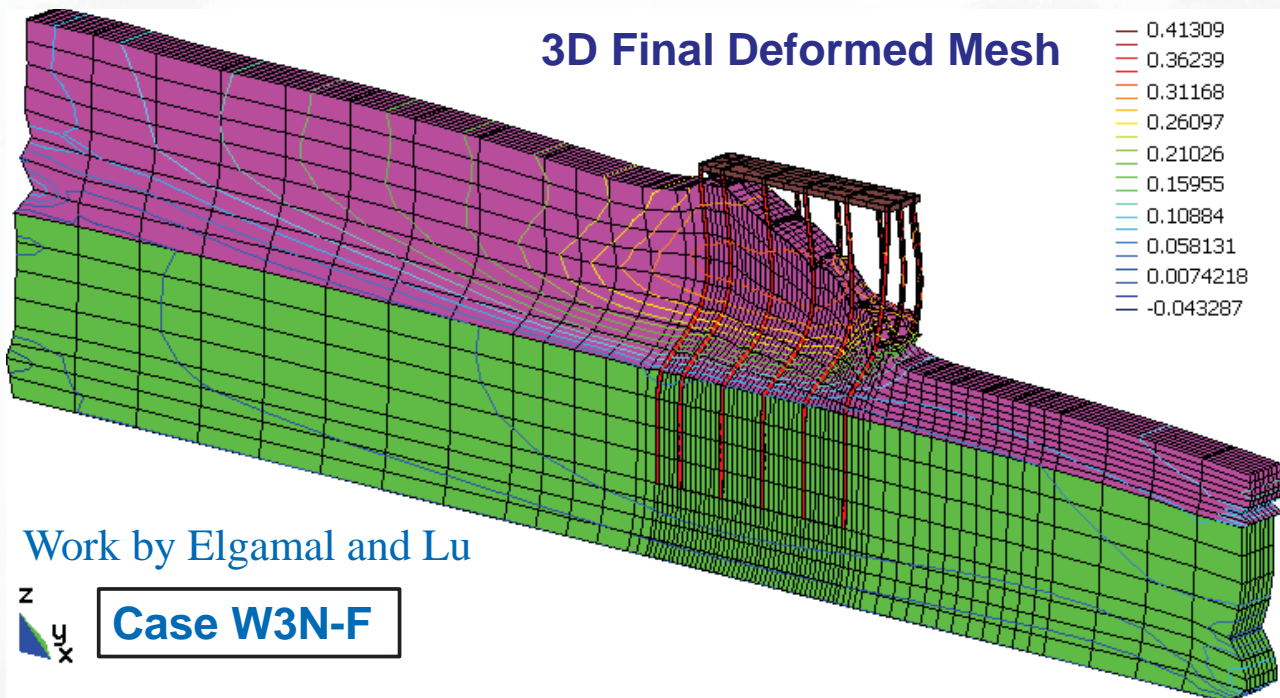
75

3D Slice of Wharf supported on pile foundation

(factor of 30)

Contour lines show longitudinal displacement in meters

3D Final Deformed Mesh



Short course notes: A. Elgamal, Chicago, Illinois, April 29 – 30, 2013

76

3D Slice of Wharf supported on pile foundation

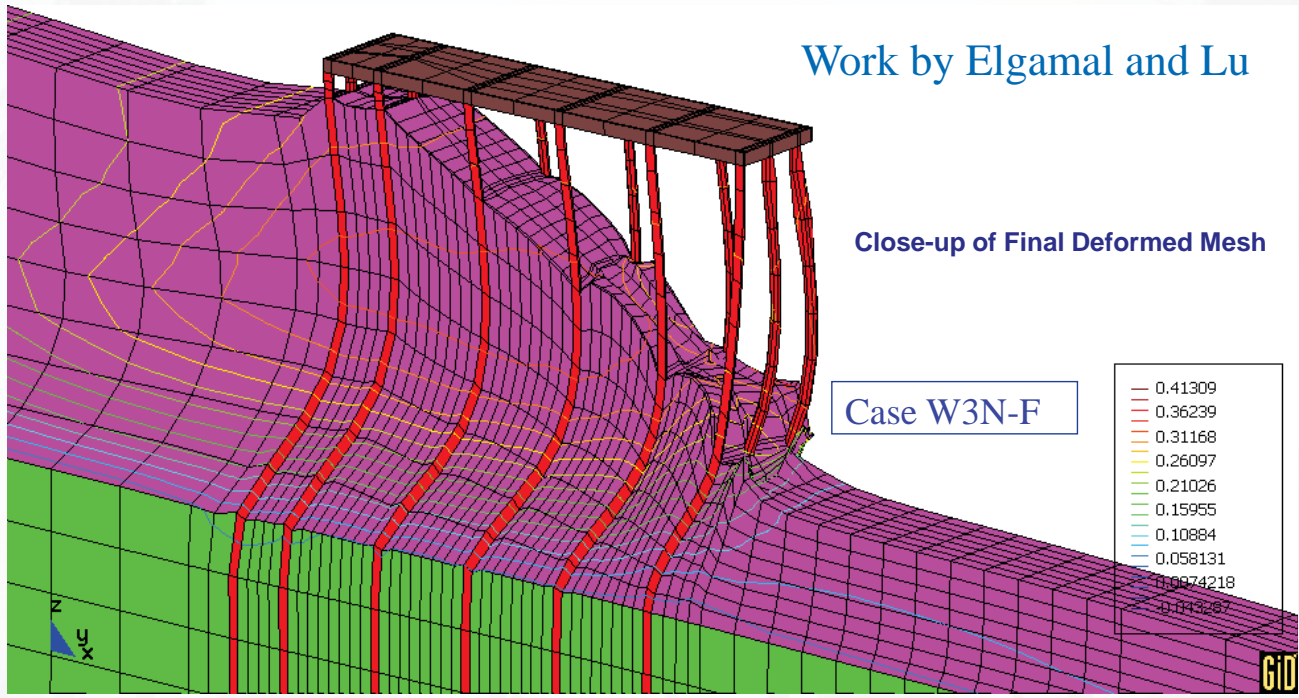
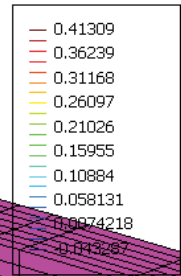
Contour lines show the longitudinal displacement in meters

(factor of 30)

Work by Elgamal and Lu

Close-up of Final Deformed Mesh

Case W3N-F

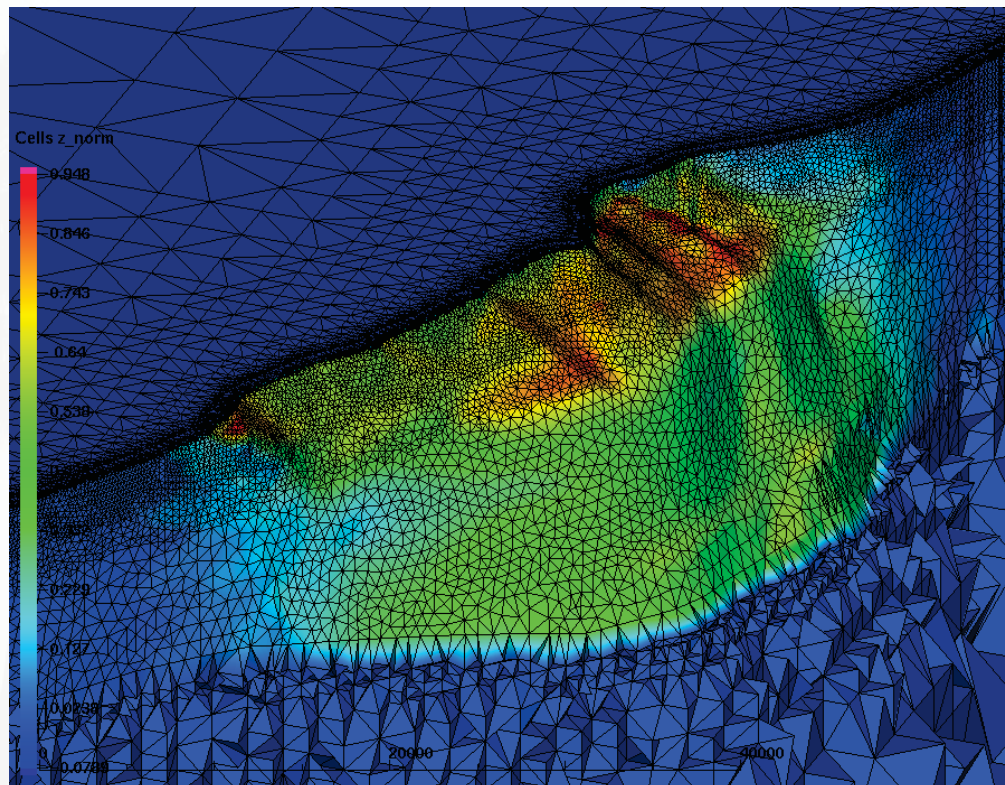


Short course notes: A. Elgamal, Chicago, Illinois, April 29 – 30, 2013

From: http://meshing.lanl.gov/proj/crustal_dyn_saf_scec_cfm/catalog.html

San Andreas Fault Finite Element Mesh

Fault definition from SCEC Community Fault Model (CFM)



Short course notes: A. Elgamal, Chicago, Illinois, April 29 – 30, 2013